

**ADVERTIMENT.** La consulta d'aquesta tesi queda condicionada a l'acceptació de les següents condicions d'ús: La difusió d'aquesta tesi per mitjà del servei TDX ([www.tesisenxarxa.net](http://www.tesisenxarxa.net)) ha estat autoritzada pels titulars dels drets de propietat intel·lectual únicament per a usos privats emmarcats en activitats d'investigació i docència. No s'autoritza la seva reproducció amb finalitats de lucre ni la seva difusió i posada a disposició des d'un lloc aliè al servei TDX. No s'autoritza la presentació del seu contingut en una finestra o marc aliè a TDX (framing). Aquesta reserva de drets afecta tant al resum de presentació de la tesi com als seus continguts. En la utilització o cita de parts de la tesi és obligat indicar el nom de la persona autora.

**ADVERTENCIA.** La consulta de esta tesis queda condicionada a la aceptación de las siguientes condiciones de uso: La difusión de esta tesis por medio del servicio TDR ([www.tesisenred.net](http://www.tesisenred.net)) ha sido autorizada por los titulares de los derechos de propiedad intelectual únicamente para usos privados enmarcados en actividades de investigación y docencia. No se autoriza su reproducción con finalidades de lucro ni su difusión y puesta a disposición desde un sitio ajeno al servicio TDR. No se autoriza la presentación de su contenido en una ventana o marco ajeno a TDR (framing). Esta reserva de derechos afecta tanto al resumen de presentación de la tesis como a sus contenidos. En la utilización o cita de partes de la tesis es obligado indicar el nombre de la persona autora.

**WARNING.** On having consulted this thesis you're accepting the following use conditions: Spreading this thesis by the TDX ([www.tesisenxarxa.net](http://www.tesisenxarxa.net)) service has been authorized by the titular of the intellectual property rights only for private uses placed in investigation and teaching activities. Reproduction with lucrative aims is not authorized neither its spreading and availability from a site foreign to the TDX service. Introducing its content in a window or frame foreign to the TDX service is not authorized (framing). This rights affect to the presentation summary of the thesis as well as to its contents. In the using or citation of parts of the thesis it's obliged to indicate the name of the author

UNIVERSITAT POLITÈCNICA DE CATALUNYA

Ph.D. Program:

AUTOMATIC CONTROL, ROBOTICS AND COMPUTER VISION

Ph.D. Thesis

CONSENSUS CONTROL IN ROBOT NETWORKS AND COOPERATIVE TELEOPERATION:  
AN OPERATIONAL SPACE APPROACH

**Carlos Iván Aldana López**

Thesis advisors: Luis Basañez Villaluenga  
Emmanuel Nuño Ortega

January 2015

Dissertation

CONSENSUS CONTROL IN ROBOT NETWORKS AND COOPERATIVE TELEOPERATION:  
AN OPERATIONAL SPACE APPROACH

by

**Carlos Iván Aldana López**

Supervisors: Luis Basañez Villaluenga  
Emmanuel Nuño Ortega

Submitted to the Institut d'Organització i Control de Sistemes Industrials in partial  
fulfillment of the requirements for the degree of

Doctor of Philosophy

at the

Universitat Politècnica de Catalunya

Barcelona, Spain. January 2015.

To my wife Mary Nuño,  
my parents Guillermina López and †Arturo Aldana,  
and my brothers Arturo and Aldo Aldana.

# CONSENSUS CONTROL IN ROBOT NETWORKS AND COOPERATIVE TELEOPERATION: AN OPERATIONAL SPACE APPROACH

Carlos Iván Aldana López

## Abstract

An interesting approach in cooperative control is to design distributed control strategies which use only local information so that a multi-agent system achieves specified behaviors. A basic behavior in cooperative control is the *consensus*. Given a multi-agent system, like a multiple robot network, it is said that the agents reach a consensus if the state of each agent converges to a common state. Examples of cooperative tasks in which consensus algorithms are employed include *formation control*, *flocking theory*, *rendezvous problems* and *synchronization*. These cooperative tasks have several possible applications, like: transportation systems (intelligent highways, air-traffic control); military systems (formation flight, surveillance, reconnaissance, cooperative attack and rendezvous) and mobile sensor networks (space-based interferometers, environmental sampling).

The solution to the consensus problems involves the design of control algorithms such that the agents can reach an agreement on their states. There are two main problems that are studied in consensus, the *leader-follower consensus* and the *leaderless consensus*. In the leader-follower consensus problem, there exists a leader that specifies the state for the whole group while in a leaderless consensus problem, there is not a priori reference state.

The main goal of this thesis is the design of operational space controllers that solve the leader-follower and the leaderless consensus problems in networks composed of multiple heterogeneous robots. Furthermore, this document proposes novel operational space control schemes for bilateral teleoperation systems. In both scenarios, different conditions are studied, such as the absence of robot velocity measurements, constant and variable time-delays in the robot's interconnection, and uncertainty in the robot's physical parameters.

Most of the previous consensus control algorithms, only work with the position or orientation but not with both. On the contrary, this dissertation deals with the entire pose of the robots that contains both the position and the orientation. Moreover, in order to render a singularity-free description of the orientation, the unit-quaternions are employed.

The dissertation provides a rigorous stability analysis of the control algorithms and presents simulations and experiments that validate the effectiveness of the proposed controllers.



## ACKNOWLEDGEMENTS

---

In the following lines I want to acknowledge and thank the people and institutions that made possible the successful completion of this thesis.

I thank Professor Luis Basañez for his constant and invaluable support in the development of this thesis. In particular, I thank him for his confidence and friendship. I am very fortunate to have had a thesis director with the human and professional quality as his, I thank him a lot for all his teachings.

To Emmanuel Nuño, my gratitude and admiration forever, his guidance and expertise were instrumental in the development of this thesis, I appreciate his patience and all the work and time he invested, but especially the friendship we have developed for many years.

Thanks to the teachers and staff at the IOC, especially to its director Raúl Suárez for his help with the administrative issues and for the nice and interesting conversations that we had. Thanks to Jan Rosell and Orestes Mas, for their comments and questions always accurate in the group meetings. I am grateful to Robert Griñó and Enric Fosas for their kindness whenever I consulted them. Thanks to Carme Martínez, Noemí Zapata and Marta Fuentes, for their always efficient assistance in the administrative matters.

My time at the IOC would not have been the same without the friendship and daily interaction that I had with my colleagues, among them: Alexander, Paolo, Leo, Josep, Carlos, Andres, Niliana, Marcos, Henry, Abiud, Isiah, Sergi, Gemma, Noe, Diana. I highly appreciate their attention to the monologues that sometimes I told them during lunch time, but also the discussions about politics, religion, movies and any interesting issue. They always made the meals very entertaining and sometimes very educational.

Thanks to Patrick Grosch for the friendship and support throughout this path. Thanks to John Hannaford for his hospitality and help during the years we have shared the flat. They made our stay at “Can Granados” very pleasant.

I thank my dear mother and much-missed father, Guillermina and Arturo, for all the love and the unconditional support that they have always given me. They are the best parents that I could have had, They are an example and a reference to me. Thanks to my two great friends that I have the fortune to have as brothers, Arturo and Aldo, for always being there, for encouraging me to follow my dreams and goals.

Thanks to my beloved wife, Mary Nuño, for everything she has done for me. In particular for listening, encouraging and always believing in me. Without her, this adventure would not have started much less finished, thanks, thanks a lot chula.

Finally, I thank the Consejo Nacional de Ciencia y Tecnología (CONACyT), for the scholarship they gave me (reference number 168998) and for the basic science project CB-129079 in which I participated. Thanks to the Secretaría de Educación Pública, for the complementary scholarship within the program “Apoyo al Posgrado”. Besides, thanks to the Spanish CICYT projects DPI2010-15446 and DPI2011-22471 within which this thesis was elaborated.

*Carlos Iván Aldana López.* Barcelona, Spain. January 2015.



## AGRADECIMIENTOS

---

En las siguientes líneas quiero reconocer y agradecer a las personas e instituciones que hicieron posible llevar a buen término esta tesis.

Al profesor Luis Basañez le agradezco su constante e invaluable apoyo en el desarrollo de esta tesis. En especial le agradezco su confianza y su amistad. Soy muy afortunado por haber tenido un director de tesis con la calidad humana y profesional como la de él, le agradezco mucho todas sus enseñanzas.

A Emmanuel Nuño mi agradecimiento y admiración por siempre, su guía y conocimientos fueron fundamentales en la elaboración de esta tesis, le agradezco la paciencia y todo el trabajo invertido, pero sobre todo la amistad que hemos podido desarrollar desde hace muchos años.

A los profesores y personal administrativo del IOC muchas gracias, en especial a su director Raúl Suárez por su ayuda con los temas de gestión y por las agradables e interesantes conversaciones que hemos tenido. Gracias a Jan Rosell y a Orestes Mas, por sus comentarios y preguntas siempre certeras en las reuniones de grupo. A Robert Griñó y Enric Fosas les agradezco su disponibilidad y amabilidad siempre que les consulté. A Carme Martínez, Noemí Zapata y Marta Fuentes les agradezco su siempre eficiente y oportuna ayuda en los temas administrativos.

Mi paso por el IOC no hubiera sido lo mismo sin la amistad y la convivencia diaria que tuve con mis compañeros, entre ellos: Alexander, Paolo, Leo, Josep, Carlos, Andrés, Niliana, Marcos, Henry, Abiud, Isiah, Sergi, Gemma, Noé, Diana. Les agradezco mucho su atención a mis monólogos durante las comidas, pero también las discusiones sobre política, religión, cine, y cualquier tema que se nos atravesara. Hicieron que las comidas siempre fueran muy amenas y algunas veces muy educativas.

A Patrick Grosch, gracias por su amistad y apoyo durante todo este camino. A John Hanford gracias por su hospitalidad y ayuda durante estos años que hemos compartido piso. Los dos hicieron que nuestra estancia en “Can Granados” fuera muy placentera.

A mi querida madre y a mi añorado padre, Guillermina y Arturo, les agradezco todo el amor y el apoyo incondicional que siempre me han dado. Sé que no pude tener mejores padres que ustedes, son un ejemplo y una referencia para mí. Y a mis dos grandes amigos que tengo la fortuna de tener como hermanos, Arturo y Aldo, gracias por estar siempre ahí, por motivarme a seguir mis sueños y metas.

A mi amada esposa, Mary Nuño, muchas gracias por todo lo que has hecho por mí, por escucharme, animarme y creer siempre en mí. Sin ti, esta aventura no hubiera empezado y mucho menos acabado, gracias por ser y estar, gracias, muchas gracias chula.

Finalmente agradezco al Consejo Nacional de Ciencia y Tecnología (CONACyT), por la beca que me otorgaron (numero de referencia: 168998) y por el proyecto de ciencia básica CB-129079 en el cual participé. Gracias a la Secretaría de Educación Pública por la beca complemento dentro del programa de “Apoyo al Posgrado”. Por ultimo, gracias a los proyectos CICYT españoles DPI2010-15446 and DPI2011-22471 dentro de los cuales se elaboró esta tesis.

*Carlos Iván Aldana López.* Barcelona, España. Enero 2015.

# CONTENTS

---

<b>List of Figures</b>	<b>XV</b>
<b>List of Tables</b>	<b>XIX</b>
<b>Notation and Acronyms</b>	<b>XXI</b>
<b>1 Introduction</b>	<b>1</b>
1.1 Context and motivation . . . . .	1
1.2 Objectives . . . . .	4
1.3 Outline of the thesis . . . . .	5
<b>2 State of the Art</b>	<b>7</b>
2.1 Consensus in networked linear dynamics agents . . . . .	8
2.2 Consensus in networked nonlinear dynamic agents . . . . .	10
2.3 Teleoperation systems . . . . .	12
2.4 Cooperative teleoperation systems . . . . .	14
2.5 Summary and open problems . . . . .	15
<b>3 Modeling</b>	<b>17</b>
3.1 Robot manipulators . . . . .	17
3.1.1 Representing the orientation . . . . .	19
3.1.2 Pose definition and kinematics . . . . .	28
3.1.3 Pose error . . . . .	31
3.1.4 Dynamics . . . . .	34
3.2 Robot networks . . . . .	38
3.2.1 Network interconnection . . . . .	38
3.2.2 Assumptions and instrumental lemmas . . . . .	39
3.3 Teleoperation systems . . . . .	42
3.3.1 SL-SR teleoperation system model . . . . .	42
3.3.2 CTS model . . . . .	43
<b>4 Consensus Control</b>	<b>47</b>
4.1 Problem statement . . . . .	47
4.2 Consensus control without velocity measurements . . . . .	51
4.2.1 Leader-follower consensus . . . . .	51
4.2.2 Leaderless consensus . . . . .	54
4.2.3 Human-robot interactions . . . . .	55

4.2.4	Remarks . . . . .	56
4.3	Consensus control with variable time-delays . . . . .	56
4.3.1	Leader-follower consensus . . . . .	56
4.3.2	Leaderless consensus . . . . .	61
4.3.3	Human-robot interactions . . . . .	62
4.3.4	Remarks . . . . .	64
4.4	Consensus control with uncertain parameters and variable time-delays . . . . .	64
4.4.1	Leader-follower consensus . . . . .	65
4.4.2	Leaderless consensus . . . . .	70
4.4.3	Human-robot interactions . . . . .	71
4.4.4	Remarks . . . . .	72
4.5	Simulation results . . . . .	74
4.5.1	Simulation platform . . . . .	74
4.5.2	Consensus control without velocity measurements results . . . . .	76
4.5.3	Consensus control with variable time-delays . . . . .	82
4.5.4	Consensus control with uncertain parameters and variable time-delays . . . . .	86
4.6	Experimental results . . . . .	92
4.6.1	Experimental validation testbed . . . . .	92
4.6.2	Consensus control without velocity measurements . . . . .	96
4.6.3	Consensus control with variable time-delays . . . . .	104
<b>5</b>	<b>Teleoperation Control</b>	<b>113</b>
5.1	Controllers for SL-SR teleoperation systems . . . . .	113
5.1.1	Teleoperation control without velocity measurements . . . . .	113
5.1.2	Teleoperation control with variable time-delays . . . . .	115
5.1.3	Teleoperation control with uncertain parameters and variable time-delays . . . . .	116
5.2	Control of cooperative teleoperation system with uncertain parameters and variable time-delays . . . . .	118
5.3	Simulation results . . . . .	120
5.4	Experimental results . . . . .	133
<b>6</b>	<b>Conclusions</b>	<b>139</b>
6.1	Conclusions and contributions . . . . .	139
6.2	Future work . . . . .	141
6.3	List of publications . . . . .	142
<b>A</b>	<b>Math and Control Background</b>	<b>145</b>
A.1	Mathematical preliminaries . . . . .	145
A.1.1	Matrix types and Kronecker product . . . . .	145
A.1.2	Vectors products and norms . . . . .	147
A.1.3	Function properties . . . . .	149
A.1.4	Norms for functions and $\mathcal{L}_q$ spaces . . . . .	150
A.1.5	Sets . . . . .	151
A.1.6	Inequalities . . . . .	152
A.1.7	Quaternions . . . . .	153

A.2	Stability concepts . . . . .	154
A.2.1	Lyapunov theory . . . . .	154
A.2.2	Input–output stability . . . . .	157
A.2.3	Passivity . . . . .	158
<b>B</b>	<b>Validation Tools</b>	<b>161</b>
B.1	Robot kinematics and dynamics . . . . .	161
B.1.1	2-DoF robot . . . . .	162
B.1.2	3-DoF robot . . . . .	163
B.1.3	3-DoF robot Omni . . . . .	170
B.1.4	7-DoF robot LWR . . . . .	172
B.2	PhanTorque libraries . . . . .	172
	<b>References</b>	<b>179</b>
	<b>Index</b>	<b>191</b>
	Keyword Index . . . . .	191
	First Authors Index . . . . .	193



## LIST OF FIGURES

---

1.1	Examples of robot networks: (left) robot network with one leader and three followers; (right) robot network composed of three robots without a leader. . . . .	3
1.2	Configurations of teleoperation systems: (left) single local and single remote (SL-SR) configuration; (right) a cooperative teleoperation system with a single local robot and, at the remote site, a cooperative system composed of two robots handling an object. . . . .	4
3.1	(a) 6-DoF robot manipulator and its joint axes; (b) pose and Cartesian coordinates frames of a robot manipulator. . . . .	18
3.2	Representation of the Euler angles ZYZ convention. . . . .	22
3.3	Representation of the Euler angles ZYX convention (yaw, pitch, roll). . . . .	23
3.4	Axis-angle orientation representation, $\mathbf{u}$ is the rotation axis (unit vector) and $\theta$ the rotation angle. . . . .	25
3.5	Description of the robot's pose and the coordinate frames used in the forward kinematics. . . . .	29
3.6	Position vectors and rotation matrices of frames $\Sigma_i$ and $\Sigma_j$ relative to the reference frame $\Sigma_W$ . . . . .	31
3.7	Examples of allowed graph topologies and their corresponding Laplacians for a five nodes network. . . . .	39
3.8	Leaderless robot network and the graph that models its interconnection. . . . .	41
3.9	Leader-follower robot network and the graph that models its interconnection. . . . .	41
3.10	SL-SR teleoperation system. . . . .	43
3.11	Teleoperation system with a single local robot and a remote cooperative system composed of two robots handling a common object. . . . .	44
4.1	Block diagram of the control scheme that solves the consensus problems without velocity measurements using the controller proposed in equation (4.14). . . . .	51
4.2	Block diagram of the control scheme that solves the consensus problem with variable time-delays in the interconnection using the controller proposed in equation (4.31). . . . .	57
4.3	Block diagram of the control scheme that solves the consensus problem with uncertain parameters and variable time-delays in the interconnection using the controller proposed in equation (4.54). . . . .	66
4.4	Robot network and interconnection graphs used in the simulations of the consensus algorithms without velocity measurements and with variable time-delays. . . . .	76
4.5	Pose of the robots for the leader-follower case using the consensus control scheme without velocity measurements. . . . .	78

4.6	Velocities of the robots for the leader-follower case using the consensus control scheme without velocity measurements. . . . .	79
4.7	Pose of the robots for the leaderless case using the consensus control scheme without velocity measurements. . . . .	80
4.8	Velocities of the robots for the leaderless case using the consensus control scheme without velocity measurements. . . . .	81
4.9	Sample of the variable time-delays. . . . .	82
4.10	Pose of the robots for the leader-follower case using the consensus control scheme with variable time-delays. . . . .	84
4.11	Velocities of the robots for the leader-follower case using the consensus control scheme with variable time-delays. . . . .	85
4.12	Pose of the robots for the leaderless case using the consensus control scheme with variable time-delays. . . . .	87
4.13	Velocities of the robots for the leaderless case using the consensus control scheme with variable time-delays. . . . .	88
4.14	Robot network and interconnection graphs used in the simulations of the consensus algorithm with uncertain parameters and variable time-delays. . . . .	89
4.15	Pose of the robots for the leader-follower case using the consensus control scheme with uncertain parameters and variable time-delays. . . . .	91
4.16	Kinematic parameters estimation for the leader-follower case using the consensus control scheme with uncertain parameters and variable time-delays. . . . .	92
4.17	Pose of the robots for the leaderless case using the consensus control scheme with uncertain parameters and variable time-delays. . . . .	93
4.18	Kinematic parameters estimation for the leaderless case using the consensus control scheme with uncertain parameters and variable time-delays. . . . .	94
4.19	Experimental validation test-bed. . . . .	95
4.20	PhanTorque_6Dof and PhanTorque_3Dof libraries. . . . .	96
4.21	Pose of the robots for the leader-follower case using the consensus control scheme without velocity measurements. . . . .	97
4.22	Velocities of the robots for the leader-follower case using the consensus control scheme without velocity measurements. . . . .	98
4.23	Pose of the robots for the leaderless case using the consensus control scheme without velocity measurements. . . . .	100
4.24	Velocities of the robots for the leaderless case using the consensus control scheme without velocity measurements. . . . .	101
4.25	Pose of the robots for the leaderless with human interaction case using the consensus control scheme without velocity measurements. . . . .	102
4.26	Velocities of the robots for the leaderless with human interaction case using the consensus control scheme without velocity measurements. . . . .	103
4.27	Sample of the variable time-delays added to the communication channel of the robot network. . . . .	104
4.28	Pose of the robots for the leader-follower case using the consensus control scheme with variable time-delays. . . . .	105
4.29	Velocities of the robots for the leader-follower case using the consensus control scheme with variable time-delays. . . . .	106



4.30	Pose of the robots for the leaderless case using the consensus control scheme with variable time-delays. . . . .	108
4.31	Velocities of the robots for the leaderless case using the consensus control scheme with variable time-delays. . . . .	109
4.32	Pose of the robots for the leaderless with human interaction case using the consensus control scheme with variable time-delays. . . . .	110
4.33	Velocities of the robots for the leaderless with human interaction case using the consensus control scheme with variable time-delays. . . . .	111
5.1	Control scheme for teleoperation systems without velocity measurements. The controller is defined in (5.1). . . . .	114
5.2	Control scheme for teleoperation systems with variable time-delays in the communication channel. The controller is defined in (5.5). . . . .	115
5.3	Control scheme for teleoperation systems with uncertain parameters and variable time-delays. The controller is defined in (5.7). . . . .	117
5.4	Control scheme for a cooperative teleoperation systems with uncertain parameters and variable time-delays. The controller is defined in (5.10). . . . .	119
5.5	Teleoperation system used in the simulations of the control algorithms without velocity measurements and with variable time-delays. . . . .	121
5.6	Teleoperation system used in the simulations of the control algorithm with uncertain parameters and variable time-delays. . . . .	121
5.7	Pose of the robots that compose the teleoperation system shown in Figure 5.5 using the control algorithm without velocity measurements. . . . .	124
5.8	Velocities of the robots that compose the teleoperation system shown in Figure 5.5 using the control algorithm without velocity measurements. . . . .	125
5.9	Pose of the robots that compose the teleoperation system shown in Figure 5.5 using the control algorithm with variable time-delays. . . . .	126
5.10	Velocities of the robots that compose the teleoperation system shown in Figure 5.5 using the control algorithm with variable time-delays. . . . .	127
5.11	Pose of the robots that compose the teleoperation system shown in Figure 5.6 using the control algorithm with uncertain parameters and variable time-delays. . . . .	128
5.12	Kinematic parameters estimation of the robots that compose the teleoperation system shown in Figure 5.6 using the control algorithm with uncertain parameters and variable time-delays. . . . .	129
5.13	Teleoperator System with the reference frame and parameters description. . . . .	129
5.14	Pose of the robots that compose the cooperative teleoperation system. . . . .	131
5.15	Velocities of the robots that compose the cooperative teleoperation system. . . . .	132
5.16	Test-bed used in the experimental validation of the teleoperation control algorithms. . . . .	133
5.17	Pose of the robots using the teleoperation control algorithm without velocity measurements. . . . .	135
5.18	Velocities of the robots using the teleoperation control algorithm without velocity measurements. . . . .	136
5.19	Pose of the robots using the teleoperation control algorithm with variable time-delays. . . . .	137

5.20 Velocities of the robots using the teleoperation control algorithm with variable time-delays. . . . .	138
B.1 2-DoF planar manipulator. . . . .	161
B.2 3-DoF planar manipulator. . . . .	163
B.3 3-DoF robot Omni. . . . .	170
B.4 7-DoF robot LWR. . . . .	172
B.5 PhanTorque_6Dof library. . . . .	174
B.6 PhanTorque_6Dof block. . . . .	174
B.7 PhanTorque_6Dof_vels block. . . . .	175
B.8 PhanTorque_3Dof library. . . . .	176
B.9 PhanTorque_3Dof block. . . . .	176
B.10 PhanTorque_3Dof_vels block. . . . .	177
B.11 PhanTorque_3Dof_tele block. . . . .	177

## LIST OF TABLES

---

4.1	Robots' structure and their physical parameters. . . . .	75
4.2	Parameters used in the simulations of the consensus control scheme without velocity measurements. . . . .	77
4.3	Upper-bounds of the variable time-delays and Gaussian distribution parameters. . . . .	82
4.4	Parameters used in the simulations of the consensus control scheme with variable time-delays. . . . .	83
4.5	Parameters of the variable time-delays. . . . .	89
4.6	Parameters used in the simulations of the consensus control scheme with uncertain parameters and variable time-delays. . . . .	90
4.7	Estimated parameters of the Premium robots. . . . .	99
4.8	Upper-bounds of the variable time-delays and Gaussian distribution parameters. . . . .	107
5.1	Robots' and object's dynamic parameters. . . . .	123
B.1	Robots' parameters description. . . . .	163
B.2	Elements of the parameters vector $\Theta$ . . . . .	165



## NOTATION AND ACRONYMS

---

### Notation

$\exists$	There exists
$\forall$	For any
$\Rightarrow$	Implies that
$\rightarrow$	Tends to
$\in$	Belongs to
$\subset$	Subset
$\equiv$	Equivalent
$:=$	Defined as
$\cup$	Set union
$\cap$	Set intersection
$\mathbb{R}$	All real numbers $\in (-\infty, \infty)$
$\mathbb{R}_{>0}$	All real numbers $\in (0, \infty)$
$\mathbb{R}_{\geq 0}$	All real numbers $\in [0, \infty)$
$\lambda_m\{\mathbf{A}\}$	Minimum eigenvalue of matrix $\mathbf{A}$
$\lambda_M\{\mathbf{A}\}$	Maximum eigenvalue of matrix $\mathbf{A}$
$ \cdot $	Euclidean norm of a vector ( <i>i.e.</i> $ \mathbf{x}  = \sqrt{x_1^2 + x_2^2 + \dots + x_n^2}$ ), or Induced norm of a matrix <i>i.e.</i> $ \mathbf{A}  = \max_{ \mathbf{x} =1}  \mathbf{A}\mathbf{x} $ for $\mathbf{A} \in \mathbb{R}^{n \times m}$ , $\mathbf{x} \in \mathbb{R}^m$
$\ \cdot\ _q$	The $\mathcal{L}_q$ norm, $q \in [1, \infty)$
$n$	Number of DoF
$i$	$i \in \bar{N} := \{1, \dots, N\}$ , where $N$ is the number of nodes of the network, or $i \in \{l, r\}$ , for local and remote manipulators
$T$	Constant time-delay
$T(t)$	Variable time-delay
$\mathbf{q}_i \in \mathbb{R}^n$	Joint position
$\mathbf{p}_i \in \mathbb{R}^3$	Robot's end-effector position relative to the world reference frame
$\boldsymbol{\xi}_i \in S^3$	Robot's end-effector unit-quaternion relative to the world reference frame
$\mathbf{x}_i \in \mathbb{R}^7$	Robot's end effector pose (position and orientation)
$\mathbf{x}_i(t - T) \in \mathbb{R}^7$	Delayed pose
$\mathbf{x}_i(t - T(t)) \in \mathbb{R}^7$	Delayed pose for variable time-delays
$\mathbf{x}_\ell \in \mathbb{R}^7$	Leader pose
$\dot{\mathbf{p}}_i \in \mathbb{R}^3$	Robot's end-effector linear velocity
$\boldsymbol{\omega}_i \in \mathbb{R}^3$	Robot's end-effector angular velocity
$\boldsymbol{\tau}_i \in \mathbb{R}^n$	Joint torques
$\mathbf{f}_i \in \mathbb{R}^6$	Cartesian forces
$\mathbf{f}_h \in \mathbb{R}^6$	Human operator forces
$\mathbf{f}_e \in \mathbb{R}^6$	Environment forces

In general, the argument of the time dependent signals is omitted, *e.g.*,  $\mathbf{x} \equiv \mathbf{x}(t)$ , except for those which are time-delayed, *e.g.*,  $\mathbf{x}(t - T(t))$ .

## General Acronyms

LFCP	Leader-Follower Consensus Problem
LCP	Leaderless Consensus Problem
PD	Proportional-Derivative
P + d	Proportional plus damping
SL-SR	Single Local and Single Remote
CTS	Cooperative Teleoperation System
DoF	Degrees of Freedom
UDP	User Datagram Protocol

## Stability Acronyms

AS	Asymptotically Stable
US	Uniformly Stable
UAS	Uniformly Asymptotically Stable
GAS	Global Asymptotically Stable
GUAS	Global Uniformly Asymptotically Stable
ISS	Input to State Stable
BIBO	Bounded Input Bounded Output

## Latin abbreviations

<i>i.e.</i>	-id est-	that is
<i>e.g.</i>	-exempli gratia-	for instance
<i>cf.</i>	-confer-	see
<i>etc.</i>	-et cetera-	and the rest
<i>et al.</i>	-et alii-	and others

## English abbreviations

s.t.	such that
------	-----------

**INTRODUCTION**

*The work reported in this thesis treats the consensus control of robot networks and the control of teleoperation systems. This chapter introduces some basic definitions of concepts used along the document and it comments on the wide applicability of the consensus in networks of dynamical systems. Furthermore, the thesis objectives are defined and the outline of the thesis is given.*

**1.1 Context and motivation**

The advances in networking and distributed computing over the last decade has motivated a prosperous research activity on distributed *cooperative control* of multi-agent systems. In addition, the cooperative control has also been motivated by the numerous of cooperative behaviors in nature, such as flocking of birds and schooling of fish. The objective in cooperative control problems is to design a distributed control strategy using only local information so that the multi-agent system achieves specified behaviors.

A basic behavior in cooperative control is the *consensus*. Given a multi-agent system it is said that the agents reach a consensus if the state of each agent converges to a common state. The solution to the consensus problems involves the design of control algorithms such that the agents can reach such agreement on their states. There are two main problems that are studied in consensus, the *leader-follower consensus* and the *leaderless consensus*. In the leader-follower consensus problem, there exists a leader that specifies the state for the whole group while in

a leaderless consensus problem, there is not an specified reference state. Necessarily, consensus algorithms are designed to be distributed, assuming only neighbor-to-neighbor interaction between agents.

Examples of cooperative tasks in which consensus algorithms are employed include *formation control*, *flocking theory*, *rendezvous problems* and *synchronization*. These cooperative tasks have a lot of possible applications, some of them are: transportation systems (intelligent highways, air-traffic control); military systems (formation flight, surveillance, reconnaissance, cooperative attack and rendezvous) and mobile sensor networks (space-based interferometers, environmental sampling).

The *operational space* control plays a major role in cooperative tasks performed by multi-robot systems, primarily if the robots are kinematically and dynamically dissimilar (heterogeneous). The operational space (also known as *task space*) is a subspace of the Special Euclidean space of dimension three, denoted  $SE(3)$ . It is well-known that the minimum number of coordinates required to define the pose (position and orientation) of an object in a three-dimensional space are six: three for the position and three for the orientation (attitude). The drawback of the minimal orientation representations (e.g., the Euler angles) is that they exhibit singularities. The *unit-quaternions* are an alternative non-minimal representation of orientation that have the key property to render a singularity-free representation which is the main motivation behind its use.

The *robot networks* are interconnected multi-robots systems. Their interconnection can be modeled using graph theory, as can be seen in the examples of Figure 1.1 where each robot is represented by a node and the information flow between robots is represented by an edge. This information flow can have constant or variable *time-delays* (time lag between when the information is sent and when it is received), which hinders the consensus among the robots. The practical applications of robot networks span different areas such as underwater and space exploration (underwater cultural heritage recovery, coordination of clusters of satellites, synchronization of spacecrafts), hazardous environments (search and rescue missions, military operations), service robotics (commercial cleaning) and in production processes, such as automotive manufacturing, where high flexibility, manipulability, and maneuverability cannot be achieved by a single robot.

A *teleoperation system* can be seen as a particular case of a robot network, since it is a type of network composed of two interconnected robots that interact with human and environmental forces. A bilateral teleoperation system enables a human operator to feel, through the local manipulator, the interaction of the remote manipulator with the environment<sup>1</sup>. Figure 1.2 (left)

---

<sup>1</sup>In this thesis control algorithms for bilateral teleoperation systems are derived and designed, thus in the rest of the present work, teleoperation system stands for bilateral teleoperation system.



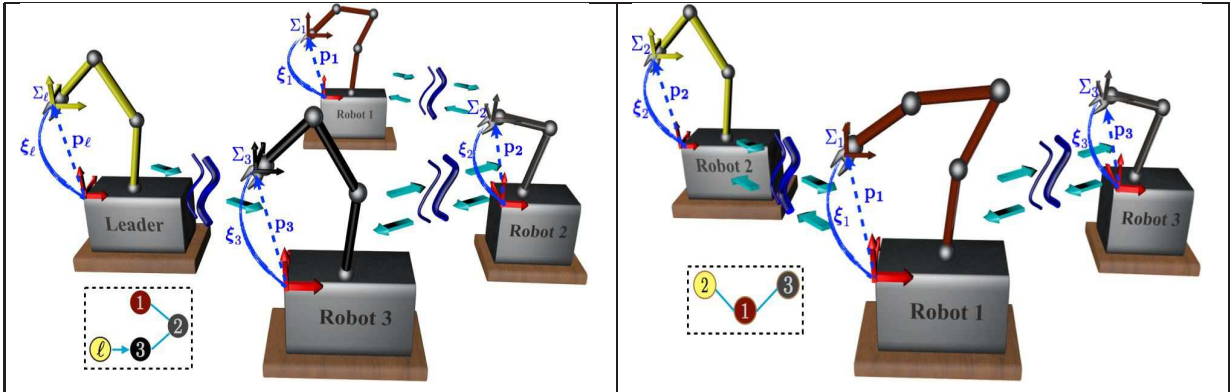


Figure 1.1: Examples of robot networks: (left) robot network with one leader and three followers; (right) robot network composed of three robots without a leader.

shows the five elements that compose a single local robot and single remote robot (SL-SR) teleoperation system: the human operator, the local robot, the communication channel, the remote robot and the environment. There are certain tasks that a single remote manipulator cannot perform well, like handling large and heavy objects and assembly and mating of mechanical parts, amongst others. In these cases, a cooperative strategy with two or more manipulators at the remote site becomes necessary, and the corresponding teleoperation system is called cooperative teleoperation system (CTS). Figure 1.2 (right) shows an example of CTS.

The leader-follower and leaderless consensus problems for first and second-order linear systems have been widely studied and, in general, the stability of the proposed control algorithms is analyzed by examining the eigenvalues of the closed-loop system matrix with the help of the algebraic graph theory, but this linear control or the one based in a linearization approximation are not guaranteed to work with a nonlinear system undergoing large dynamic changes as it is the case of robot manipulators. This fact motivates the design of appropriate control schemes that solve both consensus problems for heterogeneous robot networks. Furthermore, it should be underscored that most of the consensus algorithms only work with the position or orientation but not with both. This has an extra challenge from the fact that the angular velocity cannot be integrated to an equivalent orientation variable.

Moreover, most of the previous consensus controllers require velocity measurements. However, in general, velocity sensors are noisy and costly, and for this reason most of the robots do not have these sensors. This motivates the design of consensus and teleoperation algorithms that do not require velocity measurements. Another challenging condition are the variable time-delays that might appear in the communication channels of the interconnected robots, which affects the performance and the stability of the system, encouraging the design of control al-

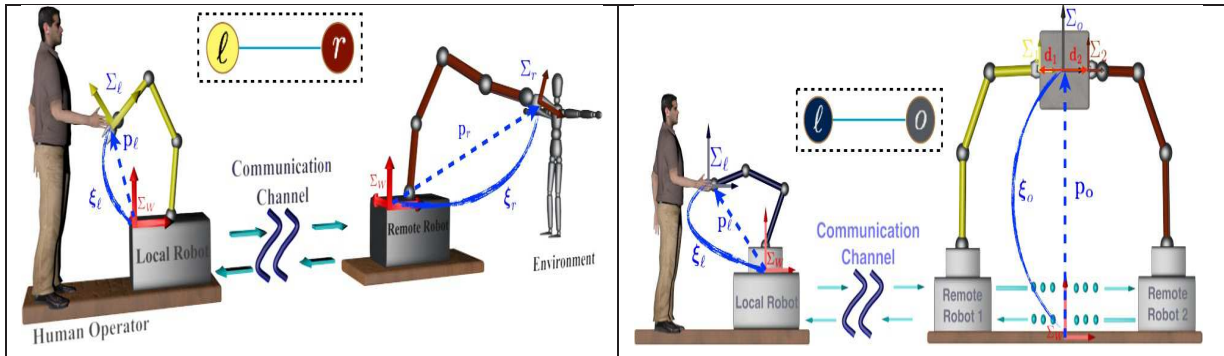


Figure 1.2: Configurations of teleoperation systems: (left) single local and single remote (SL-SR) configuration; (right) a cooperative teleoperation system with a single local robot and, at the remote site, a cooperative system composed of two robots handling an object.

gorithms robust to these communication conditions. It is also of interest the design of control schemes for networks composed of robots with uncertain dynamic and kinematic parameters, because, generally these parameters cannot be used in the control algorithms. Regarding the interconnection, the motivation is to look for the minimum possible number of interconnection among the agents of the network in order to fortify the distributed characteristic of the proposed consensus algorithms.

The derivation of control algorithms for teleoperation systems from the designed consensus algorithms confirms the idea that teleoperation systems are a particular case of robot networks. Finally, the capacity of the CTS motivates the design of control algorithms that make it simple for a human operator to teleoperate an object handled by a cooperative system at a remote site.

## 1.2 Objectives

According to the motivation stated in the last section and the literature review conclusions presented in Section 2.5, this thesis focuses on the design of control schemes that give solutions to the consensus problems of robot networks under different conditions, such as: without velocity measurements, variable time delays in the communication channels and parametric uncertainties. A common pose or a pose determined by a leader is defined as the consensus objective. Moreover, control algorithms for SL-SR teleoperation systems and CTS have to be derived from the proposed consensus algorithms. Then the main objectives are the following:

1. Design of control schemes that solve two different consensus problems in networks of heterogeneous robots (Figure 1.1). These two problems are: the leader-follower consensus problem (LFCP), where the objective is to ensure that all robot manipulators converge to a leader pose, and the leaderless consensus problem (LCP), where, in the absence of a leader, the robot manipulators have to reach an agreement pose (consensus point).
2. Design of control algorithms for teleoperation systems composed of heterogeneous robots that ensures that the pose errors, between the local robot and the remote robot, converge to zero.
3. Design of control algorithms for cooperative teleoperation systems that ensure that the pose errors, between the local robot and the object handled by the cooperative system, converge to zero.
4. Robustness of the designed controllers in front of time-delays, uncertain kinematic and dynamic parameters, orientation singularities and lack of velocity measurements.
5. Validation of the designed control algorithms with simulations and experiments.

### 1.3 Outline of the thesis

The presented work is organized in six chapters and two appendices. A brief description of their content is the following:

- **Chapter 1** describes the motivation and objectives of the present work and gives an insight of the basic concepts used along the document.
- **Chapter 2** discusses the state of the art in cooperative control, consensus and teleoperation control algorithms.
- **Chapter 3** details the kinematics and the dynamics of the robot manipulators and the network interconnection model. Besides, the dynamic model of two configurations of teleoperation systems are derived.
- **Chapter 4** proposes control schemes for the consensus of robot networks under several conditions such as time-delays, no velocity measurements and parametric uncertainty. Simulations and experimental results of the proposed algorithms are presented.
- **Chapter 5** presents control algorithms derived for SL-SR teleoperation systems and for CTS. Simulation and experimental results are also presented.

- **Chapter 6** summarizes the contributions of this work, states some concluding remarks and lists the publications derived from this work.
- **Appendix A** presents an overview of the mathematical and stability concepts used in the models derivation and controllers design.
- **Appendix B** details the kinematics and dynamics of the robots used in the simulations and the communication library developed and used in the experimental validation.

**STATE OF THE ART**

*This chapter outlines some of the most important works found in the consensus literature, which are grouped according to the agent's dynamics. The first section collects the consensus works for networks with linear dynamics agents and the second one those that consider nonlinear dynamics agents. These last are the most related to the consensus control algorithms proposed in this thesis. Two more sections are dedicated to review some interesting works in teleoperation systems. At the end of the chapter, a summary and a list of open problems are given as a result of this literature review.*

In recent years, cooperative control of multiple agent systems has received significant attention. It has been motivated by the scientific interest in cooperative behavior in nature, such as flocking of birds with coordinated wing strokes, coordinated movements by gregarious animals, social synchronization in ant colonies and beehives, coordinated light-twinkling in firefly swarms and formation of complex structures by cells in multicellular organisms (Camazine 2003; Murata and Kurokawa 2012). The objective in cooperative control is to design a distributed control strategy using only local information so that the aggregate system achieves specified behaviors, such as flocking (Lee and Spong 2007; Gu and Wang 2009), synchronization (Rodriguez-Angeles and Nijmeijer 2004; Scardovi and Sepulchre 2009; Abdessameud, Tayebi, and Polushin 2012; Hatanaka, Igarashi, Fujita, and Spong 2012), coordination (Wang and Xie 2012; Qin, Zheng, and Gao 2012), rendezvous and formation control. A fundamental approach to achieve cooperative control is *consensus*. The basic idea for consensus is that each agent updates its

control input based on the information states of its local neighbors in such a way that the final states of all agents converge to a common value. In the past decade, a tremendous amount of interesting results have been addressed for consensus problems in different formulations adapted to different types of agent dynamics and different kind of tasks. Next some of these works are commented.

## 2.1 Consensus in networked linear dynamics agents

The study of the consensus for networked dynamic systems appeared in (Jadbabaie, Lin, and Morse 2003). In this work, the authors use tools from the algebraic graph theory in order to give a theoretical explanation of the consensus behavior observed in particles systems reported in the work of Vicsek, Czirók, Ben-Jacob, Cohen, and Shochet (1995). Later, the theoretical framework for posing and solving consensus problems for a network of agents with single-integrator dynamics under a fixed or a time-varying (switching) topology and communication time-delays is introduced in (Olfati-Saber and Murray 2004) based on the work of Fax and Murray (2004). In (Ren and Beard 2005) the results of Olfati-Saber and Murray are extended to the case of directed graphs, and the authors prove that consensus in multi-agent systems with single-integrator dynamics can be achieved if and only if the switching network topology contains a directed spanning tree frequently enough as the network evolves over time. Moreover, in these last two papers (Olfati-Saber and Murray 2004; Ren and Beard 2005) the useful relation between the graph structure and eigenvalues of the associated Laplacian matrix is further analyzed. In (Moreau 2005) a set-valued Lyapunov approach to address the consensus problem with unidirectional time-dependent communication links is proposed. The aforementioned papers can be considered the key works that paved the way to recent advances in the consensus of networked systems.

Two interesting problems are studied in consensus, the *leaderless consensus problem*, in which there does not exist a leader in the network, and the *leader-follower consensus problem*, in which there exists a leader that specifies a desired state for the network's agents. In the last decade, researchers have studied both consensus problems under a variety of assumptions on the network topology (fixed or switching), presence or lack of communication delays, and directed or undirected network information flow. All these assumptions are reviewed in the remarkable survey papers (Olfati-Saber, Fax, and Murray 2007), (Ren, Beard, and Atkins 2007) and (Murray 2007), furthermore, these surveys provide a summary of the most interesting works about consensus to that date. It has to be noted that most of the works referenced in those surveys focus on agents with *first order* or *second order* dynamics *i.e.*, networks in which the dynamics

of the agents is represented by a simple integrator  $\dot{x} = u$  or has the form:  $\dot{x} = v, \dot{v} = u$  (most of the time, for mechanical systems,  $x$  and  $v$  are the position and the velocity, respectively, of each agent, and  $u$  is the input).

Recent works of consensus for first order dynamic systems extend the previous results or consider more general settings. For example, (Ren 2010a) proposes a consensus tracking algorithm explicitly accounting for bounded control effort under a directed fixed interaction topology; (Sun 2012) employs a linear matrix inequality (LMI) method to deal with the average consensus problem for directed networks with uncertain topologies as well as time-varying delays; (Terelius, Shi, and Johansson 2013) studies the consensus control for a multi-agent system with a faulty node; (Hu, Yu, Zhang, and Song 2013) investigates a group consensus problem with discontinuous information transmissions among different groups of dynamic agents.

The study of second-order consensus protocols has helped the researchers to introduce more complicated dynamics into the model of each individual agent within the general framework of multi-agent systems. It has been found that, in contrast to the first-order consensus problem, second-order consensus may fail to be achieved in many cases even if the network topology contains a directed spanning tree (Ren and Beard 2005). In (Ren and Atkins 2007) and (Ren 2008) sufficient conditions have been derived for reaching second-order consensus and some existing results are extended. Recent consensus algorithms for second-order dynamics systems are presented in (Hu and Lin 2010; Meng, Ren, Cao, and You 2011; Abdessameud and Tayebi 2011a; Qin, Zheng, and Gao 2011; Wen, Duan, Yu, and Chen 2012; Feng, Xu, Lewis, and Zhang 2013), to name a few.

The consensus control of multi-agent systems with general linear dynamics, *i.e.* networks in which the dynamics of each agent is a  $n$ -th order linear system, results more interesting in both the theory and the practice. For example, (Ni and Cheng 2010) proposes a leader-follower consensus algorithm for both fixed and switching interaction based on Riccati and Lyapunov inequalities; (Su and Huang 2012a; Su and Huang 2012c) study the leader-follower consensus problem using distributed observers for fixed and switching topologies; (Su and Huang 2012b) proposes solutions to the leaderless and the leader-follower consensus problems for general marginally stable linear multi-agent systems under switching network topology; (Wen, Li, Duan, and Chen 2013) addresses the leaderless consensus problem with discontinuous observations over a time-invariant undirected communication topology. A class of distributed observer-type protocols are designed and employed to achieve consensus; (Li, Duan, and Lewis 2014) proposes an adaptive consensus protocol to solve the leaderless and leader-follower consensus problems for the case where the communication graph is undirected and connected, and the multi-agent system is subject to different matching uncertainties.

The extensions of the linear consensus algorithms reviewed in this section to the case of nonlinear dynamic agents is not straightforward, and in the available literature there exist few papers (compared with the number of which study the consensus of linear agents) dealing with this problem.

## 2.2 Consensus in networked nonlinear dynamic agents

This dissertation studies the consensus problems for robot networks, where the considered robots are full actuated robots modeled by Euler-Lagrange equations, which are second order non-linear differential equations, but these equations can also be used to represent fully-actuated autonomous vehicles and spacecrafts. Therefore, consensus algorithms for Euler–Lagrange networked systems are specially reviewed in this section. Solutions to the consensus for a general class ( $n$ -th order) of nonlinear systems can be found in (Chopra and Spong 2005; Arcak 2007; Yu, Chen, Cao, and Kurths 2010; De Persis and Jayawardhana 2012; Hu, Su, and Lam 2013; Yu, Ren, Zheng, Chen, and Lü 2013).

The study of the consensus problems for Euler-Lagrange systems is frequently done in the generalized coordinates space, that is, in the case of robot manipulators, in the *joint space* (Rodriguez-Angeles and Nijmeijer 2004; Ren 2009; Chung and Slotine 2009; Nuño, Ortega, Basañez, and Hill 2011; Meng, Ren, Cao, and You 2011; Mei, Ren, and Ma 2011; Nuño, Sarras, Panteley, and Basañez 2012; Secchi, Sabattini, and Fantuzzi 2013). The works (Rodriguez-Angeles and Nijmeijer 2004) and (Nuño et al. 2011) present solutions to the leader-follower case, provided that the leader position is available to all the followers. In the first one, the case that only position measurements are available is studied and a set of nonlinear observers and a feedback controller are proposed. In the second paper, constant time-delays are considered and an adaptive controller is proposed. In (Nuño et al. 2012) and (Nuño et al. 2013) a solution to the leaderless case using simple proportional plus damping (P+d) controllers is reported. The work (Mei et al. 2011) proposes a sliding-based scheme for the leader-follower case assuming that the leader position and velocity are available only to a certain set of followers. (Ren 2009) discusses a proportional controller and a velocity estimator to solve the leaderless consensus problem. The work (Secchi et al. 2013) proposes a decentralized control strategy that preserves the connectivity of the communication graph of multi-agent systems. The proposed controller is robust with respect to possible data corruption in the exchange of information between the agents. (Chung and Slotine 2009) analyzes the concurrent synchronization of multiple Euler-Lagrange systems in the joint space provided that the leader trajectory is available to all the followers, the time-delays are identical and constant, the complete exact dynamics are known



and the Euler-Lagrange systems are identical. The use of adaptive controllers in (Chung and Slotine 2009) is only restricted to the leader-follower consensus problem and for the undelayed case.

The consensus problem defined in the operational space offers the capability of working with robot manipulators that are not kinematically similar (heterogeneous), and facilitates the common task definition. The term pose is employed to represent both the position and the orientation (attitude) of the robot's end-effector in the operational space. Minimal representations of the orientation are defined with three parameters, e.g., the Euler angles. In spite of their popularity, Euler angles suffer the drawbacks of representation singularities and inconsistency with the task geometry. The unit-quaternions have the key property that can render a singularity-free representation and they have been widely used in different robotics applications, see for example (Yuan 1988; Wen and Kreutz-Delgado 1991; Fjellstad 1994; Caccavale, Chiacchio, and Chiaverini 2000). An interesting survey on the use of the unit-quaternions for robot control, with a clear demonstration of their advantages over the Euler angles, is reported in (Caccavale, Siciliano, and Villani 1999).

There are several interesting papers of consensus control of multi-robot systems in the operational space but most of them only address the orientation part. Among these are the following: (Sarlette, Sepulchre, and Leonard 2009) uses an energy shaping approach to propose control laws to synchronize attitudes in a swarm of fully actuated rigid bodies; (Igarashi, Hatanaka, Fujita, and Spong 2009) develops a passivity-based velocity input law in order to achieve attitude synchronization. (Abdessameud and Tayebi 2009) proposes a synchronization control scheme, that allows the team members to align their attitudes without velocity measurements; (Ren 2007) uses unit-quaternions and full-state feedback controllers to solve both consensus problems, provided that the leader orientation is available to all the followers. Assuming complete knowledge of the system dynamics and employing the -possibly singular- modified Rodriguez parameters, Ren (2010b) presents the solution to both consensus problems. For the leaderless case, the controller does not require velocity measurements; however, for the leader-follower case, a full-state feedback scheme is needed. Abdessameud, Tayebi, and Polushin (2012) solve also both consensus problems by using a *virtual* system for each agent in the network without velocity measurements, provided that the agents physical parameters are all exactly known. Similarly, defining an auxiliary agent system, Abdessameud and Tayebi (2011b) deal with the solution to the leaderless consensus problem only under the assumption that all physical parameters are known.

Some few exceptions dealing with the complete pose are presented in the following works: (Chung, Ahsun, and Slotine 2009) proposes a decentralized translational tracking control law

based on oscillator phase synchronization, enabling coupled translational and rotational maneuvers of spacecrafts, but the proposed control laws require the knowledge of the dynamic models and time-delays are not considered; (Liu and Chopra 2012) discusses an adaptive control algorithm that use a minimal orientation representation to solve the leader-follower consensus problem; (Hatanaka, Igarashi, Fujita, and Spong 2012) presents solutions to the leaderless and leader-follower consensus problems based on the fact that the kinematics of a rigid body in the  $SE(3)$  has a passivity-like property; (Wang, Yu, and Lin 2012) provides a dual quaternion solution for the coordination of the pose of rigid bodies' networks. The last two works obviate the second order dynamical model and they only deal with the kinematical model. Using similar kinematic and dynamic adaptation schemes as (Cheah, Liu, and Slotine 2006; Gu and Wang 2009), Wang (2013a) solves the leader-follower consensus provided that the leader position is available to *all* the agents and, in (Wang 2013b) also solves the leaderless consensus problem without time-delays. These works make use of a minimal representation that exhibits singularities and it is assumed that all the agents are kinematically similar, i.e., all agents have the same degrees-of-freedom.

## 2.3 Teleoperation systems

Teleoperation systems have a large area of application in special for the work in hazardous workspaces such as nuclear plants (Launay 1998; Qian et al. 2012; Okura et al. 2013), outer space missions (Vertut and Coiffet 1985; Ge et al. 2014), surgery (Preusche et al. 2002; Seung et al. 2009), mining (Hainsworth 2001), etc.

According to the information flow direction, the teleoperation may be unilateral or bilateral. In unilateral teleoperation, the local manipulator sends position or force data to the remote and only receives, as feedback, visual information from the remote scene. But in bilateral teleoperation, position or force data are also sent from the remote robot in addition to the visual information. This allows to operators to feel, through the local manipulator, the interaction of the remote manipulator with the environment. A classification of the bilateral teleoperation works reported in the literature can be done according to the type of information interchanged between the local and remote manipulator. This include: position-position (Artigas et al. 2010; Lau and Wai 2005), position-force (Willaert et al. 2009), force-position (Le et al. 2011b) and force-force (Rubio et al. 2000; Le et al. 2011a).

The design of a controller for a teleoperation system involves a trade-off between stability and transparency (Lawrence 1993). Transparency is the property that describes how well the motion/forces of the remote environment are transmitted to the human operator and vice-versa.

The stability is the basic and minimum requirement that guarantees that the teleoperation system works. In this thesis the proposed controllers prioritize the stability over transparency. In the literature there are interesting works in which the transparency is established as priority such as (Sirouspour and Shahdi 2006; Polushin, Liu, and Lung 2007; Azorin, Aracil, Perez, Garcia, and Sabater 2008; Ahn and Ryu 2008; Aracil, Azorin, Ferre, and Peña 2013).

The communication channel generates a variety of constraints that degrade the teleoperation system performance, and also may cause instability. These include time delays, data loss, quantization errors, data packet dropouts, etc. The outstanding works (Anderson and Spong 1989) and (Niemeyer and Slotine 1991) propose, for teleoperation systems with constant time-delays, controllers based on the use of scattering and wave variable together with passivity concepts, respectively. (Nuño, Ortega, and Basañez 2010) proposes an adaptive controller to solve the constant time-delay problem that does not rely on the scattering transformation. An insightful historical survey that analyzes communication delays and other challenging conditions in teleoperation systems can be consulted in (Hokayem and Spong 2006) and a tutorial of passivity-based controllers which guarantee stability for teleoperation systems with constant and variable time-delays is given in (Nuño, Basañez, and Ortega 2011).

Most of the teleoperation schemes proposed in the literature require the knowledge of velocity measurements in their control laws (Anderson and Spong 1989; Niemeyer and Slotine 1991; Stramigioli et al. 2002; Chopra et al. 2006; Nuño et al. 2010). Few remarkable exceptions are (Garcia-Valdovinos, Parra-Vega, and Arteaga 2007) where a model dependent sliding scheme is used to control a linearized version of the local and remote manipulators; (Hua and Liu 2011) where the boundedness of the position error is proved using a high gain velocity observer; and (Nuño, Basañez, Obregon-Pulido, and Solis-Perales 2011) where a controller capable of achieving synchronization of local and remote velocities and ensuring position error convergence to zero with only position measurements is proposed.

All the previously mentioned works develop the control algorithms in the joint space. Similar as in the consensus problem, the interest in designing control laws in the operational space becomes evident when the teleoperation system is composed of robot manipulators that are kinematically dissimilar or when an object is teleoperated through a cooperative system, as will be commented in the next section. In spite of these interesting situations, there are few works in the literature that propose controllers for teleoperation systems in the operational space. (Wang and Xie 2012) proposes a control scheme robust to time-delays that achieve pose synchronization between the local and the remote robot manipulators; (Ge, Zhang, Wang, and Li 2014) adds an adaptive regulator in the typical P+d controller to compensate for the unknown gravity signal, obtaining a control algorithm robust to time-delays in the communication but us-

ing a minimal orientation representation; (Liu and Chopra 2013) proposes a semi-autonomous control framework to enable task space tracking, and besides, they use the redundancy of the slave robot to achieve several sub-tasks, such as singularity avoidance, joint limits, and collision avoidance; (Liu, Tao, and Tavakoli 2014) proposes a nonlinear adaptive controller for a teleoperation system with kinematic and dynamic uncertainties. The last two works do not consider time-delays in the communications and in the same way as most of the papers that work in the operational space, they use a minimal representation for the orientation.

## 2.4 Cooperative teleoperation systems

A cooperative strategy with two or more robot manipulators becomes necessary to perform the tasks that cannot be executed by a single manipulator. Typical cooperation examples include tasks such as handling large and heavy rigid and non-rigid objects, assembly and mating of mechanical parts and space robotics applications (Xi et al. 1996; Rodriguez-Angeles and Nijmeijer 2004; Torres et al. 2009).

In spite of the potential benefits achievable with multiple robot manipulators, the analysis and control problem become more complex due to the kinematic and the dynamic interactions imposed by the cooperation. This means that, in all those tasks requiring effective cooperation, one cannot extend the well-known results for the kinematics, dynamics, and control of a single arm. A global description of the kinematic and dynamic relationship for the multi-robot cooperative system is needed (Caccavale, Chiacchio, and Chiaverini 1999). Two main approaches have been proposed for this global description: a force decomposition of the cooperative system using “virtual sticks” (Uchiyama, Iwasawa, and Hakomori 1987) and a geometrically clear parametrization of the internal forces/moments acting on the grasped object (Williams and Khatib 1993).

As mentioned in (Uchiyama 1998), the cooperative system control problem has begun to be studied since the early 1970's, not late after the emergence of robotics technologies. Since then, different control techniques have been proposed for the control of cooperative systems, such as hybrid position/force control (Nakamura et al. 1987; Uchiyama and Dauchez 1993; Dauchez et al. 1992), feedback linearization control (Wen and Delgado 1992; Hsu 1993; Khatib 1995), joint-space control (Luecke and Lai 1997; Caccavale, Chiacchio, and Chiaverini 1999), adaptive approaches to force/motion control (Ahmad and Zribi 1993; Sun and Mills 2002; Uzmay, Burkan, and Sarikaya 2004) and as impedance control schemes (Bonitz and Hsia 1996; Moosavian and Mostafavi 2006; Caccavale et al. 2008).

Few proposals can be found in the literature about the teleoperation of multiple robot manip-

ulators. Some inspiring exceptions include (Lee and Spong 2005), where a formation of multiple manipulators is teleoperated by a single local manipulator using passive decomposition, and separating the teleoperation system into two decoupled systems: the shape system describing the cooperative grasping aspect, and the locked system representing the overall behavior of the multiple slaves, their control scheme being robust to constant time-delays and designed in the joint space; (Sirouspour 2005), where multiple local manipulators command multiple remote manipulators and each local one is coupled to one of the remote robots, the proposed control scheme uses linearized dynamics of the elements of the teleoperation system and no time-delays are considered; (Rodriguez-Seda et al. 2010) where is designed a PD controller to enforce motion tracking and formation control of master and slave vehicles under constant time-delays; (Malysz and Sirouspour 2011) where a Lyapunov-based adaptive control approach for two types of asymmetrical teleoperation systems is proposed, the first one is composed of two local manipulators and one redundant remote robot and the second is composed of one local robot and one remote robot with less DoF than the local, and the proposed control scheme does not consider time-delays; (Franchi et al. 2012) proposes a controller based on passivity for the teleoperation of a team of heterogeneous robots. The proposed control scheme allows that the remote team modifies the shape of the formation and the communication topology. Finally, (Polushin et al. 2013) proposes a control framework based on the small-gain arguments for teleoperation systems composed of multiple SL-SR pairs that interact through an environment.

This document only considers cooperative teleoperation systems composed of a single local robot and multiple cooperative remote robots, and the other configurations of asymmetrical teleoperation systems are not investigated.

## 2.5 Summary and open problems

After a review of the literature in consensus and in teleoperation, the following conclusions are derived:

- The consensus problem has attracted a great deal of attention in many fields such as physics, biology, robotics and engineering. Many existing applications, such as formation control, synchronization, coordination, flocking, and rendezvous, can be analyzed departing from the basic framework of consensus building.
- Most existing works in consensus control of multi-agent systems focus on linear systems with first-order or second-order dynamics, and in the consensus of agents with nonlinear dynamics there are few works. One reason might be the difficulty of extending the re-

sults for linear systems using the classical methods like feedback linearization because the existence of parametric uncertainties in the models.

- Most available consensus algorithms for double-integrator dynamics assume that full state information is available for feedback and therefore are generally not applicable in the case where the velocity information (second part of the state) is not available. This problem becomes relevant when the network agents are not equipped with velocity sensors, to save cost, weight and volume, or velocity is not precisely measured. Some works are proposed to treat with this problem but they require the full knowledge of the agents dynamics.
- The proposed consensus algorithms for networked robotic systems with uncertainties in both kinematics and dynamics use a minimal orientation representation and do not consider variable time-delays in the communications.
- The consensus algorithms proposed in the joint space can be used only in networks composed of robots with the same degrees of freedom (not heterogeneous).
- Teleoperation systems allows the execution of different tasks in remote environments including possibly dangerous and harmful jobs for the human operator. The teleoperation can be unilateral or bilateral. The bilateral teleoperation systems provide operators with a sense of presence in the remote environment.
- There are two major issues in bilateral teleoperation: stability and transparency. Stability guarantees that the teleoperation systems works and transparency is how well the system works.
- Cooperative robot systems can perform tasks that for a single robot are impossible. These systems have increased dexterity, improved handling capabilities, increased loading capacity, and enhanced robustness due to redundancy. Surprisingly, cooperative teleoperation has received little attention in the past even though it is the result of combining two traditional areas of robotics (teleoperation and cooperative manipulation).
- Few consensus works and teleoperation algorithms deal with the complete pose of the robots, and those that consider it, have one or more of the following characteristics:
  - Use of a minimal orientation representation.
  - Consider only the kinematics model of the agents.
  - Require the complete knowledge of the agents dynamics.
  - Time-delays are not considered.

*This chapter presents the complete dynamical description of a robot network. This description contains two basic elements: i) the dynamics of the nodes and; ii) the interconnection of the nodes. In this document it is considered that each node contains a fully-actuated, revolute joints robot manipulator. A description of this robot is given in the first section of the chapter together with the definition of the robot's pose (position and orientation). The nonlinear dynamic model in the operational space is derived from the joint space model. In the second section, the interconnection of the robots in the network is modeled using concepts of graph theory. Besides, general assumptions about the interconnection and the delays in the communication channels are defined. Finally, the operational space dynamic models of a SL-SR teleoperation system and a CTS are derived.*

### **3.1 Robot manipulators**

Serial robot manipulators are mechanical structures composed of a sequence of rigid bodies (links) interconnected by *prismatic* or *revolute joints*, required to provide a desired motion to the manipulator's end-effector. Usually each prismatic or revolute joint provides the structure with a single *degree of freedom*. A prismatic joint creates a relative translational motion between two links, whereas a revolute joint creates a relative rotational motion between them. In Figure 3.1(a) it is shown a 6-DoF with its 6 revolute joint axes. In general, each degree of freedom

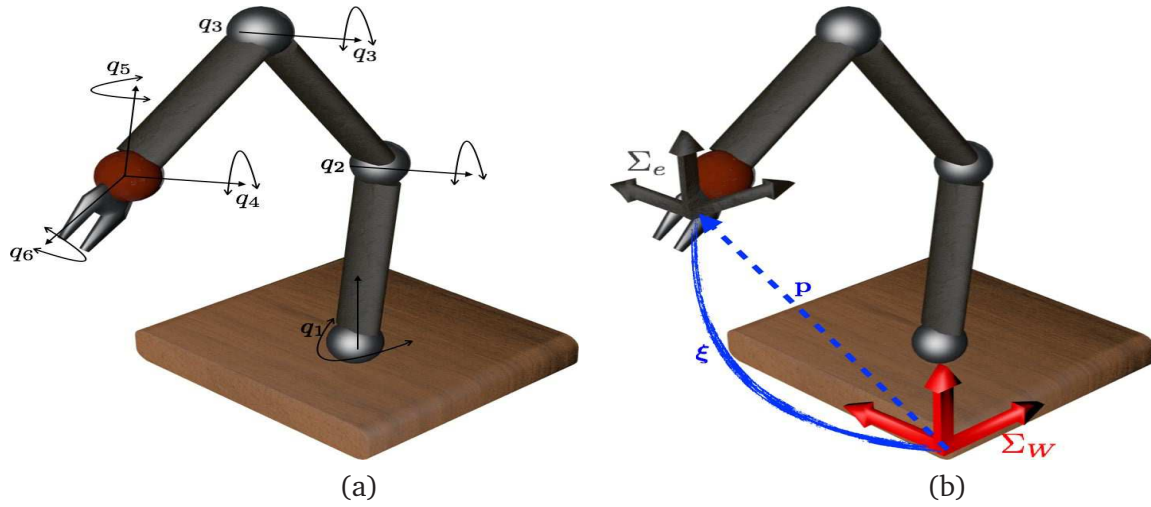


Figure 3.1: (a) 6-DoF robot manipulator and its joint axes; (b) pose and Cartesian coordinates frames of a robot manipulator.

is typically associated with a joint axis and constitutes a *joint variable*  $q_k$  ( $k=1,2,3,\dots, n$ ). These variables are commonly called the *generalized coordinates*. It is common to use the generalized coordinates vector,  $\mathbf{q} := [q_1, q_2, \dots, q_n]^T \in \mathbb{R}^n$ , to define the robot configuration.

The robot manipulators are machines designed to execute one or more tasks, with speed and precision. It is more intuitive and natural, from a robot user point of view, to describe a robotic task by specifying the pose of the robot's end-effector. The term *pose* is employed to represent both the position and the orientation (attitude) of the robot's end-effector with respect to a reference frame. This is normally done by placing a Cartesian coordinates frame at the robot's end-effector ( $\Sigma_e$ ) and compare it with respect to a fixed Cartesian reference frame ( $\Sigma_W$ ). The translational coordinates describe the position of the end-effector frame origin relative to the fixed reference frame origin, whereas the rotational coordinates describe the orientation of the end-effector frame axes relative to the reference frame axes. Figure 3.1(b) shows a graphic representation of the pose of a robot manipulator.

From the aforementioned it can be concluded that the configuration of a robot manipulator can be defined in two ways: in the *joint space*, that denotes the space in which the vector of generalized coordinates ( $\mathbf{q}$ ) is defined or in the *operational space* (also known as *task space*), in which the manipulator task is specified.



### 3.1.1 Representing the orientation

It is well-known that the minimum number of coordinates required to define the pose of an object in a three-dimensional space is six: three for the position and three for the orientation. In the case of the robots end-effector, its position with respect to the fixed reference frame is uniquely represented by the vector  $\mathbf{p} \in \mathbb{R}^3$  that describes the Cartesian coordinates of the end-effector frame origin. For the orientation of the robots end-effector there is not a generalized method to describe it. The minimal orientation representations, which are defined by three parameters, e.g., Euler angles, suffer the drawbacks of representation singularities and inconsistency with the task geometry. The non-minimal parameterizations of orientation use a set of  $3+k$  parameters, related by  $k$  constraints, in order to keep the required three degrees of freedom (Campa and de la Torre 2009). Common examples are the rotation matrices, the axis-angle pair and the unit-quaternions.

#### Rotation matrix

A rotation matrix,  $\mathbf{R}_i^j$ , describes the orientation of the coordinate frame  $\Sigma_i$  relative to the coordinate frame  $\Sigma_j$ . The columns of this  $3 \times 3$  matrix consist of the unit vectors along the axes of frame  $i$ , relative to the reference frame  $j$ . The components of  $\mathbf{R}_i^j$  are the dot products of basis vectors of the two coordinate frames,

$$\mathbf{R}_i^j = \begin{pmatrix} \mathbf{x}_i^j & \mathbf{y}_i^j & \mathbf{z}_i^j \end{pmatrix} = \begin{pmatrix} \mathbf{x}_i \cdot \mathbf{x}_j & \mathbf{y}_i \cdot \mathbf{x}_j & \mathbf{z}_i \cdot \mathbf{x}_j \\ \mathbf{x}_i \cdot \mathbf{y}_j & \mathbf{y}_i \cdot \mathbf{y}_j & \mathbf{z}_i \cdot \mathbf{y}_j \\ \mathbf{x}_i \cdot \mathbf{z}_j & \mathbf{y}_i \cdot \mathbf{z}_j & \mathbf{z}_i \cdot \mathbf{z}_j \end{pmatrix}. \quad (3.1)$$

Because the basis vectors are unit vectors and the dot product of any two unit vectors is the cosine of the angle between them, the components are commonly referred to as direction cosines.

It is worth noting that the column vectors of matrix  $\mathbf{R}_i^j$  are mutually orthogonal since they represent the unit vectors of an orthonormal frame, i.e.  $\mathbf{x}_i^j \cdot \mathbf{y}_i^j = 0$ ,  $\mathbf{z}_i^j \cdot \mathbf{x}_i^j = 0$  and  $\mathbf{y}_i^j \cdot \mathbf{z}_i^j = 0$ . Also, they have unit norm:  $\mathbf{x}_i^j \cdot \mathbf{x}_i^j = 1$ ,  $\mathbf{y}_i^j \cdot \mathbf{y}_i^j = 1$  and  $\mathbf{z}_i^j \cdot \mathbf{z}_i^j = 1$ . As a consequence,  $\mathbf{R}_i^j$  is an orthogonal matrix meaning that

$$\mathbf{R}_i^j (\mathbf{R}_i^j)^\top = (\mathbf{R}_i^j)^\top \mathbf{R}_i^j = \mathbf{I}_3. \quad (3.2)$$

From this last it follows that

$$\det(\mathbf{R}_i^j) = \pm 1. \quad (3.3)$$

$\det(\mathbf{R}_i^j) = 1$  when the coordinate frames are right-handed, while  $\det(\mathbf{R}_i^j) = -1$  if the frames are left-handed. The set of all  $3 \times 3$  matrices which satisfy (3.2) and the positive case of (3.3) is denoted  $SO(3)$  ( $SO$  abbreviates *special orthogonal*). More generally, the space of rotation matrices in  $\mathbb{R}^{m \times m}$  is defined by

$$SO(m) = \{\mathbf{R} \in \mathbb{R}^{m \times m} : \mathbf{R}\mathbf{R}^\top = \mathbf{I}_m, \det(\mathbf{R}) = +1\}. \quad (3.4)$$

In the case of spatial rotations  $m = 3$ , whereas in the case of planar rotations  $m = 2$ . Also from the property (3.2), the following interesting result is obtained

$$(\mathbf{R}_i^j)^\top = (\mathbf{R}_i^j)^{-1}. \quad (3.5)$$

Rotation matrices can be combined through simple matrix multiplication such that the orientation of frame  $i$  relative to frame  $k$  can be expressed as

$$\mathbf{R}_i^k = \mathbf{R}_j^k \mathbf{R}_i^j. \quad (3.6)$$

Besides, a rotation matrix serves as a transformation, taking coordinates of a point from one frame to another

$$\mathbf{p}^j = \mathbf{R}_i^j \mathbf{p}^i, \quad (3.7)$$

and it can be also interpreted as the matrix operator allowing rotation of a vector by a given angle  $\theta$  about an arbitrary axis

$$\mathbf{p} = \mathbf{R}_{(\cdot)}(\theta) \mathbf{p}', \quad (3.8)$$

where  $(\cdot)$  can be any axis of rotation ( $x, y, z$ ). The rotation matrices that represent the rotation of a frame by an angle  $\theta$  about the  $(\cdot)$ -axis are:

$$\mathbf{R}_x(\theta) = \begin{pmatrix} 1 & 0 & 0 \\ 0 & \cos \theta & -\sin \theta \\ 0 & \sin \theta & \cos \theta \end{pmatrix} \quad \mathbf{R}_y(\theta) = \begin{pmatrix} \cos \theta & 0 & \sin \theta \\ 0 & 1 & 0 \\ -\sin \theta & 0 & \cos \theta \end{pmatrix} \quad \mathbf{R}_z(\theta) = \begin{pmatrix} \cos \theta & -\sin \theta & 0 \\ \sin \theta & \cos \theta & 0 \\ 0 & 0 & 1 \end{pmatrix} \quad (3.9)$$

Rotation about the  $x$ -axis

Rotation about the  $y$ -axis

Rotation about the  $z$ -axis

Rotation matrix summary:

- The rotation matrix describes the mutual orientation between two coordinate frames; its column vectors are the direction cosines of the axes of the rotated frame with respect to the original frame.

- The column vectors of the rotation matrix are mutually orthogonal and have unit norm.
- A rotation matrix is a non-minimal representation of a rigid body's orientation. That is, it uses nine elements to represent an orientation instead of just three. The nine elements are not independent but related by six constraints due to the orthogonality and unit norm conditions, hence, only three of them are independent.
- The rotation matrix represents the transformation of a point coordinates expressed in two different frames with common origin.
- The rotation matrix can be used as an operator that allows the rotation of a vector in the same coordinate frame.
- $SO(3) \subset \mathbb{R}^{3 \times 3}$  is a *group* (see Appendix A for group definition) under the operation of matrix multiplication, i.e., the result of the multiplication of two rotation matrices is a rotation matrix.

### Euler angles

A representation of orientation in terms of three independent parameters constitutes a minimal representation, and it can be obtained by three successive rotations performed in a specific sequence. The Euler angles are the 3 angles of rotation  $(\varphi, \vartheta, \psi)$  when each rotation is taken about one axis in the coordinate system at every stage. For the first rotation, any of the 3 axes can be chosen as the axis of revolution, and two successive rotations must have different axes of revolution, so there are only two alternatives for the second and for the third rotations. This means there are  $3 \times 2 \times 2 = 12$  different conventions for the Euler angles (Craig 2005). The most used conventions are the *ZYZ Euler angles* and *ZYX Euler angles* (Roll-Pitch-Yaw).

#### ZYZ Euler angles

Taking the moving frame  $\Sigma_i$  and the fixed frame  $\Sigma_j$  to be initially coincident,  $\varphi$  is the rotation about the  $z$ -axis of  $\Sigma_i$ ,  $\vartheta$  is the rotation about the rotated  $y$ -axis of  $\Sigma_i$ ,  $y'$ , and finally,  $\psi$  is the rotation about the twice rotated  $z$ -axis of  $\Sigma_i$ ,  $z''$ . Then  $\varphi, \vartheta, \psi$  are the ZYZ Euler angles (Figure 3.2). The equivalent rotation matrix can be computed via post-multiplication of the matrices of elementary rotations, using (3.9), it is given by

$$\begin{aligned} \mathbf{R}(\phi) &= \mathbf{R}_z(\varphi)\mathbf{R}_{y'}(\vartheta)\mathbf{R}_{z''}(\psi) \\ &= \begin{pmatrix} c_\varphi c_\vartheta c_\psi - s_\varphi s_\vartheta & -c_\varphi c_\vartheta s_\psi - s_\varphi c_\psi & c_\varphi s_\vartheta \\ s_\varphi c_\vartheta c_\psi + c_\varphi s_\vartheta & -s_\varphi c_\vartheta s_\psi + c_\varphi c_\psi & s_\varphi s_\vartheta \\ -s_\vartheta c_\psi & s_\vartheta s_\psi & c_\vartheta \end{pmatrix}, \end{aligned} \quad (3.10)$$

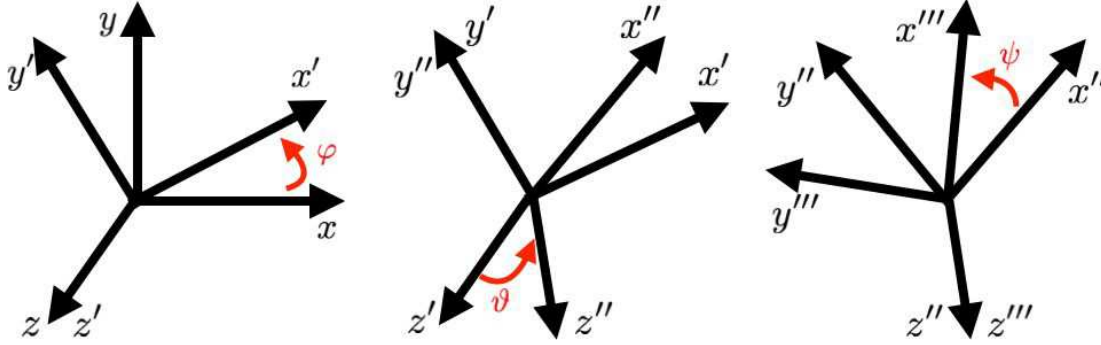


Figure 3.2: Representation of the Euler angles ZYZ convention.

where  $\phi = [\varphi \ \vartheta \ \psi]^T$  and  $c_{(\cdot)} = \cos(\cdot)$  and  $s_{(\cdot)} = \sin(\cdot)$ . The inverse problem, that consists on determining the Euler angles from a given  $\mathbf{R} \in SO(3)$ , can be solved in the following way

$$\begin{aligned}\varphi &= \text{Atan2}(r_{23}, r_{13}), \\ \vartheta &= \text{Atan2}\left(\sqrt{r_{13}^2 + r_{23}^2}, r_{33}\right), \\ \psi &= \text{Atan2}(r_{32}, -r_{31}),\end{aligned}\tag{3.11}$$

where  $r_{ij}$  are the elements of the rotation matrix (3.10) and  $\text{atan2}(y, x)$  computes  $\tan^{-1}(y/x)$  but uses the sign of both  $x$  and  $y$  to determine the quadrant in which the resulting angle lies. The above equations are not determined for values of  $s_{\vartheta} = 0$  (i.e., for  $\vartheta = n\pi$ ), and this is called a *representation singularity* i.e. the lack of a global, smooth solution to the problem of determining the Euler angles from the rotation, and it is present in all the Euler angles conventions.

### ZYX Euler angles

The ZYX Euler angles are also referred to as the yaw, pitch, and roll angles, to denote the typical changes of orientation of a ship. In this convention, the angles  $\phi = [\varphi \ \vartheta \ \psi]^T$  represent rotations defined with respect to a fixed frame. The rotation is defined by rotating about the  $x$ -axis (roll), then the  $y$ -axis (pitch), and finally the  $z$ -axis (yaw) of the fixed frame (Figure 3.3). The corresponding rotation matrix can be computed via premultiplication of the elementary rotation matrix, and it is given by

$$\begin{aligned}\mathbf{R}(\phi) &= \mathbf{R}_z(\varphi)\mathbf{R}_y(\vartheta)\mathbf{R}_x(\psi) \\ &= \begin{pmatrix} c_{\varphi}c_{\vartheta} & c_{\varphi}s_{\vartheta}s_{\psi} - s_{\varphi}c_{\psi} & c_{\varphi}s_{\vartheta}c_{\psi} + s_{\varphi}s_{\psi} \\ s_{\varphi}c_{\vartheta} & s_{\varphi}s_{\vartheta}s_{\psi} + c_{\varphi}c_{\psi} & s_{\varphi}s_{\vartheta}c_{\psi} - c_{\varphi}s_{\psi} \\ -s_{\vartheta} & c_{\vartheta}s_{\psi} & c_{\vartheta}c_{\psi} \end{pmatrix},\end{aligned}\tag{3.12}$$

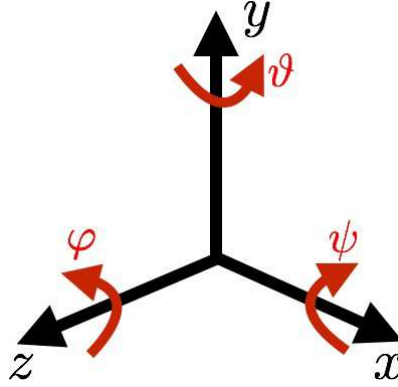


Figure 3.3: Representation of the Euler angles ZYX convention (yaw, pitch, roll).

The ZYX Euler angles can be obtained from a given  $\mathbf{R} \in SO(3)$ , in the next way

$$\begin{aligned}\varphi &= \text{Atan2}(r_{21}, r_{11}), \\ \vartheta &= \text{Atan2}\left(-r_{31}, \sqrt{r_{32}^2 + r_{33}^2}\right), \\ \psi &= \text{Atan2}(r_{32}, r_{33}).\end{aligned}\tag{3.13}$$

This solution is not determined when  $c_\vartheta = 0$ .

Euler angles summary:

- This is a minimal orientation representation, i.e., it uses only 3 parameters to represent a coordinate frame orientation.
- There are different Euler angle conventions that can be used to describe a given orientation i.e., the representation is not unique.
- All Euler angles conventions suffer representation singularities occurring when the first and last axes of rotation in the sequence lie along the same direction and causes a loss of one degree of freedom.
- Euler angle equations contain many trigonometric functions. It is a disadvantage from a computational efficiency point of view because trigonometric functions computation is very slow compared to basic arithmetic operations such as addition and multiplication.

### Axis-angle

The Euler's rotation theorem states that any displacement of a rigid body such that a point on the rigid body remains fixed, is equivalent to a single rotation about some axis that runs through the fixed point. It implies that an arbitrary rotation between two coordinate frames is equivalent to a single rotation around an axis. Thus, to completely define a rotation (or relative orientation between two frames) it is enough with an angle  $\theta \in \mathbb{R}$  and a unit vector  $\mathbf{u} = [u_x \ u_y \ u_z]^\top \in S^2 \subset \mathbb{R}^3$  in the direction of the rotation axis (Figure 3.4). This angle  $\theta$  and unit vector  $\mathbf{u}$  form the axis-angle representation. The rotation matrix corresponding to a given  $\theta$  and  $\mathbf{u}$  is given by

$$\begin{aligned} \mathbf{R}(\theta, \mathbf{u}) &= c_\theta \mathbf{I}_3 + s_\theta \mathbf{S}(\mathbf{u}) + [1 - c_\theta] \mathbf{u} \mathbf{u}^\top \\ &= \begin{pmatrix} u_x^2(1 - c_\theta) + c_\theta & u_x u_y(1 - c_\theta) - u_z s_\theta & u_x u_z(1 - c_\theta) + u_y s_\theta \\ u_x u_y(1 - c_\theta) + u_z s_\theta & u_y^2(1 - c_\theta) + c_\theta & u_y u_z(1 - c_\theta) - u_x s_\theta \\ u_x u_z(1 - c_\theta) - u_y s_\theta & u_y u_z(1 - c_\theta) + u_x s_\theta & u_z^2(1 - c_\theta) + c_\theta \end{pmatrix}, \end{aligned} \quad (3.14)$$

where  $\mathbf{S}(\cdot)$  is the skew-symmetric matrix operator defined in (a.4) and  $c_\theta$  and  $s_\theta$  represent  $\cos(\theta)$  and  $\sin(\theta)$ , respectively. It should be noticed that  $\mathbf{R}(-\theta, -\mathbf{u}) = \mathbf{R}(\theta, \mathbf{u})$ , so that, for a given orientation, represented by  $\mathbf{R}$ , the axis-angle pair is not unique, but double, whenever  $\theta \neq 2n\pi$ . The inverse mapping  $SO(3) \rightarrow \mathbb{R} \times S^2$  can be calculated in the following way

$$\begin{aligned} \theta &= \cos^{-1} \left( \frac{r_{11} + r_{22} + r_{33} - 1}{2} \right), \\ \mathbf{u} &= \frac{1}{2\sin(\theta)} \begin{bmatrix} r_{32} - r_{23} \\ r_{13} - r_{31} \\ r_{21} - r_{12} \end{bmatrix}, \end{aligned} \quad (3.15)$$

it can be seen that the last equations are not well defined when  $\theta = 0$ .

Axis-angle summary:

- It is a geometrically meaningful definition of orientation.
- This is a non-minimal orientation representation because it uses four parameters to represent the orientation of a rigid body. The auxiliary relationship (restriction) that resolves this is the unit magnitude of vector  $\mathbf{u}$ .
- In spite of the four parameters, this representation presents singularities when  $\theta = 0$ , in this situation the unit vector  $\mathbf{u}$  can be defined arbitrary. Besides, the axis-angle pair is not unique, but double, for a given rotation ( $\mathbf{R}(-\theta, -\mathbf{u}) = \mathbf{R}(\theta, \mathbf{u})$ ).

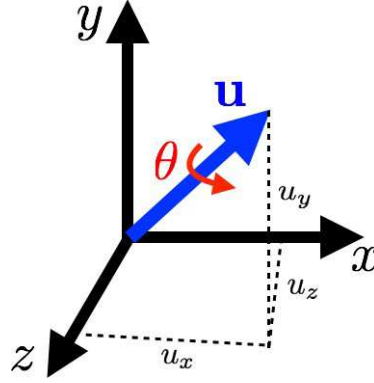


Figure 3.4: Axis-angle orientation representation,  $\mathbf{u}$  is the rotation axis (unit vector) and  $\theta$  the rotation angle.

### Unit-quaternions

Quaternions, first devised by the 19th-century Irish mathematician William Rowan Hamilton, generalize complex numbers and can be used to represent orientations. In Section A.1.7 the quaternions ( $\alpha$ ) and their basic algebra operations are formally defined. The *unit-quaternions* are the subset of all  $\alpha \in \mathbb{H}$  such that their norm ( $\mathcal{N}(\alpha)$ ), fulfills the condition

$$\mathcal{N}(\alpha) = a_0^2 + a_1^2 + a_2^2 + a_3^2 = 1.$$

In this thesis, the unit-quaternion is represented by the greek letter  $\xi$  and its four real elements by  $\eta, \beta_1, \beta_2, \beta_3 \in \mathbb{R}$ . The unit-quaternion<sup>2</sup>  $\xi \in S^3$  can be split in two elements: one scalar term  $\eta \in \mathbb{R}$ , and one vectorial term  $\beta \in \mathbb{R}^3$ . Thus

$$\xi := \begin{bmatrix} \eta \\ \beta \end{bmatrix} \in S^3 \subset \mathbb{R}^4,$$

using this notation the unit norm constraint can be expressed as

$$\eta^2 + \beta^\top \beta = 1. \quad (3.16)$$

The unit-quaternion has a clear geometrical meaning, since it can be described as a special

<sup>2</sup>The set  $S^3 \subset \mathbb{R}^4$  represents an unitary sphere of dimension three and it is defined as  $S^3 := \{\xi \in \mathbb{R}^4 : |\xi|^2 = 1\}$ .

axis-angle representation in the following way

$$\begin{aligned}\eta &= \cos\left(\frac{\theta}{2}\right), \\ \boldsymbol{\beta} &= \sin\left(\frac{\theta}{2}\right) \mathbf{u}.\end{aligned}\tag{3.17}$$

It is worth noting that, differently from the angle/axis representation, a rotation by  $-\theta$  about  $-\mathbf{u}$  gives the same unit-quaternion as that associated with a rotation by  $\theta$  about  $\mathbf{u}$ , this solves the non-uniqueness problem of the axis-angle representation.

The rotation matrix can be defined in terms of the unit-quaternion parameters in the following way (Campa 2005):

$$\begin{aligned}\mathbf{R}(\eta, \boldsymbol{\beta}) &= (\eta^2 - \boldsymbol{\beta}^\top \boldsymbol{\beta}) \mathbf{I}_3 + 2\eta \mathbf{S}(\boldsymbol{\beta}) + 2\boldsymbol{\beta} \boldsymbol{\beta}^\top = \mathbf{I}_3 + 2\eta \mathbf{S}(\boldsymbol{\beta}) + 2\mathbf{S}^2(\boldsymbol{\beta}) \\ &= \begin{pmatrix} \eta^2 + \beta_1^2 - \beta_2^2 - \beta_3^2 & 2(\beta_1\beta_2 - \eta\beta_3) & 2(\beta_1\beta_3 + \eta\beta_2) \\ 2(\beta_1\beta_2 + \eta\beta_3) & \eta^2 - \beta_1^2 + \beta_2^2 - \beta_3^2 & 2(\beta_2\beta_3 - \eta\beta_1) \\ 2(\beta_1\beta_3 - \eta\beta_2) & 2(\beta_2\beta_3 + \eta\beta_1) & \eta^2 - \beta_1^2 - \beta_2^2 + \beta_3^2 \end{pmatrix}.\end{aligned}\tag{3.18}$$

It has to be noted that

$$\mathbf{R}(-\eta, -\boldsymbol{\beta}) = \mathbf{R}(\eta, \boldsymbol{\beta}),\tag{3.19}$$

i.e.,  $\boldsymbol{\xi}$  and  $-\boldsymbol{\xi}$  represent the same orientation, meaning that  $S^3$  is a double cover of  $SO(3)$ . But, unlike the axis-angle pair, the unit-quaternions give a global (no singularities) parameterization of orientation.

Several algorithms exist in the literature to extract the unit-quaternion  $\boldsymbol{\xi}$  from the rotation matrix  $\mathbf{R} \in SO(3)$  (Klumpp 1976; Spurrier 1978; Craig 2005; Markley 2008), the main differences among them being the numerical accuracy and computational efficiency; an interesting one appears in (Siciliano et al. 2009):

$$\begin{bmatrix} \eta \\ \beta_1 \\ \beta_2 \\ \beta_3 \end{bmatrix} = \frac{1}{2} \begin{bmatrix} \sqrt{r_{11} + r_{22} + r_{33} + 1} \\ \text{sgn}(r_{32} - r_{23}) \sqrt{r_{11} - r_{22} - r_{33} + 1} \\ \text{sgn}(r_{13} - r_{31}) \sqrt{r_{22} - r_{11} - r_{33} + 1} \\ \text{sgn}(r_{21} - r_{12}) \sqrt{r_{33} - r_{22} - r_{11} + 1} \end{bmatrix},\tag{3.20}$$

where  $\text{sgn}(x) = 1$  for  $x \geq 0$  and  $\text{sgn}(x) = -1$  for  $x < 0$ . In this algorithm it has been implicitly assumed  $\eta \geq 0$ , that corresponds to an angle  $\theta \in [-\pi, \pi]$  and thus any rotation can be described.



Sequences of rotations are represented by products of unit-quaternions i.e., if  $\pm\xi_1, \pm\xi_2 \in S^3$  are the unit-quaternions corresponding to the rotation matrices  $\mathbf{R}_1, \mathbf{R}_2 \in SO(3)$ , respectively, then:

$$\mathbf{R}_1\mathbf{R}_2 \in SO(3) \Leftrightarrow \xi_1 \odot \xi_2 = \begin{bmatrix} \eta_1 \\ \beta_1 \end{bmatrix} \odot \begin{bmatrix} \eta_2 \\ \beta_2 \end{bmatrix} = \begin{bmatrix} \eta_1\eta_2 - \beta_1^T\beta_2 \\ \eta_1\beta_2 + \eta_2\beta_1 + \mathbf{S}(\beta_1)\beta_2 \end{bmatrix} \in S^3, \quad (3.21)$$

where  $\odot$  is the symbol used to represent the quaternion multiplication defined in (a.11). The transformations of a vector  $\mathbf{x}$  by a rotation matrix  $\mathbf{R}$ , given by (3.7) and (3.8) can be performed with quaternion multiplication in the following way:

$$\mathbf{R}\mathbf{x} \in \mathbb{R}^3 \Leftrightarrow \xi \odot \bar{\mathbf{x}} \odot \xi^* \in \mathbb{R}^4, \quad (3.22)$$

where  $\xi$  is the unit-quaternion corresponding to  $\mathbf{R}$ ,  $\xi^*$  is the unit-quaternion conjugate defined in (a.8) and  $\bar{\mathbf{x}} = [0 \ \mathbf{x}^T]^T \in \mathbb{H}$  is formed adding a null scalar part to the corresponding vector.

Unit-quaternions summary:

- This is a non-minimal orientation representation, since it uses four parameters subject to a unit norm.
- The unit-quaternions give a global (no singularities) parameterization of orientation.
- It is a geometrically meaningful definition of orientation since it can be described as a special axis-angle representation.
- In the group of unit-quaternions is possible to define a complete algebra, as detailed in (Chou 1992), owing to this, every operation with rotation matrices is possible with the corresponding unit-quaternions (Natale 2003).
- The unit-quaternions yields a double covering of  $SO(3)$  i.e.,  $\xi$  and  $-\xi$  represent the same physical orientation.

### Orientation representation conclusions

It is a fundamental topological fact that singularities can never be eliminated in any 3-dimensional representation of  $SO(3)$  (Murray, Li, and Sastry 1994). Based on this, the use of a non-minimal orientation representation avoids the singularities problem. From the non-minimal representations reviewed in this section, the rotation matrix and the unit-quaternions are the representations that are free of singularities. The main drawbacks of the rotation matrices are their number

of parameters (9 parameters) and the 6 constraints that are not given explicitly. In the literature (Shuster 1993; Natale 2003; Caccavale, Siciliano, and Villani 1999), the unit-quaternions are recognized to be the best option to represent the orientation, some of their interesting properties have been reviewed in this section. The unit-quaternions are used in this thesis to describe the orientation of the robots' end-effectors and consequently for the design of the consensus algorithms.

### 3.1.2 Pose definition and kinematics

In this work the pose of the robot's end-effector relative to a fixed reference frame is denoted by

$$\mathbf{x} = \begin{bmatrix} \mathbf{p} \\ \boldsymbol{\xi} \end{bmatrix} \subset \mathbb{R}^7, \quad (3.23)$$

where  $\mathbf{p} \in \mathbb{R}^3$  is the position vector and  $\boldsymbol{\xi} \in S^3$  the orientation unit-quaternion. In Figure 3.5 is shown a graphic representation of the robot's pose. The pose is defined relative to the world reference frame  $\Sigma_W$ . The superscript  $W$  used to describe the reference to the world coordinated frame will be omitted in the following, i.e.,  $\mathbf{p} \equiv \mathbf{p}^W$ ,  $\boldsymbol{\xi} \equiv \boldsymbol{\xi}^W$ ,  $\mathbf{R} \equiv \mathbf{R}^W$ . A way to obtain the pose of the robot is through the forward kinematics, that consists on finding the position and orientation of the end-effector relative to a fixed reference frame given the positions of all the  $n$ -joints and the values of all the geometric link parameters. It reduces to find an equivalent  $4 \times 4$  homogeneous transformation matrix that relates the spatial displacement and rotation of the end-effector frame with respect to the fixed reference frame:

$$\mathbf{T}_e = \mathbf{T}_0 \mathbf{T}_n^0(\mathbf{q}) \mathbf{T}_e^n = \begin{pmatrix} \mathbf{R}_e(\mathbf{q}) & \mathbf{p}_e(\mathbf{q}) \\ 0 & 1 \end{pmatrix}, \quad (3.24)$$

where  $\mathbf{T}_0$  and  $\mathbf{T}_e^n$  are two constant homogeneous transformations describing the pose of Frame 0 with respect to the world reference frame, and of the end-effector frame with respect to Frame  $n$ , respectively (Figure 3.5).

The relation between the joint velocities  $\dot{\mathbf{q}}$  and the linear  $\dot{\mathbf{p}}$  and angular  $\boldsymbol{\omega}$  velocities of the robot's end-effector, expressed also relative to a fixed reference frame, is given by

$$\mathbf{v} = \begin{bmatrix} \dot{\mathbf{p}} \\ \boldsymbol{\omega} \end{bmatrix} = \mathbf{J}(\mathbf{q}) \dot{\mathbf{q}}, \quad (3.25)$$

where  $\mathbf{v} \in \mathbb{R}^6$  and  $\mathbf{J}(\mathbf{q}) \in \mathbb{R}^{6 \times n}$  is the *geometric Jacobian* matrix (hereafter referred just as *Jacobian*). Using the principle of the virtual work, the following relation between joint torque  $\boldsymbol{\tau}$

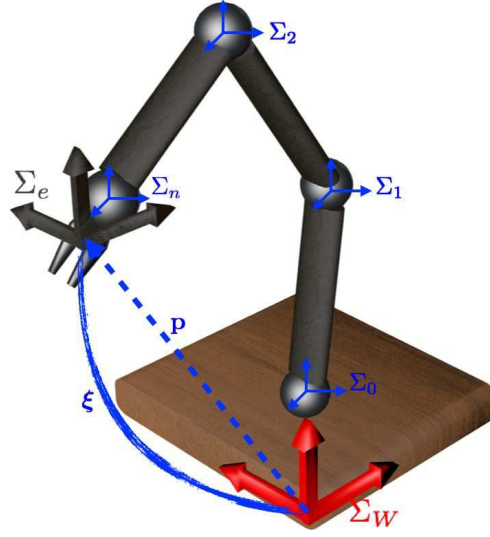


Figure 3.5: Description of the robot's pose and the coordinate frames used in the forward kinematics.

and the Cartesian forces  $\mathbf{f}$  is obtained

$$\boldsymbol{\tau} = \mathbf{J}^\top(\mathbf{q})\mathbf{f}, \quad (3.26)$$

where  $\boldsymbol{\tau} \in \mathbb{R}^n$ ,  $\mathbf{f} \in \mathbb{R}^6$ ,  $\mathbf{f} := (\mathbf{h}^\top, \mathbf{m}^\top)^\top$  and  $\mathbf{h}, \mathbf{m} \in \mathbb{R}^3$  represent the Cartesian linear forces and moments, respectively. Pre-multiplying (3.25) by the Jacobian pseudo-inverse  $\mathbf{J}^\dagger(\mathbf{q})$  and differentiating, yields

$$\ddot{\mathbf{q}} = \mathbf{J}^\dagger(\mathbf{q})\dot{\mathbf{v}} + \dot{\mathbf{J}}^\dagger(\mathbf{q})\mathbf{v}. \quad (3.27)$$

The following are some interesting properties of the Jacobian matrix:

**P1.** For all  $\mathbf{q} \in \mathbb{R}^n$ , the Jacobian matrix  $\mathbf{J}(\mathbf{q}) \in \mathbb{R}^{6 \times n}$  is a bounded operator.

**P2.** The kinematic relation (3.25) satisfies:

$$\mathbf{v} = \mathbf{J}(\mathbf{q})\dot{\mathbf{q}} = \mathbf{Y}_K(\mathbf{q}, \dot{\mathbf{q}})\boldsymbol{\theta}_K,$$

where  $\mathbf{Y}_K \in \mathbb{R}^{6 \times m_K}$  is the kinematic regressor matrix and  $\boldsymbol{\theta}_K \in \mathbb{R}^{m_K}$  is a constant vector containing the  $m_k$  kinematic physical parameters (link lengths, center of mass distances, etc.).

The relation between the time-derivative of the unit-quaternion and the angular velocity,

relative to the world reference frame, is (Fjellstad 1994; Campa and Camarillo 2008)

$$\dot{\boldsymbol{\xi}}_i = \frac{1}{2}\mathbf{U}(\boldsymbol{\xi})\boldsymbol{\omega}, \quad (3.28)$$

where

$$\mathbf{U}(\boldsymbol{\xi}) := \begin{bmatrix} -\boldsymbol{\beta}^\top \\ \eta\mathbf{I}_3 - \mathbf{S}(\boldsymbol{\beta}) \end{bmatrix} \in \mathbb{R}^{4 \times 3}. \quad (3.29)$$

Using the normality condition and the skew-symmetric matrix  $\mathbf{S}(\cdot)$  properties (a.5), it holds that:

$$\begin{aligned} \mathbf{U}^\top(\boldsymbol{\xi})\mathbf{U}(\boldsymbol{\xi}) &= \begin{bmatrix} -\boldsymbol{\beta} & \eta\mathbf{I}_3 + \mathbf{S}(\boldsymbol{\beta}) \end{bmatrix} \begin{bmatrix} -\boldsymbol{\beta}^\top \\ \eta\mathbf{I}_3 - \mathbf{S}(\boldsymbol{\beta}) \end{bmatrix} \\ &= \boldsymbol{\beta}\boldsymbol{\beta}^\top + \eta^2\mathbf{I}_3 - \mathbf{S}^2(\boldsymbol{\beta}) \\ &= \eta^2\mathbf{I}_3 + \boldsymbol{\beta}^\top\boldsymbol{\beta}\mathbf{I}_3 = (\eta^2 + \boldsymbol{\beta}^\top\boldsymbol{\beta})\mathbf{I}_3 \\ &= \mathbf{I}_3, \end{aligned} \quad (3.30)$$

hence  $\text{rank}(\mathbf{U}(\boldsymbol{\xi})) = 3$ . Using (3.28) and (3.30), the following useful relation is derived:

$$\begin{aligned} |\dot{\boldsymbol{\xi}}|^2 &= \dot{\boldsymbol{\xi}}^\top \dot{\boldsymbol{\xi}} \\ &= \frac{1}{4}\boldsymbol{\omega}^\top \mathbf{U}^\top(\boldsymbol{\xi})\mathbf{U}(\boldsymbol{\xi})\boldsymbol{\omega} \\ &= \frac{1}{4}|\boldsymbol{\omega}|^2. \end{aligned} \quad (3.31)$$

Using this last and the fact that  $|\dot{\mathbf{x}}|^2 = |\dot{\mathbf{p}}|^2 + |\dot{\boldsymbol{\xi}}|^2$ , the square norm of the velocity can be expressed as

$$\begin{aligned} |\mathbf{v}|^2 &= |\dot{\mathbf{p}}|^2 + |\boldsymbol{\omega}|^2 \\ &= |\dot{\mathbf{p}}|^2 + 4|\dot{\boldsymbol{\xi}}|^2 \\ &= |\dot{\mathbf{x}}|^2 + 3|\dot{\boldsymbol{\xi}}|^2. \end{aligned} \quad (3.32)$$

Besides, from (3.29) and using (a.5), it follows that

$$\mathbf{U}^\top(\boldsymbol{\xi})\boldsymbol{\xi} = \begin{bmatrix} -\boldsymbol{\beta} & \eta\mathbf{I}_3 + \mathbf{S}(\boldsymbol{\beta}) \end{bmatrix} \begin{bmatrix} \eta \\ \boldsymbol{\beta} \end{bmatrix} = \mathbf{0}_4. \quad (3.33)$$

From (3.30) and (3.33) and noting that  $\mathbf{U}(\boldsymbol{\xi})$  is linear in  $\boldsymbol{\xi}$ , the following properties can be derived (Fjellstad 1994):

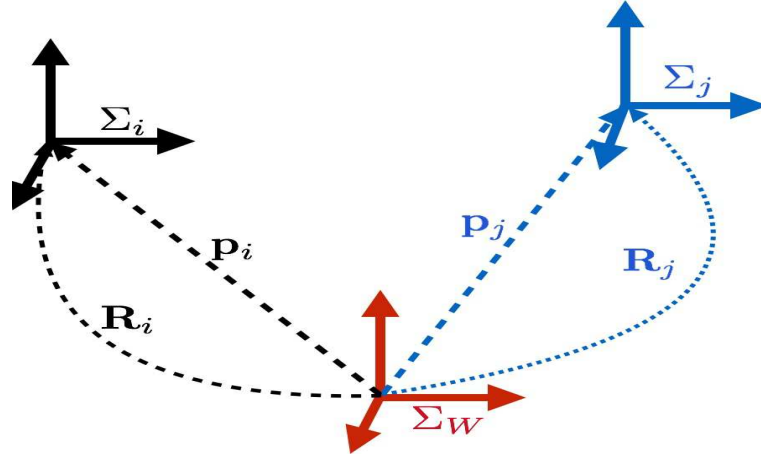


Figure 3.6: Position vectors and rotation matrices of frames  $\Sigma_i$  and  $\Sigma_j$  relative to the reference frame  $\Sigma_W$ .

**P3.** For all  $\xi \in S^3$ ,  $\mathbf{U}^\top(\xi)\mathbf{U}(\xi) = \mathbf{I}_3$ . Hence,  $\text{rank}(\mathbf{U}(\xi)) = 3$  and  $\ker(\mathbf{U}^\top(\xi)) = \text{span}(\xi)$ .

**P4.** For all  $\xi \in S^3$  and  $\dot{\xi} \in \mathbb{R}^4$ ,  $\dot{\mathbf{U}}(\xi) = \mathbf{U}(\dot{\xi})$ .

**P5.** Since, for all  $\xi \in S^3$ ,  $|\xi| = 1$  then  $\mathbf{U}(\xi)$  is a bounded operator.

Finally, defining  $\Phi(\xi) \in \mathbb{R}^{6 \times 7}$  as the block-diagonal matrix:

$$\begin{aligned} \Phi(\xi) &:= \text{diag}(\mathbf{I}_3, \frac{1}{2}\mathbf{U}^\top(\xi)) \\ &= \begin{bmatrix} \mathbf{I}_3 & \mathbf{0}_{3 \times 4} \\ \mathbf{0}_3 & \frac{1}{2}\mathbf{U}^\top(\xi_i) \end{bmatrix}, \end{aligned} \quad (3.34)$$

it holds that

$$\dot{\mathbf{x}} = \begin{bmatrix} \dot{\mathbf{p}} \\ \dot{\xi} \end{bmatrix} = \Phi^\top(\xi)\mathbf{v}. \quad (3.35)$$

### 3.1.3 Pose error

This section analyzes the position and orientation errors between two different frames,  $\Sigma_i$  and  $\Sigma_j$ , relative to a fixed reference frame  $\Sigma_W$ , as shown in Figure 3.6.

The position error vector,  $\tilde{\mathbf{p}}_{ij} \in \mathbb{R}^3$  is simply the difference between the origin of  $\Sigma_i$  and the

origin of  $\Sigma_j$ , that is

$$\tilde{\mathbf{P}}_{ij} = \mathbf{p}_i - \mathbf{p}_j. \quad (3.36)$$

The orientation error calculation is not as simple as the position case, because it depends on the representation of orientation and its group's algebra. In the case that the orientation of  $\Sigma_i$  and  $\Sigma_j$  is represented by the rotation matrices  $\mathbf{R}_i$  and  $\mathbf{R}_j$ , respectively, three different way can be used to define an error matrix (Wen and Kreutz-Delgado 1991; Fjellstad 1994; Campa 2005):

- $\tilde{\mathbf{R}}_{i-j} := \mathbf{R}_i - \mathbf{R}_j$
- $\tilde{\mathbf{R}}_{ji} := \mathbf{R}_j^\top \mathbf{R}_i$
- $\tilde{\mathbf{R}}_{ij} := \mathbf{R}_i \mathbf{R}_j^\top$

In the first case,  $\tilde{\mathbf{R}}_{i-j} = \mathbf{0}$  would mean no orientation error between the two reference frame, however  $\tilde{\mathbf{R}}_{i-j}$  is not a rotation matrix since  $SO(3)$  has not group structure under matrix addition. The other two options,  $\tilde{\mathbf{R}}_{ji}$  and  $\tilde{\mathbf{R}}_{ij}$  are a better approach because both are rotation matrices. For these,  $\tilde{\mathbf{R}}_{ji} = \mathbf{I}_3$  and  $\tilde{\mathbf{R}}_{ij} = \mathbf{I}_3$  would mean that  $\Sigma_i$  and  $\Sigma_j$  have the same orientation. The rotation matrix  $\tilde{\mathbf{R}}_{ji}$  is commonly used in applications of autonomous vehicles (satellites, submarines, etc.) in which the pose is relative to the moving object.

In this thesis  $\tilde{\mathbf{R}}_{ij}$  is used but in the unit-quaternion parameterization. The unit-quaternion describing such orientation error is given by

$$\begin{aligned} \tilde{\boldsymbol{\xi}}_{ij} = \boldsymbol{\xi}_i \odot \boldsymbol{\xi}_j^* &= \begin{bmatrix} \tilde{\eta}_{ij} \\ \tilde{\boldsymbol{\beta}}_{ij} \end{bmatrix} = \begin{bmatrix} \boldsymbol{\xi}_i^\top \boldsymbol{\xi}_j \\ \eta_j \boldsymbol{\beta}_i - \eta_i \boldsymbol{\beta}_j - \mathbf{S}(\boldsymbol{\beta}_i) \boldsymbol{\beta}_j \end{bmatrix} \\ &= \begin{bmatrix} \eta_i \eta_j + \boldsymbol{\beta}_i^\top \boldsymbol{\beta}_j \\ -\mathbf{U}^\top(\boldsymbol{\xi}_i) \boldsymbol{\xi}_j \end{bmatrix}, \end{aligned} \quad (3.37)$$

where  $\odot$  denotes the quaternion product,  $\boldsymbol{\xi}_{(\cdot)}^* = [\eta_{(\cdot)}, -\boldsymbol{\beta}_{(\cdot)}^\top]^\top$  is the quaternion conjugate, and  $\mathbf{S}(\cdot)$  is the skew-symmetric matrix operator. The no disparity condition (no orientation error) is given by

$$\boldsymbol{\xi}_i = \pm \boldsymbol{\xi}_j \Leftrightarrow \tilde{\boldsymbol{\xi}}_{ij} = \begin{bmatrix} \pm 1 \\ \mathbf{0} \end{bmatrix}. \quad (3.38)$$

It should be underscored that  $\tilde{\boldsymbol{\beta}}_{ij} = \mathbf{0}$  implies that  $\boldsymbol{\xi}_i = \pm \boldsymbol{\xi}_j$ . This, in turn, implies that  $\mathbf{U}^\top(\boldsymbol{\xi}_i) \boldsymbol{\xi}_j = \mathbf{0}_3$ . In order to clarify this, the following proposition is defined.

**PROPOSITION 3.1:**

The orientation of the coordinate frames  $\Sigma_i$  and  $\Sigma_j$ , represented by the unit-quaternions  $\xi_i$  and  $\xi_j$ , respectively, is the same if and only if the vector component of the unit-quaternion  $\tilde{\xi}_{ij}$ , defined in (3.37), is equal to zero, i.e.,

$$\xi_i = \pm \xi_j \Leftrightarrow \tilde{\beta}_{ij} = \mathbf{0}.$$

*Proof.* This proof follows the same procedure as in Proposition 1 in (Yuan 1988). From (3.37) and  $\tilde{\beta}_{ij} = \mathbf{0}$  it follows that

$$\eta_j \beta_i - \eta_i \beta_j = \mathbf{S}(\beta_i) \beta_j.$$

Since  $(\eta_j \beta_i - \eta_i \beta_j)$  and  $\mathbf{S}(\beta_i) \beta_j$  are orthogonal to each other, the above equation only holds if  $\beta_i$  and  $\beta_j$  are parallel, hence  $\mathbf{S}(\beta_i) \beta_j = \mathbf{0}$ . Thus

$$\beta_i = \frac{\eta_i}{\eta_j} \beta_j, \quad (3.39)$$

moreover,  $\tilde{\beta}_{ij} = \mathbf{0}$  and the normality condition of the quaternions, implies that

$$\tilde{\eta}_{ij} = \eta_i \eta_j + \beta_i^\top \beta_j = \pm 1. \quad (3.40)$$

Finally, substituting (3.39) in (3.40), results

$$\begin{aligned} \eta_i \eta_j + \frac{\eta_i}{\eta_j} |\beta_j|^2 &= \pm 1 \\ \eta_i (\eta_j^2 + |\beta_j|^2) &= \pm \eta_j, \end{aligned}$$

hence  $\eta_i = \pm \eta_j$ , which in turn implies that  $\beta_i = \pm \beta_j$ . This corresponds to the same orientation in  $SE(3)$ .  $\diamond \diamond \diamond$

Using (3.29) and (3.33) the following relation can be derived

$$\begin{aligned} \mathbf{U}^\top(\xi_i)(\xi_i - \xi_j) &= \begin{bmatrix} -\beta_i & \eta_i \mathbf{I}_3 + \mathbf{S}(\beta_i) \end{bmatrix} \left( \begin{bmatrix} \eta_i \\ \beta_i \end{bmatrix} - \begin{bmatrix} \eta_j \\ \beta_j \end{bmatrix} \right) \\ &= \begin{bmatrix} \eta_j \beta_{i1} & -\eta_i \beta_{j1} & -\beta_{j3} \beta_{i2} + \beta_{j2} \beta_{i3} \\ \eta_j \beta_{i2} & -\eta_i \beta_{j2} & \beta_{j3} \beta_{i1} - \beta_{j1} \beta_{i3} \\ \eta_j \beta_{i3} & -\eta_i \beta_{j3} & -\beta_{j2} \beta_{i1} + \beta_{j1} \beta_{i2} \end{bmatrix} \\ &= \eta_j \beta_i - \eta_i \beta_j - \mathbf{S}(\beta_i) \beta_j \\ &= \tilde{\beta}_{ij}. \end{aligned} \quad (3.41)$$

Finally, for  $\tilde{\omega}_{ij} = \omega_i - \omega_j$ , it also holds that (Wen and Kreutz-Delgado 1991; Campa and Camarillo 2008)

$$\dot{\tilde{\xi}}_{ij} = \frac{1}{2} \begin{bmatrix} -\tilde{\beta}_{ij}^\top \\ \tilde{\eta}_{ij} \mathbf{I}_3 + \mathbf{S}(\tilde{\beta}_{ij}) \end{bmatrix} \tilde{\omega}_{ij} - \begin{bmatrix} 0 \\ \mathbf{S}(\tilde{\beta}_{ij}) \end{bmatrix} \omega_i. \quad (3.42)$$

### 3.1.4 Dynamics

This section describes the dynamics of a robot manipulator using a set of nonlinear, second-order, ordinary differential equations which depend on the kinematic and inertial properties of the robot. There are two general methods for the derivation of the dynamic equations of motion, the *Newton-Euler formulation*, that allows to obtain the dynamic model in a recursive form, so that it is computationally more efficient and the *Euler-Lagrange formulation* which is an energy based method that requires only the kinetic and potential energies of the system to be computed and the resulting equations can be obtained in closed form, allowing detailed analysis of the properties of the system. In the literature there exist several works that study both formulations, like (Murray et al. 1994; Craig 2005; Spong et al. 2005; Siciliano et al. 2009). Here the Euler-Lagrange formulation is used in order to derive the joint space dynamic model.

#### Joint space dynamics

Let  $\mathcal{K}(\mathbf{q}, \dot{\mathbf{q}})$  and  $\mathcal{U}(\mathbf{q})$  be the kinetic and potential energies of the system defined in the generalized coordinates  $\mathbf{q} \in \mathbb{R}^n$ ; then the Lagrangian function  $\mathcal{L}(\mathbf{q}, \dot{\mathbf{q}})$  is defined as

$$\mathcal{L}(\mathbf{q}, \dot{\mathbf{q}}) = \mathcal{K}(\mathbf{q}, \dot{\mathbf{q}}) - \mathcal{U}(\mathbf{q}).$$

The equations of motion for a mechanical system are given by

$$\frac{d}{dt} \left( \frac{\partial \mathcal{L}(\mathbf{q}, \dot{\mathbf{q}})}{\partial \dot{\mathbf{q}}} \right) - \frac{\partial \mathcal{L}(\mathbf{q}, \dot{\mathbf{q}})}{\partial \mathbf{q}} = \boldsymbol{\tau}, \quad (3.43)$$

where  $\boldsymbol{\tau} \in \mathbb{R}^n$  are the torques applied at the joints by the robot's actuator. In general, for mechanical systems such as robot manipulators, the kinetic energy  $\mathcal{K}(\mathbf{q}, \dot{\mathbf{q}})$  is given by

$$\mathcal{K}(\mathbf{q}, \dot{\mathbf{q}}) = \frac{1}{2} \dot{\mathbf{q}}^\top \bar{\mathbf{M}}(\mathbf{q}) \dot{\mathbf{q}},$$



where  $\bar{\mathbf{M}}(\mathbf{q}) \in \mathbb{R}^{n \times n}$  is the inertia matrix. Using this definition of kinetic energy in (3.43) the equations of motion become

$$\frac{d}{dt} \left( \frac{\partial}{\partial \dot{\mathbf{q}}} \left( \frac{1}{2} \dot{\mathbf{q}}^\top \bar{\mathbf{M}}(\mathbf{q}) \dot{\mathbf{q}} \right) \right) - \frac{\partial}{\partial \mathbf{q}} \left( \frac{1}{2} \dot{\mathbf{q}}^\top \bar{\mathbf{M}}(\mathbf{q}) \dot{\mathbf{q}} \right) + \frac{\partial}{\partial \mathbf{q}} \mathcal{U}(\mathbf{q}) = \boldsymbol{\tau},$$

resulting,

$$\bar{\mathbf{M}}(\mathbf{q}) \ddot{\mathbf{q}} + \dot{\bar{\mathbf{M}}}(\mathbf{q}) \dot{\mathbf{q}} - \frac{\partial}{\partial \mathbf{q}} \left( \frac{1}{2} \dot{\mathbf{q}}^\top \bar{\mathbf{M}}(\mathbf{q}) \dot{\mathbf{q}} \right) + \frac{\partial}{\partial \mathbf{q}} \mathcal{U}(\mathbf{q}) = \boldsymbol{\tau}.$$

Now defining

$$\bar{\mathbf{C}}(\mathbf{q}, \dot{\mathbf{q}}) \dot{\mathbf{q}} = \dot{\bar{\mathbf{M}}}(\mathbf{q}) \dot{\mathbf{q}} - \frac{\partial}{\partial \mathbf{q}} \left( \frac{1}{2} \dot{\mathbf{q}}^\top \bar{\mathbf{M}}(\mathbf{q}) \dot{\mathbf{q}} \right), \quad (3.44)$$

and  $\bar{\mathbf{g}}(\mathbf{q}) = \frac{\partial}{\partial \mathbf{q}} \mathcal{U}(\mathbf{q})$ , the nonlinear dynamic model of a robot manipulator in the joint space can finally be expressed as

$$\bar{\mathbf{M}}(\mathbf{q}) \ddot{\mathbf{q}} + \bar{\mathbf{C}}(\mathbf{q}, \dot{\mathbf{q}}) \dot{\mathbf{q}} + \bar{\mathbf{g}}(\mathbf{q}) = \boldsymbol{\tau}. \quad (3.45)$$

where  $\bar{\mathbf{g}}(\mathbf{q}) \in \mathbb{R}^n$  is the gravitational torques vector and  $\bar{\mathbf{C}}(\mathbf{q}, \dot{\mathbf{q}}) \in \mathbb{R}^{n \times n}$  is the Coriolis and centrifugal effects matrix and may be not unique, but the vector  $\bar{\mathbf{C}}(\mathbf{q}, \dot{\mathbf{q}}) \dot{\mathbf{q}}$  is indeed unique. A useful Coriolis matrix is the one defined using the Christoffel symbols of the first kind, that is (Kelly, Santibáñez, and Loria 2005)

$$\bar{c}_{ij} = \sum_{k=1}^n \bar{c}_{ijk} \dot{q}_k,$$

with

$$\bar{c}_{ijk} = \frac{1}{2} \left( \frac{\partial \bar{m}_{ij}}{\partial q_k} + \frac{\partial \bar{m}_{ik}}{\partial q_j} - \frac{\partial \bar{m}_{jk}}{\partial q_i} \right),$$

where,  $\bar{m}_{ij}$  and  $\bar{c}_{ij}$  denote the  $ij$ th element of the inertia and Coriolis matrices, respectively.

The joint space dynamic model (3.45) enjoys of the following properties (Kelly, Santibáñez, and Loria 2005):

**P6.**  $\bar{\mathbf{M}}(\mathbf{q})$  is symmetric and there exist  $\lambda_m, \lambda_M > 0$  such that

$$0 < \lambda_m \mathbf{I}_n \leq \bar{\mathbf{M}}(\mathbf{q}) \leq \lambda_M \mathbf{I}_n < \infty$$

**P7.** The matrix  $\dot{\bar{\mathbf{M}}}(\mathbf{q}) - 2\bar{\mathbf{C}}(\mathbf{q}, \dot{\mathbf{q}})$  is skew-symmetric, for  $\bar{\mathbf{C}}(\mathbf{q}, \dot{\mathbf{q}})$  defined via the Christoffel symbols of the first kind.

**P8.** For any  $\phi \in \mathbb{R}^n$ , (3.45) satisfies

$$\bar{\mathbf{M}}(\mathbf{q})\dot{\phi} + \bar{\mathbf{C}}(\mathbf{q}, \dot{\mathbf{q}})\phi - \bar{\mathbf{g}}(\mathbf{q}) = \mathbf{Y}_D(\mathbf{q}, \dot{\mathbf{q}}, \phi, \dot{\phi})\boldsymbol{\theta}_D$$

where  $\mathbf{Y}_D \in \mathbb{R}^{n \times m}$  is a regressor matrix of known functions and  $\boldsymbol{\theta}_D \in \mathbb{R}^m$  is a constant vector containing the  $m$  dynamical parameters (link masses, moments of inertia, etc.) of the robot.

### Operational space dynamics

Operational space (also known as task space) is the space in which high-level motion and force commands are issued and executed. To develop an operational space model which can be adopted for both redundant and non-redundant manipulators, it is then convenient to start from the joint space model.

From (3.25), the joint velocity is given by

$$\dot{\mathbf{q}} = \mathbf{J}^\dagger(\mathbf{q})\mathbf{v}, \quad (3.46)$$

substituting, (3.46), (3.27) and (3.26) in (3.45) gives,

$$\bar{\mathbf{M}}(\mathbf{q})(\mathbf{J}^\dagger(\mathbf{q})\dot{\mathbf{v}} + \dot{\mathbf{J}}^\dagger(\mathbf{q})\mathbf{v}) + \bar{\mathbf{C}}(\mathbf{q}, \dot{\mathbf{q}})\mathbf{J}^\dagger(\mathbf{q})\mathbf{v} + \bar{\mathbf{g}}(\mathbf{q}) = \mathbf{J}^\top \mathbf{f},$$

premultiplying by  $(\mathbf{J}^\top)^\dagger$  and defining

$$\begin{aligned} \mathbf{M}(\mathbf{q}) &:= (\mathbf{J}^\top)^\dagger \bar{\mathbf{M}}(\mathbf{q})\mathbf{J}^\dagger, & \mathbf{g}(\mathbf{q}) &:= (\mathbf{J}^\top)^\dagger \bar{\mathbf{g}}(\mathbf{q}), \\ \mathbf{C}(\mathbf{q}, \dot{\mathbf{q}}) &:= (\mathbf{J}^\top)^\dagger (\bar{\mathbf{M}}(\mathbf{q})\dot{\mathbf{J}}^\dagger + \bar{\mathbf{C}}(\mathbf{q}, \dot{\mathbf{q}})\mathbf{J}^\dagger), \end{aligned} \quad (3.47)$$

the operational space dynamic model can finally be expressed as

$$\mathbf{M}(\mathbf{q})\dot{\mathbf{v}} + \mathbf{C}(\mathbf{q}, \dot{\mathbf{q}})\mathbf{v} + \mathbf{g}(\mathbf{q}) = \mathbf{f}. \quad (3.48)$$

The operational space model (3.48) has the following well-known properties (Spong et al. 2005; Siciliano et al. 2009) :

**P9.**  $\mathbf{M}(\mathbf{q})$  is symmetric positive definite and there exist  $\lambda_m, \lambda_M > 0$  such that

$$0 < \lambda_m \mathbf{I}_6 \leq \mathbf{M}(\mathbf{q}) \leq \lambda_M \mathbf{I}_6 < \infty.$$

**P10.** The matrix  $\dot{\mathbf{M}}(\mathbf{q}) - 2\mathbf{C}(\mathbf{q}, \dot{\mathbf{q}})$  is skew-symmetric.

**P11.** For all  $\mathbf{q}, \dot{\mathbf{q}}, \mathbf{v}$ , there exists  $\kappa \in \mathbb{R}_{>0}$  such that

$$|\mathbf{C}(\mathbf{q}, \dot{\mathbf{q}})\mathbf{v}| \leq \kappa|\mathbf{v}|^2.$$

**P12.** If  $\mathbf{v}, \dot{\mathbf{v}} \in \mathcal{L}_\infty$  then  $\frac{d}{dt}\mathbf{C}(\mathbf{q}, \dot{\mathbf{q}})$  is a bounded operator.

**P13.** For any  $\phi \in \mathbb{R}^6$ , (3.48) satisfies

$$\mathbf{M}(\mathbf{q})\dot{\phi} + \mathbf{C}(\mathbf{q}, \dot{\mathbf{q}})\phi - \mathbf{g}(\mathbf{q}) = \mathbf{Y}(\mathbf{q}, \dot{\mathbf{q}}, \phi, \dot{\phi})\boldsymbol{\theta},$$

where  $\mathbf{Y} \in \mathbb{R}^{6 \times m}$  is a regressor matrix of known functions and  $\boldsymbol{\theta} \in \mathbb{R}^m$  is a constant vector containing the dynamical parameters (link masses, moments of inertia, etc.).

**Remark 3.1** (Passivity of the Robot Manipulators). The robot manipulator modeled as (3.48) is passive from input  $\mathbf{f}$  to output  $\mathbf{v}$ . This can be proved using the total energy function

$$\mathcal{E}(\mathbf{v}, \mathbf{q}) = \mathcal{K}(\mathbf{v}) + \mathcal{U}(\mathbf{q}), \quad (3.49)$$

where  $\mathcal{K}$  is the kinetic energy given by

$$\mathcal{K}(\mathbf{v}) = \frac{1}{2}\mathbf{v}^\top \mathbf{M}(\mathbf{q})\mathbf{v}, \quad (3.50)$$

and  $\mathcal{U}(\mathbf{q})$  is the gravity potential energy such that  $\bar{\mathbf{g}}(\mathbf{q}) := \frac{\partial \mathcal{U}}{\partial \mathbf{q}}$ . The time derivative of (3.49) evaluated on the system trajectories ( $\dot{\mathbf{v}} = \mathbf{M}^{-1}(\mathbf{q})(\mathbf{f} - \mathbf{C}(\mathbf{q}, \dot{\mathbf{q}})\mathbf{v} - \mathbf{g}(\mathbf{q}))$ ), using the skew-symmetric property **P10**, is given by

$$\dot{\mathcal{E}}(\mathbf{v}, \mathbf{q}) = \mathbf{v}^\top \mathbf{f} - \mathbf{g}(\mathbf{q})^\top \mathbf{v} + \frac{d}{dt}\mathcal{U}(\mathbf{q}),$$

noting that  $\frac{d}{dt}\mathcal{U}(\mathbf{q}) = \frac{\partial \mathcal{U}}{\partial \mathbf{q}}\dot{\mathbf{q}} = \bar{\mathbf{g}}^\top(\mathbf{q})\dot{\mathbf{q}}$  and using (3.47), results

$$\dot{\mathcal{E}}(\mathbf{v}, \mathbf{q}) = \mathbf{v}^\top \mathbf{f},$$

integrating from 0 to  $t$ , yields

$$\mathcal{E}(t) - \mathcal{E}(0) = \int_0^t \mathbf{v}^\top(\sigma)\mathbf{f}(\sigma)d\sigma,$$

Thus,

$$\int_0^t \mathbf{v}^\top(\sigma) \mathbf{f}(\sigma) d\sigma \geq -\mathcal{E}(0), \quad (3.51)$$

It means that the robot manipulator has bounded extractable energy  $\mathcal{E}(0)$ . Besides, it proofs that (3.48) represents a passive map from force  $\mathbf{f}$  to velocity  $\mathbf{v}$  (see Section A.2.3).

## 3.2 Robot networks

This work studies network systems composed of  $N$  robot manipulators (agents). Each agent is regarded as a node in a graph ( $\mathcal{G}$ ), where every  $i$ th-node,  $i \in \bar{N} := \{1, \dots, N\}$ , is modeled as a  $n_i$ -DoF robot manipulator in the operational space as in (3.48), thus the dynamic of the  $i$ th-node can be expressed as

$$\mathbf{M}_i(\mathbf{q}_i) \dot{\mathbf{v}}_i + \mathbf{C}_i(\mathbf{q}_i, \dot{\mathbf{q}}_i) \mathbf{v}_i + \mathbf{g}_i(\mathbf{q}_i) = \mathbf{f}_i. \quad (3.52)$$

In this thesis the robots of the network are considered *heterogeneous*, so they can have different numbers of DoF, i.e.,  $n_i \neq n_j$ , for  $j \neq i$ , and  $j \in \bar{N}$ . In the next section, graph theory is used to model the robot network interconnection.

### 3.2.1 Network interconnection

In a multi-agent system, each agent can communicate with other agents which are defined as its neighbors in a graph. A graph  $\mathcal{G} = (\bar{N}, \mathcal{M}, \mathcal{A})$  consists of a node set  $\bar{N} = \{1, \dots, N\}$ , an edge set  $\mathcal{M} \subseteq \bar{N} \times \bar{N}$  and a weighted adjacency matrix  $\mathcal{A} = [a_{ij}] \in \mathbb{R}^{N \times N}$ .

A graph is called a *directed graph* if the edge set is composed by ordered pairs of nodes and each edge,  $(i, j) \in \mathcal{M}$ , denotes that agent  $j$  can obtain information from agent  $i$ , but not necessarily vice-versa. For the edge  $(i, j)$ ,  $i$  is the parent node and  $j$  is the child node. In contrast to a directed graph, the pair of nodes in an *undirected graph* are unordered, where the edge  $(i, j)$  denotes that agent  $i$  and  $j$  can obtain information from each other.

A path in a graph is an ordered sequence of nodes such that any pair of consecutive nodes in the sequence is linked by an edge of the graph. A graph is connected if there exists a path between any two nodes. If a graph is not connected, then it is composed of multiple connected components, that is, multiple connected subgraphs. An *undirected graph* is connected if there is an undirected path (a sequence of undirected edges) between every pair of distinct nodes.

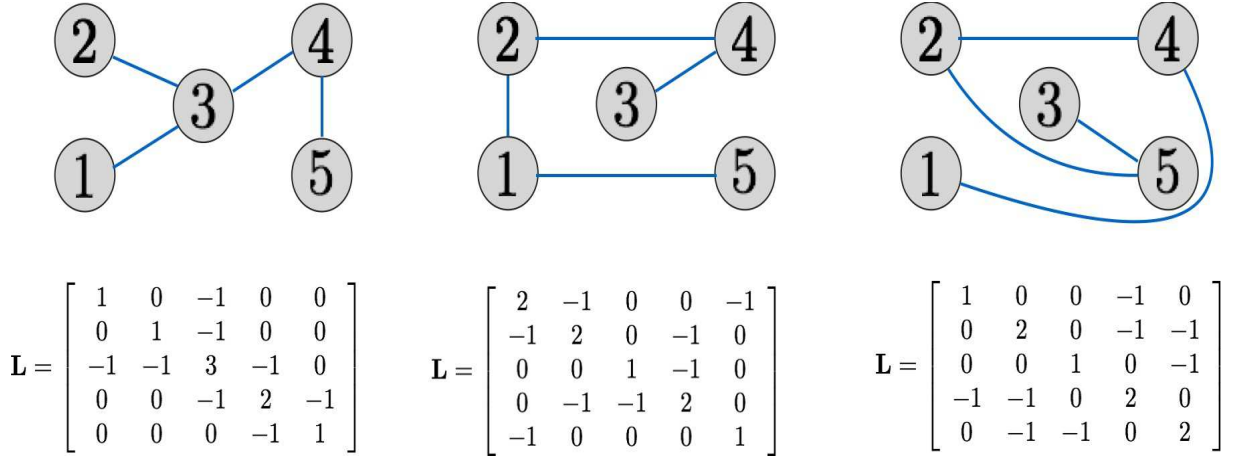


Figure 3.7: Examples of allowed graph topologies and their corresponding Laplacians for a five nodes network.

For an undirected graph the elements of the adjacency matrix  $a_{ij}$  are defined as  $a_{ij} > 0$  if  $(i, j) \in \mathcal{M}$  and  $a_{ij} = 0$  otherwise.  $\mathcal{N}_i$  is the set of nodes transmitting information to the  $i$ th node. The graph in-degree matrix  $\mathcal{I} \in \mathbb{R}^{N \times N}$  is a diagonal matrix whose elements are defined as  $\mathcal{I}_i := \sum_{j \in \mathcal{N}_i} a_{ij}$ . The graph Laplacian matrix  $\mathbf{L} := [\ell_{ij}] \in \mathbb{R}^{N \times N}$  is defined, via the in-degree and the adjacency matrices, as  $\mathbf{L} = \mathcal{I} - \mathcal{A}$ . Equivalently,

$$\ell_{ij} = \begin{cases} \sum_{j \in \mathcal{N}_i} a_{ij} & i = j \\ -a_{ij} & i \neq j \end{cases}. \quad (3.53)$$

### 3.2.2 Assumptions and instrumental lemmas

In this thesis, the interconnection of the  $N$  robot manipulators is described via the graph Laplacian matrix and, in order to ensure that the interconnection forces are generated by a gradient of a potential function, the following assumption is used:

**A1.** The robot network graph is *undirected and connected*.

Note that, the assumption **A1** allows arbitrary undirected connected communication topologies and not only the restrictive all-to-all or ring communication topologies. Figure 3.7 shows some examples of allowed interconnection topologies and their corresponding Laplacian matrices.

By construction,  $\mathbf{L}$  has a zero row sum, i.e.,  $\mathbf{L}\mathbf{1}_N = \mathbf{0}_N$ . Moreover, assumption **A1**, en-

sures that  $\mathbf{L}$  is symmetric, has a single zero-eigenvalue and the rest of its spectrum has positive real parts (Olfati-Saber and Murray 2004). Thus,  $\text{rank}(\mathbf{L}) = N - 1$ . Using these facts, it is straightforward to show that, for any  $\mathbf{z} \in \mathbb{R}^N$ ,

$$\mathbf{z}^\top \mathbf{L} \mathbf{z} = \frac{1}{2} \sum_{i \in \bar{N}} \sum_{j \in \mathcal{N}_i} a_{ij} (z_i - z_j)^2 \geq 0,$$

Furthermore,

$$\frac{d}{dt} \mathbf{z}^\top \mathbf{L} \mathbf{z} = 2 \dot{\mathbf{z}}^\top \mathbf{L} \mathbf{z} = 2 \sum_{i \in \bar{N}} \dot{z}_i \sum_{j \in \mathcal{N}_i} a_{ij} (z_i - z_j). \quad (3.54)$$

The following Lemma is based on the assumption **A1**, and its proof employs the previous Laplacian matrix properties. This lemma is useful in the stability proof of the controllers derived in this work.

**LEMMA 3.1:**

Consider a network satisfying the assumption **A1**. Then

$$\sum_{i \in \bar{N}} \sum_{j \in \mathcal{N}_i} a_{ij} \left( (\dot{\mathbf{x}}_i + \dot{\mathbf{x}}_j)^\top (\mathbf{x}_i - \mathbf{x}_j) \right) = 0. \quad (3.55)$$

*Proof.* Adding and subtracting the term  $\mathbf{x}_i^\top \dot{\mathbf{x}}_i$  to the terms inside the parenthesis of expression (3.55) and doing some algebra, yields

$$\begin{aligned} (\dot{\mathbf{x}}_i + \dot{\mathbf{x}}_j)^\top (\mathbf{x}_i - \mathbf{x}_j) &= \dot{\mathbf{x}}_i^\top (\mathbf{x}_i - \mathbf{x}_j) - \mathbf{x}_i^\top (\dot{\mathbf{x}}_i - \dot{\mathbf{x}}_j) + \mathbf{x}_i^\top \dot{\mathbf{x}}_i - \mathbf{x}_j^\top \dot{\mathbf{x}}_j \\ &= \dot{\mathbf{x}}_i^\top (\mathbf{x}_i - \mathbf{x}_j) - \mathbf{x}_i^\top (\dot{\mathbf{x}}_i - \dot{\mathbf{x}}_j) + \rho_i - \rho_j, \end{aligned}$$

where the scalar  $\rho_{(\cdot)}$  is defined as  $\rho_{(\cdot)} := \mathbf{x}_{(\cdot)}^\top \dot{\mathbf{x}}_{(\cdot)}$ . Now, using (3.53) and since

$$\sum_{i \in \bar{N}} \sum_{j \in \mathcal{N}_i} a_{ij} (\rho_i - \rho_j) = \mathbf{1}_N^\top \mathbf{L} \boldsymbol{\rho} = 0,$$

it is straightforward to show, using the fact that the Laplacian matrix is symmetric, that

$$\sum_{i \in \bar{N}} \sum_{j \in \mathcal{N}_i} a_{ij} (\dot{\mathbf{x}}_i + \dot{\mathbf{x}}_j)^\top (\mathbf{x}_i - \mathbf{x}_j) = \mathbf{x}^\top \left( (\mathbf{L}^\top - \mathbf{L}) \otimes \mathbf{I}_7 \right) \dot{\mathbf{x}} = 0,$$

where  $\boldsymbol{\rho} := [\rho_1, \dots, \rho_N]^\top \in \mathbb{R}^N$  and  $\mathbf{x} := [\mathbf{x}_1^\top, \dots, \mathbf{x}_N^\top]^\top$ ,  $\dot{\mathbf{x}} := [\dot{\mathbf{x}}_1^\top, \dots, \dot{\mathbf{x}}_1^\top]^\top \in \mathbb{R}^{7N}$ . ◇◇◇

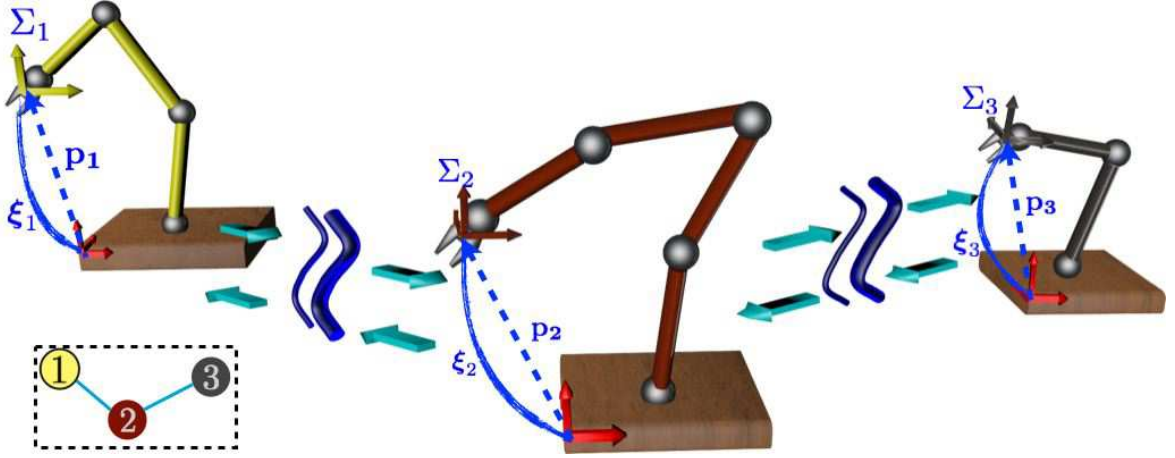


Figure 3.8: Leaderless robot network and the graph that models its interconnection.

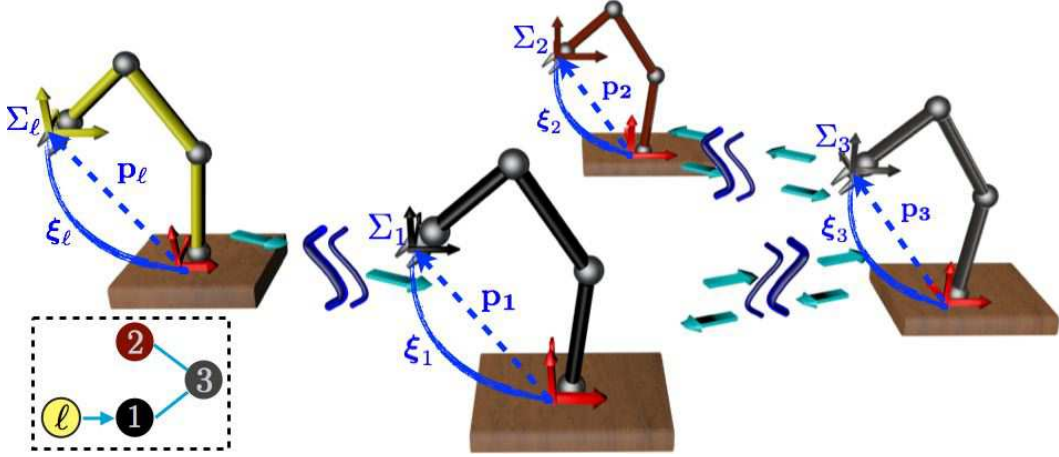


Figure 3.9: Leader-follower robot network and the graph that models its interconnection.

This thesis proposes consensus algorithms for robots networks without a leader (leaderless), and for robot networks with a leader (leader-follower). Examples of both configurations are shown in Figure 3.8 and Figure 3.9, respectively. The leaderless interconnection fulfils the assumption **A1** and it is modeled with the Laplacian matrix defined as in (3.53). With regards to the leader-follower interconnection, the following assumption is also made:

**A2.** At least one of the  $N$  follower robots has direct access to the leader's constant pose  $x_\ell$ , *i.e.*, there exists at least one directed edge from the leader to any of the  $N$  followers.

The Assumptions **A1** and **A2** ensure that the leader pose is *globally reachable* from any  $i$ th node. The following lemma defines a composed Laplacian ( $L_\ell$ ) that models the interconnections

with the leader. It has been borrowed from Chapter 1, Lemma 1.6 of (Cao and Ren 2011).

**LEMMA 3.2:**

Consider a non-negative diagonal matrix  $\mathbf{B} := \text{diag}(b_{1\ell}, \dots, b_{N\ell}) \in \mathbb{R}^{N \times N}$  and suppose that, at least, one  $b_{i\ell}$  is strictly positive, i.e., there exists some  $b_{i\ell} > 0$ . Assume that **A1** holds, then the following matrix

$$\mathbf{L}_\ell = \mathbf{L} + \mathbf{B}, \quad (3.56)$$

is symmetric, positive definite and of full rank.  $\diamond$

When time-delays are present in the interconnection of the followers network, the following assumption is considered

**A3.** The information exchange, from the  $j$ -th robot to the  $i$ -th robot, is subject to a variable time-delay  $T_{ji}(t)$  with a known upper-bound  ${}^*T_{ji}$ . Hence, it holds that  $0 \leq T_{ji}(t) \leq {}^*T_{ji} < \infty$ . Additionally, the time-delays have first and second bounded derivatives.

A fundamental lemma for the stability analysis of the consensus algorithms that consider variable time-delays, proposed and proved as Lemma 1 in Nuño, Basañez, Ortega, and Spong (2009), is the following:

**LEMMA 3.3:**

For any vector signals  $\mathbf{x}, \mathbf{y} \in \mathbb{R}^n$ , any variable time-delay  $0 \leq T(t) \leq {}^*T < \infty$  and any constant  $\alpha > 0$ , the following inequality holds

$$-2 \int_0^t \mathbf{x}^\top(\sigma) \int_{-T(\sigma)}^0 \mathbf{y}(\sigma + \theta) d\theta d\sigma \leq \alpha \|\mathbf{x}\|_2^2 + \frac{{}^*T^2}{\alpha} \|\mathbf{y}\|_2^2. \quad (3.57)$$

$\diamond$

### 3.3 Teleoperation systems

#### 3.3.1 SL-SR teleoperation system model

A teleoperation system, with a single local robot ( $\ell$ ) and a single remote robot ( $r$ ) as shown in Figure 3.10, can be seen as a particular case of a robot network with  $\bar{N} = \{1, 2\}$  and a Laplacian given by

$$\mathbf{L} = \begin{bmatrix} 1 & -1 \\ -1 & 1 \end{bmatrix}.$$



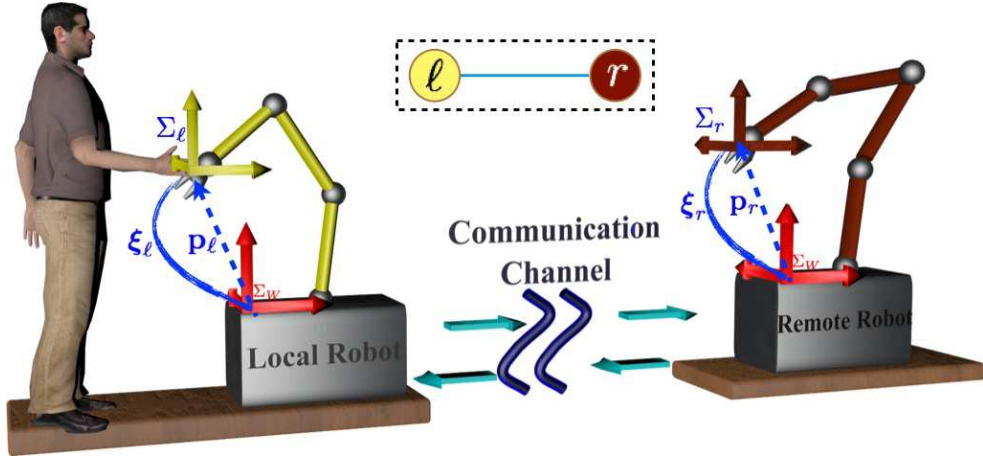


Figure 3.10: SL-SR teleoperation system.

Based on this last and on the node dynamics defined in (3.52), the operational space dynamic model of the teleoperation system is given by

$$\left. \begin{aligned} \mathbf{M}_\ell(\mathbf{q}_\ell)\dot{\mathbf{v}}_\ell + \mathbf{C}_\ell(\mathbf{q}_\ell, \dot{\mathbf{q}}_\ell)\mathbf{v}_\ell + \mathbf{g}_\ell(\mathbf{q}_\ell) &= \mathbf{f}_h - \mathbf{f}_\ell \\ \mathbf{M}_r(\mathbf{q}_r)\dot{\mathbf{v}}_r + \mathbf{C}_r(\mathbf{q}_r, \dot{\mathbf{q}}_r)\mathbf{v}_r + \mathbf{g}_r(\mathbf{q}_r) &= \mathbf{f}_r - \mathbf{f}_e \end{aligned} \right\}, \quad (3.58)$$

where  $\mathbf{f}_h := [\mathbf{h}_h^\top, \mathbf{m}_h^\top]^\top$  and  $\mathbf{f}_e := [\mathbf{h}_e^\top, \mathbf{m}_e^\top]^\top$  are the linear forces and moments induced by the human and environment, respectively.

### 3.3.2 CTS model

Another configuration for the teleoperation system defined in the last section is with a cooperative system composed of  $\mathcal{J}$  robot manipulators grasping a object at the remote site. In Figure 3.11 is shown an example with  $\mathcal{J} = 2$  and the associated reference frames. The following assumption is made about the cooperative system:

**A4.** All the  $\mathcal{J}$  end-effectors of the cooperative system are firmly attached to a rigid object, i.e., there is not relative motion between any of the  $\mathcal{J}$  end-effectors and the rigid object.

The operational space dynamics for each of the  $\mathcal{J}$  robot manipulators is similar to (3.48) and is given by

$$\mathbf{M}_i(\mathbf{q}_i)\ddot{\mathbf{r}}_i + \mathbf{C}_i(\mathbf{q}_i, \dot{\mathbf{q}}_i)\dot{\mathbf{r}}_i + \mathbf{g}_i(\mathbf{q}_i) = \mathbf{f}_i - \mathbf{f}_{o,i}, \quad (3.59)$$

where  $\mathbf{f}_{o,i} := [\mathbf{h}_{o,i}^\top, \mathbf{m}_{o,i}^\top]^\top$  are the linear forces and moments applied to the object.

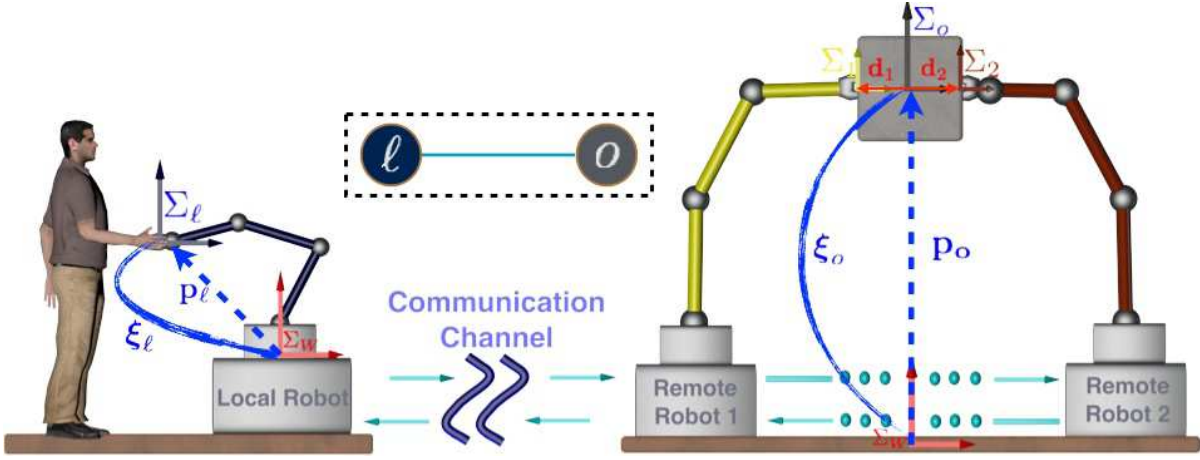


Figure 3.11: Teleoperation system with a single local robot and a remote cooperative system composed of two robots handling a common object.

The dynamical model of the object is given by

$$\mathbf{M}_o(\mathbf{r}_o)\dot{\mathbf{v}}_o + \mathbf{C}_o(\mathbf{r}_o, \dot{\mathbf{r}}_o)\mathbf{v}_o + \mathbf{g}_o(\mathbf{r}_o) = \mathbf{f}_o - \mathbf{f}_e, \quad (3.60)$$

where  $\mathbf{v}_o = [\dot{\mathbf{p}}_o^\top, \dot{\boldsymbol{\omega}}_o^\top]^\top$ ,  $\dot{\mathbf{v}}_o = [\ddot{\mathbf{p}}_o^\top, \ddot{\boldsymbol{\omega}}_o^\top]^\top$  stand for the object's velocities and accelerations, which can be obtained, due to A4, from any manipulator of the cooperative system.  $\mathbf{M}_o(\mathbf{r}_o)$ ,  $\mathbf{C}_o(\mathbf{r}_o, \dot{\mathbf{r}}_o)$ ,  $\mathbf{g}_o(\mathbf{r}_o)$  represent the inertia matrix, the Coriolis matrix and the gravity vector, respectively.  $\mathbf{f}_o = [\mathbf{h}_o^\top, \mathbf{m}_o^\top]^\top$  is the vector of the resultant linear forces and moments applied on the object by the  $\mathcal{J}$  robot manipulators and  $\mathbf{f}_e = [\mathbf{h}_e^\top, \mathbf{m}_e^\top]^\top$  is the vector of linear forces and moments exerted on the object by the environment.

The linear forces and moments acting on the object fulfill

$$\mathbf{h}_o = \sum_{i=1}^{\mathcal{J}} \mathbf{h}_{o,i}, \quad \mathbf{m}_o = \sum_{i=1}^{\mathcal{J}} \mathbf{m}_{o,i} + \sum_{i=1}^{\mathcal{J}} \mathbf{m}_{h_{o,i}}, \quad (3.61)$$

where  $\mathbf{m}_{h_{o,i}}$  are the moments generated by the linear forces  $\mathbf{h}_{o,i}$ . Relation (3.61) can be rewritten in matrix form as

$$\mathbf{f}_o = \sum_{i=1}^{\mathcal{J}} \mathbf{W}_i \mathbf{f}_i = \mathbf{W} \mathbf{f}, \quad (3.62)$$

where  $\mathbf{W} := [\mathbf{W}_1 \ \cdots \ \mathbf{W}_{\mathcal{J}}] \in \mathbb{R}^{6 \times 6\mathcal{J}}$ ,  $\mathbf{f} := [\mathbf{f}_1^\top, \dots, \mathbf{f}_{\mathcal{J}}^\top]^\top \in \mathbb{R}^{6\mathcal{J}}$  and  $\mathbf{W}_i \in \mathbb{R}^{6 \times 6}$  is a full row rank matrix called the grasp matrix (Walker, Freeman, and Marcus 1991) that relates the resultant forces and moments of the object with the linear forces and moments applied by the

$i$ -end effector at the contact point and is given by

$$\mathbf{W}_i = \begin{bmatrix} \mathbf{I}_3 & \mathbf{0}_3 \\ \mathbf{S}(\mathbf{d}_i) & \mathbf{I}_3 \end{bmatrix}, \quad (3.63)$$

where  $\mathbf{d}_i \in \mathbb{R}^3$ , defined as  $\mathbf{d}_i = [d_{i,x}, d_{i,y}, d_{i,z}]^\top$ , describes the position from the origin of the coordinate frame  $\Sigma_o$  to the origin of  $\Sigma_i$  with respect to  $\Sigma_W$ , see Figure 3.11. Invoking the principle of virtual work and using A4, returns the following relation

$$\dot{\mathbf{v}}_i = \mathbf{W}_i^\top \dot{\mathbf{v}}_o, \quad (3.64)$$

and hence  $\ddot{\mathbf{v}}_i = \mathbf{W}_i^\top \ddot{\mathbf{v}}_o + \dot{\mathbf{W}}_i^\top \dot{\mathbf{v}}_o$ . Therefore we can express the dynamical model (3.59) in the object's frame as

$$\mathbf{M}_i \mathbf{W}_i^\top \dot{\mathbf{v}}_o + \mathbf{M}_i \dot{\mathbf{W}}_i^\top \mathbf{v}_o + \mathbf{C}_i \mathbf{W}_i^\top \mathbf{v}_o + \mathbf{g}_i = \mathbf{f}_i - \mathbf{f}_{o,i}. \quad (3.65)$$

Replacing (3.62) in (3.60) and using (3.65), the complete *remote cooperative system dynamic model* is given by

$$\mathbf{M}_{rcs} \dot{\mathbf{v}}_o + \mathbf{C}_{rcs} \mathbf{v}_o + \mathbf{g}_{rcs} = \sum_{i=1}^{\mathcal{J}} \mathbf{W}_i \mathbf{f}_i - \mathbf{f}_e, \quad (3.66)$$

where

$$\begin{aligned} \mathbf{M}_{rcs} &:= \mathbf{M}_o + \sum_{i=1}^{\mathcal{J}} \mathbf{W}_i \mathbf{M}_i \mathbf{W}_i^\top, \\ \mathbf{C}_{rcs} &:= \mathbf{C}_o + \sum_{i=1}^{\mathcal{J}} \mathbf{W}_i \left[ \mathbf{M}_i \dot{\mathbf{W}}_i^\top + \mathbf{C}_i \mathbf{W}_i^\top \right], \\ \mathbf{g}_{rcs} &:= \mathbf{g}_o + \sum_{i=1}^{\mathcal{J}} \mathbf{W}_i \mathbf{g}_i. \end{aligned}$$

The dynamic model (3.66) also fulfills the properties **P9** to **P13**. This is based on the properties of each robot and on the boundedness and full rank properties of the grasp matrix.

Finally, the operational space dynamic model of the cooperative teleoperation system (CTS) is given by

$$\left. \begin{aligned} \mathbf{M}_\ell(\mathbf{q}_\ell) \dot{\mathbf{v}}_\ell + \mathbf{C}_\ell(\mathbf{q}_\ell, \dot{\mathbf{q}}_\ell) \mathbf{v}_\ell + \mathbf{g}_\ell(\mathbf{q}_\ell) &= \mathbf{f}_h - \mathbf{f}_\ell \\ \mathbf{M}_{rcs} \dot{\mathbf{v}}_o + \mathbf{C}_{rcs} \mathbf{v}_o + \mathbf{g}_{rcs} &= \sum_{i=1}^{\mathcal{J}} \mathbf{W}_i \mathbf{f}_i - \mathbf{f}_e \end{aligned} \right\}. \quad (3.67)$$



## CONSENSUS CONTROL

*This chapter presents three control schemes designed to solve the leader-follower and leaderless pose consensus problems of robot networks. The first scheme is designed for networks composed of robots that lack of velocity measurements. The second scheme is for robot networks with variable time-delays in the communication channels and the third scheme is for networks that are composed of robots with parametric uncertainty and variable time-delays in their communications. All the control schemes are distributed and designed to be implemented in networks of heterogeneous robots.*

## 4.1 Problem statement

Consider a network of  $N$  heterogeneous Euler-Lagrange systems in the operational space of the form (3.48). Assume that the interconnection fulfills the Assumption **A1** for the leaderless networks and the Assumptions **A1** and **A2** for the leader-follower networks. The objective is to find the controllers to solve the following two consensus problems:

**LFCP Leader-Follower Consensus Problem:** The network of  $N$  followers has to be regulated at a given constant leader pose  $\mathbf{x}_\ell := [\mathbf{p}_\ell^\top, \boldsymbol{\xi}_\ell^\top]^\top \in \mathbb{R}^7$ , provided that  $\mathbf{x}_\ell$  is only available to a certain set of followers. Hence, for all  $i \in \bar{N}$ ,

$$\lim_{t \rightarrow \infty} |\mathbf{v}_i(t)| = 0, \quad \lim_{t \rightarrow \infty} \mathbf{x}_i(t) = \mathbf{x}_\ell. \quad (4.1)$$

**LCP Leaderless Consensus Problem:** In the absence of a leader, the network of  $N$  agents has to asymptotically reach a consensus pose, denoted  $\mathbf{x}_c := [\mathbf{p}_c^\top, \boldsymbol{\xi}_c^\top]^\top \in \mathbb{R}^7$ . Hence, for all  $i \in \bar{N}$

$$\lim_{t \rightarrow \infty} |\mathbf{v}_i(t)| = 0, \quad \lim_{t \rightarrow \infty} \mathbf{x}_i(t) = \mathbf{x}_c. \quad (4.2)$$

The controllers have to be designed taking into account one or multiple of the following scenarios:

- Networks composed of robots without velocity measurements.
- Networks with variable time-delays in the communication channels.
- Networks composed of robots with uncertain kinematic and dynamic parameters and variable time-delay in their communications.

◇

The following lemmas are instrumental in the definition of the equilibrium points and the stability proofs of the proposed consensus algorithms.

**LEMMA 4.1** (Leader-follower network equilibrium points):

Suppose that, for a leader-follower network, Assumptions A1 and A2 hold. Then, the following equation

$$b_{i\ell} \Phi(\boldsymbol{\xi}_i) \mathbf{e}_{i\ell} + \sum_{j \in \mathcal{N}_i} a_{ij} \Phi(\boldsymbol{\xi}_i) \mathbf{e}_{ij} = \mathbf{0}_6, \quad (4.3)$$

where the matrix  $\Phi(\boldsymbol{\xi}_i)$  is defined in (3.34) and  $\mathbf{e}_{ij}$  is the interconnection error defined as

$$\mathbf{e}_{ij} := \mathbf{x}_i - \mathbf{x}_j, \quad (4.4)$$

has only two possible solutions, for all  $i \in \bar{N}$ , namely

$$(\mathbf{v}_i, \mathbf{p}_i, \boldsymbol{\xi}_i) = (\mathbf{0}_6, \mathbf{p}_\ell, \boldsymbol{\xi}_\ell), \quad (4.5)$$

and

$$(\mathbf{v}_i, \mathbf{p}_i, \boldsymbol{\xi}_i) = (\mathbf{0}_6, \mathbf{p}_\ell, -\boldsymbol{\xi}_\ell). \quad (4.6)$$

◇

*Proof.* Using (3.23), (3.33) and (3.34), the equation (4.3) can be separated in the following two equations,

$$b_{i\ell}(\mathbf{p}_i - \mathbf{p}_\ell) + \sum_{j \in \mathcal{N}_i} a_{ij}(\mathbf{p}_i - \mathbf{p}_j) = \mathbf{0}_3, \quad (4.7)$$

$$-b_{i\ell} \mathbf{U}^\top(\boldsymbol{\xi}_i) \boldsymbol{\xi}_\ell - \sum_{j \in \mathcal{N}_i} a_{ij} \mathbf{U}^\top(\boldsymbol{\xi}_i) \boldsymbol{\xi}_j = \mathbf{0}_3. \quad (4.8)$$

Defining,  $\mathbf{p} := [\mathbf{p}_1^\top, \dots, \mathbf{p}_N^\top]^\top$ , (4.7) can be written as

$$(\mathbf{B} \otimes \mathbf{I}_3)(\mathbf{p} - (\mathbf{1}_N \otimes \mathbf{p}_\ell)) + (\mathbf{L} \otimes \mathbf{I}_3)\mathbf{p} = \mathbf{0}_{3N},$$

where  $\otimes$  is the standard Kronecker product detailed in (a.1),  $\mathbf{B}$  is defined in Lemma 3.2 and  $\mathbf{L}$  is the Laplacian matrix defined in (3.53). Thus, since  $\mathbf{L}\mathbf{1}_N = \mathbf{0}_N$ , the last expression can be simplified as

$$(\mathbf{L}_\ell \otimes \mathbf{I}_3)(\mathbf{p} - (\mathbf{1}_N \otimes \mathbf{p}_\ell)) = \mathbf{0}_{3N},$$

where  $\mathbf{L}_\ell$  is defined in Lemma 3.2. Further, Lemma 3.2 and the Kronecker product properties ensure that  $\text{rank}(\mathbf{L}_\ell \otimes \mathbf{I}_3) = 3N$ ; thus, for all  $i \in \bar{N}$ ,  $\mathbf{p}_i = \mathbf{p}_\ell$  is the only solution to (4.7).

Now, defining  $\boldsymbol{\xi} := [\boldsymbol{\xi}_1^\top, \dots, \boldsymbol{\xi}_N^\top]^\top$  and  $\bar{\mathbf{U}} := \text{diag}(\mathbf{U}(\boldsymbol{\xi}_1), \dots, \mathbf{U}(\boldsymbol{\xi}_N)) \in \mathbb{R}^{4N \times 3N}$ , (4.8) can be written as

$$\bar{\mathbf{U}}^\top (\mathbf{A} \otimes \mathbf{I}_4)(\boldsymbol{\xi} - (\mathbf{1}_N \otimes \boldsymbol{\xi}_\ell)) + \bar{\mathbf{U}}^\top (\mathbf{L} \otimes \mathbf{I}_4)(\boldsymbol{\xi} - (\mathbf{1}_N \otimes \boldsymbol{\xi}_\ell)) = \mathbf{0}_{3N},$$

or, what is the same,  $\bar{\mathbf{U}}^\top (\mathbf{L}_\ell \otimes \mathbf{I}_4)(\boldsymbol{\xi} - (\mathbf{1}_N \otimes \boldsymbol{\xi}_\ell)) = \mathbf{0}_{3N}$ . Defining  $\mathbf{y} := (\mathbf{L}_\ell \otimes \mathbf{I}_4)(\boldsymbol{\xi} - (\mathbf{1}_N \otimes \boldsymbol{\xi}_\ell))$ , yields

$$\bar{\mathbf{U}}^\top(\boldsymbol{\xi})\mathbf{y} = \mathbf{0}_{3N}.$$

Note that this equation has only two possible solutions, namely  $\mathbf{y} = \mathbf{0}_{4N}$  or  $\mathbf{y} \in \ker(\bar{\mathbf{U}}^\top(\boldsymbol{\xi}))$ . On one hand,  $\mathbf{y} = \mathbf{0}_{4N}$  implies that  $\boldsymbol{\xi} = (\mathbf{1}_N \otimes \boldsymbol{\xi}_\ell)$ , because  $(\mathbf{L}_\ell \otimes \mathbf{I}_4)$  is of full rank. Hence this implies consensus at  $\boldsymbol{\xi}_i = \boldsymbol{\xi}_\ell$ . On the other hand, (4.8) can be also written as

$$-\mathbf{U}^\top(\boldsymbol{\xi}_i) \left[ b_{i\ell} \boldsymbol{\xi}_\ell + \sum_{j \in \mathcal{N}_i} a_{ij} \boldsymbol{\xi}_j \right] = \mathbf{0}_3,$$

and the other possible solutions have to live in  $\ker(\mathbf{U}^\top(\boldsymbol{\xi}_i))$ , which are in the  $\text{span}(\boldsymbol{\xi}_i)$ . This is due to the fact that  $b_{i\ell} \boldsymbol{\xi}_\ell + \sum_{j \in \mathcal{N}_i} a_{ij} \boldsymbol{\xi}_j$  vanishes only when  $\boldsymbol{\xi}_i = \boldsymbol{\xi}_\ell$ , because of the properties of matrix  $\mathbf{L}_\ell$ .

Now, since there is, at least one  $b_{i\ell} > 0$  for all  $i \in \bar{N}$ , then for any node  $i$ ,  $\boldsymbol{\xi}_i \in \text{span}(b_{i\ell} \boldsymbol{\xi}_\ell +$

$\sum_{j \in \mathcal{N}_i} a_{ij} \xi_j$ ), which are nothing but linear combinations of the leader unit-quaternion and the neighbors unit-quaternions. Hence, together with properties of matrix  $\mathbf{L}_\ell$  and the normality condition of the unit-quaternions, yields  $\xi_i = \pm \xi_\ell$  as the only possible solution to (4.8).  $\diamond \diamond \diamond$

**LEMMA 4.2** (Leaderless network equilibrium points):

Consider a leaderless network that fulfills **A1**. Then, the equation

$$\sum_{j \in \mathcal{N}_i} a_{ij} \Phi(\xi) \mathbf{e}_{ij} = \mathbf{0}_6, \quad (4.9)$$

where  $\Phi(\xi)$  is defined in (3.34) and  $\mathbf{e}_{ij}$  in (4.4), has only the following solutions for any  $\mathbf{p}_c \in \mathbb{R}^3$  and  $\xi_c \in S^3$ :

$$(\mathbf{v}_i, \mathbf{p}_i, \xi_i) = (\mathbf{0}_6, \mathbf{p}_c, \xi_c), \quad (4.10)$$

and

$$(\mathbf{v}_i, \mathbf{p}_i, \xi_i) = (\mathbf{0}_6, \mathbf{p}_c, -\xi_c). \quad (4.11)$$

$\diamond$

*Proof.* Following *verbatim* the steps of the proof of Lemma 4.1, it is easy to see that equation (4.1) can be separated in the two following equations:

$$(\mathbf{L} \otimes \mathbf{I}_3) \mathbf{p} = \mathbf{0}_{3N}, \quad (4.12)$$

and

$$\bar{\mathbf{U}}^\top (\mathbf{L} \otimes \mathbf{I}_4) \xi = \mathbf{0}_{3N}. \quad (4.13)$$

On one hand, since  $\text{rank}(\mathbf{L} \otimes \mathbf{I}_3) = 3(N - 1)$  due to **A1**, it can be seen that  $\mathbf{p} = (\mathbf{1}_N \otimes \mathbf{p}_c)$ , for any  $\mathbf{p}_c \in \mathbb{R}^3$ , is the only solution to (4.12). On the other hand, the trivial solution  $\xi = (\mathbf{1}_N \otimes \xi_c)$ , for any  $\xi_c \in S^3$ , satisfies (4.13). However, the fact that  $\text{rank}(\bar{\mathbf{U}}) = 3N$  and **P3** ensure that  $\xi_i = \pm \xi_c$ , for all  $i \in \bar{N}$ , are the only two possible solutions.  $\diamond \diamond \diamond$



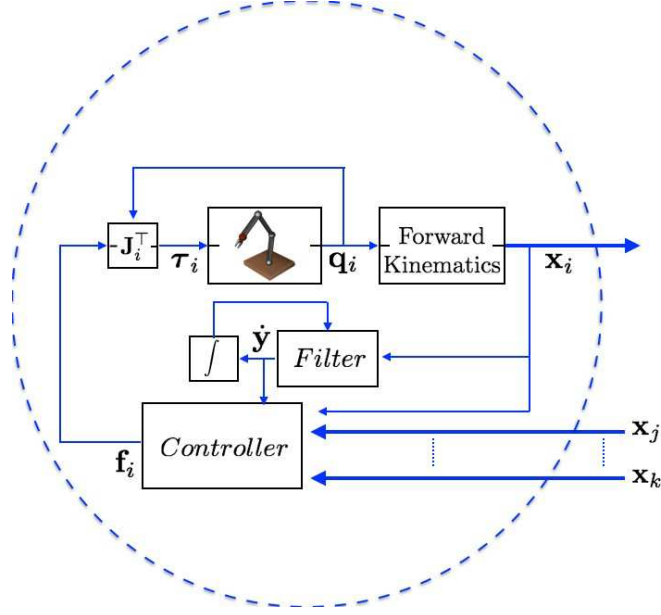


Figure 4.1: Block diagram of the control scheme that solves the consensus problems without velocity measurements using the controller proposed in equation (4.14).

## 4.2 Consensus control without velocity measurements

### 4.2.1 Leader-follower consensus

In order to solve the consensus problem in networks of robots without velocity measurements, the following controller is proposed

$$\left. \begin{aligned} \dot{\mathbf{y}}_i &= \mathbf{x}_i - k_{yi}\mathbf{y}_i \\ \mathbf{f}_i &= -k_i b_{i\ell} \Phi(\boldsymbol{\xi}_i) \mathbf{e}_{i\ell} - k_i \sum_{j \in \mathcal{N}_i} a_{ij} \Phi(\boldsymbol{\xi}_i) \mathbf{e}_{ij} + \mathbf{g}_i(\mathbf{q}_i) - d_i \Phi(\boldsymbol{\xi}_i) \dot{\mathbf{y}}_i \end{aligned} \right\} \quad (4.14)$$

where, for any pair  $(i, j)$ ,

$$\mathbf{e}_{ij} := \mathbf{x}_i - \mathbf{x}_j, \quad (4.15)$$

$\mathbf{y}_i \in \mathbb{R}^7$  is the filter state whose time derivative is used to indirectly inject damping, instead of the linear and angular velocities,  $k_i, d_i, k_{yi} \in \mathbb{R}_{>0}$  are the controller gains,  $\Phi(\boldsymbol{\xi})$  is defined in (3.34), and  $b_{i\ell} > 0$  if the leader's pose  $\mathbf{x}_\ell$  is available to the  $i$ th robot manipulator and  $b_{i\ell} = 0$ , otherwise. Figure 4.1 shows a block diagram of this control scheme.

The closed-loop system of (3.52) with (4.14) is

$$\left. \begin{aligned} \dot{\mathbf{y}}_i &= \mathbf{x}_i - k_{yi}\mathbf{y}_i \\ \dot{\mathbf{v}}_i &= -\mathbf{M}_i^{-1}(\mathbf{q}_i) \left[ \mathbf{C}_i(\mathbf{q}_i, \dot{\mathbf{q}}_i) \mathbf{v}_i + k_i b_{i\ell} \Phi(\boldsymbol{\xi}_i) \mathbf{e}_{i\ell} + k_i \sum_{j \in \mathcal{N}_i} a_{ij} \Phi(\boldsymbol{\xi}_i) \mathbf{e}_{ij} + d_i \Phi(\boldsymbol{\xi}_i) \dot{\mathbf{y}}_i \right] \end{aligned} \right\} \quad (4.16)$$

It can be seen that the equilibrium ( $\mathbf{v}_i = \dot{\mathbf{y}}_i = 0$ ) of the closed-loop (4.16) is the same as in (4.3), which in turn implies, using Lemma 4.1, that the two different equilibrium points, for all  $i \in \bar{N}$ , are:

$$(\mathbf{v}_i, \dot{\mathbf{y}}_i, \mathbf{p}_i, \boldsymbol{\xi}_i) = (\mathbf{0}_6, \mathbf{0}_7, \mathbf{p}_\ell, \boldsymbol{\xi}_\ell), \quad (4.17)$$

and

$$(\mathbf{v}_i, \dot{\mathbf{y}}_i, \mathbf{p}_i, \boldsymbol{\xi}_i) = (\mathbf{0}_6, \mathbf{0}_7, \mathbf{p}_\ell, -\boldsymbol{\xi}_\ell). \quad (4.18)$$

Even though  $\boldsymbol{\xi}_i = \boldsymbol{\xi}_\ell$  and  $\boldsymbol{\xi}_i = -\boldsymbol{\xi}_\ell$  represent the same orientation, in the proof of Proposition 4.1, it is shown that  $\boldsymbol{\xi}_i = -\boldsymbol{\xi}_\ell$  corresponds to an unstable equilibrium point.

**PROPOSITION 4.1:**

Consider a network of  $N$  robot manipulators, in the operational space, whose dynamics fulfills (3.52) and in closed-loop with the controller (4.14). Suppose that the Assumptions **A1** and **A2** hold. Furthermore, it is assumed that velocity measurements of the robots are not available. Under these conditions, the **LFCP** is solved, i.e.,

$$\lim_{t \rightarrow \infty} |\mathbf{v}_i(t)| = \lim_{t \rightarrow \infty} |\mathbf{e}_{i\ell}(t)| = 0, \quad \forall i \in \bar{N}.$$

Moreover,  $\boldsymbol{\xi}_i = \boldsymbol{\xi}_\ell$  is part of the asymptotically stable equilibrium point.  $\diamond$

*Proof.* Consider the following energy-like function

$$\mathcal{V}_i := \frac{1}{k_i} \mathcal{K}_i(\mathbf{v}_i) + \frac{b_{i\ell}}{2} |\mathbf{x}_i - \mathbf{x}_\ell|^2 + \frac{1}{4} \sum_{j \in \mathcal{N}_i} a_{ij} |\mathbf{x}_i - \mathbf{x}_j|^2, \quad (4.19)$$

where  $\mathcal{K}_i$  is the kinetic energy of the  $i$ th robot manipulator defined in (3.50), and the other two terms are the potential energy stored in a virtual leader-follower spring and in the virtual spring of every connected pair of robot manipulators  $(i, j)$ , respectively. Note that  $\mathcal{V}_i$  is positive definite and radially unbounded with regards to  $\mathbf{v}_i$ ,  $|\mathbf{x}_i - \mathbf{x}_\ell|$  and  $|\mathbf{x}_i - \mathbf{x}_j|$ , for all  $i \in \bar{N}$  and  $j \in \mathcal{N}_i$ .

Using (3.35), **P10** and the fact that  $\dot{\mathbf{x}}_\ell = \mathbf{0}_7$  ensure that  $\dot{\mathcal{V}}_i$ , evaluated along (4.16), is given by

$$\begin{aligned} \dot{\mathcal{V}}_i &= -\frac{d_i}{k_i} \dot{\mathbf{x}}_i^\top (\mathbf{x}_i - k_{yi} \mathbf{y}_i) - \sum_{j \in \mathcal{N}_i} a_{ij} \left( \dot{\mathbf{x}}_i^\top (\mathbf{x}_i - \mathbf{x}_j) - \frac{1}{2} (\dot{\mathbf{x}}_i - \dot{\mathbf{x}}_j)^\top (\mathbf{x}_i - \mathbf{x}_j) \right) \\ &= -\frac{d_i}{k_i} \dot{\mathbf{x}}_i^\top (\mathbf{x}_i - k_{yi} \mathbf{y}_i) - \frac{1}{2} \sum_{j \in \mathcal{N}_i} a_{ij} \left( (\dot{\mathbf{x}}_i + \dot{\mathbf{x}}_j)^\top (\mathbf{x}_i - \mathbf{x}_j) \right). \end{aligned} \quad (4.20)$$

Consider now the following total energy-like function

$$\mathcal{E} := \sum_{i \in \bar{N}} \left[ \mathcal{V}_i + \frac{d_i}{2k_i} |\mathbf{x}_i - k_{yi} \mathbf{y}_i|^2 \right], \quad (4.21)$$

where the second term is the scaled  $i$ th controller potential energy. The derivative of this total energy-like function is given by

$$\begin{aligned} \dot{\mathcal{E}} &= \sum_{i \in \bar{N}} \left[ \dot{\mathcal{V}}_i + \frac{d_i}{k_i} (\mathbf{x}_i - k_{yi} \mathbf{y}_i)^\top (\dot{\mathbf{x}}_i - k_{yi} \dot{\mathbf{y}}_i) \right] \\ &= \sum_{i \in \bar{N}} \left[ \frac{1}{2} \sum_{j \in \mathcal{N}_i} a_{ij} \left( (\dot{\mathbf{x}}_i + \dot{\mathbf{x}}_j)^\top (\mathbf{x}_i - \mathbf{x}_j) \right) - \frac{d_i k_{yi}}{k_i} |\mathbf{x}_i - k_{yi} \mathbf{y}_i|^2 \right]. \end{aligned}$$

According to Lemma 3.1, the first term inside the brackets in the last expression is equal to zero and thus,

$$\dot{\mathcal{E}} = - \sum_{i \in \bar{N}} \frac{d_i k_{yi}}{k_i} |\mathbf{x}_i - k_{yi} \mathbf{y}_i|^2 \leq 0. \quad (4.22)$$

On one hand, from (4.16),  $\mathbf{x}_i - k_{yi} \mathbf{y}_i = \mathbf{0}_7$  implies that  $\dot{\mathbf{y}}_i = \mathbf{0}_7$  and hence  $\ddot{\mathbf{y}}_i = \mathbf{0}_7$ . Noting that  $\ddot{\mathbf{y}}_i = \dot{\mathbf{x}}_i - k_{yi} \dot{\mathbf{y}}_i$  it also holds that  $\dot{\mathbf{x}}_i = \mathbf{0}_7$ . Now, since  $\mathbf{U}_i(\boldsymbol{\xi}_i)$  is a full column rank matrix, using (3.28) and  $\dot{\mathbf{x}}_i = \mathbf{0}_7$  implies that  $\mathbf{v}_i = \mathbf{0}_6$  and hence  $\dot{\mathbf{v}}_i = \mathbf{0}_6$ .

On the other hand,  $\mathcal{E}$  is positive definite and radially unbounded with regards to  $\mathbf{v}_i$ ,  $\mathbf{x}_i - \mathbf{x}_\ell$ ,  $\mathbf{x}_i - \mathbf{x}_j$  and  $\mathbf{x}_i - k_{yi} \mathbf{y}_i$ . Furthermore,  $\mathcal{E} \geq 0$  and  $\dot{\mathcal{E}} \leq 0$  ensures that  $\mathcal{E}(t) \leq \mathcal{E}(0)$  for all  $t$ . Recalling, the two possible equilibrium points (4.17) and (4.18) of the closed-loop system, and using (4.19) it is proved that  $\boldsymbol{\xi}_i = -\boldsymbol{\xi}_\ell$  corresponds to a maximum energy point. Since  $\mathcal{E}$  is a decreasing function, any perturbation from  $\boldsymbol{\xi}_i = -\boldsymbol{\xi}_\ell$  will drive the system to  $\boldsymbol{\xi}_i = \boldsymbol{\xi}_\ell$ , which corresponds to a minimum energy point. Hence, the equilibrium point (4.18) is unstable.

From this last and the fact that  $\mathbf{x}_i - k_{yi} \mathbf{y}_i = \mathbf{0}_7$  is inside the largest invariant set at which  $\dot{\mathcal{E}}$  vanishes, LaSalle's Invariant Theorem ensures that (4.17) is asymptotically stable for all the state space except at the unstable equilibrium point (4.18). This completes the proof.  $\diamond \diamond \diamond$

### 4.2.2 Leaderless consensus

The controller proposed to solve the **LCP** is also (4.14) but with  $b_{i\ell} = 0$  for all  $i \in \bar{N}$ . In this case, the closed-loop system becomes,

$$\left. \begin{aligned} \dot{\mathbf{y}}_i &= \mathbf{x}_i - k_{yi}\mathbf{y}_i \\ \dot{\mathbf{v}}_i &= -\mathbf{M}_i^{-1}(\mathbf{q}_i) \left[ \mathbf{C}_i(\mathbf{q}_i, \dot{\mathbf{q}}_i)\mathbf{v}_i + k_i \sum_{j \in \mathcal{N}_i} a_{ij}\mathbf{e}_{ij} + d_i\boldsymbol{\Psi}_i\dot{\mathbf{y}}_i \right] \end{aligned} \right\} \quad (4.23)$$

The equilibrium points of (4.23) fulfill  $\sum_{j \in \mathcal{N}_i} a_{ij}\tilde{\mathbf{p}}_{ij} = \mathbf{0}_3$  and  $\sum_{j \in \mathcal{N}_i} a_{ij}\tilde{\boldsymbol{\beta}}_{ij} = \mathbf{0}_3$ ,  $\forall i \in \bar{N}$  and using Lemma 4.2 it can be seen that the only two possible solutions are:

$$(\mathbf{v}_i, \dot{\mathbf{y}}_i, \mathbf{p}_i, \boldsymbol{\xi}_i) = (\mathbf{0}_6, \mathbf{0}_7, \mathbf{p}_c, \boldsymbol{\xi}_c), \quad (4.24)$$

and

$$(\mathbf{v}_i, \dot{\mathbf{y}}_i, \mathbf{p}_i, \boldsymbol{\xi}_i) = (\mathbf{0}_6, \mathbf{0}_7, \mathbf{p}_c, -\boldsymbol{\xi}_c). \quad (4.25)$$

#### PROPOSITION 4.2:

Consider a network of  $N$  robot manipulators, in the operational space, whose dynamics fulfills (3.52) and in closed-loop with the controller (4.14), with  $b_{i\ell} = 0$  for all  $i \in \bar{N}$ . If the Assumption **A1** holds and no velocity measurements of the robots are available, this controller solves the **LCP**, i.e.,  $\lim_{t \rightarrow \infty} |\mathbf{v}_i(t)| = 0$ ,  $\lim_{t \rightarrow \infty} \mathbf{x}_i(t) = \mathbf{x}_c$ ,  $\forall i \in \bar{N}$  and some  $\mathbf{x}_c \subset \mathbb{R}^7$ . Moreover,  $\boldsymbol{\xi}_i = \boldsymbol{\xi}_c$  is part of the asymptotically stable equilibrium.  $\diamond$

*Proof.* Similar to the proof of Proposition 4.1, the following total energy function based on (4.21) with  $b_{i\ell} = 0$  is proposed,

$$\mathcal{E} := \sum_{i \in \bar{N}} \left[ \frac{1}{k_i} \mathcal{K}_i(\mathbf{v}_i) + \frac{1}{4} \sum_{j \in \mathcal{N}_i} a_{ij} |\mathbf{x}_i - \mathbf{x}_j|^2 + \frac{d_i}{2k_i} |\mathbf{x}_i - k_{yi}\mathbf{y}_i|^2 \right]. \quad (4.26)$$

$\dot{\mathcal{E}}$ , evaluated along (4.23), satisfies (4.22). The rest of the proof follows *verbatim* the proof of Proposition 4.1. In this case, LaSalle's Invariant Theorem ensures that the equilibrium point (4.24) is almost globally asymptotically stable for all  $i \in \bar{N}$ .  $\diamond \diamond \diamond$

### 4.2.3 Human-robot interactions

Now, in the case that human forces  $\mathbf{f}_{h,i} := [\mathbf{h}_{h,i}^\top, \mathbf{m}_{h,i}^\top]^\top \in \mathbb{R}^6$  are injected into one or multiple robots, the dynamics (3.52) change to

$$\mathbf{M}_i(\mathbf{q}_i)\dot{\mathbf{v}}_i + \mathbf{C}_i(\mathbf{q}_i, \dot{\mathbf{q}}_i)\mathbf{v}_i + \mathbf{g}_i(\mathbf{q}_i) = \mathbf{f}_i + c_i\mathbf{f}_{h,i}, \quad (4.27)$$

where  $c_i = 1$  if a human interacts with robot  $i$  and  $c_i = 0$ , otherwise.

Since, in the leader-follower case, the equilibrium point  $(\mathbf{v}_i, \mathbf{p}_i, \boldsymbol{\xi}_i) = (\mathbf{0}_6, \mathbf{p}_\ell, \boldsymbol{\xi}_\ell)$  is *almost* globally attractive, when the human operator applies some forces the equilibrium point is changed. However, once the human forces become zero, all robots converge asymptotically to the point  $(\mathbf{0}_6, \mathbf{p}_\ell, \boldsymbol{\xi}_\ell)$ .

In the leaderless case, since the equilibrium point  $(\mathbf{v}_i, \mathbf{p}_i, \boldsymbol{\xi}_i) = (\mathbf{0}_6, \mathbf{p}_c, \boldsymbol{\xi}_c)$  is *almost* globally attractive for some  $\mathbf{p}_c \in \mathbb{R}^3$  and  $\boldsymbol{\xi}_c \in S^3$ , when the human operator applies forces the consensus point is dynamically changed and when the human forces become zero, if the robots are not in consensus, they find another consensus point that might be different from the original point. This fact increases the applicability of the leaderless consensus algorithm in the sense that the robot network can be *driven* by one or multiple human operators, which allows a wide range of practical implementations such as the formation control or the teleoperation of networks of robots by one or multiple operators. Motivated by these applications, the leaderless scheme is studied.

Hence, the closed-loop system (4.27) and (4.14), with all  $b_{i\ell} = 0$ , is

$$\left. \begin{aligned} \dot{\mathbf{y}}_i &= \mathbf{x}_i - k_{yi}\mathbf{y}_i \\ \dot{\mathbf{v}}_i &= -\mathbf{M}_i^{-1}(\mathbf{q}_i) \left[ \mathbf{C}_i(\mathbf{q}_i, \dot{\mathbf{q}}_i)\mathbf{v}_i + k_i \sum_{j \in \mathcal{N}_i} a_{ij} \mathbf{e}_{ij} + d_i \boldsymbol{\Psi}_i \dot{\mathbf{y}}_i - c_i \mathbf{f}_{h,i} \right] \end{aligned} \right\} \quad (4.28)$$

**PROPOSITION 4.3:**

*Assume that A1 holds. Suppose that one or multiple human operators inject forces in one or multiple robot manipulators whose dynamics satisfy (4.27). Then, the controller (4.14), with all  $b_{i\ell} = 0$ , ensures that  $\dot{\mathbf{y}}_i \in \mathcal{L}_\infty \cap \mathcal{L}_2$  and  $\mathbf{v}_i, \mathbf{e}_{ij} \in \mathcal{L}_\infty$  for all  $i \in \bar{N}$  and  $j \in \mathcal{N}_i$ , if the human operator is passive from force to velocity, that is,  $\forall t$  and  $\gamma_i \geq 0$  the following inequality holds*

$$-\int_0^t \mathbf{v}_i^\top(\sigma) \mathbf{f}_{h,i}(\sigma) d\sigma + \gamma_i \geq 0. \quad (4.29)$$

◇

*Proof.* The proof is established using the following energy function

$$\mathcal{T}_i := \frac{1}{k_i} \mathcal{K}_i(\mathbf{v}_i) + \frac{1}{4} \sum_{j \in \mathcal{N}_i} a_{ij} |\mathbf{x}_i - \mathbf{x}_j|^2 + \frac{c_i}{k_i} \left( \gamma_i - \int_0^t \mathbf{v}_i^\top(\sigma) \mathbf{f}_{h,i}(\sigma) d\sigma \right). \quad (4.30)$$

Using Lemma 3.1, P10 and relation (3.35) ensure that  $\dot{\mathcal{T}}_i$ , evaluated along (4.28), satisfies  $\dot{\mathcal{T}}_i = \dot{\mathcal{V}}_i$ , where  $\dot{\mathcal{V}}_i$  is defined in (4.20). Following *verbatim* the same steps after (4.20) in Proposition 4.1, it can be deduced that  $\mathcal{T}$  is positive definite and radially unbounded with regards to to  $\mathbf{v}_i$ ,  $\mathbf{x}_i - \mathbf{x}_j$  and  $\mathbf{x}_i - k_{yi} \mathbf{y}_i$ . Furthermore,  $\mathcal{T} \geq 0$  and  $\dot{\mathcal{T}} \leq 0$  ensures that  $\dot{\mathbf{y}}_i \in \mathcal{L}_2$  and  $\mathbf{v}_i, \dot{\mathbf{y}}_i, \mathbf{e}_{ij} \in \mathcal{L}_\infty$ .  $\diamond \diamond \diamond$

#### 4.2.4 Remarks

**Remark 4.1.** The case of a network with only two agents without velocity measurements exchanging information via the Laplacian matrix  $\mathbf{L} = \begin{bmatrix} 1 & -1 \\ -1 & 1 \end{bmatrix}$  is detailed in the next chapter. This is the scenario of a teleoperation system composed of one local and one remote robot manipulators with interaction with human and environment forces.

**Remark 4.2.** A clear theoretical extension of the proposed scheme is the inclusion of time-delays in the network interconnection. For this extension other Lyapunov–Krasovskii or Lyapunov–Razumikhin functionals to prove stability with time-delays need to be found or a strategy using an observer as in (Astolfi, Ortega, and Venkatraman 2010; Sarras, Nuño, Basañez, and Kinnaert ) can be followed. The disadvantage of the observer strategy is that the complete dynamic of the robot manipulators has to be known.

### 4.3 Consensus control with variable time-delays

#### 4.3.1 Leader-follower consensus

The controller presented in this section considers variable time-delays in the interconnection of all the robot manipulators and under this condition the LFCEP has to be solved. The proposed solution is established with the following operational space P+d injection controller

$$\mathbf{f}_i = -k_i b_{i\ell} \Phi(\boldsymbol{\xi}_i)(\mathbf{x}_i - \mathbf{x}_\ell) - k_i \sum_{j \in \mathcal{N}_i} a_{ij} \Phi(\boldsymbol{\xi}_i) \mathbf{e}_{ij} - d_i \mathbf{v}_i + \mathbf{g}_i(\mathbf{q}_i), \quad (4.31)$$

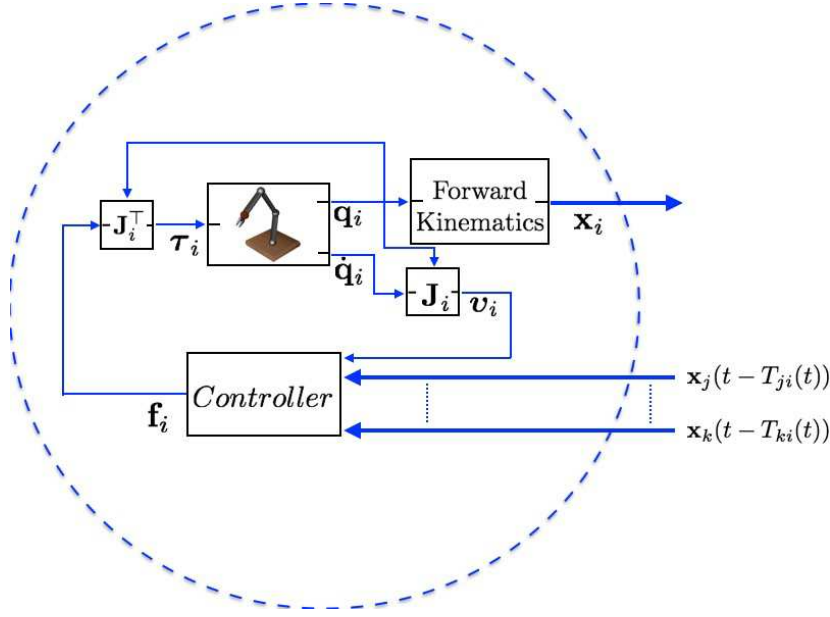


Figure 4.2: Block diagram of the control scheme that solves the consensus problem with variable time-delays in the interconnection using the controller proposed in equation (4.31).

where  $k_i, d_i \in \mathbb{R}_{>0}$  are the controller gains,  $b_{i\ell} > 0$  if the leader pose  $\mathbf{x}_\ell$  is available to the  $i$ th robot manipulator and  $b_{i\ell} = 0$ , otherwise. The interconnection error  $\mathbf{e}_{ij}$ , for any pair of robots  $(i, j)$ , is given by

$$\mathbf{e}_{ij} = \mathbf{x}_i - \mathbf{x}_j(t - T_{ji}(t)). \quad (4.32)$$

Figure 4.2 shows a block diagram of this control scheme. The closed-loop system of (3.52) with (4.31) is

$$\dot{\mathbf{v}}_i = -\mathbf{M}_i^{-1}(\mathbf{q}_i) \left[ \mathbf{C}_i(\mathbf{q}_i, \dot{\mathbf{q}}_i) \mathbf{v}_i + d_i \mathbf{v}_i + k_i b_{i\ell} \Phi(\boldsymbol{\xi}_i) (\mathbf{x}_i - \mathbf{x}_\ell) + k_i \sum_{j \in \mathcal{N}_i} a_{ij} \Phi(\boldsymbol{\xi}_i) \mathbf{e}_{ij} \right]. \quad (4.33)$$

This closed-loop system has two possible equilibria. Proposition 4.4 formally states this fact and Proposition 4.5 shows that one of them corresponds to an unstable equilibrium point.

**PROPOSITION 4.4:**

*If the Assumptions A1 and A2 are fulfilled, then the closed-loop system (4.33) has the following two different equilibrium points, for all  $i \in \bar{N}$ ,*

$$(\mathbf{v}_i, \mathbf{p}_i, \boldsymbol{\xi}_i) = (\mathbf{0}_6, \mathbf{p}_\ell, \boldsymbol{\xi}_\ell), \quad (4.34)$$

and

$$(\mathbf{v}_i, \mathbf{p}_i, \boldsymbol{\xi}_i) = (\mathbf{0}_6, \mathbf{p}_\ell, -\boldsymbol{\xi}_\ell). \quad (4.35)$$

◇

*Proof.* The possible equilibria of (4.33) satisfy  $\mathbf{v}_i = \mathbf{0}_6$  and thus  $b_{i\ell}\Phi(\boldsymbol{\xi}_i)\mathbf{e}_{i\ell} + \sum_{j \in \mathcal{N}_i} a_{ij}\Phi(\boldsymbol{\xi}_i)\mathbf{e}_{ij} = \mathbf{0}_6$ , which in turn implies that

$$b_{i\ell}(\mathbf{p}_i - \mathbf{p}_\ell) + \sum_{j \in \mathcal{N}_i} a_{ij}(\mathbf{p}_i - \mathbf{p}_j(t - T_{ji}(t))) = \mathbf{0}_3, \quad (4.36)$$

$$-b_{i\ell}\mathbf{U}^\top(\boldsymbol{\xi}_i)\boldsymbol{\xi}_\ell - \sum_{j \in \mathcal{N}_i} a_{ij}\mathbf{U}^\top(\boldsymbol{\xi}_i)\boldsymbol{\xi}_j(t - T_{ji}(t)) = \mathbf{0}_3. \quad (4.37)$$

Since,

$$\mathbf{p}_j(t - T_{ji}(t)) = \mathbf{p}_j - \int_{t-T_{ji}(t)}^t \dot{\mathbf{p}}_j(\sigma) d\sigma, \quad (4.38)$$

$$\boldsymbol{\xi}_j(t - T_{ji}(t)) = \boldsymbol{\xi}_j - \int_{t-T_{ji}(t)}^t \dot{\boldsymbol{\xi}}_j(\sigma) d\sigma, \quad (4.39)$$

and the fact that at the equilibrium,  $\int_{t-T_{ji}(t)}^t \dot{\mathbf{p}}_j(\sigma) d\sigma = \mathbf{0}_3$  and  $\int_{t-T_{ji}(t)}^t \dot{\boldsymbol{\xi}}_j(\sigma) d\sigma = \mathbf{0}_4$ , allows to write (4.36) and (4.37) as

$$\begin{aligned} b_{i\ell}(\mathbf{p}_i - \mathbf{p}_\ell) + \sum_{j \in \mathcal{N}_i} a_{ij}(\mathbf{p}_i - \mathbf{p}_j) &= \mathbf{0}_3, \\ -b_{i\ell}\mathbf{U}^\top(\boldsymbol{\xi}_i)\boldsymbol{\xi}_\ell - \sum_{j \in \mathcal{N}_i} a_{ij}\mathbf{U}^\top(\boldsymbol{\xi}_i)\boldsymbol{\xi}_j &= \mathbf{0}_3. \end{aligned}$$

These two equations are the same as the equations (4.7) and (4.8). The rest of the proof follows *verbatim* as the proof of Lemma 4.1. ◇◇◇

**PROPOSITION 4.5:**

If the Assumptions A1, A2 and A3 hold, the controller (4.31) solves the LFCEP provided that, for any  $\alpha_i, \alpha_j > 0$ , damping  $d_i$  satisfies

$$2d_i > k_i \left( \ell_{ii}\alpha_i + \sum_{j \in \mathcal{N}_i} a_{ji} \frac{*T_{ji}^2}{\alpha_j} \right), \quad \forall i \in \bar{N}. \quad (4.40)$$

Furthermore, the equilibrium (4.35) is unstable and the equilibrium (4.34) is asymptotically stable everywhere except at  $(\mathbf{0}_6, \mathbf{p}_\ell, -\boldsymbol{\xi}_\ell)$ . ◇



*Proof.* Using the energy-like function (4.19), and evaluating its time-derivative along (4.33), together with P10, relation (3.35) and the fact that  $\dot{\mathbf{x}}_\ell = \mathbf{0}_7$ , results in

$$\begin{aligned}\dot{\mathcal{V}}_i &= -\frac{d_i}{k_i}|\mathbf{v}_i|^2 - \sum_{j \in \mathcal{N}_i} a_{ij} \left[ \dot{\mathbf{x}}_i^\top \mathbf{e}_{ij} - \frac{1}{2}(\dot{\mathbf{x}}_i - \dot{\mathbf{x}}_j)^\top (\mathbf{x}_i - \mathbf{x}_j) \right] \\ &= -\frac{d_i}{k_i}|\mathbf{v}_i|^2 - \sum_{j \in \mathcal{N}_i} a_{ij} \dot{\mathbf{x}}_i^\top \int_{t-T_{ji}(t)}^t \dot{\mathbf{x}}_j(\sigma) d\sigma - \frac{1}{2} \sum_{j \in \mathcal{N}_i} a_{ij} (\dot{\mathbf{x}}_i + \dot{\mathbf{x}}_j)^\top (\mathbf{x}_i - \mathbf{x}_j).\end{aligned}\quad (4.41)$$

Hence, taking  $\mathcal{V} = \sum_{i \in \bar{N}} \mathcal{V}_i$  yields

$$\dot{\mathcal{V}} = - \sum_{i \in \bar{N}} \left[ \frac{d_i}{k_i} |\mathbf{v}_i|^2 + \sum_{j \in \mathcal{N}_i} a_{ij} \dot{\mathbf{x}}_i^\top \int_{t-T_{ji}(t)}^t \dot{\mathbf{x}}_j(\sigma) d\sigma + \frac{1}{2} \sum_{j \in \mathcal{N}_i} a_{ij} (\dot{\mathbf{x}}_i + \dot{\mathbf{x}}_j)^\top (\mathbf{x}_i - \mathbf{x}_j) \right],$$

after applying Lemma 3.1,  $\dot{\mathcal{V}}$  becomes

$$\dot{\mathcal{V}} = - \sum_{i \in \bar{N}} \left[ \frac{d_i}{k_i} |\mathbf{v}_i|^2 + \sum_{j \in \mathcal{N}_i} a_{ij} \dot{\mathbf{x}}_i^\top \int_{t-T_{ji}(t)}^t \dot{\mathbf{x}}_j(\sigma) d\sigma \right].$$

Since  $\mathcal{V}$  does not qualify as a Lyapunov Function, *i.e.*,  $\dot{\mathcal{V}} < 0$ , it is possible to integrate  $\dot{\mathcal{V}}$  from 0 to  $t$  and then apply Lemma 3.3 to the double integral terms. Furthermore, using (3.32), it yields,

$$\mathcal{V}(t) - \mathcal{V}(0) = - \sum_{i \in \bar{N}} \frac{d_i}{k_i} \left[ \int_\ell^t |\dot{\mathbf{x}}_i(\theta)|^2 d\theta + 3 \int_\ell^t |\dot{\boldsymbol{\xi}}_i(\theta)|^2 d\theta \right] - \sum_{i \in \bar{N}} \sum_{j \in \mathcal{N}_i} a_{ij} \int_\ell^t \dot{\mathbf{x}}_i^\top(\theta) \int_{\theta-T_{ji}(\theta)}^\theta \dot{\mathbf{x}}_j(\sigma) d\sigma d\theta,$$

and, for any  $\alpha_i > 0$  and  $i \in \bar{N}$ ,

$$\mathcal{V}(t) - \mathcal{V}(0) \leq - \sum_{i \in \bar{N}} \frac{d_i}{k_i} \left( \|\dot{\mathbf{x}}_i\|_2^2 + 3 \|\dot{\boldsymbol{\xi}}_i\|_2^2 \right) + \sum_{i \in \bar{N}} \sum_{j \in \mathcal{N}_i} a_{ij} \left( \frac{\alpha_i}{2} \|\dot{\mathbf{x}}_i\|_2^2 + \frac{*T_{ji}^2}{2\alpha_j} \|\dot{\mathbf{x}}_j\|_2^2 \right).$$

Moreover, recalling that  $\ell_{ii} = \sum_{j \in \mathcal{N}_i} a_{ij}$  then it holds that

$$\mathcal{V}(t) - \mathcal{V}(0) \leq - \sum_{i \in \bar{N}} \frac{3d_i}{k_i} \|\dot{\boldsymbol{\xi}}_i\|_2^2 + \sum_{i \in \bar{N}} \sum_{j \in \mathcal{N}_i} a_{ij} \frac{*T_{ji}^2}{2\alpha_j} \|\dot{\mathbf{x}}_j\|_2^2 - \sum_{i \in \bar{N}} \sum_{j \in \mathcal{N}_i} a_{ij} \left( \frac{d_i}{k_i \ell_{ii}} - \frac{\alpha_i}{2} \right) \|\dot{\mathbf{x}}_i\|_2^2,$$

which can be further written as

$$\mathcal{V}(t) + \sum_{i \in \bar{N}} \frac{3d_i}{k_i} \|\dot{\boldsymbol{\xi}}_i\|_2^2 + \mathbf{1}_N^\top \boldsymbol{\Psi} [\|\dot{\mathbf{x}}_1\|_2^2, \dots, \|\dot{\mathbf{x}}_N\|_2^2]^\top \leq \mathcal{V}(0),$$

where

$$\Psi = \begin{bmatrix} \frac{d_1}{k_1} - \frac{\ell_{11}\alpha_1}{2} & -\frac{a_{12}^*T_{21}^2}{2\alpha_1} & \dots & -\frac{a_{1N}^*T_{N1}^2}{2\alpha_1} \\ -\frac{a_{21}^*T_{12}^2}{2\alpha_2} & \frac{d_2}{k_2} - \frac{\ell_{22}\alpha_2}{2} & \dots & -\frac{a_{2N}^*T_{N2}^2}{2\alpha_2} \\ \vdots & \vdots & \ddots & \vdots \\ -\frac{a_{N1}^*T_{1N}^2}{2\alpha_N} & -\frac{a_{N2}^*T_{2N}^2}{2\alpha_N} & \dots & \frac{d_N}{k_N} - \frac{\ell_{NN}\alpha_N}{2} \end{bmatrix}. \quad (4.42)$$

Clearly, if  $d_i$  is set according to (4.40) then there exists  $\boldsymbol{\mu} \in \mathbb{R}^N$ , defined as  $\boldsymbol{\mu} := \Psi^\top \mathbf{1}_N$ , such that  $\mu_i > 0$ , for all  $i \in \bar{N}$ . Hence

$$\mathcal{V}(t) + \sum_{i \in \bar{N}} \left( \frac{3d_i}{k_i} \|\dot{\boldsymbol{\xi}}_i\|_2^2 + \mu_i \|\dot{\mathbf{x}}_i\|_2^2 \right) \leq \mathcal{V}(0). \quad (4.43)$$

Therefore,  $\dot{\mathbf{x}}_i \in \mathcal{L}_2$  and  $\mathcal{V} \in \mathcal{L}_\infty$ . This last implies that  $\mathbf{v}_i, |\mathbf{x}_i - \mathbf{x}_\ell|, |\mathbf{x}_i - \mathbf{x}_j| \in \mathcal{L}_\infty$ , for all  $i \in \bar{N}$  and  $j \in \mathcal{N}_i$ . All these bounded signals together with P11 and the fact that  $|\boldsymbol{\xi}_i| = 1$  ensure, from the closed-loop system (4.33), that  $\dot{\mathbf{v}} \in \mathcal{L}_\infty$ . Additionally, from (3.35),  $\dot{\mathbf{x}}_i \in \mathcal{L}_2$  implies that  $\mathbf{v}_i \in \mathcal{L}_2$ . Barbălat's Lemma with  $\mathbf{v}_i \in \mathcal{L}_\infty \cap \mathcal{L}_2$  and  $\dot{\mathbf{v}}_i \in \mathcal{L}_\infty$  supports the fact that  $\lim_{t \rightarrow \infty} \mathbf{v}_i(t) = \mathbf{0}_6$ , which in turn implies from (3.35) that  $\lim_{t \rightarrow \infty} \dot{\mathbf{x}}_i(t) = \mathbf{0}_7$ .

Boundedness of  $\dot{\mathbf{v}}_i, \mathbf{v}_i, |\mathbf{x}_i - \mathbf{x}_\ell|$  and  $|\mathbf{x}_i - \mathbf{x}_j|$ , together with P12, imply that  $\dot{\mathbf{v}}_i$  is uniformly continuous. Moreover, since

$$\lim_{t \rightarrow \infty} \int_0^t \dot{\mathbf{v}}_i(\sigma) d\sigma = \lim_{t \rightarrow \infty} \mathbf{v}_i(t) - \mathbf{v}_i(0) = -\mathbf{v}_i(0),$$

then  $\lim_{t \rightarrow \infty} \dot{\mathbf{v}}_i(t) = \mathbf{0}_6$ .

According to Proposition 4.4, it holds that, when  $\lim_{t \rightarrow \infty} \mathbf{v}_i(t) = \lim_{t \rightarrow \infty} \dot{\mathbf{v}}_i(t) = \mathbf{0}_6$ , the closed-loop system (4.33) has only two possible equilibrium points, namely (4.34) and (4.35). Using (4.19) it is shown that (4.34) corresponds to a minimum energy point and since  $\mathcal{V}(t)$  is a decreasing function, *i.e.*,  $\mathcal{V}(t) \leq \mathcal{V}(0)$ , any perturbation from (4.35) will drive the system to (4.34). Hence,  $(\mathbf{v}_i, \mathbf{p}_i, \boldsymbol{\xi}_i) = (\mathbf{0}_6, \mathbf{p}_\ell, \boldsymbol{\xi}_\ell)$  is asymptotically stable everywhere except at the unstable equilibrium point (4.35). This concludes the proof.  $\diamond \diamond \diamond$

### 4.3.2 Leaderless consensus

The solution to the LCP makes use of the P+d controller (4.31) but with all  $b_{i\ell} = 0$ , which means that there is not any leader pose available to the followers. In this case, the closed-loop system becomes

$$\dot{\mathbf{v}}_i = -\mathbf{M}_i^{-1}(\mathbf{q}_i) \left[ \mathbf{C}_i(\mathbf{q}_i, \dot{\mathbf{q}}_i) \mathbf{v}_i + d_i \mathbf{v}_i + k_i \sum_{j \in \mathcal{N}_i} a_{ij} \Phi(\boldsymbol{\xi}_i) \mathbf{e}_{ij} \right]. \quad (4.44)$$

Following *verbatim* the steps of the proof of Proposition 4.4, with  $b_{i\ell} = 0$ , it can be shown that the equilibrium points of the closed-loop (4.44) must satisfy  $\sum_{j \in \mathcal{N}_i} a_{ij} \Phi(\boldsymbol{\xi}_i) \mathbf{e}_{ij} = \mathbf{0}_6$ , and according to the Lemma 4.2, the closed-loop system (4.44) has two possible equilibrium points, namely

$$(\mathbf{v}_i, \mathbf{p}_i, \boldsymbol{\xi}_i) = (\mathbf{0}_6, \mathbf{p}_c, \boldsymbol{\xi}_c), \quad (4.45)$$

and

$$(\mathbf{v}_i, \mathbf{p}_i, \boldsymbol{\xi}_i) = (\mathbf{0}_6, \mathbf{p}_c, -\boldsymbol{\xi}_c). \quad (4.46)$$

The following proposition formally describes the solution to the LCP.

**PROPOSITION 4.6:**

Suppose that **A1** and **A3** hold, then controller (4.31), with  $b_{i\ell} = 0$ , solves the LCP provided that damping  $d_i$  satisfies (4.40), for any  $\alpha_i, \alpha_j > 0$ . Furthermore, the equilibrium  $(\mathbf{0}_6, \mathbf{p}_c, \boldsymbol{\xi}_c)$  is asymptotically stable everywhere except at  $(\mathbf{0}_6, \mathbf{p}_c, -\boldsymbol{\xi}_c)$ .  $\diamond$

*Proof.* This proof follows the same procedure of the proof of Proposition 4.5. Hence, only the main steps are given. Using (4.19) with  $b_{i\ell} = 0$  yields

$$\mathcal{V}_i := \frac{1}{k_i} \mathcal{K}_i(\mathbf{v}_i) + \frac{1}{4} \sum_{j \in \mathcal{N}_i} a_{ij} |\mathbf{x}_i - \mathbf{x}_j|^2. \quad (4.47)$$

Let us now define  $\mathcal{V} := \sum_{i \in \bar{N}} \mathcal{V}_i$ . **P10**, Lemma 3.1 and relation (3.35) allow to show that  $\dot{\mathcal{V}}$ , evaluated along (4.44), satisfies

$$\dot{\mathcal{V}} = - \sum_{i \in \bar{N}} \left[ \frac{d_i}{k_i} |\mathbf{v}_i|^2 + \sum_{j \in \mathcal{N}_i} a_{ij} \dot{\mathbf{x}}_i^\top \int_{t-T_{ji}(t)}^t \dot{\mathbf{x}}_j(\sigma) d\sigma \right].$$

After integration, from 0 to  $t$ , invoking Lemma 3.3 and using (3.32), for any  $\alpha_i > 0$  and  $i \in \bar{N}$ , yields

$$\mathcal{V}(t) - \mathcal{V}(0) \leq - \sum_{i \in \bar{N}} \frac{3d_i}{k_i} \|\dot{\boldsymbol{\xi}}_i\|_2^2 + \sum_{i \in \bar{N}} \sum_{j \in \mathcal{N}_i} a_{ij} \frac{{}^*T_{ji}^2}{2\alpha_j} \|\dot{\mathbf{x}}_j\|_2^2 - \sum_{i \in \bar{N}} \sum_{j \in \mathcal{N}_i} a_{ij} \left( \frac{d_i}{k_i \ell_{ii}} - \frac{\alpha_i}{2} \right) \|\dot{\mathbf{x}}_i\|_2^2.$$

Setting  $d_i$  satisfying (4.40) ensures that there exists  $\mu_i > 0$  such that

$$\mathcal{V}(t) + \sum_{i \in \bar{N}} \left( \frac{3d_i}{k_i} \|\dot{\boldsymbol{\xi}}_i\|_2^2 + \mu_i \|\dot{\mathbf{x}}_i\|_2^2 \right) \leq \mathcal{V}(0).$$

The rest of the proof follows *verbatim* the last part of the proof of Proposition 4.5 with the additional fact that, in this case,  $(\mathbf{v}_i, \mathbf{p}_i, \boldsymbol{\xi}_i) = (\mathbf{0}_6, \mathbf{p}_c, \boldsymbol{\xi}_c)$  corresponds to the minimum energy equilibria, for any  $\mathbf{x}_c \subset \mathbb{R}^7$ . Thus, it is an asymptotically stable equilibrium point everywhere except at the unstable equilibrium point  $(\mathbf{0}_6, \mathbf{p}_c, -\boldsymbol{\xi}_c)$ .  $\diamond \diamond \diamond$

### 4.3.3 Human-robot interactions

As in section 4.2.3, the effects of the human interaction for the leaderless consensus are studied in this section. In this case the closed-loop system of (4.27) with (4.31), with all  $b_{i\ell} = 0$ , is given by

$$\dot{\mathbf{v}}_i = -\mathbf{M}_i^{-1}(\mathbf{q}_i) \left[ \mathbf{C}_i(\mathbf{q}_i, \dot{\mathbf{q}}_i) \mathbf{v}_i + d_i \mathbf{v}_i + k_i \sum_{j \in \mathcal{N}_i} a_{ij} \boldsymbol{\Phi}(\boldsymbol{\xi}_i) \mathbf{e}_{ij} - c_i \mathbf{f}_{h,i} \right]. \quad (4.48)$$

#### PROPOSITION 4.7:

Assume that A1 and A3 hold. Suppose that one or multiple human operators inject forces in one or multiple robot manipulators whose dynamics satisfy (4.27). Then the controller (4.31), with all  $b_{i\ell} = 0$ , ensures that  $\mathbf{v}_i \in \mathcal{L}_\infty \cap \mathcal{L}_2$  and  $|\mathbf{x}_i - \mathbf{x}_j| \in \mathcal{L}_\infty$ , for all  $i \in \bar{N}$  and  $j \in \mathcal{N}_i$ , if

i) condition (4.40) is satisfied for any  $\alpha_i, \alpha_j > 0$  and the human operator is passive from force to velocity, that is, the inequality (4.29) holds.

ii) the following damping condition is fulfilled, for any  $\delta_i, \alpha_i, \alpha_j > 0$  and  $c_i \in \{0, 1\}$ ,

$$2d_i > c_i \delta_i + k_i \left( \ell_{ii} \alpha_i + \sum_{j \in \mathcal{N}_i} a_{ji} \frac{{}^*T_{ji}^2}{\alpha_j} \right). \quad (4.49)$$

$\diamond$

*Proof.* The proof of claim i) is established using the energy function defined in (4.30). Using (3.35) and P10 ensure that  $\dot{\mathcal{T}}_i$ , evaluated along (4.48), satisfies  $\dot{\mathcal{T}}_i = \dot{\mathcal{V}}_i$ , where  $\dot{\mathcal{V}}_i$  is defined in (4.41). Since  $\mathcal{T}_i$  is positive definite and radially unbounded w.r.t.  $\mathbf{v}_i$  and  $|\mathbf{x}_i - \mathbf{x}_j|$ , following *verbatim* the same steps after (4.41) in Proposition 4.5, it is shown that  $\mathbf{v}_i \in \mathcal{L}_\infty \cap \mathcal{L}_2$  and  $|\mathbf{x}_i - \mathbf{x}_j| \in \mathcal{L}_\infty$ .

The proof of claim ii) employs the energy function given in (4.47). In this case,  $\dot{\mathcal{V}}_i$  evaluated along (4.48) yields

$$\dot{\mathcal{V}}_i = -\frac{d_i}{k_i}|\mathbf{v}_i|^2 + \frac{c_i}{k_i}\mathbf{v}_i^\top \mathbf{f}_{h,i} - \sum_{j \in \mathcal{N}_i} a_{ij} \dot{\mathbf{x}}_i^\top \int_{t-T_{ji}(t)}^t \dot{\mathbf{x}}_j(\sigma) d\sigma - \frac{1}{2} \sum_{j \in \mathcal{N}_i} a_{ij} (\dot{\mathbf{x}}_i + \dot{\mathbf{x}}_j)^\top (\mathbf{x}_i - \mathbf{x}_j),$$

following a similar procedure as in the proof of Proposition 4.6, using  $\mathcal{V} = \sum_{i \in \bar{N}} \mathcal{V}_i$ , it holds that

$$\dot{\mathcal{V}} = - \sum_{i \in \bar{N}} \left[ \frac{d_i}{k_i} |\mathbf{v}_i|^2 + \sum_{j \in \mathcal{N}_i} a_{ij} \dot{\mathbf{x}}_i^\top \int_{t-T_{ji}(t)}^t \dot{\mathbf{x}}_j(\sigma) d\sigma - \frac{c_i}{k_i} \mathbf{v}_i^\top \mathbf{f}_{h,i} \right],$$

invoking Young's inequality, for any  $\delta_i > 0$ , to the crossed term  $\frac{c_i}{k_i} \mathbf{v}_i^\top \mathbf{f}_{h,i}$  results in

$$\dot{\mathcal{V}} \leq - \sum_{i \in \bar{N}} \left[ \frac{1}{k_i} \left( d_i - \frac{c_i \delta_i}{2} \right) |\mathbf{v}_i|^2 - \frac{c_i}{2\delta_i k_i} |\mathbf{f}_{h,i}|^2 + \sum_{j \in \mathcal{N}_i} a_{ij} \dot{\mathbf{x}}_i^\top \int_{t-T_{ji}(t)}^t \dot{\mathbf{x}}_j(\sigma) d\sigma \right].$$

Integrating  $\dot{\mathcal{V}}$  from 0 to  $t$  and invoking Lemma 3.3 yields

$$\mathcal{V}(t) + \sum_{i \in \bar{N}} \frac{3}{k_i} \left( d_i - \frac{c_i \delta_i}{2} \right) \|\dot{\boldsymbol{\xi}}_i\|_2^2 + \mathbf{1}_N^\top (\boldsymbol{\Psi} - \boldsymbol{\Theta}) \left[ \|\dot{\mathbf{x}}_1\|_2^2, \dots, \|\dot{\mathbf{x}}_N\|_2^2 \right]^\top \leq \mathcal{V}(0) + \sum_{i \in \bar{N}} \frac{c_i}{2\delta_i k_i} \|\mathbf{f}_{h,i}\|_2^2,$$

where  $\boldsymbol{\Psi}$  has been defined in (4.42) and  $\boldsymbol{\Theta} := \text{diag}(\frac{c_1 \delta_1}{2k_1}, \dots, \frac{c_N \delta_N}{2k_N})$ . Since  $\delta_i$  can be chosen as small as desired,  $d_i > \frac{c_i \delta_i}{2}$  is always satisfied. Furthermore, if  $d_i$  is set satisfying (4.49) then there exists  $\epsilon \in \mathbb{R}^N$ , defined as  $\epsilon := (\boldsymbol{\Psi} - \boldsymbol{\Theta})^\top \mathbf{1}_N$ , such that  $\epsilon_i > 0$ , for all  $i \in \bar{N}$ . Hence

$$\mathcal{V}(t) + \sum_{i \in \bar{N}} \epsilon_i \|\dot{\mathbf{x}}_i\|_2^2 \leq \mathcal{V}(0) + \sum_{i \in \bar{N}} \frac{c_i}{2\delta_i k_i} \|\mathbf{f}_{h,i}\|_2^2. \quad (4.50)$$

Now, the fact that  $\mathbf{f}_{h,i} \in \mathcal{L}_2$  ensures that  $\dot{\mathbf{x}}_i \in \mathcal{L}_2$  and  $\mathcal{V} \in \mathcal{L}_\infty$ , which in turn implies that  $\mathbf{v}_i, |\mathbf{x}_i - \mathbf{x}_j| \in \mathcal{L}_\infty$ . Additionally, from (3.35),  $\dot{\mathbf{x}}_i \in \mathcal{L}_2$  implies that  $\mathbf{v}_i \in \mathcal{L}_2$ .  $\diamond \diamond \diamond$

#### 4.3.4 Remarks

**Remark 4.3.** If the network is composed by only two agents exchanging information via the Laplacian matrix  $\mathbf{L} = \begin{bmatrix} 1 & -1 \\ -1 & 1 \end{bmatrix}$ , then condition (4.40) is satisfied if the controller gains are set as  $4d_1d_2 > (*T_{12} + *T_{21})^2 k_1 k_2$ . This scenario defines a teleoperation system composed of one local and one remote manipulator and is detailed in the next chapter.

**Remark 4.4.** In order to obtain a physical interpretation of the damping condition (4.40), let us further elaborate on (4.40) focussing on the case that all  $\alpha_i$  are equal, i.e.,  $\alpha_i = \alpha$  for all  $i \in \bar{N}$  and any  $\alpha > 0$ . This yields

$$2d_i\alpha > k_i \left( \ell_{ii}\alpha^2 + \sum_{j \in \mathcal{N}_i} a_{ji} *T_{ji}^2 \right),$$

which is an inequality of the form  $x_1\alpha^2 + x_2\alpha + x_3 > 0$ , where  $x_1 := -k_i\ell_{ii}$ ,  $x_2 := 2d_i$  and  $x_3 := -k_i \sum_{j \in \mathcal{N}_i} a_{ji} *T_{ji}^2$ . Clearly, a sufficient condition for the existence of a real positive  $\alpha$  is  $x_2^2 - 4x_1x_3 > 0$  that is

$$d_i > k_i \sqrt{\ell_{ii} \sum_{j \in \mathcal{N}_i} a_{ji} *T_{ji}^2}. \quad (4.51)$$

Note that the P+d controller interconnects the agents via a virtual spring. Without delays such interconnection is passive and, by injecting any positive damping  $d_i$ , the leader-follower and the leaderless consensus problems can be solved. However, the interconnection delays *generate* extra energy and the interconnection is not longer passive. Condition (4.51) can be interpreted as the amount of extra damping that has to be injected in the system in order to dissipate the energy generated by the interconnecting delays. Obviously, this generated energy is a function of the bound of the delays  $*T_{ji}$  and the interconnection *strength* given by  $k_i$  and  $a_{ji}$ .

## 4.4 Consensus control with uncertain parameters and variable time-delays

The scheme proposed in this section considers the case when the kinematic and the dynamic physical parameters of the robots are uncertain and there exist variable time-delays in the interconnection channels. Under these conditions the proposed controller solves the **LF**CP and the **L**CP.

Due to kinematic uncertainties, the real Jacobian cannot be employed in the controller. Therefore, the present scheme, based on the property **P2**, makes use of an estimated Jacobian that satisfies the following relation

$$\hat{\mathbf{J}}_i(\mathbf{q}_i)\dot{\mathbf{q}}_i = \mathbf{Y}_{Ki}(\mathbf{q}_i, \dot{\mathbf{q}}_i)\hat{\boldsymbol{\theta}}_{Ki}, \quad (4.52)$$

Furthermore, since the Jacobian is not available, the operational space model (3.52) cannot be employed here. Thus, the controller is designed in the joint space (3.45), where, the dynamics of the  $i$ th node is given by

$$\bar{\mathbf{M}}_i(\mathbf{q}_i)\ddot{\mathbf{q}}_i + \bar{\mathbf{C}}_i(\mathbf{q}_i, \dot{\mathbf{q}}_i)\dot{\mathbf{q}}_i + \bar{\mathbf{g}}_i(\mathbf{q}_i) = \boldsymbol{\tau}_i. \quad (4.53)$$

#### 4.4.1 Leader-follower consensus

The proposed adaptive controller that solves the **LFCP** is given by

$$\boldsymbol{\tau}_i = -\mathbf{Y}_{Di}(\mathbf{q}_i, \dot{\mathbf{q}}_i, \phi_i, \dot{\phi}_i)\hat{\boldsymbol{\theta}}_{Di} - \kappa_i \hat{\mathbf{J}}_i^\top(\mathbf{q}_i)\hat{\mathbf{J}}_i(\mathbf{q}_i)\boldsymbol{\epsilon}_i, \quad (4.54)$$

where  $\kappa_i \in \mathbb{R}_{>0}$ . The controller is based on **P8** and relation (4.52). Two estimation laws are designed, the first one is for the estimation of the kinematic parameters,  $\hat{\boldsymbol{\theta}}_{Ki}$ , given by

$$\dot{\hat{\boldsymbol{\theta}}}_{Ki} := \boldsymbol{\Gamma}_{Ki}\mathbf{Y}_{Ki}^\top(\mathbf{q}_i, \dot{\mathbf{q}}_i) \left[ \mathbf{v}_i + \hat{\mathbf{J}}_i(\mathbf{q}_i)\phi_i \right], \quad (4.55)$$

with  $\boldsymbol{\Gamma}_{Ki} = \boldsymbol{\Gamma}_{Ki}^\top > 0$ . The second one is for the estimation of the dynamic parameters,  $\hat{\boldsymbol{\theta}}_{Di}$ ,

$$\dot{\hat{\boldsymbol{\theta}}}_{Di} := \boldsymbol{\Gamma}_{Di}\mathbf{Y}_{Di}^\top\boldsymbol{\epsilon}_i, \quad (4.56)$$

with  $\boldsymbol{\Gamma}_{Di} = \boldsymbol{\Gamma}_{Di}^\top > 0$ . The auxiliary signals,  $\boldsymbol{\epsilon}_i$  and  $\phi_i$ , that are used by the control law (4.54) and the estimation laws (4.55) and (4.56), are defined as

$$\boldsymbol{\epsilon}_i := \dot{\mathbf{q}}_i + \phi_i, \quad (4.57)$$

$$\phi_i := \hat{\mathbf{J}}_i^\dagger(\mathbf{q}_i)\boldsymbol{\Phi}(\boldsymbol{\xi}_i)\mathbf{e}_i, \quad (4.58)$$

$$\dot{\phi}_i = \hat{\mathbf{J}}_i^\dagger(\mathbf{q}_i)\boldsymbol{\Phi}(\boldsymbol{\xi}_i)\mathbf{e}_i + \hat{\mathbf{J}}_i^\dagger(\mathbf{q}_i)\frac{d}{dt}(\boldsymbol{\Phi}(\boldsymbol{\xi}_i)\mathbf{e}_i) \quad (4.59)$$

$$= \hat{\mathbf{J}}_i^\dagger(\mathbf{q}_i)\boldsymbol{\Phi}(\boldsymbol{\xi}_i)\mathbf{e}_i + \hat{\mathbf{J}}_i^\dagger(\mathbf{q}_i) \left[ \dot{\boldsymbol{\Phi}}(\boldsymbol{\xi}_i)\mathbf{e}_i + \boldsymbol{\Phi}(\boldsymbol{\xi}_i)\dot{\mathbf{e}}_i \right], \quad (4.60)$$

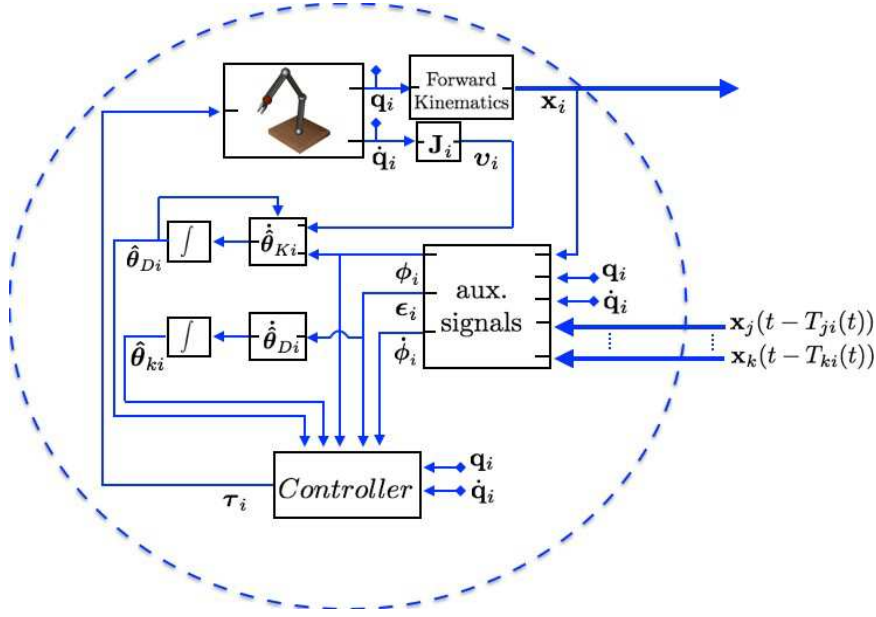


Figure 4.3: Block diagram of the control scheme that solves the consensus problem with uncertain parameters and variable time-delays in the interconnection using the controller proposed in equation (4.54).

where  $e_i$  is the pose error, between the  $i$ th robot, and the leader and its neighbors, it is defined as

$$e_i := b_{i\ell}(\mathbf{x}_i - \mathbf{x}_\ell) + \sum_{j \in \mathcal{N}_i} a_{ij} [\mathbf{x}_i - \mathbf{x}_j(t - T_{ji}(t))], \quad (4.61)$$

and its derivative is given by

$$\dot{e}_i = b_{i\ell} \dot{\mathbf{x}}_i + \sum_{j \in \mathcal{N}_i} a_{ij} \left[ \dot{\mathbf{x}}_i - (1 - \dot{T}_{ji}(t)) \dot{\mathbf{x}}_j(t - T_{ji}(t)) \right], \quad (4.62)$$

where  $b_{i\ell} > 0$  if the leader's pose  $\mathbf{x}_\ell$  is available to the  $i$ th robot and  $b_{i\ell} = 0$ , otherwise.

The control law (4.54) applied to (4.53) yields the following closed-loop system

$$\bar{\mathbf{M}}_i(\mathbf{q}_i) \dot{e}_i + \bar{\mathbf{C}}_i(\mathbf{q}_i, \dot{\mathbf{q}}_i) e_i + \kappa_i \hat{\mathbf{J}}_i^\top(\mathbf{q}_i) \hat{\mathbf{J}}_i(\mathbf{q}_i) e_i = \mathbf{Y}_{Di} \tilde{\boldsymbol{\theta}}_{Di}, \quad (4.63)$$

with  $\tilde{\boldsymbol{\theta}}_{Di} := \boldsymbol{\theta}_{Di} - \hat{\boldsymbol{\theta}}_{Di}$ . Figure 4.3 shows a block diagram of this control scheme.

#### PROPOSITION 4.8:

Consider a robot network in which the kinematic and the dynamic parameters are uncertain and the Assumptions **A1**, **A2** and **A3** hold. Additionally assume that, for any  $\alpha_i > 0$ , the following



condition is fulfilled

$$1 > \sum_{j \in \mathcal{N}_i} a_{ij} \left( \alpha_i + \frac{*T_{ji}^2}{\alpha_j} \right). \quad (4.64)$$

Then, the controller given by (4.54), (4.57), (4.58) and (4.59) together with the kinematic and dynamic parameter estimation laws (4.55) and (4.56), respectively, solves the **LFCEP** everywhere except when  $(\dot{\mathbf{x}}_i(0), \mathbf{p}_i(0), \boldsymbol{\xi}_i(0)) = (\mathbf{0}_7, \mathbf{p}_\ell, -\boldsymbol{\xi}_\ell)$  for all  $i \in \bar{N}$ .  $\diamond$

*Proof.* As usual in the adaptive control design, consider the following energy-like function

$$\mathcal{W}_i = \frac{1}{2} \left[ \boldsymbol{\epsilon}_i^\top \bar{\mathbf{M}}_i(\mathbf{q}_i) \boldsymbol{\epsilon}_i + \tilde{\boldsymbol{\theta}}_{Di}^\top \boldsymbol{\Gamma}_{Di}^{-1} \tilde{\boldsymbol{\theta}}_{Di} \right], \quad (4.65)$$

evaluating  $\dot{\mathcal{W}}_i$  along (4.63), using **P7**, the fact that  $\dot{\tilde{\boldsymbol{\theta}}}_{Di} = -\dot{\tilde{\boldsymbol{\theta}}}_{Di}$ , and the estimation law (4.56) yields

$$\dot{\mathcal{W}}_i = -\kappa_i |\hat{\mathbf{J}}_i(\mathbf{q}_i) \boldsymbol{\epsilon}_i|^2 \leq 0, \quad (4.66)$$

since  $\mathcal{W}_i$  is positive definite and radially unbounded with regards to  $\boldsymbol{\epsilon}_i$  and  $\tilde{\boldsymbol{\theta}}_{Di}$  and  $\dot{\mathcal{W}}_i \leq 0$ , the signals  $\hat{\mathbf{J}}_i(\mathbf{q}_i) \boldsymbol{\epsilon}_i \in \mathcal{L}_2$  and  $\boldsymbol{\epsilon}_i, \tilde{\boldsymbol{\theta}}_{Di} \in \mathcal{L}_\infty$ . Now, pre-multiplying (4.57) by  $\hat{\mathbf{J}}_i(\mathbf{q}_i)$  and using (3.25) and (4.52) yields

$$\hat{\mathbf{J}}_i(\mathbf{q}_i) \boldsymbol{\epsilon}_i = \mathbf{v}_i + \hat{\mathbf{J}}_i(\mathbf{q}_i) \boldsymbol{\phi}_i + \mathbf{Y}_{Ki}(\mathbf{q}_i, \dot{\mathbf{q}}_i) \tilde{\boldsymbol{\theta}}_{Ki},$$

hence,  $\dot{\mathcal{W}}_i$  can be rewritten as

$$\dot{\mathcal{W}}_i = -\kappa_i \left[ |\mathbf{v}_i + \hat{\mathbf{J}}_i(\mathbf{q}_i) \boldsymbol{\phi}_i|^2 + |\mathbf{Y}_{Ki}(\mathbf{q}_i, \dot{\mathbf{q}}_i) \tilde{\boldsymbol{\theta}}_{Ki}|^2 \right] - 2\kappa_i \tilde{\boldsymbol{\theta}}_{Ki}^\top \mathbf{Y}_{Ki}^\top(\mathbf{q}_i, \dot{\mathbf{q}}_i) \left[ \mathbf{v}_i + \hat{\mathbf{J}}_i(\mathbf{q}_i) \boldsymbol{\phi}_i \right].$$

The form of  $\dot{\mathcal{W}}_i$  motivates to propose the following function

$$\mathcal{Z}_i = \frac{1}{\kappa_i} \mathcal{W}_i + \tilde{\boldsymbol{\theta}}_{Ki}^\top \boldsymbol{\Gamma}_{Ki}^{-1} \tilde{\boldsymbol{\theta}}_{Ki}, \quad (4.67)$$

then, using the kinematic parameters estimation law (4.55), the derivative of the function (4.67) is given by

$$\begin{aligned} \dot{\mathcal{Z}}_i &= -|\mathbf{v}_i + \hat{\mathbf{J}}_i(\mathbf{q}_i) \boldsymbol{\phi}_i|^2 - |\mathbf{Y}_{Ki}(\mathbf{q}_i, \dot{\mathbf{q}}_i) \tilde{\boldsymbol{\theta}}_{Ki}|^2 \\ &= -|\mathbf{v}_i|^2 - 2\mathbf{v}_i^\top \hat{\mathbf{J}}_i(\mathbf{q}_i) \boldsymbol{\phi}_i - |\hat{\mathbf{J}}_i(\mathbf{q}_i) \boldsymbol{\phi}_i|^2 - |\mathbf{Y}_{Ki}(\mathbf{q}_i, \dot{\mathbf{q}}_i) \tilde{\boldsymbol{\theta}}_{Ki}|^2, \end{aligned}$$

using the definition of  $\boldsymbol{\phi}_i$  given in the equation (4.58), together with (3.35), ensures that

$$\dot{\mathcal{Z}}_i = -|\mathbf{v}_i|^2 - |\boldsymbol{\Phi}(\boldsymbol{\xi}_i) \mathbf{e}_i|^2 - |\mathbf{Y}_{Ki} \tilde{\boldsymbol{\theta}}_{Ki}|^2 - 2\dot{\mathbf{x}}_i^\top \mathbf{e}_i.$$

Now, a total energy-like function,  $\mathcal{H}_i$ , is proposed as

$$\mathcal{H}_i = \mathcal{Z}_i + b_{i\ell} |\mathbf{x}_i - \mathbf{x}_\ell|^2 + \frac{1}{2} \sum_{j \in \mathcal{N}_i} a_{ij} |\mathbf{x}_i - \mathbf{x}_j|^2. \quad (4.68)$$

After some simple algebraic manipulations and using (4.61),  $\dot{\mathcal{H}}_i$  is given by

$$\dot{\mathcal{H}}_i = -|\mathbf{v}_i|^2 - |\Phi(\boldsymbol{\xi}_i) \mathbf{e}_i|^2 - \sum_{j \in \mathcal{N}_i} a_{ij} (\dot{\mathbf{x}}_i + \dot{\mathbf{x}}_j)^\top (\mathbf{x}_i - \mathbf{x}_j) - |\mathbf{Y}_{Ki} \tilde{\boldsymbol{\theta}}_{Ki}|^2 - 2 \sum_{j \in \mathcal{N}_i} a_{ij} \dot{\mathbf{x}}_i^\top \int_{t-T_{ji}(t)}^t \dot{\mathbf{x}}_j(\sigma) d\sigma,$$

where, to obtain the last expression, the following transformation has been used

$$\int_{t-T_{ji}(t)}^t \dot{\mathbf{x}}_j(\sigma) d\sigma = \mathbf{x}_j - \mathbf{x}_j(t - T_{ji}(t)).$$

Hence, taking  $\mathcal{H} = \sum_{i \in \bar{N}} \mathcal{H}_i$  and using Lemma 3.1 and relation (3.32), it holds that

$$\dot{\mathcal{H}} = - \sum_{i \in \bar{N}} \left[ |\dot{\mathbf{x}}_i|^2 + 3|\dot{\boldsymbol{\xi}}_i|^2 + |\Phi(\boldsymbol{\xi}_i) \mathbf{e}_i|^2 + |\mathbf{Y}_{Ki} \tilde{\boldsymbol{\theta}}_{Ki}|^2 \right] - 2 \sum_{i \in \bar{N}} \sum_{j \in \mathcal{N}_i} a_{ij} \dot{\mathbf{x}}_i^\top \int_{t-T_{ji}(t)}^t \dot{\mathbf{x}}_j(\sigma) d\sigma. \quad (4.69)$$

$\mathcal{H}$  does not qualify as a Lyapunov Function, i.e., it does not satisfy  $\dot{\mathcal{H}} < 0$ . Then,  $\dot{\mathcal{H}}$  is integrated from 0 to  $t$  and the Lemma 3.3 is applied to the double integral terms with  $\alpha_i \in \mathbb{R}_{>0}$ . This yields

$$\mathcal{H}(0) \geq \mathcal{H}(t) + \sum_{i \in \bar{N}} \left( \|\Phi(\boldsymbol{\xi}_i) \mathbf{e}_i\|_2^2 + \|\mathbf{Y}_{Ki} \tilde{\boldsymbol{\theta}}_{Ki}\|_2^2 \right) + \sum_{i \in \bar{N}} \sum_{j \in \mathcal{N}_i} a_{ij} \left[ \left( \frac{1}{\ell_{ii}} - \alpha_i \right) \|\dot{\mathbf{x}}_i\|_2^2 - \frac{*T_{ji}^2}{\alpha_i} \|\dot{\mathbf{x}}_j\|_2^2 \right],$$

where the fact that  $\ell_{ii} := \sum_{j \in \mathcal{N}_i} a_{ij}$  has also been used. Defining the matrix  $\mathbf{\Lambda} \in \mathbb{R}^{N \times N}$  as

$$\mathbf{\Lambda} := \begin{bmatrix} 1 - \ell_{11} \alpha_1 & -\frac{a_{12} * T_{21}^2}{\alpha_1} & \dots & -\frac{a_{1N} * T_{N1}^2}{\alpha_1} \\ -\frac{a_{12} * T_{12}^2}{\alpha_2} & 1 - \ell_{22} \alpha_2 & \dots & -\frac{a_{2N} * T_{N2}^2}{\alpha_2} \\ \vdots & \vdots & \ddots & \vdots \\ -\frac{a_{1N} * T_{1N}^2}{\alpha_N} & -\frac{a_{2N} * T_{2N}^2}{\alpha_N} & \dots & 1 - \ell_{NN} \alpha_N \end{bmatrix},$$

yields  $\mathcal{H}(0) \geq \mathcal{H}(t) + \sum_{i \in \bar{N}} \left( \|\Phi(\boldsymbol{\xi}_i) \mathbf{e}_i\|_2^2 + \|\mathbf{Y}_{Ki} \tilde{\boldsymbol{\theta}}_{Ki}\|_2^2 \right) + \mathbf{1}_N^\top \mathbf{\Lambda} [\|\dot{\mathbf{x}}_1\|_2^2, \dots, \|\dot{\mathbf{x}}_N\|_2^2]^\top$ .

Setting all  $\alpha_i$  and the interconnection weights  $a_{ij}$  such that the condition (4.64) is fulfilled,

there exists  $\boldsymbol{\mu} \in \mathbb{R}^N$ , defined as  $\boldsymbol{\mu} := \boldsymbol{\Lambda}^\top \mathbf{1}_N$ , such that  $\mu_i > 0$ , for all  $i \in \bar{N}$ . Hence

$$\mathcal{H}(0) \geq \mathcal{H}(t) + \sum_{i \in \bar{N}} \left( \|\Phi(\boldsymbol{\xi}_i) \mathbf{e}_i\|_2^2 + \|\mathbf{Y}_{K_i} \tilde{\boldsymbol{\theta}}_{K_i}\|_2^2 + \mu_i \|\dot{\mathbf{x}}_i\|_2^2 \right).$$

Since  $\mathcal{H}(0)$  is a positive constant and  $\mathcal{H}(t) > 0$ , then  $\Phi(\boldsymbol{\xi}_i) \mathbf{e}_i, \mathbf{Y}_{K_i} \tilde{\boldsymbol{\theta}}_{K_i}, \dot{\mathbf{x}}_i \in \mathcal{L}_2$  and  $\mathcal{H} \in \mathcal{L}_\infty$ . Furthermore,  $\mathcal{H}$  is positive definite and radially unbounded with regards to  $\boldsymbol{\epsilon}_i, \tilde{\boldsymbol{\theta}}_{D_i}, \tilde{\boldsymbol{\theta}}_{K_i}, |\mathbf{x}_i - \mathbf{x}_\ell|, |\mathbf{x}_i - \mathbf{x}_j|$ , hence  $\mathcal{H} \in \mathcal{L}_\infty$  ensures that all these signals are also bounded.

On one hand, **P5**,  $\dot{\mathbf{x}}_i \in \mathcal{L}_2$  and  $\tilde{\boldsymbol{\theta}}_{K_i}, |\mathbf{x}_i - \mathbf{x}_\ell|, |\mathbf{x}_i - \mathbf{x}_j| \in \mathcal{L}_\infty$ , for all  $i \in \bar{N}$  and  $j \in \mathcal{N}_i$ , together with **P1** imply that  $\Phi(\boldsymbol{\xi}_i) \mathbf{e}_i, \phi_i \in \mathcal{L}_\infty$ . On the other hand,  $\boldsymbol{\epsilon}_i, \phi_i \in \mathcal{L}_\infty$  ensures that  $\dot{\mathbf{q}}_i \in \mathcal{L}_\infty$ , which together with **P1** and **P5**, implies that  $\dot{\mathbf{x}}_i \in \mathcal{L}_\infty$ . Boundedness of  $\dot{\mathbf{x}}_i$  and **A3** implies that  $\dot{\boldsymbol{\epsilon}}_i$  is also bounded.

Hence the Assumption **A3**, the properties **P1** and **P5**, and boundedness of  $\dot{\mathbf{q}}_i, \dot{\mathbf{x}}_i$  and  $\dot{\boldsymbol{\epsilon}}_i$  imply that  $\dot{\phi}_i \in \mathcal{L}_\infty$  and, consequently,  $\frac{d}{dt} (\Phi(\boldsymbol{\xi}_i) \mathbf{e}_i) \in \mathcal{L}_\infty$ . Now, boundedness of all these signals ensure, from the closed-loop system (4.63), that  $\dot{\boldsymbol{\epsilon}}_i \in \mathcal{L}_\infty$ . Since  $\dot{\boldsymbol{\epsilon}}_i = \dot{\mathbf{q}}_i + \dot{\phi}_i$ ,  $\dot{\mathbf{q}}_i \in \mathcal{L}_\infty$ . Furthermore,  $\ddot{\mathbf{x}}_i = \Phi^\top(\boldsymbol{\xi}_i) \left[ \mathbf{J}_i(\mathbf{q}_i) \ddot{\mathbf{q}}_i + \dot{\mathbf{J}}_i(\mathbf{q}_i) \dot{\mathbf{q}}_i \right] + \dot{\Phi}^\top(\boldsymbol{\xi}_i) \mathbf{J}_i(\mathbf{q}_i) \dot{\mathbf{q}}_i$ , thus **P1**, **P5**, and  $\dot{\mathbf{x}}_i, \dot{\mathbf{q}}_i, \dot{\mathbf{q}}_i \in \mathcal{L}_\infty$  ensure that  $\ddot{\mathbf{x}}_i \in \mathcal{L}_\infty$ .

Finally,  $\Phi(\boldsymbol{\xi}_i) \mathbf{e}_i, \dot{\mathbf{x}}_i \in \mathcal{L}_2 \cap \mathcal{L}_\infty$  and  $\frac{d}{dt} (\Phi(\boldsymbol{\xi}_i) \mathbf{e}_i), \ddot{\mathbf{x}}_i \in \mathcal{L}_\infty$  yields, by Barbálat's Lemma,

$$\lim_{t \rightarrow \infty} |\Phi(\boldsymbol{\xi}_i(t)) \mathbf{e}_i(t)| = \lim_{t \rightarrow \infty} |\dot{\mathbf{x}}_i(t)| = 0,$$

and, from **P3** and (3.35),  $\lim_{t \rightarrow \infty} |\mathbf{v}_i(t)| = 0$ . Note that  $\lim_{t \rightarrow \infty} |\dot{\mathbf{x}}_i(t)| = 0$  implies that  $\int_{t-T_{j_i}(t)}^t \dot{\mathbf{x}}_j(\sigma) d\sigma = \mathbf{x}_j - \mathbf{x}_j(t - T_{j_i}(t)) = \mathbf{0}_7$ . This and  $\Phi(\boldsymbol{\xi}_i) \mathbf{e}_i = \mathbf{0}_6$  ensure that

$$b_{i\ell}(\mathbf{p}_i - \mathbf{p}_\ell) + \sum_{j \in \mathcal{N}_i} a_{ij}(\mathbf{p}_i - \mathbf{p}_j) = \mathbf{0}_3, \quad (4.70)$$

$$b_{i\ell} \mathbf{U}^\top(\boldsymbol{\xi}_i)(\boldsymbol{\xi}_i - \boldsymbol{\xi}_\ell) + \sum_{j \in \mathcal{N}_i} a_{ij} \mathbf{U}^\top(\boldsymbol{\xi}_i)(\boldsymbol{\xi}_i - \boldsymbol{\xi}_j) = \mathbf{0}_3. \quad (4.71)$$

in base of these two equations and the Lemma 4.1, it can be ensured that the two different equilibrium points, for all  $i \in \bar{N}$ , are:

$$(\mathbf{v}_i, \mathbf{p}_i, \boldsymbol{\xi}_i) = (\mathbf{0}_6, \mathbf{p}_\ell, \boldsymbol{\xi}_\ell), \quad (4.72)$$

and

$$(\mathbf{v}_i, \mathbf{p}_i, \boldsymbol{\xi}_i) = (\mathbf{0}_6, \mathbf{p}_\ell, -\boldsymbol{\xi}_\ell). \quad (4.73)$$

Using (4.68) it can be shown that  $\boldsymbol{\xi}_i = \boldsymbol{\xi}_\ell$  corresponds to a minimum energy point and, since

$\mathcal{H}(t)$  is a decreasing function, *i.e.*,  $\mathcal{H}(0) \geq \mathcal{H}(t)$  for all  $t \geq 0$ , any perturbation from the other equilibrium point  $\xi_i = -\xi_\ell$  will drive the system to  $\xi_i = \xi_\ell$ . Hence, the equilibrium point (4.72) is asymptotically stable everywhere except at the unstable equilibrium point (4.73). This concludes the proof.  $\diamond \diamond \diamond$

#### 4.4.2 Leaderless consensus

The LCP is solved using the same controller as in the LFCEP with the only difference being the absence of the leader and thus  $b_{i\ell} = 0$ , for all  $i \in \bar{N}$ .

##### PROPOSITION 4.9:

Consider a robot network in which the kinematic and the dynamic parameters are uncertain and the Assumptions A1 and A3 hold. Additionally assume that, for any  $\alpha_i > 0$ , condition (4.64) holds. Then, in the absence of a leader, the controller given by (4.54), (4.57), (4.58) and (4.59) together with the kinematic and dynamic parameter estimation laws (4.55) and (4.56), respectively, solves the LCP everywhere except when  $(\dot{\mathbf{x}}_i(0), \mathbf{p}_i(0), \xi_i(0)) = (\mathbf{0}_7, \mathbf{p}_c, -\xi_c)$  for all  $i \in \bar{N}$ .  $\diamond$

*Proof.* The proof follows *verbatim* the proof of Proposition 4.8 and hence only the main steps are given. In this case,  $b_{i\ell} = 0$  and the error equation (4.61) becomes

$$\mathbf{e}_i = \sum_{j \in \mathcal{N}_i} a_{ij} [\mathbf{x}_i - \mathbf{x}_j(t - T_{ji}(t))].$$

Furthermore, the total energy-like function (4.68) transforms to

$$\mathcal{H}_i = \mathcal{Z}_i + \frac{1}{2} \sum_{j \in \mathcal{N}_i} a_{ij} |\mathbf{x}_i - \mathbf{x}_j|^2.$$

Taking  $\mathcal{H} = \sum_{i \in \bar{N}} \mathcal{H}_i$ , yields the same time-derivative as in (4.69). Following the same procedure after (4.69), it is proved, also by the Barbălat's Lemma, that

$$\lim_{t \rightarrow \infty} |\Phi(\xi_i(t)) \mathbf{e}_i(t)| = \lim_{t \rightarrow \infty} |\dot{\mathbf{x}}_i(t)| = 0.$$

In this case, (4.70) and (4.71), respectively, become

$$\begin{aligned} \sum_{j \in \mathcal{N}_i} a_{ij} (\mathbf{p}_i - \mathbf{p}_j) &= \mathbf{0}_3, \\ \sum_{j \in \mathcal{N}_i} a_{ij} \mathbf{U}^\top(\xi_i) (\xi_i - \xi_j) &= \mathbf{0}_3. \end{aligned}$$

and using this time the Lemma 4.2, it can be shown that the two equilibrium points, for all  $i \in \bar{N}$ , are:

$$(\mathbf{v}_i, \mathbf{p}_i, \boldsymbol{\xi}_i) = (\mathbf{0}_6, \mathbf{p}_c, \boldsymbol{\xi}_c),$$

and

$$(\mathbf{v}_i, \mathbf{p}_i, \boldsymbol{\xi}_i) = (\mathbf{0}_6, \mathbf{p}_c, -\boldsymbol{\xi}_c).$$

Similar to the proof of Proposition 4.8,  $\boldsymbol{\xi}_i = \boldsymbol{\xi}_c$  corresponds to a minimum energy point and since  $\mathcal{H}(t)$  is a decreasing function, any perturbation from  $\boldsymbol{\xi}_i = -\boldsymbol{\xi}_c$  will drive the system to  $\boldsymbol{\xi}_i = \boldsymbol{\xi}_c$ . Hence,  $(\mathbf{v}_i, \mathbf{p}_i, \boldsymbol{\xi}_i) = (\mathbf{0}_6, \mathbf{p}_c, \boldsymbol{\xi}_c)$  is asymptotically stable everywhere except at the unstable equilibrium point  $(\mathbf{v}_i, \mathbf{p}_i, \boldsymbol{\xi}_i) = (\mathbf{0}_6, \mathbf{p}_c, -\boldsymbol{\xi}_c)$ . This concludes the proof.  $\diamond \diamond \diamond$

### 4.4.3 Human-robot interactions

As in section 4.2.3, the effects of the human interaction for the leaderless consensus are studied in this section. The node's dynamic in the joint space when human forces are injected is given by

$$\bar{\mathbf{M}}_i(\mathbf{q}_i)\ddot{\mathbf{q}}_i + \bar{\mathbf{C}}_i(\mathbf{q}_i, \dot{\mathbf{q}}_i)\dot{\mathbf{q}}_i + \bar{\mathbf{g}}_i(\mathbf{q}_i) = \boldsymbol{\tau}_i + c_i\boldsymbol{\tau}_{h,i} \quad (4.74)$$

where  $\boldsymbol{\tau}_{h,i}$  are the joint torques corresponding to the forces exerted by the human and  $c_i = 1$  if a human interacts with robot  $i$  and  $c_i = 0$ , otherwise. The control law (4.54) with  $b_{i\ell} = 0$  applied to (4.74) yields the following closed-loop system

$$\bar{\mathbf{M}}_i(\mathbf{q}_i)\dot{\boldsymbol{\epsilon}}_i + \bar{\mathbf{C}}_i(\mathbf{q}_i, \dot{\mathbf{q}}_i)\boldsymbol{\epsilon}_i + \kappa_i \hat{\mathbf{J}}_i^\top(\mathbf{q}_i)\hat{\mathbf{J}}_i(\mathbf{q}_i)\boldsymbol{\epsilon}_i = \mathbf{Y}_{Di}\tilde{\boldsymbol{\theta}}_{Di} + c_i\boldsymbol{\tau}_{h,i}. \quad (4.75)$$

#### PROPOSITION 4.10:

*Suppose a robot network in which the kinematic and the dynamic parameters are uncertain and the Assumptions A1 and A3 hold. Besides, one or multiple human operators inject forces in one or multiple robot manipulators whose dynamics satisfy (4.74). Then controller given by (4.54), (4.57), (4.58) and (4.59) together with the kinematic and dynamic parameter estimation laws (4.55) and (4.56), ensures that  $\boldsymbol{\epsilon}_i \in \mathcal{L}_\infty$ , for all  $i \in \bar{N}$  and  $j \in \mathcal{N}_i$ , if the joint torques injected by the human are bounded, i.e.  $\boldsymbol{\tau}_{h,i} \in \mathcal{L}_\infty$*

*Proof.* Using (4.65), evaluating  $\dot{\mathcal{W}}_i$  along (4.75) and following a similar procedure to the proof of Proposition 4.8, results

$$\dot{\mathcal{W}}_i = -\kappa_i |\hat{\mathbf{J}}_i(\mathbf{q}_i)\boldsymbol{\epsilon}_i|^2 + c_i \boldsymbol{\epsilon}_i^\top \boldsymbol{\tau}_{h,i}.$$

Using Young's inequality, yields

$$\dot{\mathcal{W}}_i \leq -\kappa_i |\hat{\mathbf{J}}_i(\mathbf{q}_i)\boldsymbol{\epsilon}_i|^2 + c_i \frac{\kappa_i}{2} |\hat{\mathbf{J}}_i(\mathbf{q}_i)\boldsymbol{\epsilon}_i|^2 + c_i \frac{|\boldsymbol{\tau}_{h,i}|^2}{2\kappa_i}, \quad (4.76)$$

note that if  $c_i = 0$ , the last equation is equal to (4.66) with which boundedness of  $\boldsymbol{\epsilon}_i$  is proved. But if  $c_i = 1$ , (4.76) can be simplified to

$$\dot{\mathcal{W}}_i \leq -\frac{\kappa_i}{2} |\hat{\mathbf{J}}_i(\mathbf{q}_i)\boldsymbol{\epsilon}_i|^2 + \frac{|\boldsymbol{\tau}_{h,i}|^2}{2\kappa_i}.$$

Since  $\boldsymbol{\tau}_{h,i} \in \mathcal{L}_\infty$ , clearly, if  $|\hat{\mathbf{J}}_i(\mathbf{q}_i)\boldsymbol{\epsilon}_i|^2 > \frac{|\boldsymbol{\tau}_{h,i}|^2}{\kappa_i^2}$  then it exists  $\rho > 0$  such that  $\dot{\mathcal{W}}_i \leq -\rho |\hat{\mathbf{J}}_i(\mathbf{q}_i)\boldsymbol{\epsilon}_i|^2$ . This last and the fact that  $\mathcal{W}_i$  is positive definite and radially unbounded with regards to  $\boldsymbol{\epsilon}_i$  ensure that  $\boldsymbol{\epsilon}_i \in \mathcal{L}_\infty$ .  $\diamond \diamond \diamond$

#### 4.4.4 Remarks

**Remark 4.5.** If no kinematic uncertainties are considered, the control scheme can be analyzed and designed using the operational space dynamic model (3.52). In this case, the auxiliary signals and control law are defined in the following way

$$\boldsymbol{\epsilon}_i := \mathbf{v}_i + \boldsymbol{\phi}_i \quad (4.77)$$

$$\dot{\boldsymbol{\epsilon}}_i = \dot{\mathbf{v}}_i + \dot{\boldsymbol{\phi}}_i \quad (4.78)$$

where

$$\boldsymbol{\phi}_i := \boldsymbol{\Phi}(\boldsymbol{\xi}_i)\mathbf{e}_i \quad (4.79)$$

$$\dot{\boldsymbol{\phi}}_i = \dot{\boldsymbol{\Phi}}(\boldsymbol{\xi}_i)\mathbf{e}_i + \boldsymbol{\Phi}(\boldsymbol{\xi}_i)\dot{\mathbf{e}}_i. \quad (4.80)$$

with  $\mathbf{e}_i$  and  $\dot{\mathbf{e}}_i$  defined by the equations (4.61) and (4.62), respectively.

The adaptive controller is given by:

$$\begin{aligned} \mathbf{f}_i &= -(\hat{\mathbf{M}}_i(\mathbf{q}_i)\dot{\boldsymbol{\phi}}_i + \hat{\mathbf{C}}_i(\mathbf{q}_i, \dot{\mathbf{q}}_i)\boldsymbol{\phi}_i - \hat{\mathbf{g}}_i(\mathbf{q}_i)) - \kappa_i \boldsymbol{\epsilon}_i \\ &= -\mathbf{Y}_i(\mathbf{q}_i, \dot{\mathbf{q}}_i, \boldsymbol{\phi}_i, \dot{\boldsymbol{\phi}}_i)\hat{\boldsymbol{\theta}}_i - \kappa_i \boldsymbol{\epsilon}_i, \end{aligned} \quad (4.81)$$

with the parameter estimation law defined as

$$\dot{\hat{\boldsymbol{\theta}}}_i := \boldsymbol{\Gamma}_i \mathbf{Y}_i^\top \boldsymbol{\epsilon}_i, \quad (4.82)$$

The control law (4.81) applied to (3.52) yields the following closed-loop system

$$\mathbf{M}_i(\mathbf{q}_i)\dot{\boldsymbol{\epsilon}}_i + \mathbf{C}_i(\mathbf{q}_i, \dot{\mathbf{q}}_i)\boldsymbol{\epsilon}_i + \kappa_i\boldsymbol{\epsilon}_i = \mathbf{Y}_i\tilde{\boldsymbol{\theta}}_i, \quad (4.83)$$

with  $\tilde{\boldsymbol{\theta}}_i := \boldsymbol{\theta}_i - \hat{\boldsymbol{\theta}}_i$ . The stability proofs for the **LFCP** and **LCP** using the control law and the auxiliary signals defined in the present Remark can be performed following *verbatim* the same steps of the proof of the propositions (4.8) and (4.9), respectively.

**Remark 4.6.** When the interconnection time-delays are negligible, the pose error (4.61) becomes

$$\mathbf{e}_i = b_{i\ell}(\mathbf{x}_i - \mathbf{x}_\ell) + \sum_{j \in \mathcal{N}_i} a_{ij}(\mathbf{x}_i - \mathbf{x}_j)$$

and thus (4.69) yields  $\dot{\mathcal{H}} = - \sum_{i \in \bar{N}} \left[ |\dot{\mathbf{x}}_i|^2 + 3|\dot{\boldsymbol{\xi}}_i|^2 + |\boldsymbol{\Phi}(\boldsymbol{\xi}_i)\mathbf{e}_i|^2 + |\mathbf{Y}_{K_i}\tilde{\boldsymbol{\theta}}_{K_i}|^2 \right]$ . In this case, the proof of the solution to both consensus problems can be easily established invoking LaSalle's Invariance Theorem.

**Remark 4.7.** Similar to the Assumptions in (Nuño, Ortega, Basañez, and Hill 2011; Liu and Chopra 2012; Wang 2013a), the proposed controller can also solve the leader-follower problem for a dynamic leader provided that the leader trajectory is available to *all* the agents and that it is bounded up to its third derivative. In such a case, the pose error (4.61) becomes

$$\mathbf{e}_i = -b_{i\ell}\dot{\mathbf{x}}_\ell + b_{i\ell}\tilde{\mathbf{x}}_i + \sum_{j \in \mathcal{N}_i} a_{ij} [\tilde{\mathbf{x}}_i - \tilde{\mathbf{x}}_j(t - T_{ji}(t))]$$

where  $\tilde{\mathbf{x}}_i := \mathbf{x}_i - \mathbf{x}_\ell$  and  $b_{i\ell} > 0$ , for all  $i \in \bar{N}$ .

**Remark 4.8.** Following the same idea of (Liu and Chopra 2012; Zegeroglu, Dawson, Walker, and Setlur 2004) and since the robot manipulators can be redundant, the proposed controller can be designed to solve the consensus problems and, at the same time, to perform a subtask objective (e.g., mechanical limit avoidance or obstacle avoidance). For example, let us propose the subtask error as

$$\boldsymbol{\phi}_i := \left[ \mathbf{I}_{n_i} - \hat{\mathbf{J}}_i^\dagger(\mathbf{q}_i) \hat{\mathbf{J}}_i(\mathbf{q}_i) \right] (\dot{\mathbf{q}}_i - \dot{\mathbf{q}}_{di}),$$

where  $\dot{\mathbf{q}}_{di} \in \mathbb{R}^{n_i}$  is the desired velocity of the subtask. As usual in trajectory tracking control,  $\dot{\mathbf{q}}_{di}$  is assumed bounded up to its third derivative.

Redesigning (4.58) as

$$\boldsymbol{\phi}_i = \hat{\mathbf{J}}_i^\dagger(\mathbf{q}_i)\boldsymbol{\Phi}(\boldsymbol{\xi}_i)\mathbf{e}_i - \left[ \mathbf{I}_{n_i} - \hat{\mathbf{J}}_i^\dagger(\mathbf{q}_i)\hat{\mathbf{J}}_i(\mathbf{q}_i) \right] \dot{\mathbf{q}}_{di},$$

it holds that

$$\hat{\mathbf{J}}_i(\mathbf{q}_i)\phi_i = \Phi(\xi_i)\mathbf{e}_i,$$

where the property of the Moore-Penrose pseudo-inverse matrix  $\hat{\mathbf{J}}_i(\mathbf{q}_i)\hat{\mathbf{J}}_i^\dagger(\mathbf{q}_i) = \mathbf{I}_6$  has been used to obtain this expression. Thus the rest of the proof remains the same for each consensus problem with the additional fact that  $\mathbf{e}_{si}$  converges to zero by noting that, in this case,

$$\begin{aligned} \epsilon_i &= \dot{\mathbf{q}}_i + \phi_i \\ &= \dot{\mathbf{q}}_i + \hat{\mathbf{J}}_i^\dagger(\mathbf{q}_i)\Phi(\xi_i)\mathbf{e}_i - \left[\mathbf{I}_{n_i} - \hat{\mathbf{J}}_i^\dagger(\mathbf{q}_i)\hat{\mathbf{J}}_i(\mathbf{q}_i)\right]\dot{\mathbf{q}}_{di}. \end{aligned}$$

Thus, pre-multiplying the previous equation by  $\left[\mathbf{I}_{n_i} - \hat{\mathbf{J}}_i^\dagger(\mathbf{q}_i)\hat{\mathbf{J}}_i(\mathbf{q}_i)\right]$  yields

$$\left[\mathbf{I}_{n_i} - \hat{\mathbf{J}}_i^\dagger(\mathbf{q}_i)\hat{\mathbf{J}}_i(\mathbf{q}_i)\right]\epsilon_i = \mathbf{e}_{si},$$

hence if  $\epsilon_i$  converges to zero so does  $\mathbf{e}_{si}$ .

It should be underscored that the motions in the joint space due to  $\dot{\mathbf{q}}_{di}$  lie in the null space of  $\hat{\mathbf{J}}_i(\mathbf{q}_i)$  thus they do not induce any motion in the  $SE(3)$ .

## 4.5 Simulation results

This section presents the simulation results that show the effectiveness of the consensus control schemes reported in this chapter. First the simulation platform is detailed and then the simulation experiments and their results are commented.

### 4.5.1 Simulation platform

The simulations are carried on using Matlab<sup>®</sup> and Simulink<sup>®</sup> version 8.3. Two heterogeneous robot networks are designed and programmed to evaluate the consensus algorithms. The first one, which is shown in Figure 4.4, is composed of one 3-DoF planar robot (Node 4), two 3-DoF robots Omni (Node 2 and Node 5) and two 7-DoF robots LWR (Node 1 and Node 3). The second network, shown in Figure 4.14, is composed of one 2-DoF planar robot (Node 1), one 3-DoF planar robot (Node 3) and two 3-DoF robots Omni (Node 2 and Node 4). In Table 4.1 it can be observed a description of the robots used in the networks and the values of their physical parameters. The direct kinematics, the Jacobians, and the dynamic models of the robots are detailed in Appendix B. The algorithm defined in the paper (Spurrer 1978), that is computationally more efficient than (3.20), is used to derive the unit-quaternions from the rotation matrices.



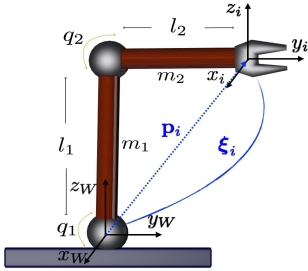
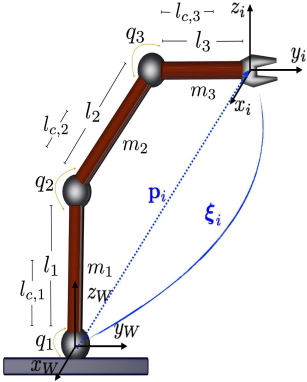
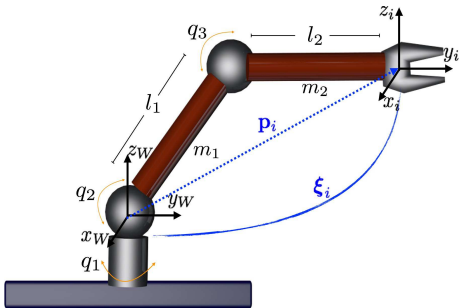
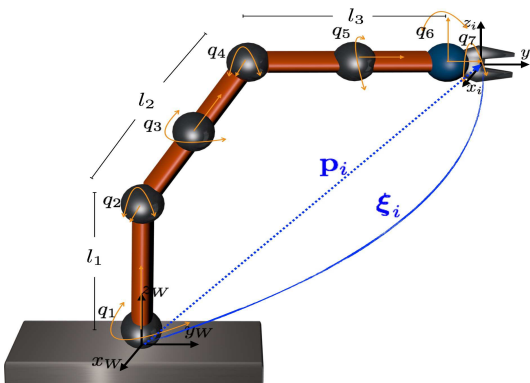
Robots	Mass(kg) Inertia(kg m <sup>2</sup> )	Length(m) C. of mass(m)
	<p><u>2-DoF Robot</u>  <math>m_1=0.3</math>  <math>m_2=0.2</math></p>	<p><u>2-DoF Robot</u>  <math>l_1=0.135</math>  <math>l_2=0.135</math></p>
	<p><u>3-DoF Robot</u>  <math>m_1=0.25</math>  <math>m_2=0.15</math>  <math>m_3=0.10</math>  <math>I_1=0.0055</math>  <math>I_2=0.005</math>  <math>I_3=0.0025</math></p>	<p><u>3-DoF Robot</u>            Network Figure 4.4  <math>l_1=0.40</math> <math>l_2=0.30</math>  <math>l_3=0.25</math> <math>lc_1=0.20</math>            Network Figure 4.14  <math>l_1=0.20</math> <math>l_2=0.15</math>  <math>l_3=0.10</math> <math>lc_1=0.10</math>  <math>lc_2=0.07</math> <math>lc_3=0.05</math></p>
	<p><u>3-DoF Robot Omni</u>  <math>m_1=0.035</math>  <math>m_2=0.1</math>  <math>I_{1x}=0.00001</math>  <math>I_{1y}=0.0002126</math>  <math>I_{1z}=0.0002126</math>  <math>I_{2x}=0.00001</math>  <math>I_{2y}=0.0006075</math>  <math>I_{2z}=0.0006075</math></p>	<p><u>3-DoF Robot Omni</u>            Network Figure 4.4  <math>l_1=0.27</math> <math>l_2=0.27</math>            Network Figure 4.14  <math>l_1=0.135</math>  <math>l_2=0.135</math></p>
	<p><u>7-DoF Robot LWR</u>            These parameters can be found in (Bargsten et al. 2013)</p>	<p><u>7-DoF Robot LWR</u>            These parameters can be found in (Bargsten et al. 2013)</p>

Table 4.1: Robots' structure and their physical parameters.

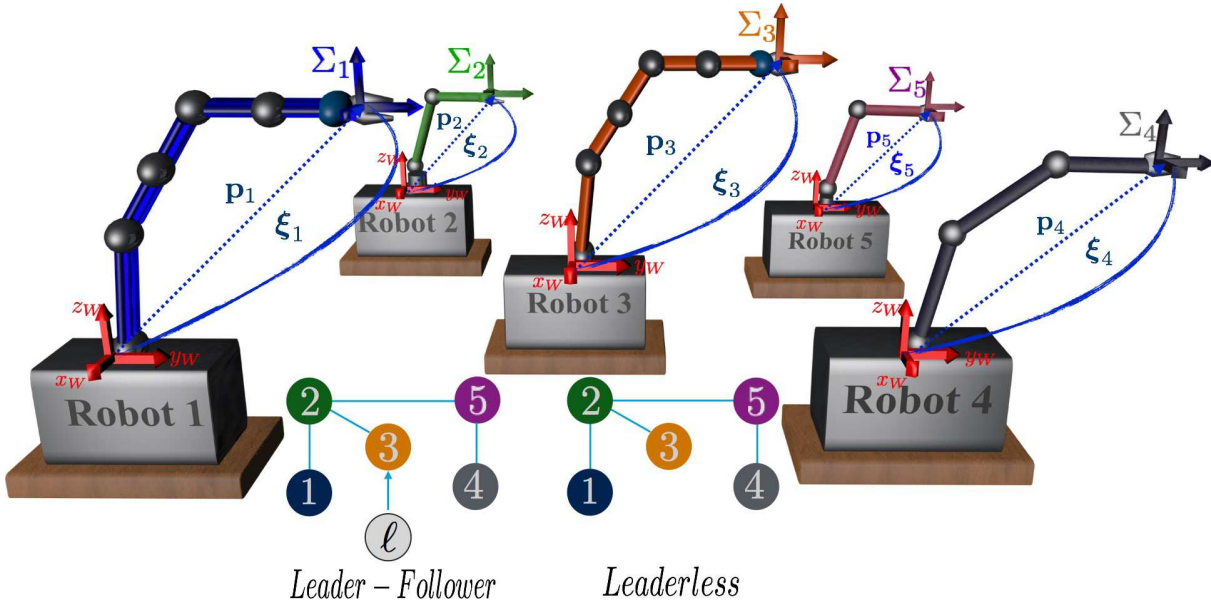


Figure 4.4: Robot network and interconnection graphs used in the simulations of the consensus algorithms without velocity measurements and with variable time-delays.

#### 4.5.2 Consensus control without velocity measurements results

The control scheme proposed in Section 4.2 is implemented in the heterogeneous robot network depicted in Figure 4.4, the robots being interconnected as shown by the interconnection graphs of this figure.

##### Leader-Follower case

In this case, only Node 3 receives the leader constant reference pose with a interconnection weight set to  $b_{3\ell} = 2$ , and the rest of the robots do not receive the leader pose, hence  $b_{i\ell} = 0$  for  $i \in \{1, 2, 4, 5\}$ . The followers network interconnection weights  $a_{ij}$  are set to:  $a_{12} = a_{21} = 0.7$ ,  $a_{23} = a_{32} = 0.8$ ,  $a_{24} = a_{42} = 0.7$  and  $a_{45} = a_{54} = 0.8$ , defining the following Laplacian matrix

$$\mathbf{L} = \begin{bmatrix} 0.7 & -0.7 & 0 & 0 & 0 \\ -0.7 & 2.2 & -0.8 & -0.7 & 0 \\ 0 & -0.8 & 0.8 & 0 & 0 \\ 0 & -0.7 & 0 & 1.5 & -0.8 \\ 0 & 0 & 0 & -0.8 & 0.8 \end{bmatrix}.$$

The controller gains employed in this simulation can be seen in Table 4.2. The performance of the leader-follower control scheme is shown in Figures 4.5 and 4.6. The position and the

	Leader-follower			Leaderless		
	$k_i$	$d_i$	$k_{yi}$	$k_i$	$d_i$	$k_{yi}$
Robot 1	50	200	50	100	200	50
Robot 2	5	160	600	2	150	500
Robot 2	20	200	50	100	200	50
Robot 4	100	150	5	200	200	5
Robot 5	5	160	600	2	150	500

Table 4.2: Parameters used in the simulations of the consensus control scheme without velocity measurements.

orientation (represented with unit-quaternions) behaviors are shown in the Figures 4.5.(a) and 4.5.(b). It is observed that the five robots of the network have different initial poses and how, after 8 seconds, they converge to the leader pose defined as

$$\mathbf{x}_\ell = [0, 0.1552, 0.5031, 0.7066, -0.0264, 0.0264, 0.7066]^\top$$

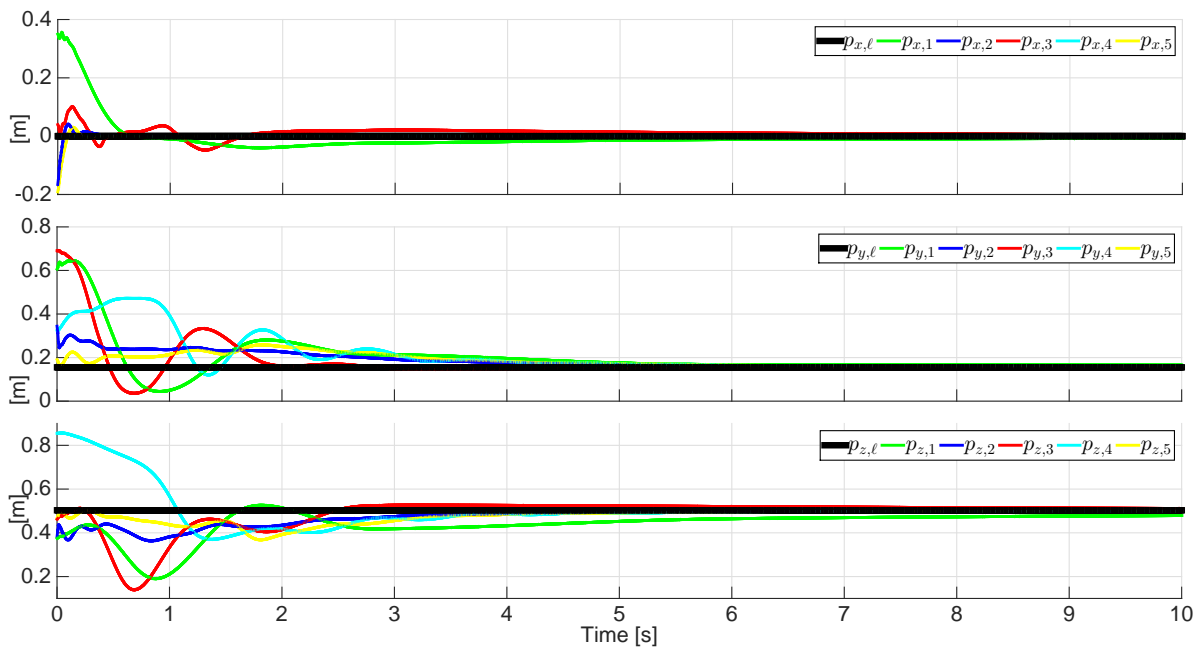
This leader pose has been defined taking into account the common task space of all the robots. The Figures 4.6.(a) and 4.6.(b) depict the linear and angular velocities for each robot manipulator, and it is observed that they converge to zero.

### Leaderless case

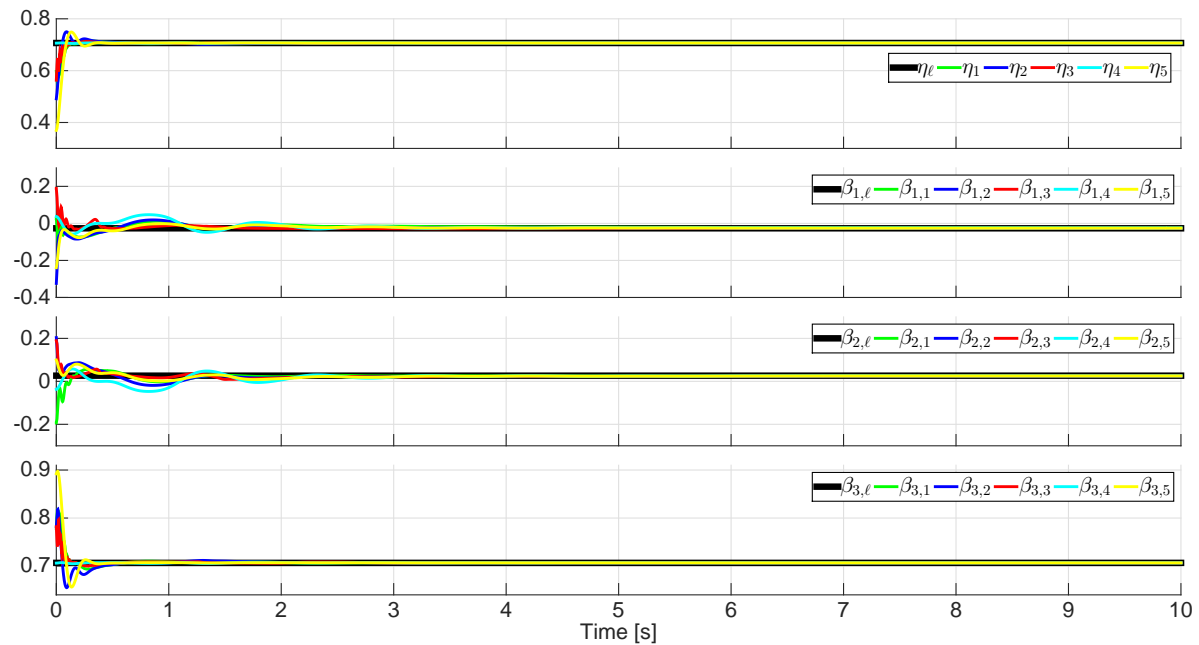
The network interconnection weights  $a_{ij}$  are set to:  $a_{12} = a_{21} = 0.4$ ,  $a_{23} = a_{32} = 0.5$ ,  $a_{24} = a_{42} = 0.4$  and  $a_{45} = a_{54} = 0.5$ , defining the following Laplacian matrix

$$\mathbf{L} = \begin{bmatrix} 0.4 & -0.4 & 0 & 0 & 0 \\ -0.4 & 1.3 & -0.5 & -0.4 & 0 \\ 0 & -0.5 & 0.5 & 0 & 0 \\ 0 & -0.4 & 0 & 0.8 & -0.4 \\ 0 & 0 & 0 & -0.4 & 0.4 \end{bmatrix}.$$

In Table 4.2 are shown the controller gains used in this simulation. The position and the orientation behaviors are shown in Figures 4.7.(a) and 4.7.(b). It is observed, that without a leader reference, the pose of the five robots converge to a common pose. Figures 4.8.(a) and 4.8.(b) show the linear and angular velocities for each robot manipulator, and it is observed that they converge to zero.

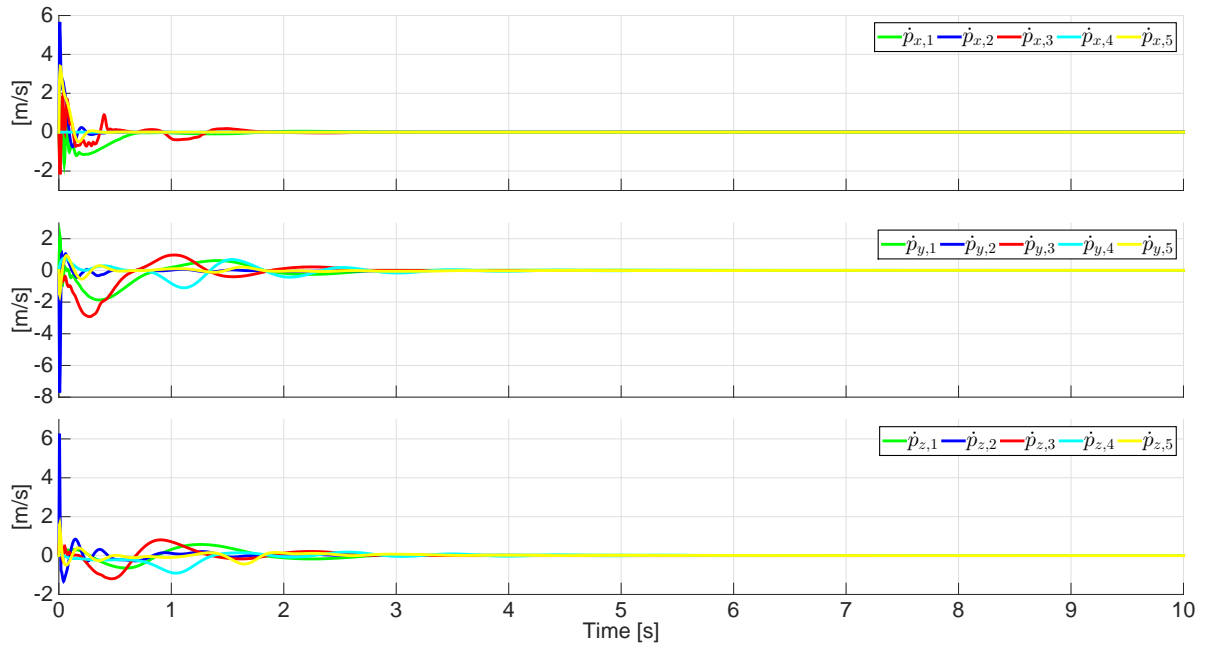


(a) Positions

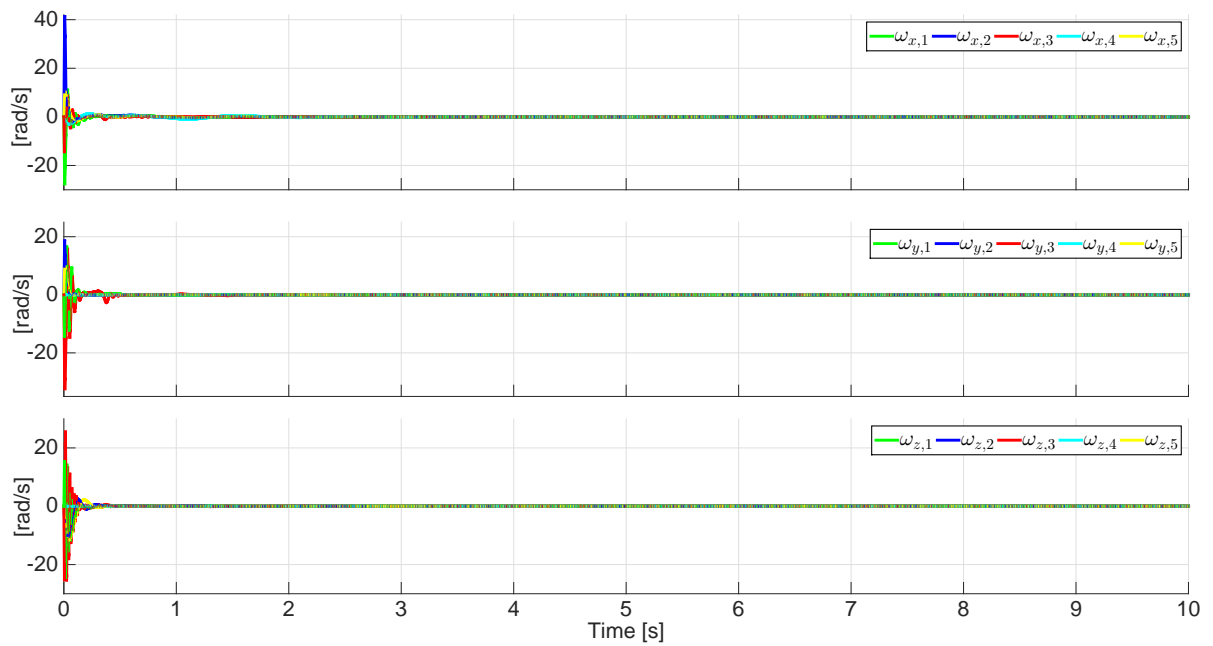


(b) Unit-quaternions (Orientations)

Figure 4.5: Pose of the robots for the leader-follower case using the consensus control scheme without velocity measurements.

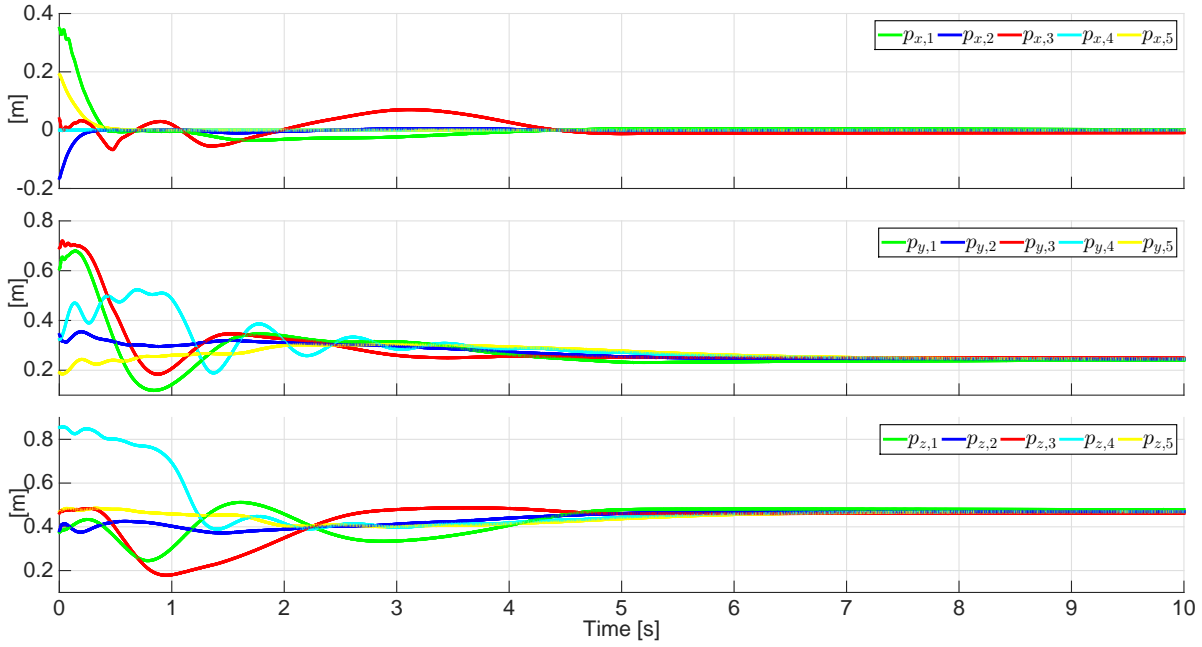


(a) Linear velocities

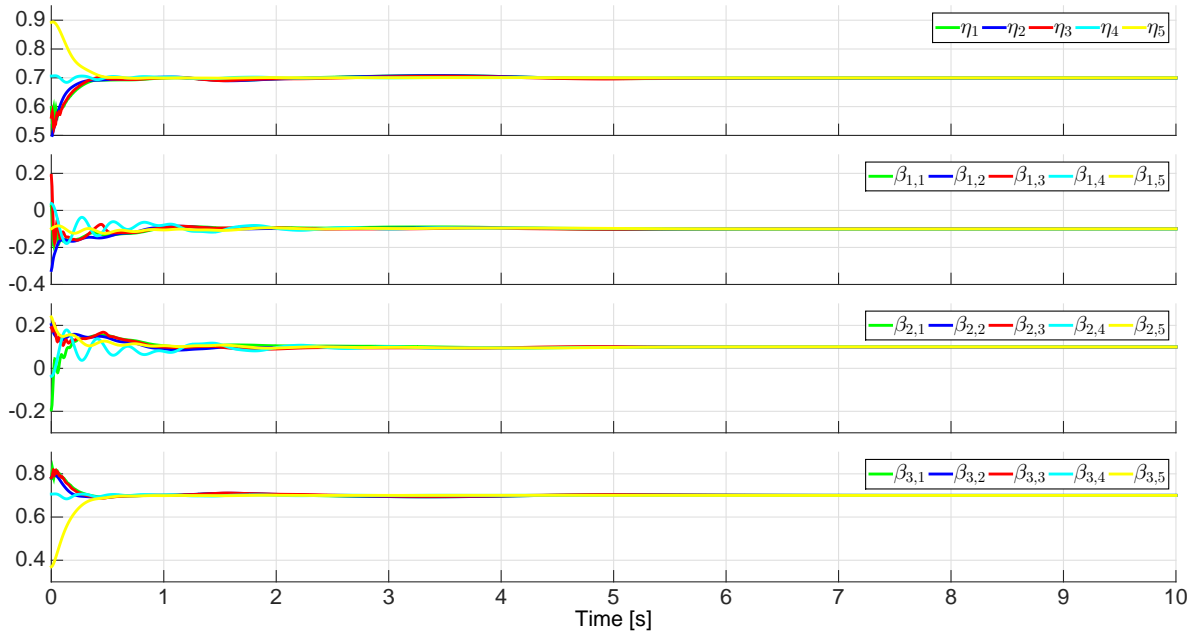


(b) Angular velocities

Figure 4.6: Velocities of the robots for the leader-follower case using the consensus control scheme without velocity measurements.

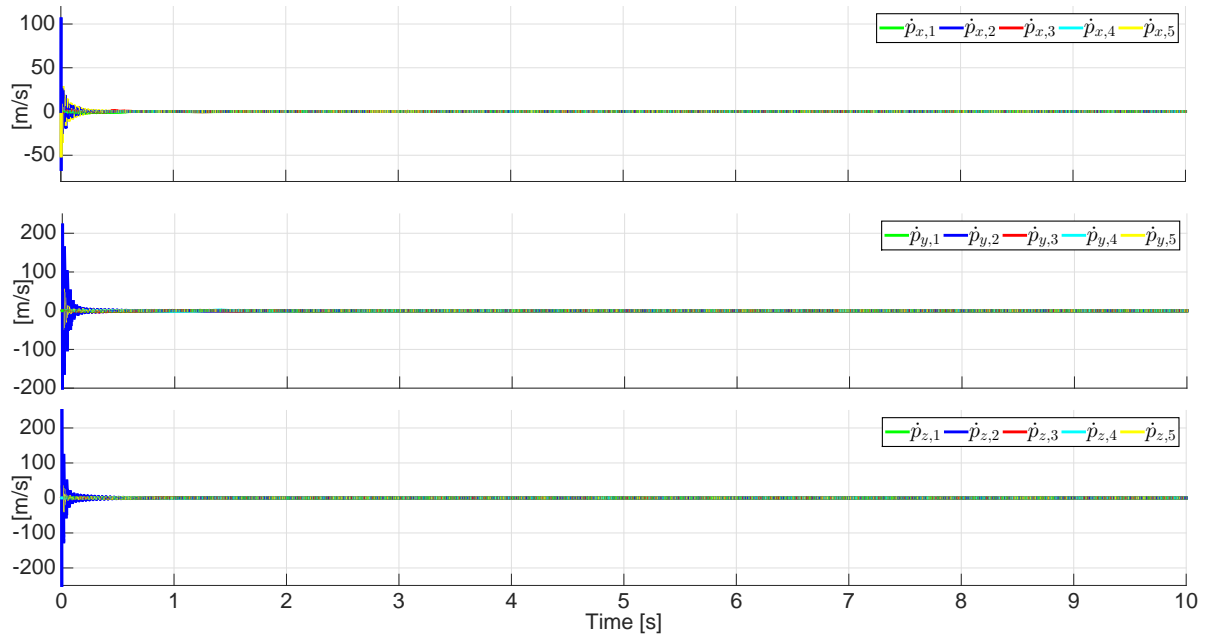


(a) Positions

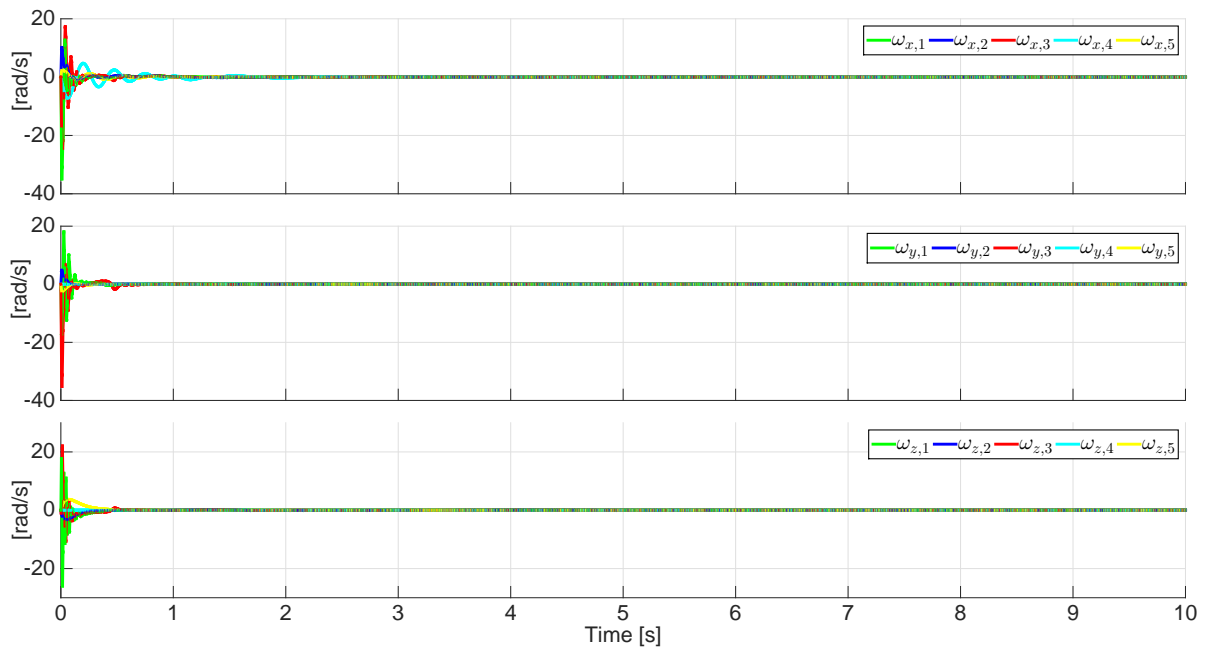


(b) Unit-quaternions (Orientations)

Figure 4.7: Pose of the robots for the leaderless case using the consensus control scheme without velocity measurements.



(a) Linear velocities



(b) Angular velocities

Figure 4.8: Velocities of the robots for the leaderless case using the consensus control scheme without velocity measurements.

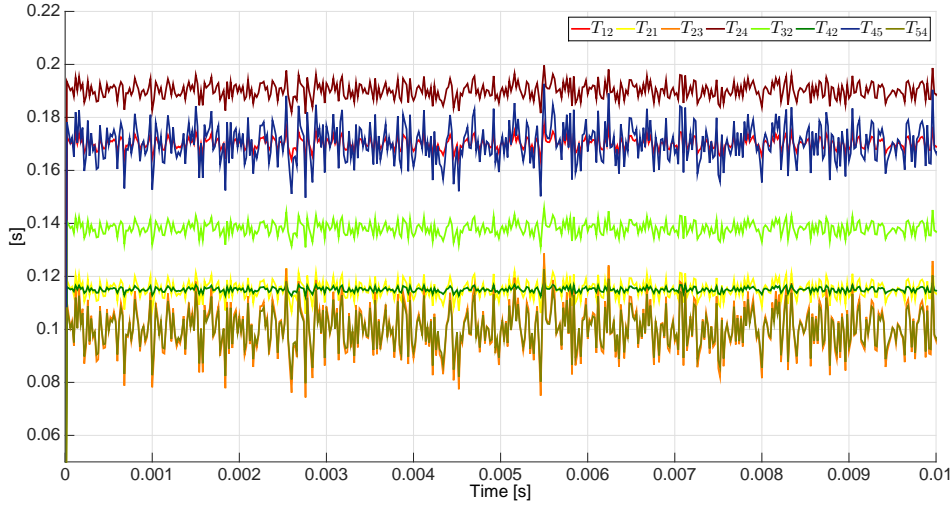


Figure 4.9: Sample of the variable time-delays.

$*T_{ji}$ [s]	Mean [s]	Variance [ $\mu s$ ]
$*T_{12}=0.20$	0.17	5
$*T_{21}=0.13$	0.115	10
$*T_{23}=0.14$	0.10	80
$*T_{24}=0.22$	0.19	9
$*T_{32}=0.15$	0.138	6
$*T_{42}=0.12$	0.115	0.8
$*T_{45}=0.20$	0.17	50
$*T_{54}=0.13$	0.10	50

Table 4.3: Upper-bounds of the variable time-delays and Gaussian distribution parameters.

### 4.5.3 Consensus control with variable time-delays

The robot network and the interconnection graphs depicted in Figure 4.4 are used in the simulations of the consensus control scheme proposed in Section 4.3. Figure 4.9 shows a small time window of the variable time-delays in the interconnection of the robots. These variable delays emulate an ordinary UDP/IP internet interconnection with a normal Gaussian distribution (Salvo-Rossi, Romano, Palmieri, and Iannello 2006). The parameters of the distributions (mean and variance) together with the delays upper bounds are given in Table 4.3.

#### Leader-Follower case

The Node 3 receives the leader constant reference pose with a interconnection weight set to  $b_{3\ell} = 2$ . The rest of the robots do not receive the leader pose, hence  $b_{i\ell} = 0$  for  $i \in \{1, 2, 4, 5\}$ . The followers network interconnection weights are set to:  $a_{12} = a_{21} = 1.5$ ,  $a_{23} = a_{32} = 2$ ,



	Leader-follower			Leaderless		
	$k_i$	$d_i$	$\alpha_i$	$k_i$	$d_i$	$\alpha_i$
Robot 1	25	7	0.3	40	10	0.4
Robot 2	20	25	0.4	40	18	0.3
Robot 2	25	9	0.3	60	18	0.6
Robot 4	20	17	0.4	40	24	0.7
Robot 5	20	9	0.3	40	14	0.8

Table 4.4: Parameters used in the simulations of the consensus control scheme with variable time-delays.

$a_{24} = a_{42} = 1.5$  and  $a_{45} = a_{54} = 2$ , defining the following Laplacian matrix

$$\mathbf{L} = \begin{bmatrix} 1.5 & -1.5 & 0 & 0 & 0 \\ -1.5 & 5 & -2 & -1.5 & 0 \\ 0 & -2 & 2 & 0 & 0 \\ 0 & -1.5 & 0 & 3.5 & -2 \\ 0 & 0 & 0 & -2 & 2 \end{bmatrix}.$$

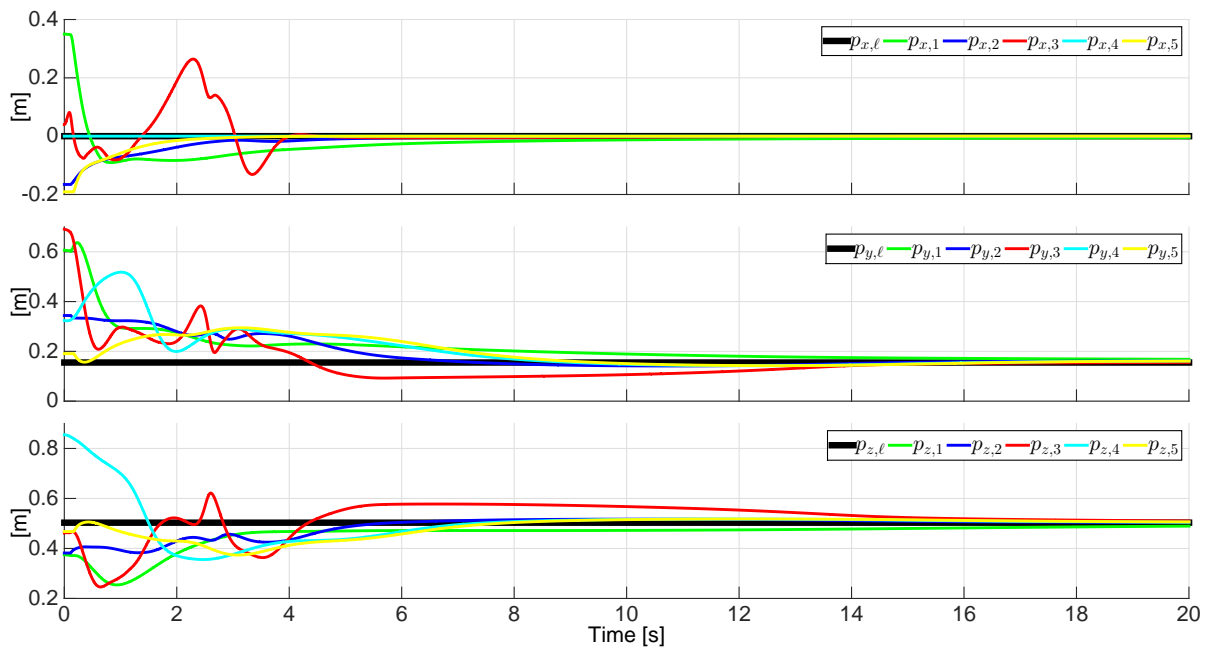
The controller gains and the  $\alpha_i$ , that fulfill condition (4.40), can be seen in Table 4.4. The performance of the leader-follower control scheme is shown in Figures 4.10 and 4.11. Figures 4.10.(a) and 4.10.(b) show the position and the orientation behaviors of the robots. It takes 15 seconds to the five robots, that begin at different initial pose, to converge to the leader pose  $\mathbf{x}_\ell$  (same as in the consensus control without velocity measurement simulation). Figures 4.11.(a) and 4.11.(b) show the linear and angular velocities for each robot manipulator, and it is observed that they converge to zero.

#### Leaderless case

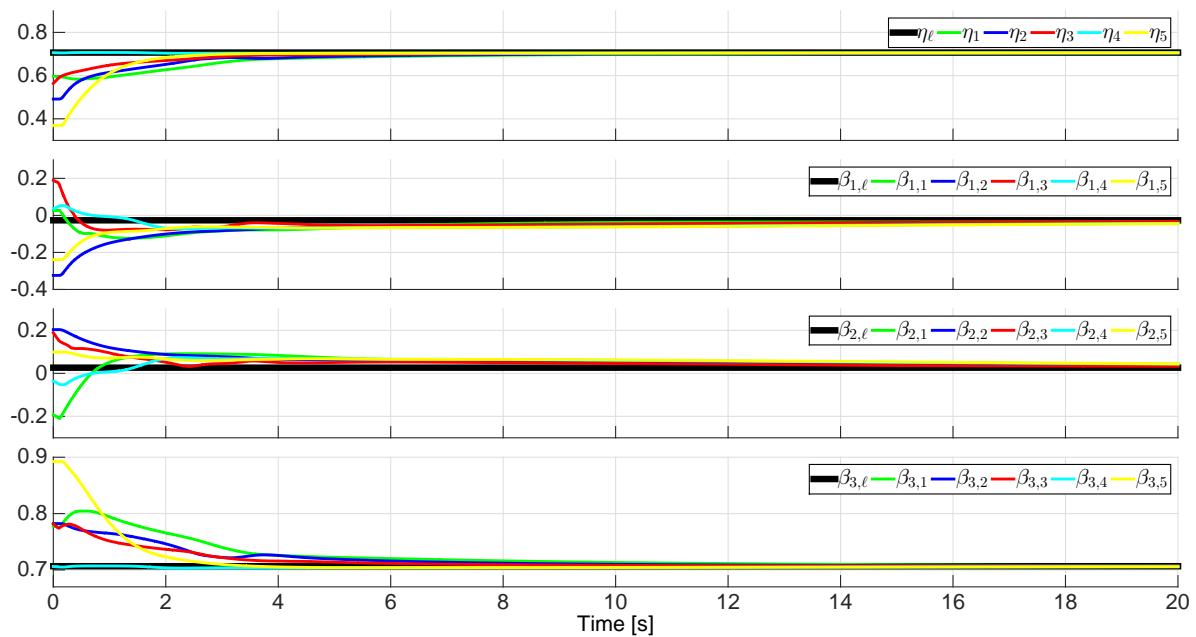
The network interconnection weights  $a_{ij}$  are set to:  $a_{12} = a_{21} = 0.8$ ,  $a_{23} = a_{32} = 0.9$ ,  $a_{24} = a_{42} = 0.8$  and  $a_{45} = a_{54} = 0.7$ , defining the following Laplacian matrix

$$\mathbf{L} = \begin{bmatrix} 0.8 & -0.8 & 0 & 0 & 0 \\ -0.8 & 2.5 & -0.9 & -0.8 & 0 \\ 0 & -0.9 & 0.9 & 0 & 0 \\ 0 & -0.8 & 0 & 1.5 & -0.7 \\ 0 & 0 & 0 & -0.7 & 0.7 \end{bmatrix}.$$

Table 4.4 shows the controller parameters used in this simulation. Figures 4.12.(a) and 4.12.(b) show how after 12 seconds the pose of the five robots converge to a common pose from

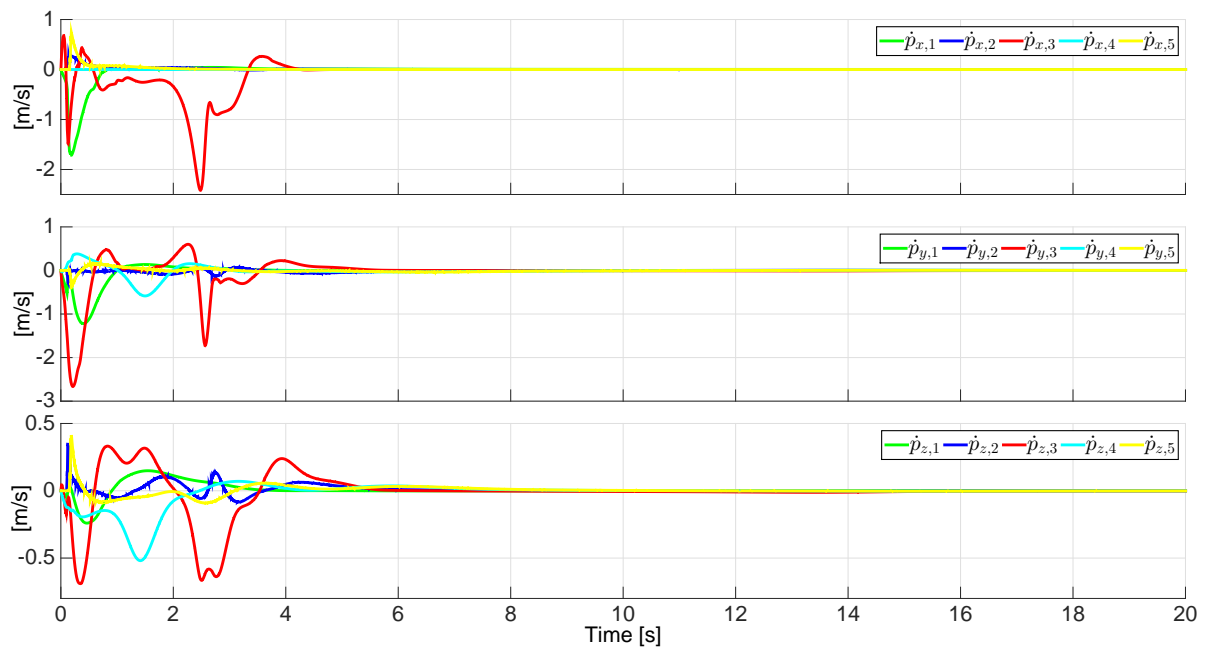


(a) Positions

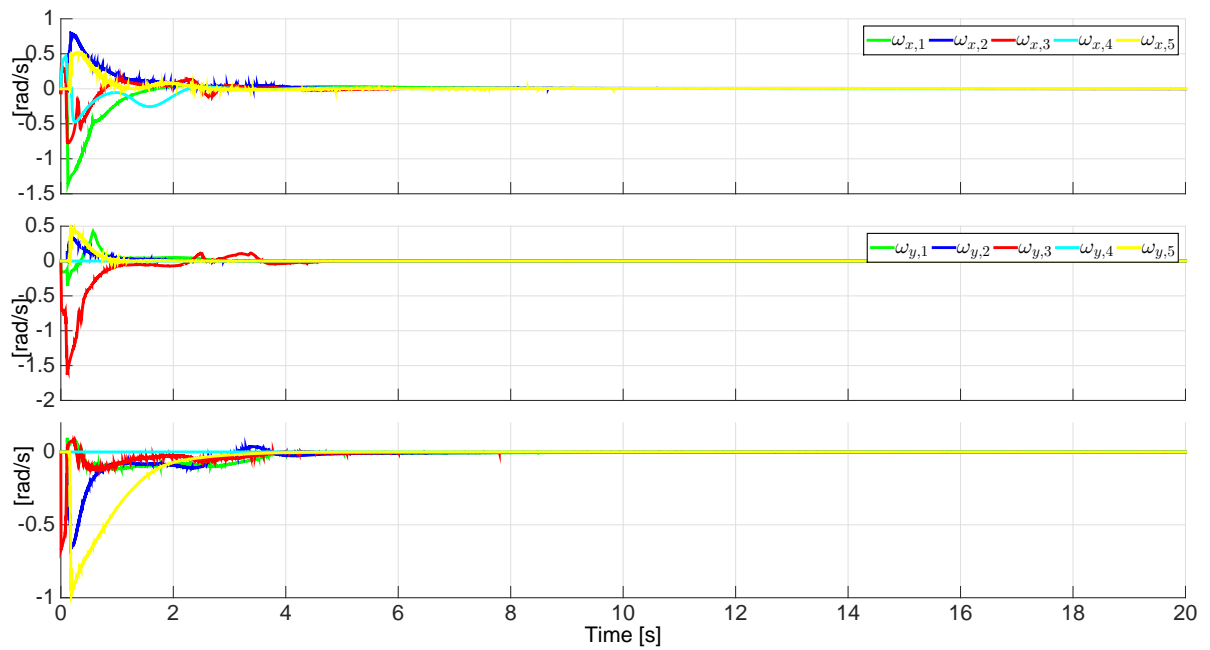


(b) Unit-quaternions (Orientations)

Figure 4.10: Pose of the robots for the leader-follower case using the consensus control scheme with variable time-delays.



(a) Linear velocities



(b) Angular velocities

Figure 4.11: Velocities of the robots for the leader-follower case using the consensus control scheme with variable time-delays.

different initial poses. The convergence to zero of the linear and angular velocities can be seen in Figures 4.13.(c) and 4.13.(d), respectively.

#### 4.5.4 Consensus control with uncertain parameters and variable time-delays

The Figure 4.14 depicts the heterogeneous robot network and the interconnection graphs used in the simulation of the consensus control scheme with uncertain kinematic and dynamic parameters and variable time-delays proposed in Section 4.4. The kinematic regressors of the robots, required by the control algorithm, are the following:

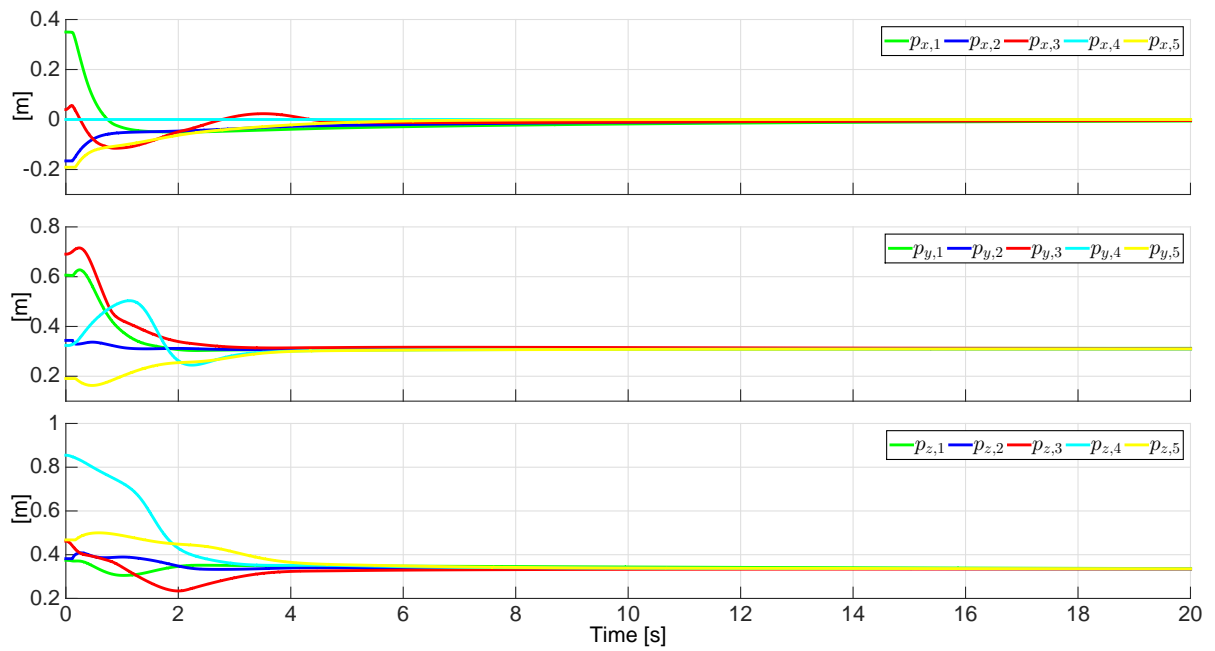
$$\mathbf{Y}_{K,2-DoF} = \begin{bmatrix} 0 & 0 \\ -s_1\dot{q}_1 & -s_{12}\dot{q}_1 - s_{12}\dot{q}_2 \\ c_1\dot{q}_1 & c_{12}\dot{q}_1 + c_{12}\dot{q}_2 \\ 0 & 0 \\ 0 & 0 \\ 0 & 0 \end{bmatrix}$$

$$\mathbf{Y}_{K,3-DoF} = \begin{bmatrix} 0 & 0 & 0 \\ -s_1\dot{q}_1 & -s_{12}\dot{q}_1 - s_{12}\dot{q}_2 & -s_{123}\dot{q}_1 - s_{123}\dot{q}_2 - s_{123}\dot{q}_3 \\ c_1\dot{q}_1 & c_{12}\dot{q}_1 + c_{12}\dot{q}_2 & c_{123}\dot{q}_1 + c_{123}\dot{q}_2 + c_{123}\dot{q}_3 \\ 0 & 0 & 0 \\ 0 & 0 & 0 \\ 0 & 0 & 0 \end{bmatrix}$$

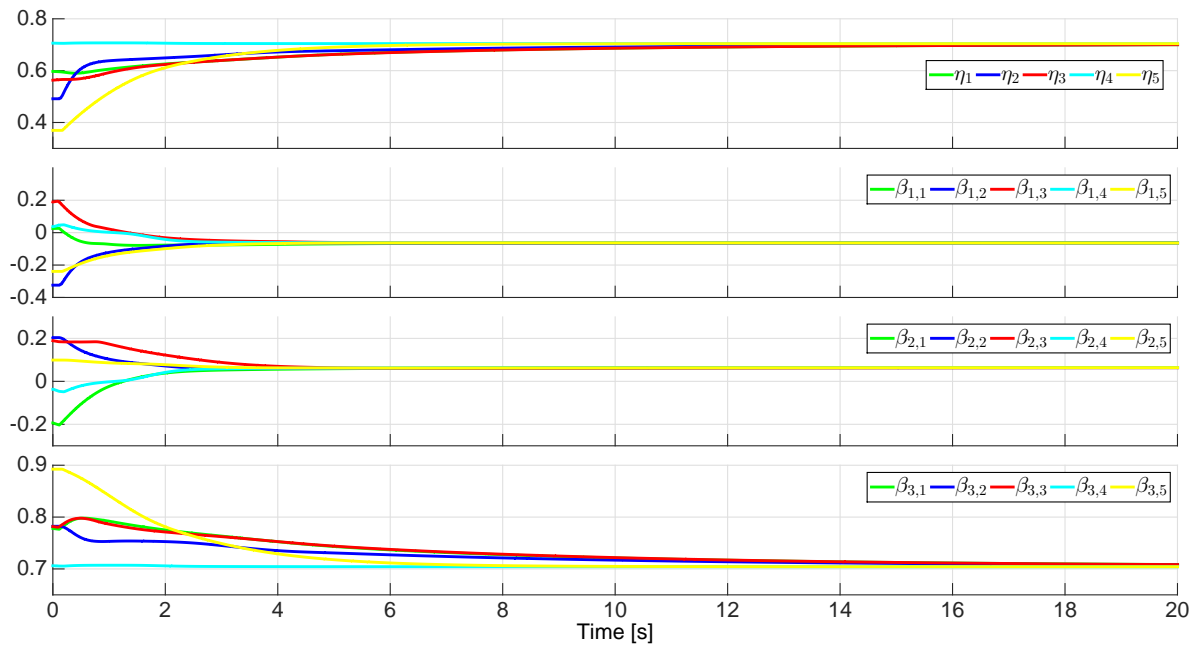
$$\mathbf{Y}_{K,Omnii} = \begin{bmatrix} s_1s_2\dot{q}_2 - c_1c_2\dot{q}_1 & s_{23}s_1\dot{q}_2 - c_{23}c_1\dot{q}_1 + s_{23}s_1\dot{q}_3 \\ -c_2c_1\dot{q}_1 - c_1s_2\dot{q}_2 & -c_{23}s_1\dot{q}_1 - s_{23}c_1\dot{q}_2 - s_{23}c_1\dot{q}_3 \\ c_2\dot{q}_2 & c_{23}\dot{q}_2 + c_{23}\dot{q}_3 \\ 0 & 0 \\ 0 & 0 \\ 0 & 0 \end{bmatrix}$$

The kinematic parameters vectors are defined as  $\boldsymbol{\theta}_{K,2-DoF} = [l_1, l_2]$ ,  $\boldsymbol{\theta}_{K,3-DoF} = [l_1, l_2, l_3]$  and  $\boldsymbol{\theta}_{K,Omnii} = [l_1, l_2]$ . For these simulations, the initial conditions for the estimated kinematic parameters are set to:  $\hat{\boldsymbol{\theta}}_{K,2-DoF}(0) = [0.03, 0.02]^\top$ ,  $\hat{\boldsymbol{\theta}}_{K,3-DoF}(0) = [0.08, 0.11, 0.08]^\top$ ,  $\hat{\boldsymbol{\theta}}_{K,Omnii_2}(0) = [0.05, 0.01]^\top$  and  $\hat{\boldsymbol{\theta}}_{K,Omnii_4}(0) = [0.04, 0.02]^\top$ , where *Omnii*<sub>2</sub> and *Omnii*<sub>4</sub> means Omni of Node 2 and Omni of Node 4, respectively.

The dynamic regressors are derived from the robots' dynamic models detailed in Appendix

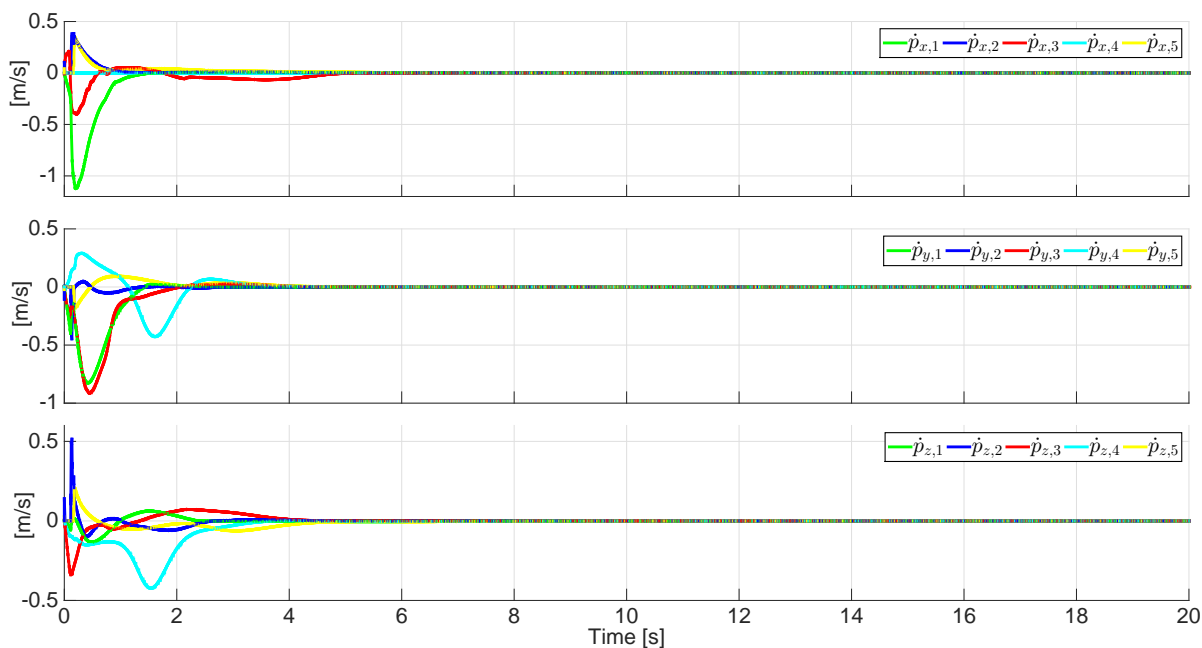


(a) Positions

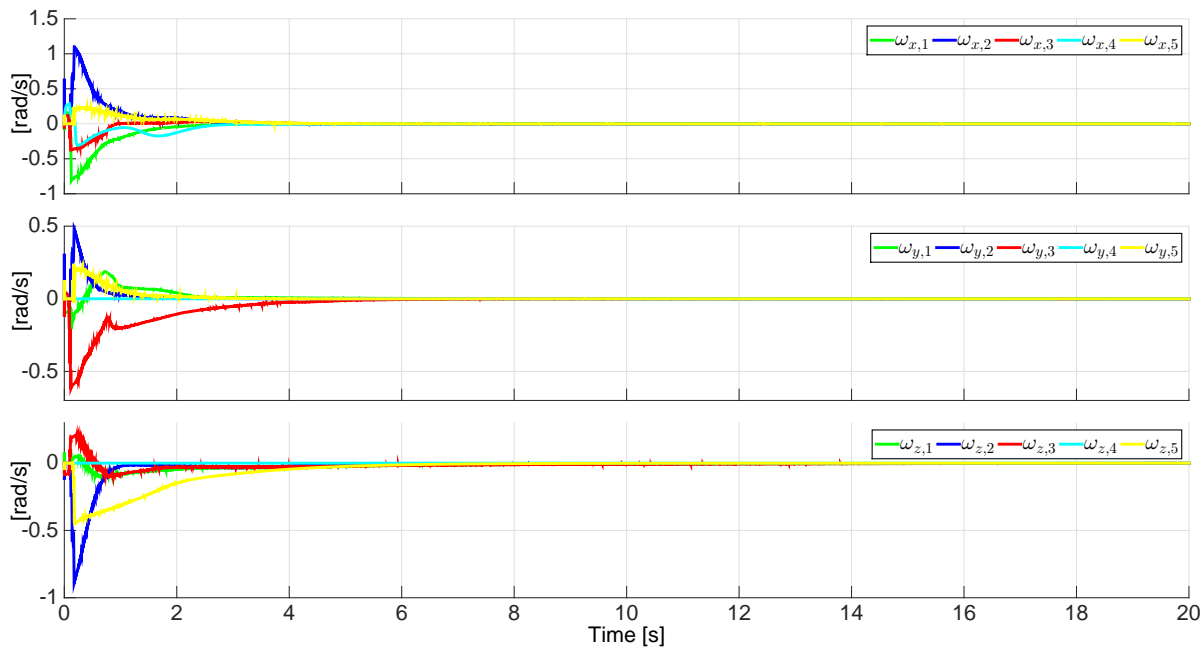


(b) Unit-quaternions (Orientations)

Figure 4.12: Pose of the robots for the leaderless case using the consensus control scheme with variable time-delays.



(a) Linear velocities



(b) Angular velocities

Figure 4.13: Velocities of the robots for the leaderless case using the consensus control scheme with variable time-delays.

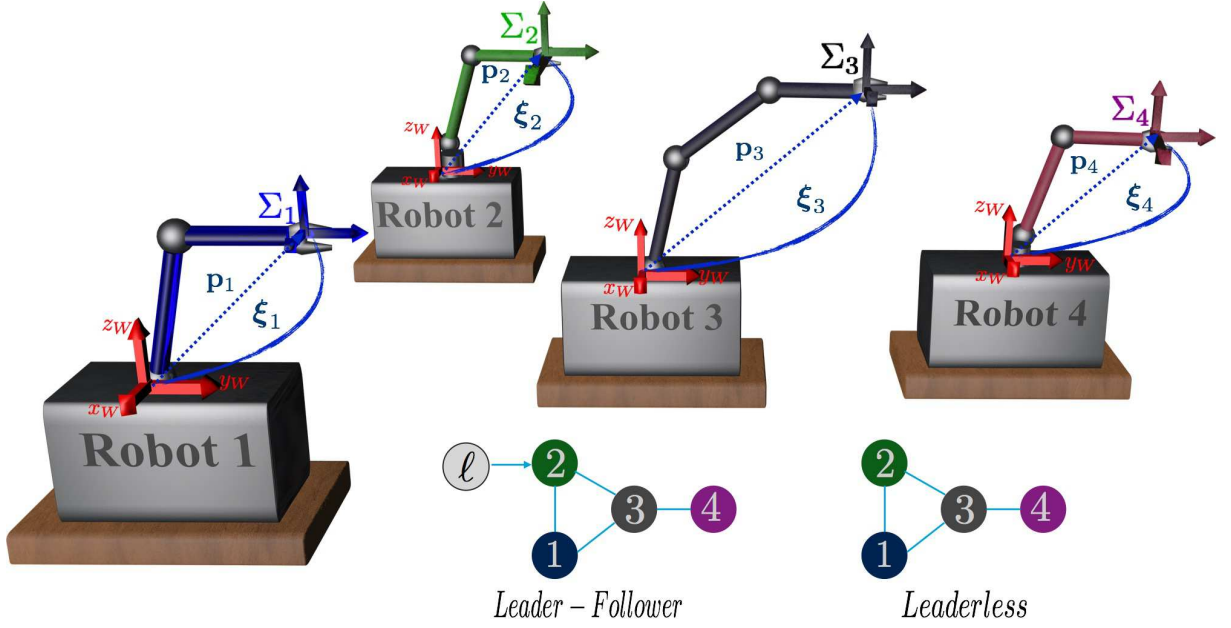


Figure 4.14: Robot network and interconnection graphs used in the simulations of the consensus algorithm with uncertain parameters and variable time-delays.

B. The initial estimated dynamic parameters are set to zero in these experiments. The variable time-delays between the nodes are given by  $T_{ji} = \rho + a_1 \sin(\vartheta_1 t) + a_2 \sin(\vartheta_2 t)$ , and in Table 4.5 are listed the values of the parameters for all the interconnection's delays.

#### Leader-follower case

In this case, only Node 2 receives the leader constant pose defined as

$$\mathbf{x}_\ell = [0, 0.2202, 0.1471, 0.5879, -0.3928, 0.3928, 0.5879]^\top.$$

Delay	$\rho$	$a_1$	$\vartheta_1(\text{rad/s})$	$a_2$	$\vartheta_2(\text{rad/s})$
$T_{21}$	0.12	0.05	7	0.06	27
$T_{31}$	0.09	0.03	2	0.05	14
$T_{12}$	0.14	0.03	5	0.08	23
$T_{32}$	0.14	0.06	2	0.08	13
$T_{13}$	0.11	0.04	3	0.07	27
$T_{23}$	0.08	0.03	8	0.05	18
$T_{43}$	0.13	0.05	4	0.07	29
$T_{34}$	0.11	0.05	6	0.06	30

Table 4.5: Parameters of the variable time-delays.

	Leader-follower				Leaderless			
	$\kappa_i$	$\Gamma_{Di}$	$\Gamma_{Ki}$	$\alpha_i$	$\kappa_i$	$\Gamma_{Di}$	$\Gamma_{Ki}$	$\alpha_i$
Robot 1	30	$80\mathbf{I}_5$	$50\mathbf{I}_2$	0.217	30	$80\mathbf{I}_5$	$50\mathbf{I}_5$	0.30
Robot 2	25	$90\mathbf{I}_8$	$50\mathbf{I}_2$	0.259	50	$80\mathbf{I}_5$	$50\mathbf{I}_5$	0.33
Robot 2	30	$80\mathbf{I}_9$	$50\mathbf{I}_3$	0.279	30	$80\mathbf{I}_5$	$50\mathbf{I}_5$	0.25
Robot 4	50	$80\mathbf{I}_8$	$50\mathbf{I}_2$	0.990	50	$80\mathbf{I}_5$	$50\mathbf{I}_5$	0.43

Table 4.6: Parameters used in the simulations of the consensus control scheme with uncertain parameters and variable time-delays.

The interconnection weights  $b_{i\ell}$  are set to  $b_{2\ell} = 1$  and  $b_{i\ell} = 0$  for  $i \in \{1, 3, 4\}$ . The followers interconnection weights are:  $a_{12} = a_{21} = 1.5$ ,  $a_{13} = a_{31} = 0.8$ ,  $a_{23} = a_{32} = 0.7$  and  $a_{34} = a_{43} = 0.8$ , defining the following Laplacian matrix

$$\mathbf{L} = \begin{bmatrix} 2.3 & -1.5 & -0.8 & 0 \\ -1.5 & 2.2 & -0.7 & 0 \\ -0.8 & -0.7 & 2.3 & -0.8 \\ 0 & 0 & -0.8 & 0.8 \end{bmatrix},$$

these weights fulfill (4.64) using the  $\alpha_i$  shown in Table 4.5. In this table are also defined the controllers gains. Figures 4.15.(a) and 4.15.(b) show the position and the orientation behavior of the robot network. It can be appreciated that the movement of the 2-DoF and 3-DoF robots is only in the plane defined by the coordinates  $(z, y)$ . Besides, it is observed that despite the time-delays and the differences in the robots initial conditions, the robots asymptotically converge to the leader pose. Figure 4.16 depicts the kinematic parameter estimation for each robot manipulator.

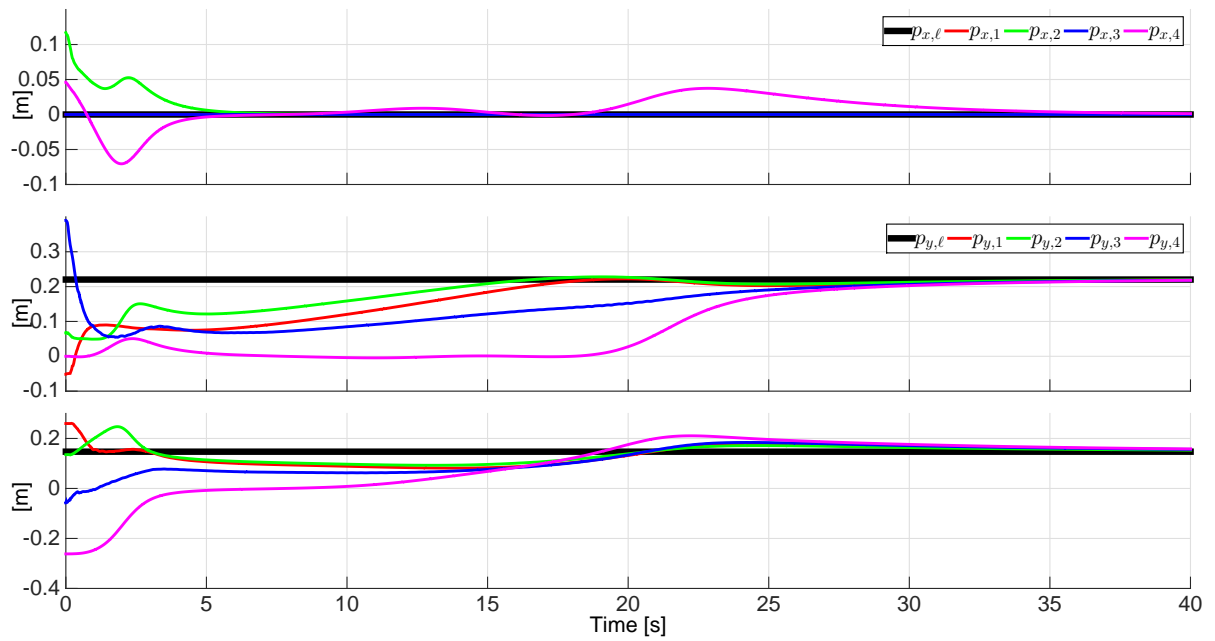
#### Leaderless case

The interconnection weights are set to  $a_{12} = a_{21} = 1$ ,  $a_{13} = a_{31} = 0.8$ ,  $a_{23} = a_{32} = 0.5$  and  $a_{34} = a_{43} = 1.2$ , defining the following Laplacian matrix

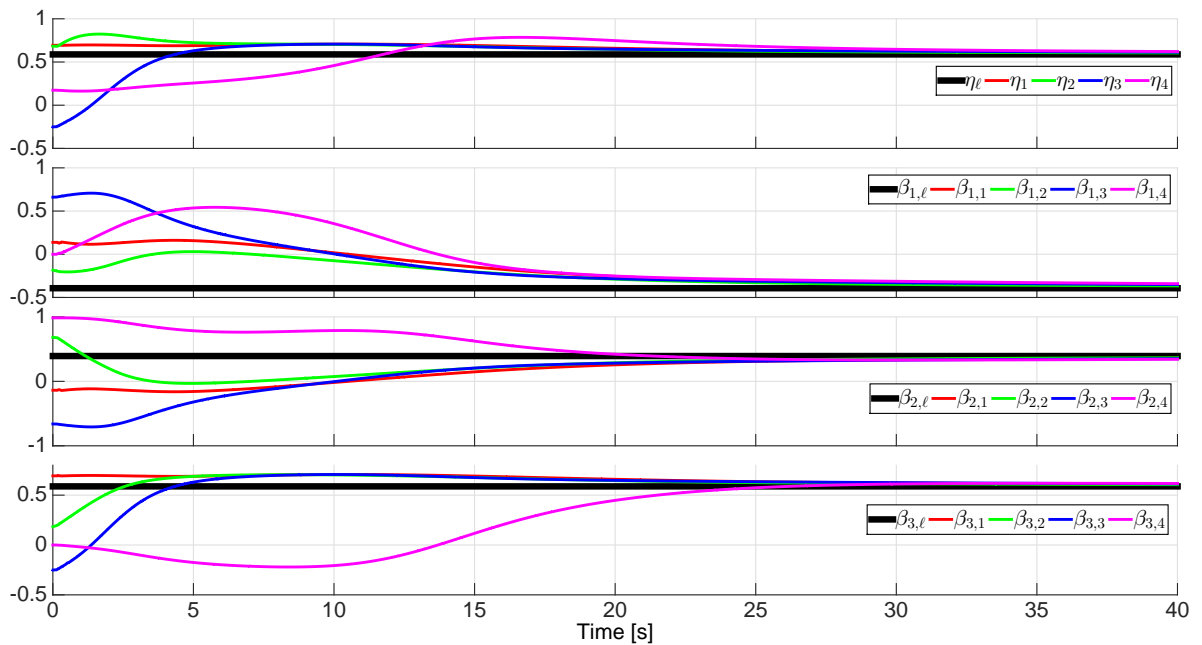
$$\mathbf{L} = \begin{bmatrix} 1.8 & -1 & -0.8 & 0 \\ -1 & 1.5 & -0.5 & 0 \\ -0.8 & -0.5 & 2.5 & -1.2 \\ 0 & 0 & -1.2 & 1.2 \end{bmatrix},$$

these weights fulfill (4.64) using the  $\alpha_i$  which are defined with the controllers gains of Table 4.6. The robot network pose behavior is shown in Fig. 4.17. It can be observed that the network asymptotically reaches a consensus pose. The kinematic estimated parameters are shown in Fig. 4.18.





(a) Positions



(b) Unit-quaternions (Orientations)

Figure 4.15: Pose of the robots for the leader-follower case using the consensus control scheme with uncertain parameters and variable time-delays.

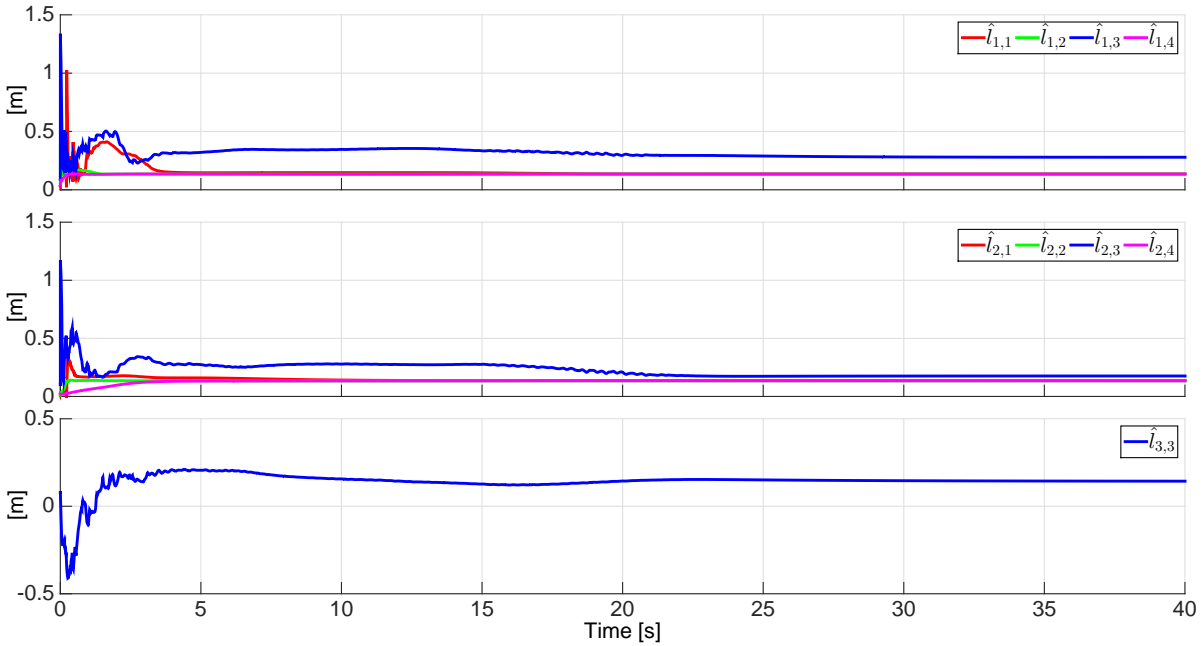


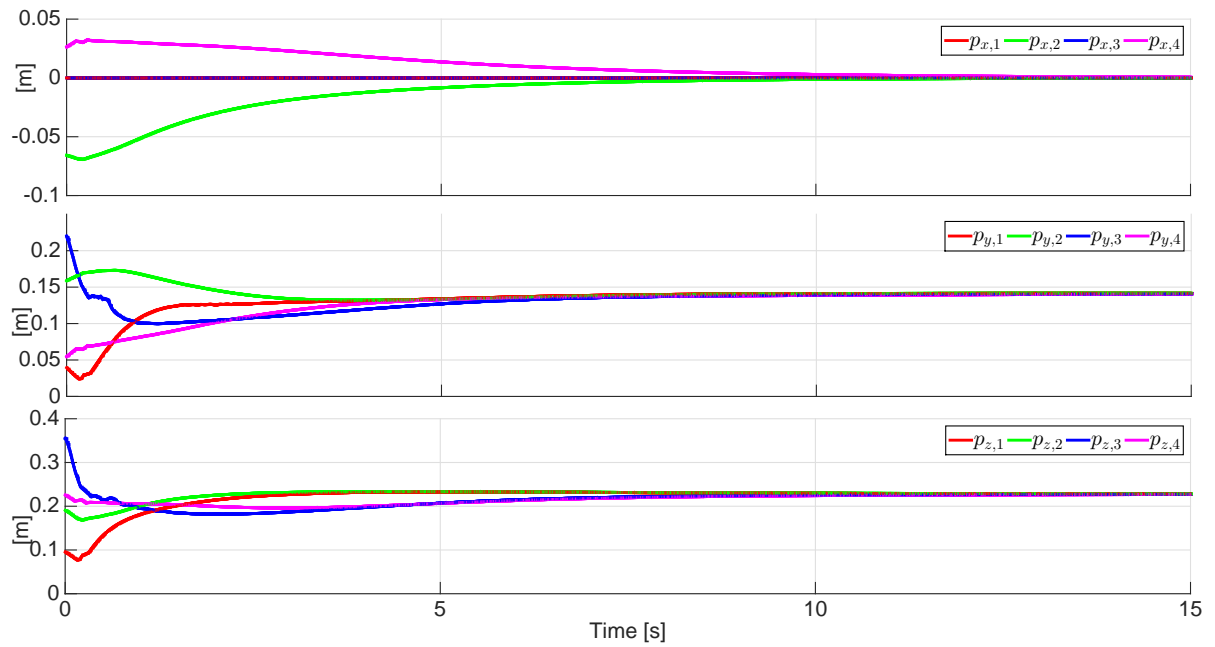
Figure 4.16: Kinematic parameters estimation for the leader-follower case using the consensus control scheme with uncertain parameters and variable time-delays.

## 4.6 Experimental results

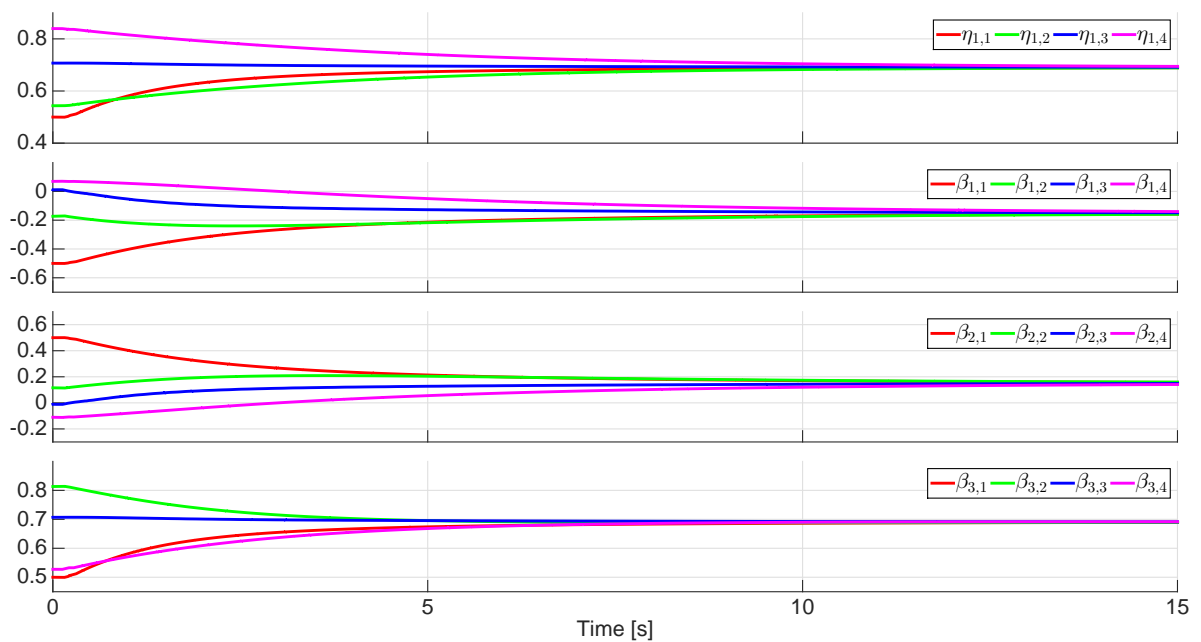
This section presents the experimental validation of the consensus control schemes proposed in Sections 4.2 and 4.3. It was not possible to perform experiments with the controller proposed in Section 4.4 due to the lack of the robots dynamic regressors. The section begins with the description of the test-bed used in the experimental validation and then the experiments and their results are commented.

### 4.6.1 Experimental validation testbed

The test-bed and the interconnection graphs of the robot networks employed in the experimental validation are depicted in Figure 4.19. The test-bed consists of one PHANTOM Premium 1.5<sup>®</sup>, one PHANTOM Premium 1.5 High Force<sup>®</sup> and one PHANTOM Omni<sup>®</sup>. The Premium devices have six fully actuated DoF and the Omni has six sensed DoF but only three of them are actuated. These devices are commercially available from Geomagic<sup>®</sup>. The controllers have been programmed using Matlab<sup>®</sup> version 7.11 and Simulink<sup>®</sup> version 7.6. The communication between Simulink and the robots is done using Simulink libraries developed in the context of this work, called *PhanTorque\_6Dof* and *PhanTorque\_3Dof* (Figure B.2) that are described in Appendix B along with the Jacobians of the robots. The data transmission of the robots' pose is done through UDP ports in the laboratory local network. As with the simulation, the algorithm



(a) Positions



(b) Unit-quaternions (Orientations)

Figure 4.17: Pose of the robots for the leaderless case using the consensus control scheme with uncertain parameters and variable time-delays.

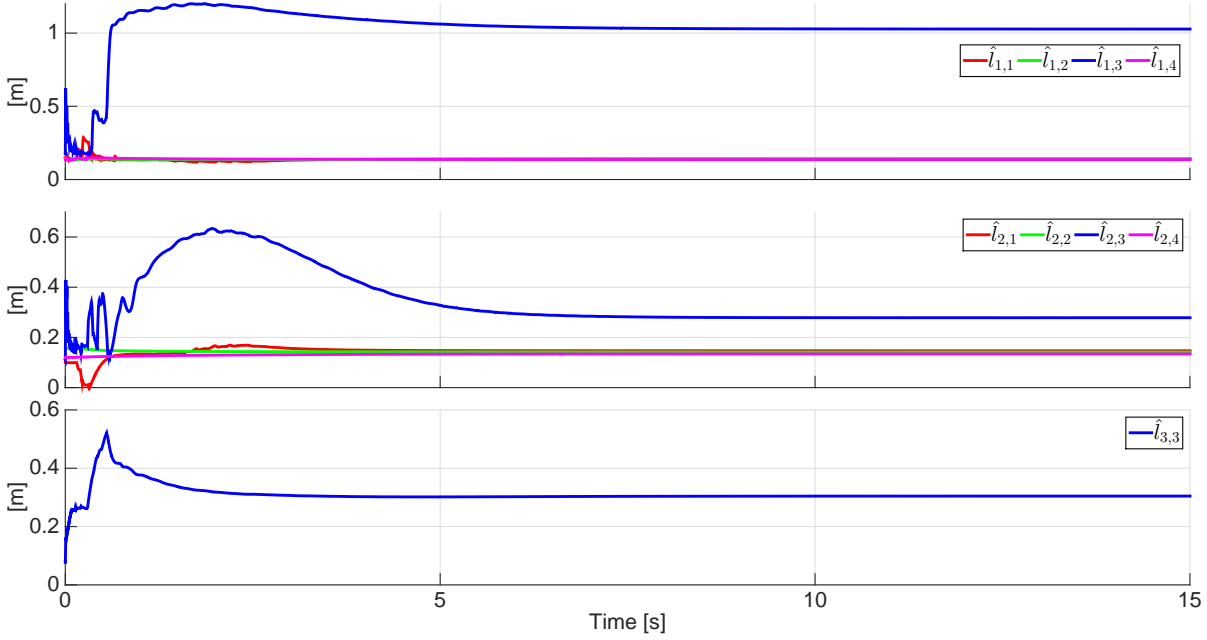


Figure 4.18: Kinematic parameters estimation for the leaderless case using the consensus control scheme with uncertain parameters and variable time-delays.

detailed in (Spurrer 1978) is used to derive the unit-quaternions.

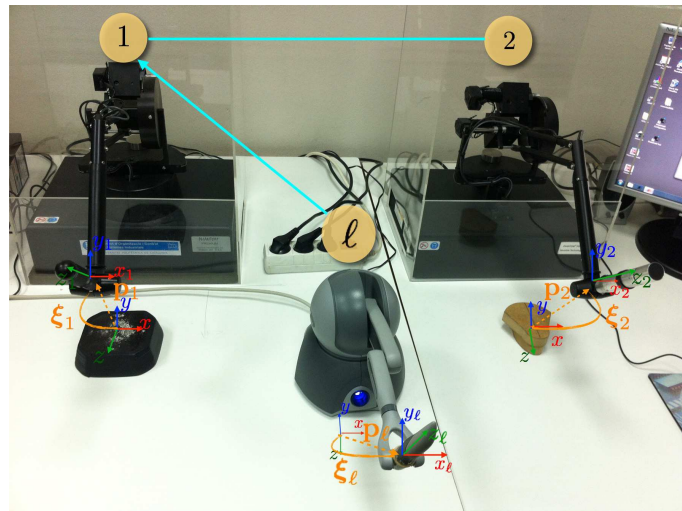
The gravitational torque vectors of the two Premium devices have been calculated as the gradient of the potential energy of the robot links  $l_1$ ,  $l_2$  and  $l_3$ . Table 4.7 depicts the link lengths and the masses involved in the potential energy calculation. The corresponding gravity vector is:

$$\mathbf{g}_i(\mathbf{q}_i) = g \begin{bmatrix} 0 \\ (m_{1i}lc_{1i}+m_{2i}l_{1i}+m_{3i}l_{1i}) \cos(q_{2i})+(m_{2i}lc_{2i}+m_{3i}l_{2i}) \sin(q_{3i})+m_{3i}l_{3i} \cos(q_{3i}+q_{5i}) \\ (m_{2i}lc_{2i}+m_{3i}l_{2i}) \sin(q_{3i})+m_{3i}lc_{3i} \cos(q_{3i}+q_{5i}) \\ m_{3i}lc_{3i} \sin(q_{3i}+q_{5i}) \sin(q_{4i}) \\ m_{3i}lc_{3i} \cos(q_{3i}) \cos(q_{5i}) \\ 0 \end{bmatrix},$$

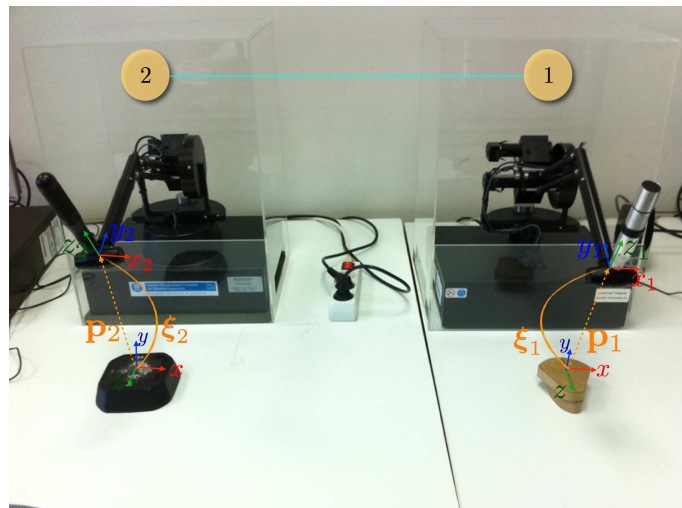
where  $g$  is the gravity acceleration constant and the rest of the parameters are defined in Table 4.7. The gravity vector of the Omni is given by

$$\mathbf{g}(\mathbf{q}) = \begin{bmatrix} 0 \\ m_3l_2 \sin(q_2 + q_3) + (m_3l_2 + m_2l_1) \cos(q_2) \\ m_3l_2 \sin(q_2 + q_3) \end{bmatrix},$$

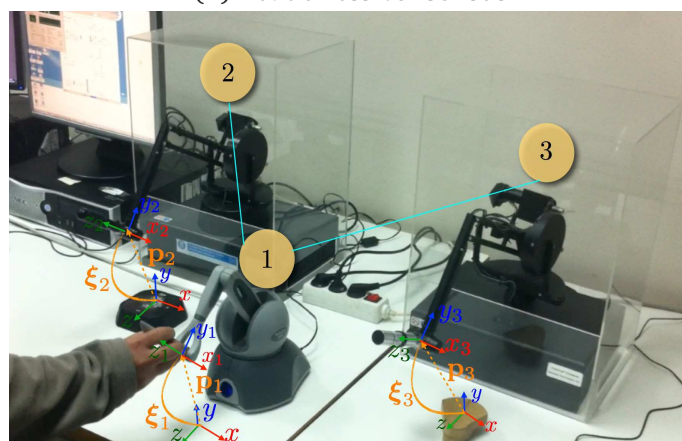
and its physical parameters have been experimentally estimated yielding  $l_1 = 0.16$ ,  $l_2 = 0.19$ ,  $m_2 = 0.02$  and  $m_3 = 0.055$  (Nuño, Sarras, Panteley, and Basañez 2012).



(a) Leader-follower consensus



(b) Leaderless consensus



(c) Leaderless consensus with human-robot interactions

Figure 4.19: Experimental validation test-bed.

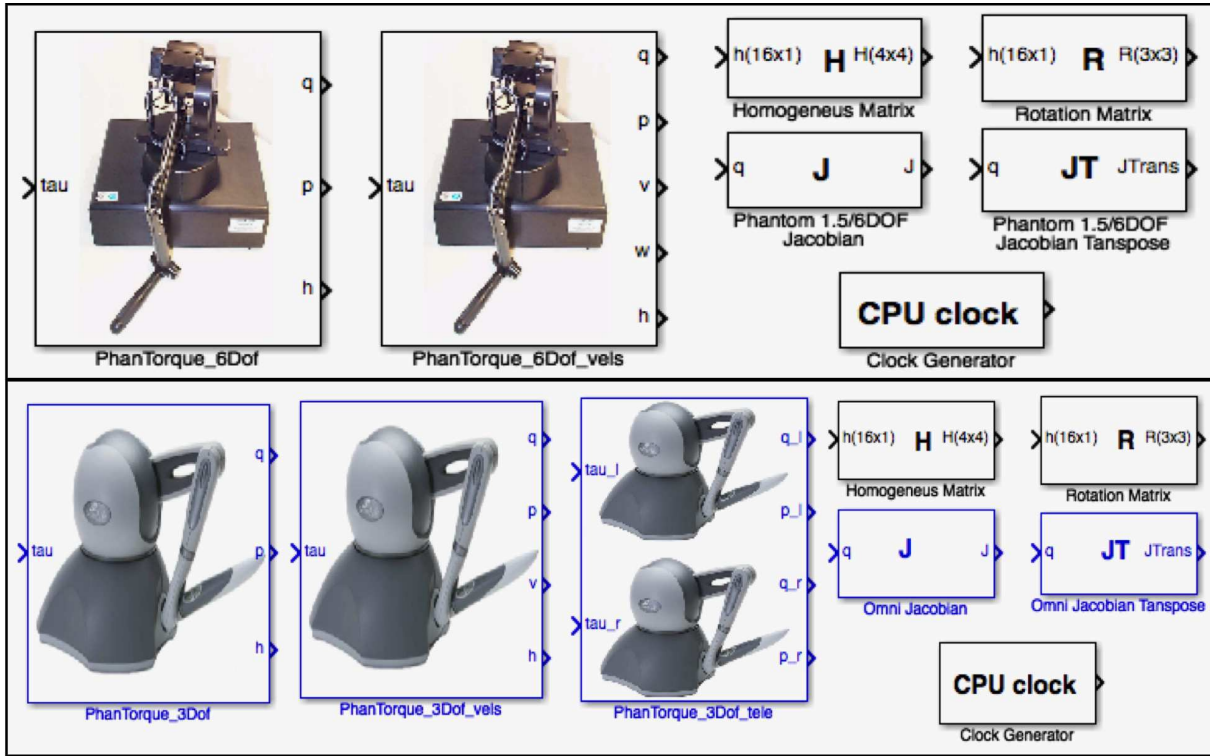


Figure 4.20: PhanTorque\_6Dof and PhanTorque\_3Dof libraries.

#### 4.6.2 Consensus control without velocity measurements

##### Leader-follower case

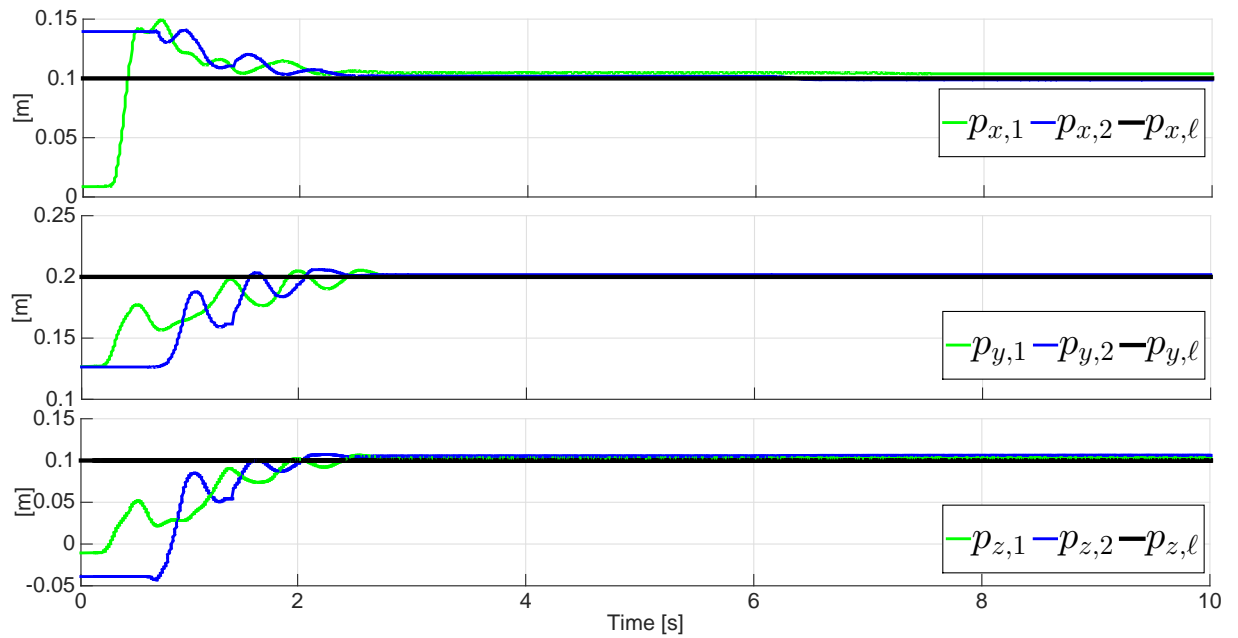
The network configuration used in this experiment is shown in Figure 4.19.(a). The Omni robot is employed as the leader ( $\ell$ ) and it sends its constant pose to only Node 1, hence  $b_{1\ell} = 1$  and  $b_{2\ell} = 0$ . The interconnection weights of the follower network are  $a_{12} = a_{21} = 1$ , defining the following Laplacian matrix

$$L = \begin{bmatrix} 1 & -1 \\ -1 & 1 \end{bmatrix}. \quad (4.84)$$

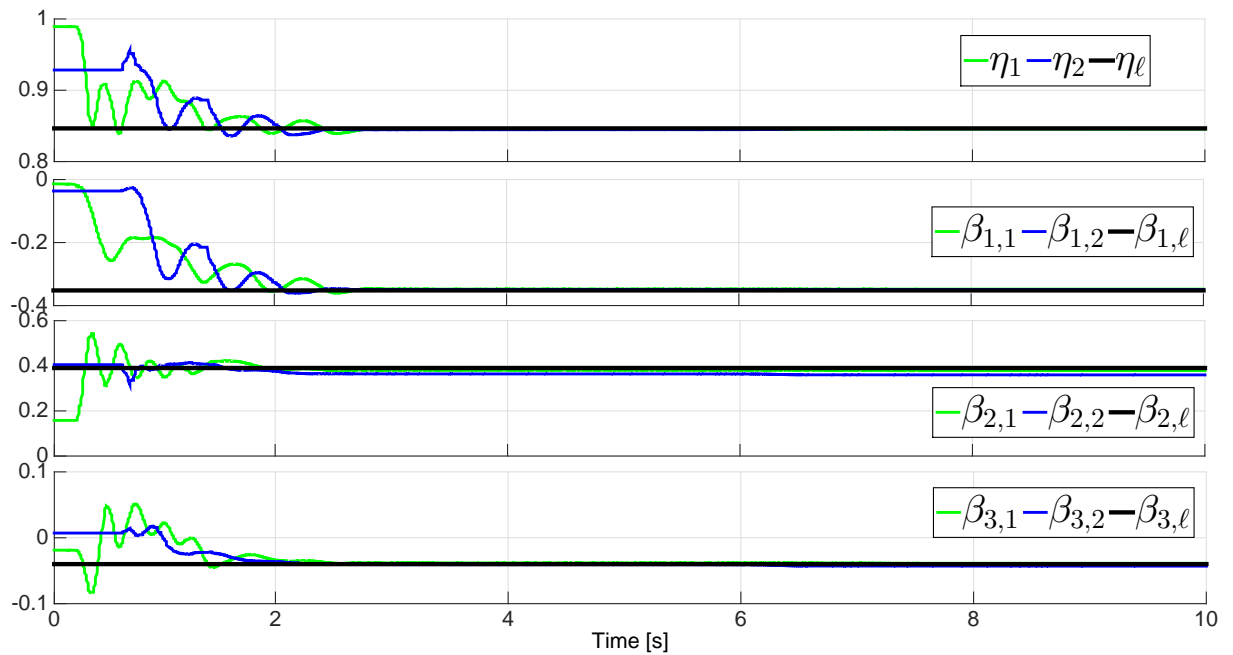
The controller gains have been set to  $k_1 = 20$ ,  $d_1 = 3$ ,  $k_2 = 14$ ,  $d_2 = 10$  and  $k_{y1} = k_{y2} = 1000$ . Figures 4.21.(a) and 4.21.(b) show that, despite the differences in initial conditions, the robots of Node 1 and Node 2 reach the leader pose after two seconds. The behavior of the linear and angular velocities are shown in Figures 4.22.(a) and 4.22.(b), respectively.

##### Leaderless case

The leaderless consensus control scheme is validated through two different scenarios: without external forces (Proposition 4.2) and when a human operator injects forces to one of the agents in the network (Proposition 4.3).

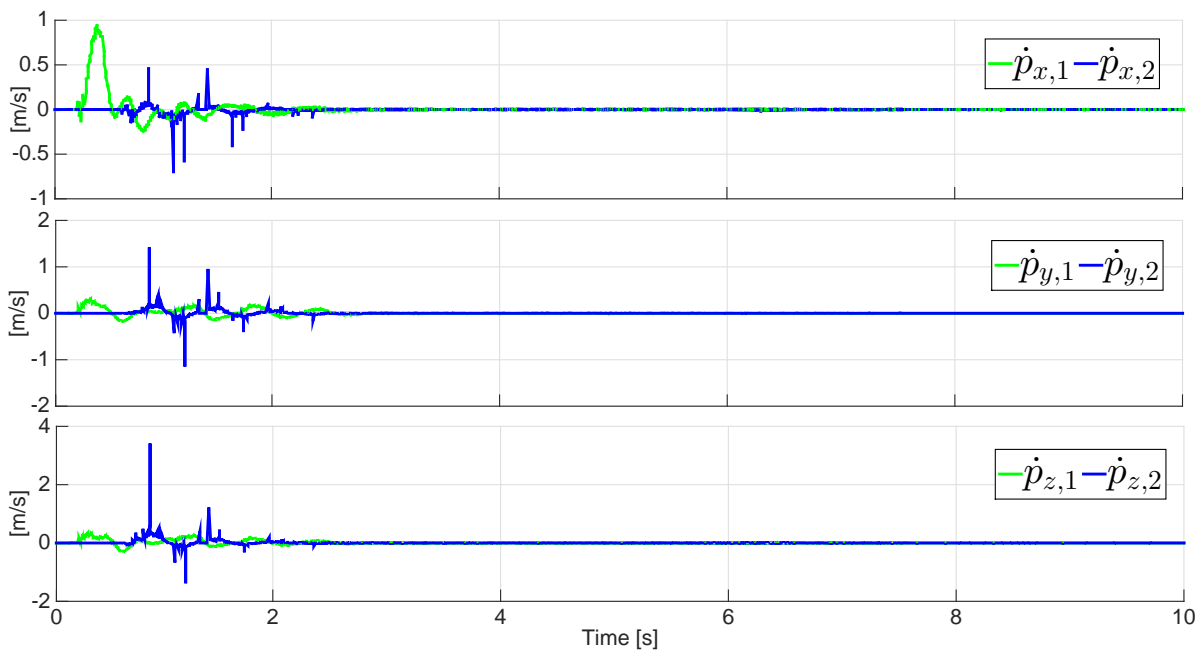


(a) Positions

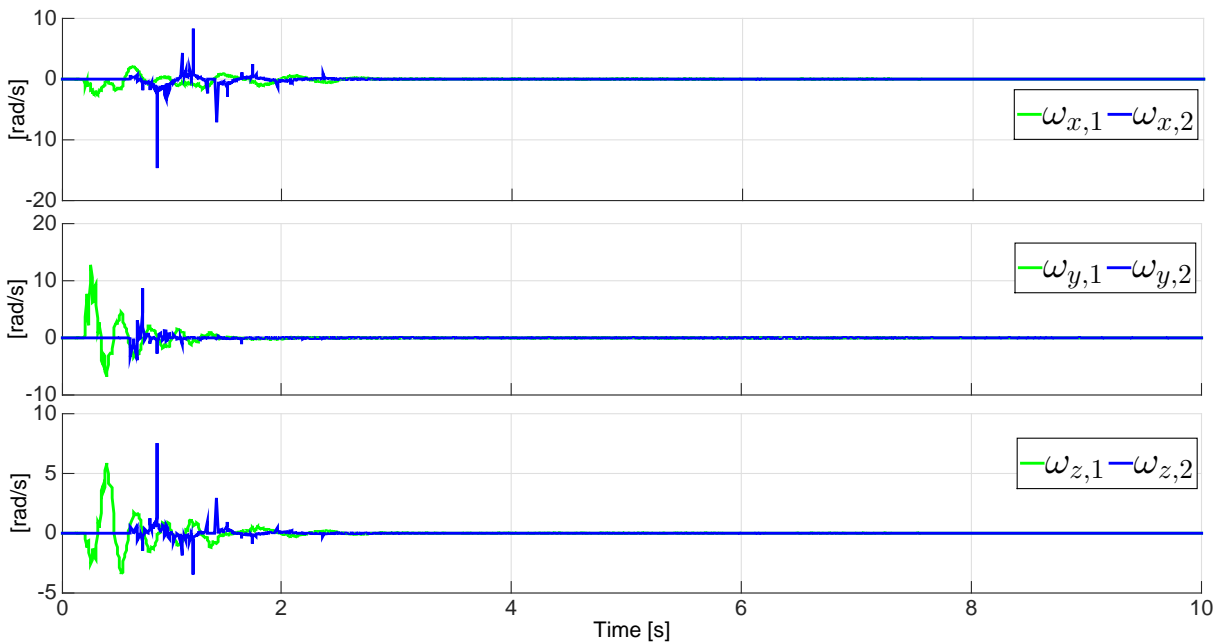


(b) Unit-quaterrions (Orientations)

Figure 4.21: Pose of the robots for the leader-follower case using the consensus control scheme without velocity measurements.



(a) Linear velocities



(b) Angular velocities

Figure 4.22: Velocities of the robots for the leader-follower case using the consensus control scheme without velocity measurements.



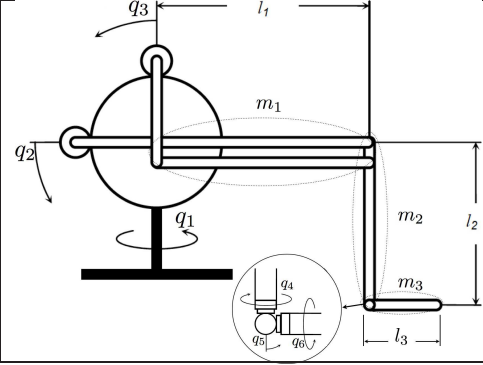
	Parameter	Premium 1.5HF	Premium 1.5
	Masses (kg)	$m_1=0.0056$ $m_2=0.005$ $m_3=0.09$	$m_1=0.026$ $m_2=0.01$ $m_3=0.09$
	Lengths (m)	$l_1=0.21$ $l_2=0.21$ $l_3=0.1$	$l_1=0.21$ $l_2=0.21$ $l_3=0.07$
	Center of masses (m)	$lc_1=0.105$ $lc_2=0.21$ $lc_3=0.1$	$lc_1=0.105$ $lc_2=0.21$ $lc_3=0.07$

Table 4.7: Estimated parameters of the Premium robots.

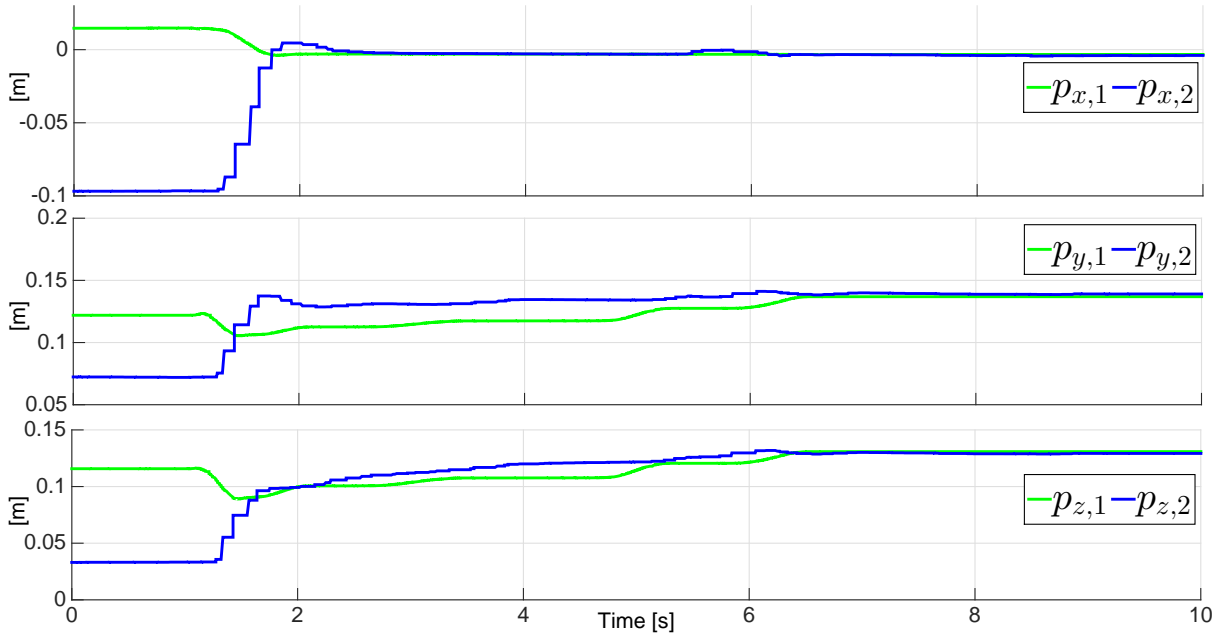
Figure 4.19.(b) shows the network configuration used for the validation of the leaderless consensus control without external forces. The controller parameters are set to  $k_1 = 7$ ,  $d_1 = 7$ ,  $k_2 = 10$ ,  $d_2 = 10$ , and  $k_{y1} = k_{y2} = 1000$ . The Laplacian matrix is the same of (4.84). The time evolution of the two robots pose is depicted in Figures 4.23.(a) and 4.23.(b). During the first seconds only the gravity compensation (4.84) is applied to the robots, which allows to set different initial conditions. From 1.1s, the controllers (4.14) with  $b_{1\ell} = b_{2\ell} = 0$  are activated in the two robots, and this makes the robots converge to a common pose after five seconds. The linear and angular velocities are shown in Figures 4.24.(a) and Figure 4.24.(b), respectively.

#### Leaderless case with human interactions

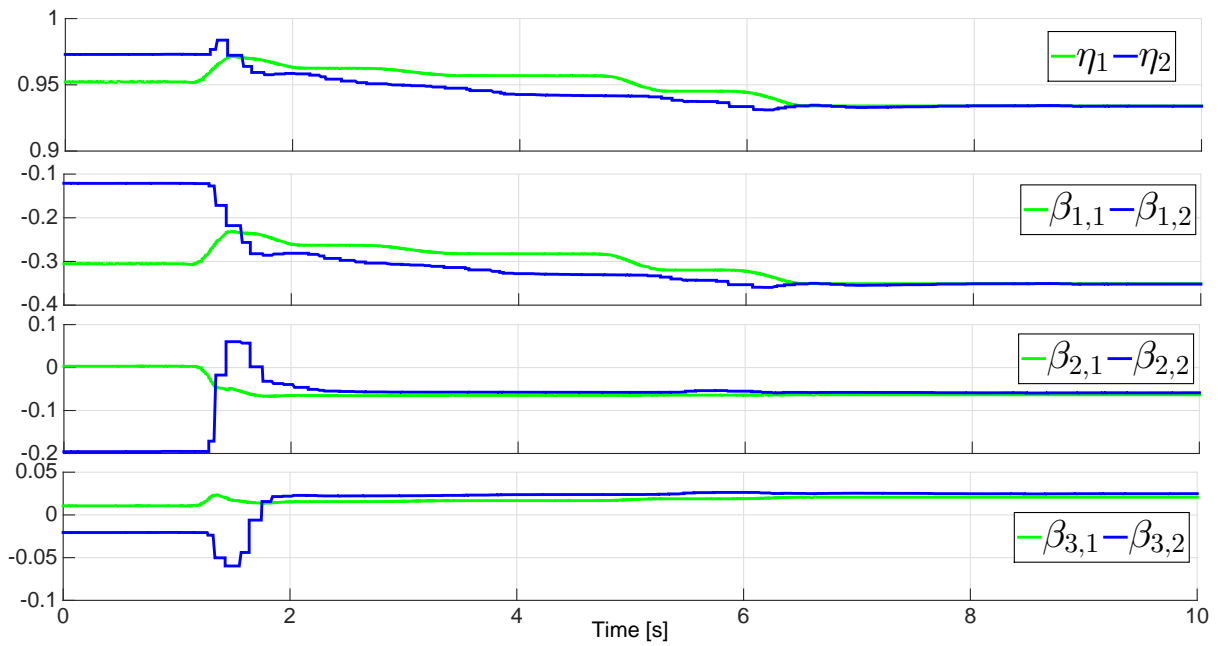
Figure 4.19.(c) shows the setup used for this experiment. The controller gains have been set to  $k_1 = 5$ ,  $d_1 = 1$ ,  $k_2 = 20$ ,  $d_2 = 3$ ,  $k_3 = 17$ ,  $d_3 = 1.5$ , and  $k_{y1} = k_{y2} = 1000$ . The interconnection weights are set to:  $a_{12} = a_{13} = a_{21} = a_{31} = 1$ , defining the following Laplacian matrix,

$$\mathbf{L} = \begin{bmatrix} 2 & -1 & -1 \\ -1 & 1 & 0 \\ -1 & 0 & 1 \end{bmatrix}.$$

Since the Omni device has only three actuated DoF, the human operator compensates the gravity effects of the non-actuated DoF. Moreover, the human operator injects forces to the Omni robot resulting in a human controlled motion of the device. Figures 4.25.(a) and 4.25.(b) show the pose behavior of the three robots of the network. It can be observed that during the first nine seconds the robots are in the same initial pose, then, from the second 9 to second 115, the human operator injects forces such that the Omni robot moves. In the last five seconds the Omni is moved to the initial pose and it is left there. It can be appreciated that the pose errors are small and bounded when human forces are injected to the network. The linear and the angular velocities are shown in Figures 4.26.(a) and 4.26.(b), respectively.

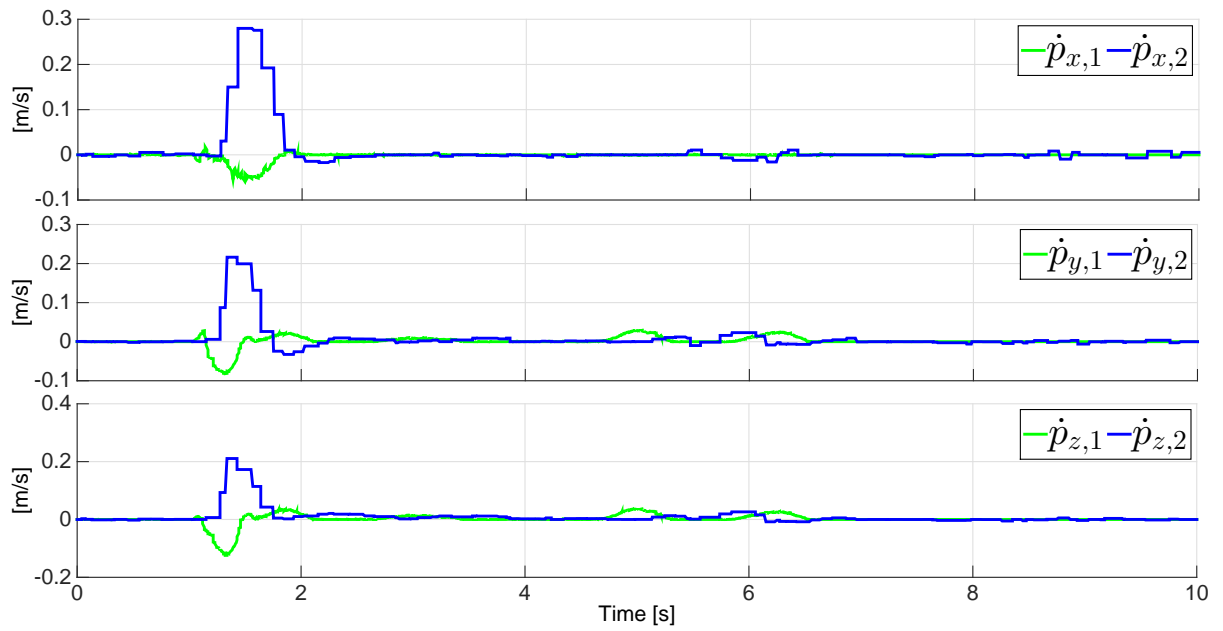


(a) Positions

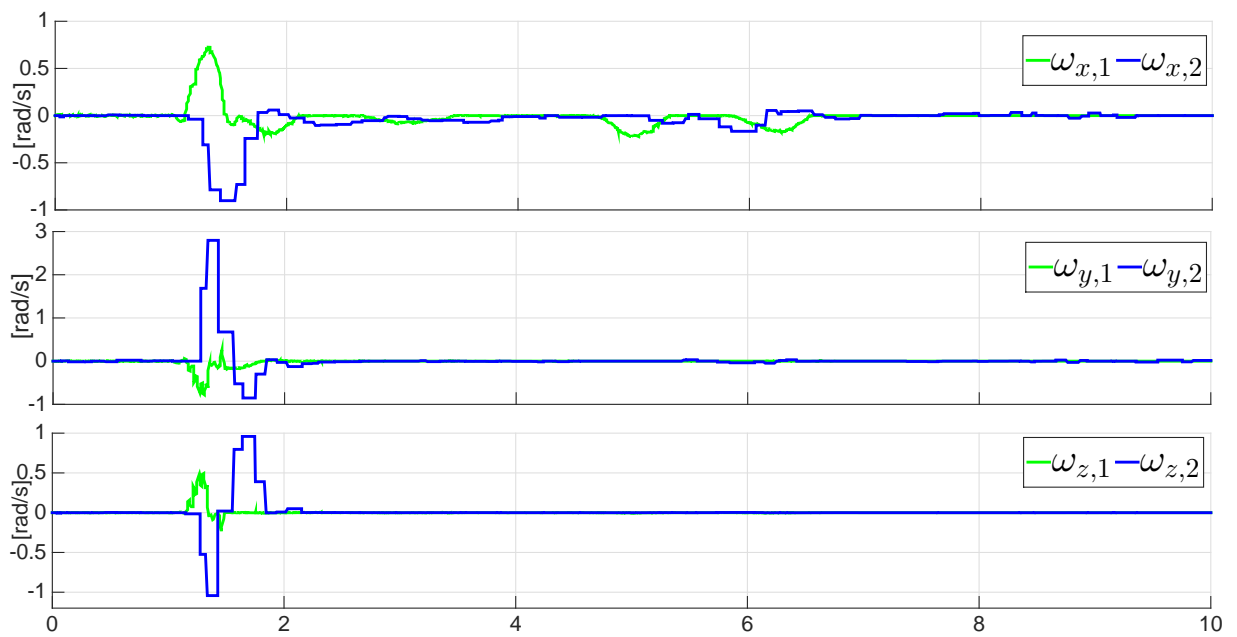


(b) Unit-quaternions (Orientations)

Figure 4.23: Pose of the robots for the leaderless case using the consensus control scheme without velocity measurements.

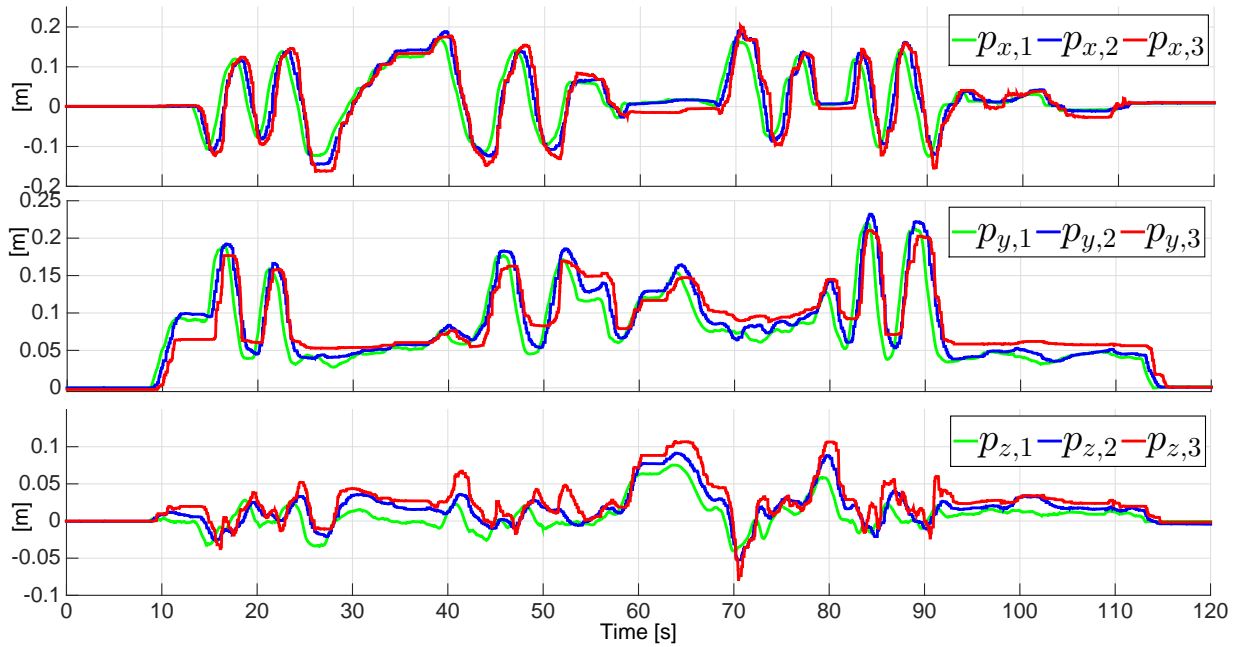


(a) Linear velocities

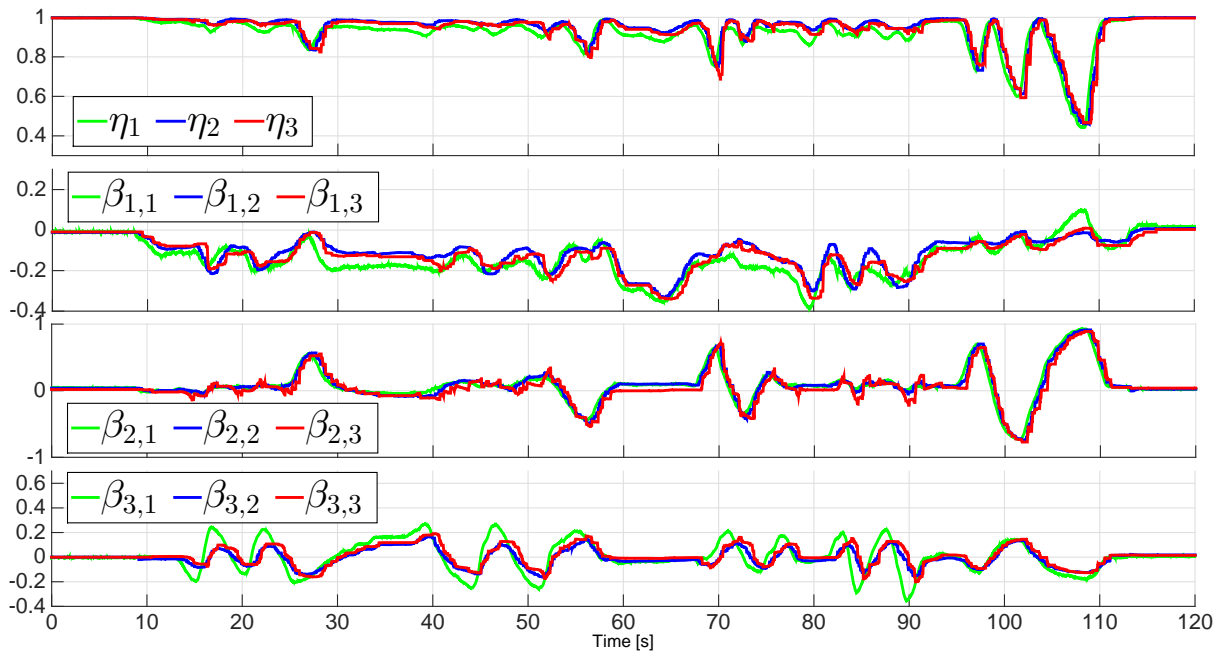


(b) Angular velocities

Figure 4.24: Velocities of the robots for the leaderless case using the consensus control scheme without velocity measurements.

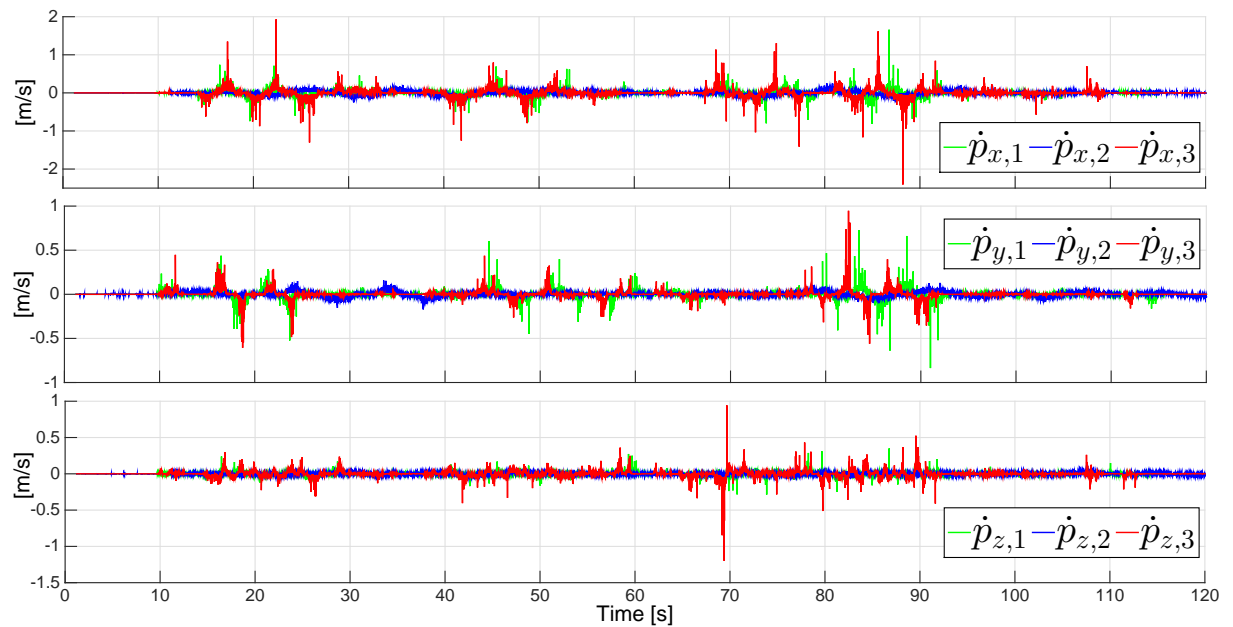


(a) Positions

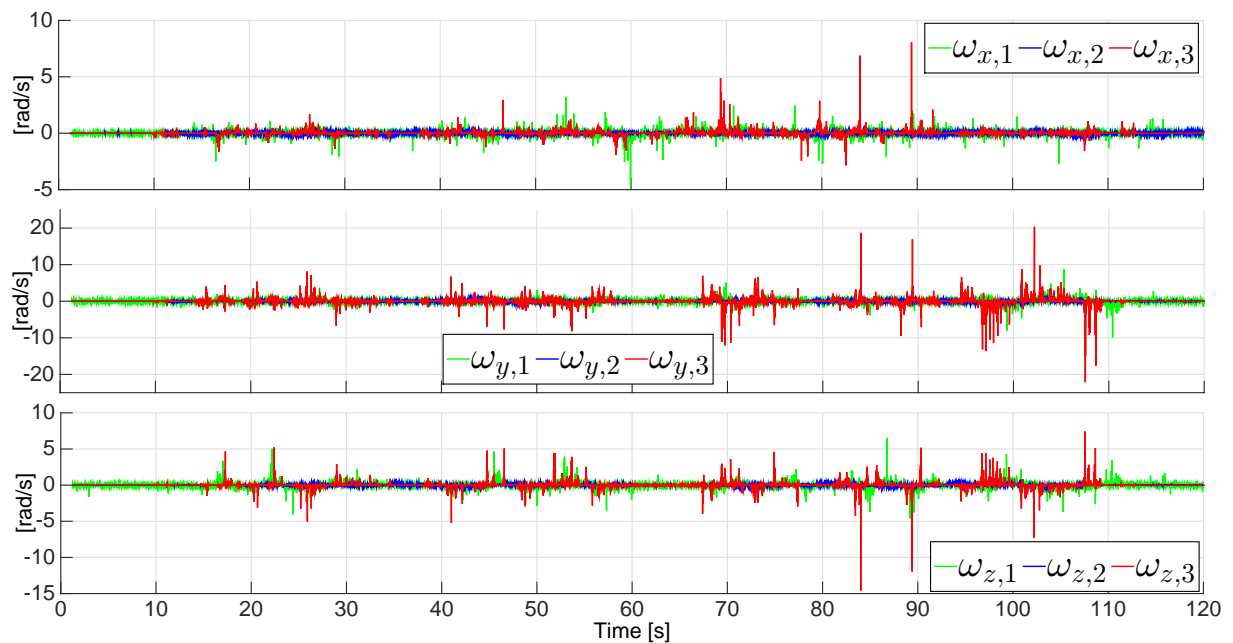


(b) Unit-quatrnions (Orientations)

Figure 4.25: Pose of the robots for the leaderless with human interaction case using the consensus control scheme without velocity measurements.



(a) Linear velocities



(b) Angular velocities

Figure 4.26: Velocities of the robots for the leaderless with human interaction case using the consensus control scheme without velocity measurements.

### 4.6.3 Consensus control with variable time-delays

A transcontinental communication has been emulated In the laboratory local network by adding artificially delays with a normal Gaussian distribution (Salvo-Rossi et al. 2006), as those used in the simulations. A small time window of these variable time-delays is shown in the Figure 4.27

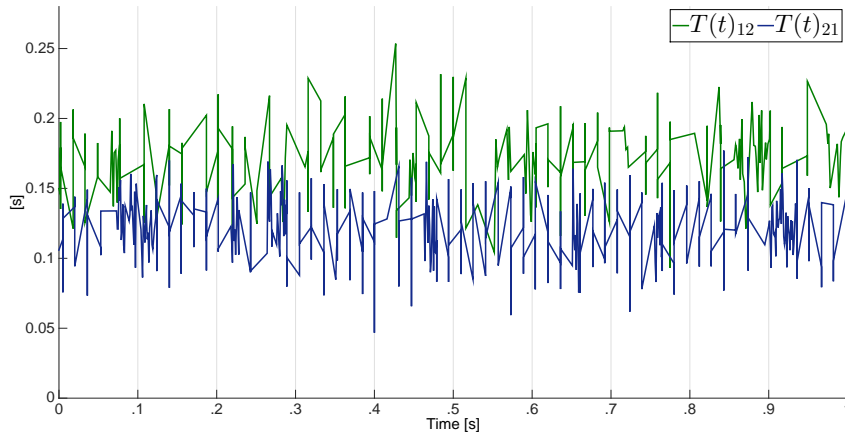


Figure 4.27: Sample of the variable time-delays added to the communication channel of the robot network.

#### Leader-follower case

Figure 4.19.(a) shows the network's interconnection for the leader-follower case, in which the leader constant pose has been made available only to Node 1 ( $b_{1\ell} = 1$  and  $b_{2\ell} = 0$ ). The interconnection weights, among Node 1 and Node 2, are set as  $a_{12} = a_{21} = 0.6$ , defining the following Laplacian matrix

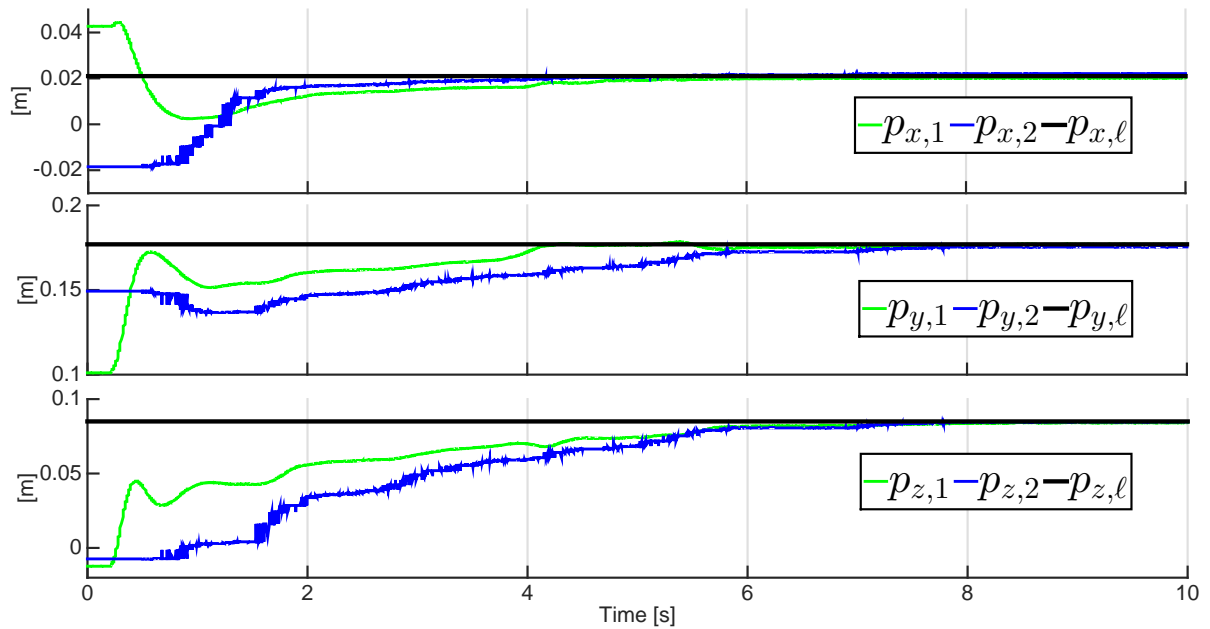
$$\mathbf{L} = \begin{bmatrix} 0.6 & -0.6 \\ -0.6 & 0.6 \end{bmatrix}.$$

The proportional and damping injection gains are  $k_1=10$ ,  $d_1=1.4$ ,  $k_2=7$ ,  $d_2=1.25$  for  $\alpha_1=0.3$ ,  $\alpha_2=0.35$ . The statistical parameters of the induced delays are 0.12s and 0.17s, for the corresponding mean, and 0.0004s and 0.0005s, for the corresponding variances. The practical upper-bounds are  ${}^*T_{12}=0.25$ s and  ${}^*T_{21}=0.19$ s.

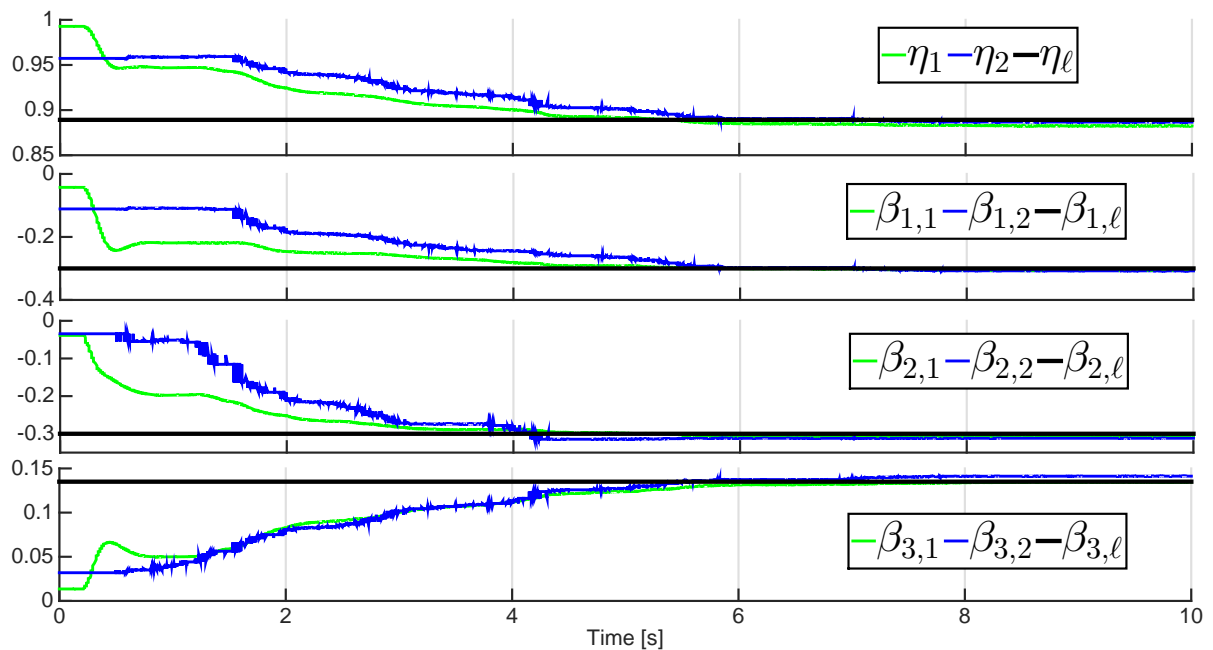
Figure 4.28.(a) and Figure 4.28.(b) show that despite the initial poses differences of the two robots and the variable time-delays in their communication channel, both robots asymptotically reach the leader pose. In Figures. 4.29.(a) and 4.29.(b), it can be observed that velocities converge to zero.

#### Leaderless case

This case is evaluated using the robot network depicted in Figure 4.19.(b), The interconnection weights are set to  $a_{12} = a_{21} = 0.7$ , defining the following Laplacian matrix

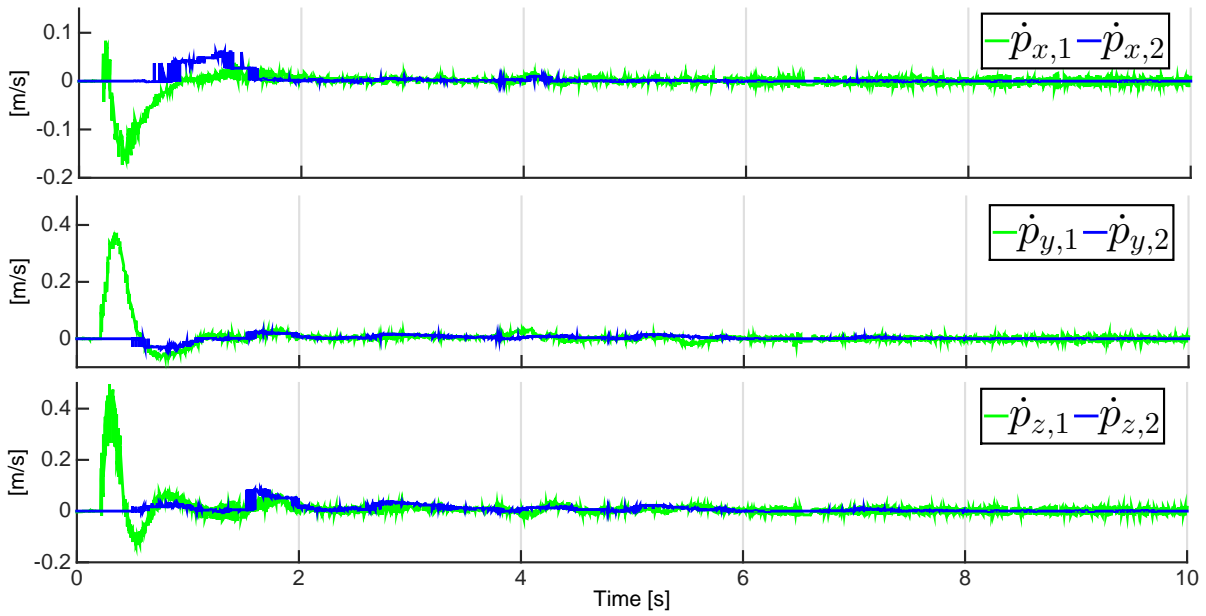


(a) Positions

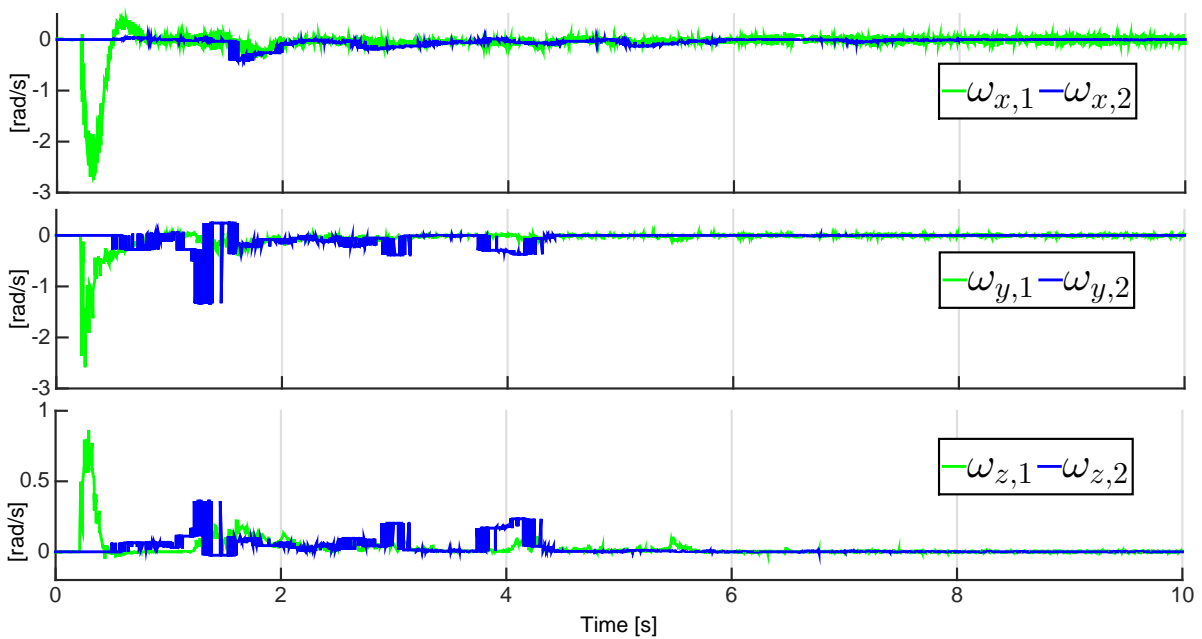


(b) Unit-quaternions (Orientations)

Figure 4.28: Pose of the robots for the leader-follower case using the consensus control scheme with variable time-delays.



(a) Linear velocities



(b) Angular velocities

Figure 4.29: Velocities of the robots for the leader-follower case using the consensus control scheme with variable time-delays.



$$\mathbf{L} = \begin{bmatrix} 0.7 & -0.7 \\ -0.7 & 0.7 \end{bmatrix}.$$

The proportional and damping injection gains are  $k_1=3.5$ ,  $d_1=1.4$ ,  $k_2=3.6$ ,  $d_2=1.25$  for  $\alpha_1=0.3$ ,  $\alpha_2=0.4$ . The variable time-delays parameters are the same as in the previous case. It can be observed in Figure 4.30, in coherence with the Proposition 4.6, how the two robots converge to a common pose from their different initial poses, the velocities behavior being shown in the Figure 4.31. Several experiments of this case have been performed changing the initial conditions, resulting in a different pose agreement for each case.

#### Leaderless case with human interactions

Using the robot network depicted in Figure 4.19.(c) the consensus control scheme detailed in Proposition 4.7 is evaluated. The interconnection weights are set to  $a_{12} = a_{21} = 0.8$  and  $a_{13} = a_{31} = 0.9$ , defining the following Laplacian

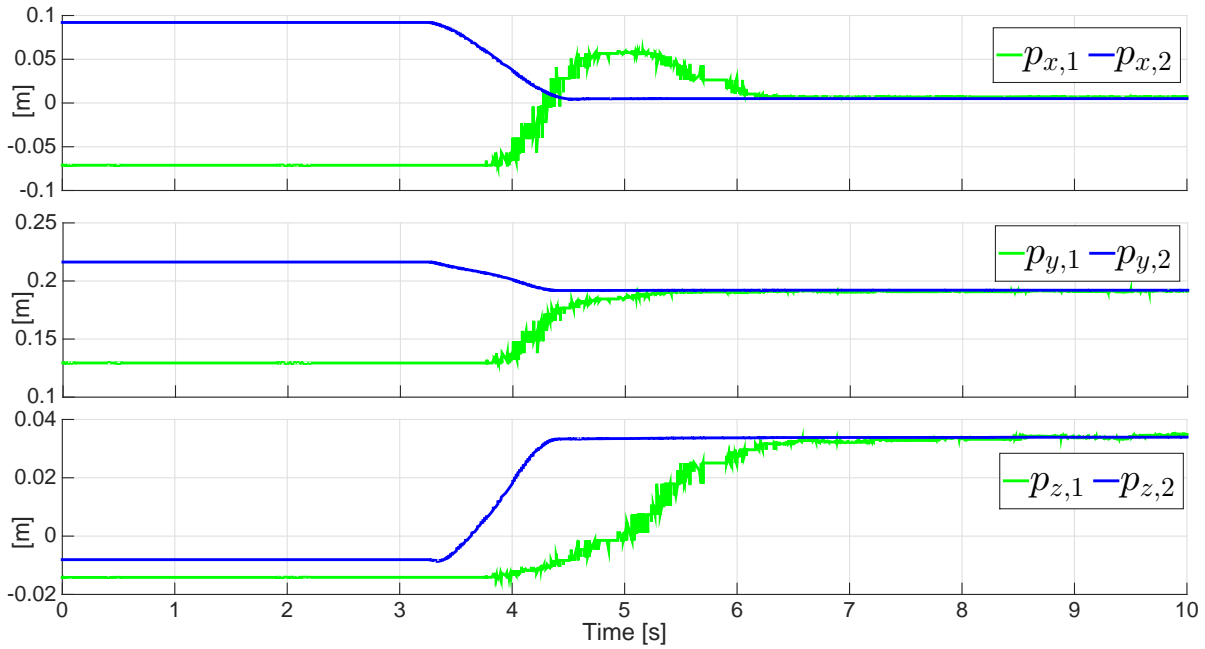
$$\mathbf{L} = \begin{bmatrix} 1.7 & -0.8 & -0.9 \\ -0.8 & 0.8 & 0 \\ -0.9 & 0 & 0.9 \end{bmatrix}.$$

The proportional and damping injection gains are  $k_1=4$ ,  $d_1=1.1$ ,  $k_2=9$ ,  $d_2=1.9$  and  $k_3=5$ ,  $d_3=1.3$  for  $\alpha_1=0.2$ ,  $\alpha_2=0.3$  and  $\alpha_3=0.35$ . The statistical parameters and upper-bounds of the variable time-delays are shown in Table 4.8.

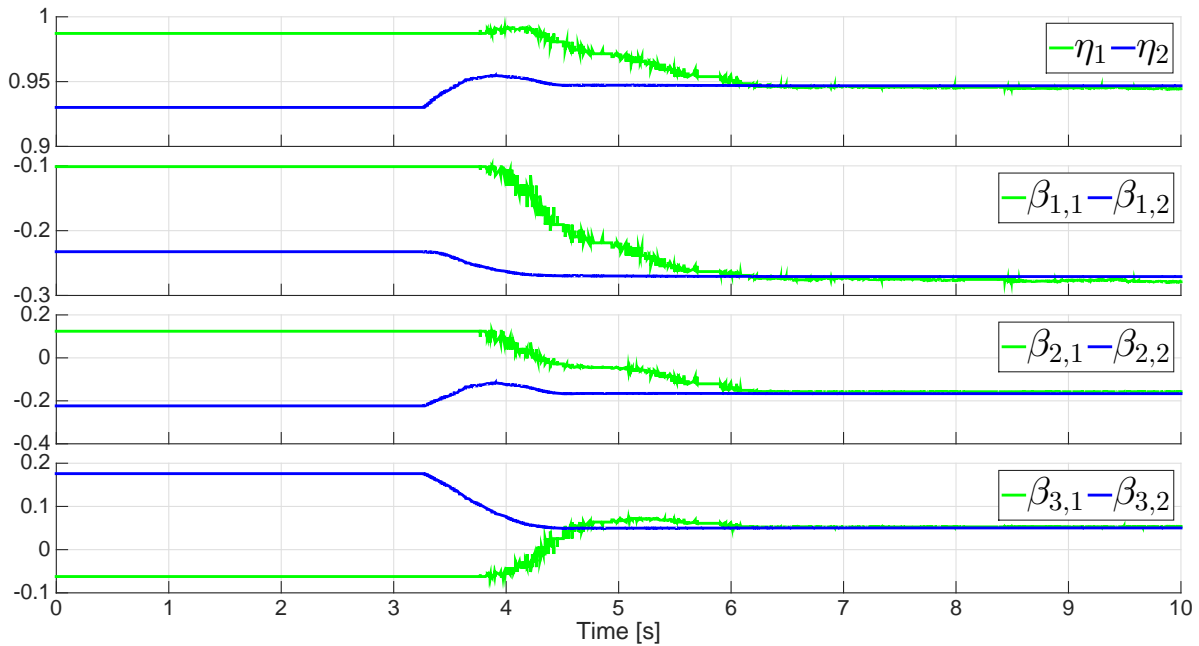
Figures 4.32.(a) and 4.32.(b) show the pose behavior of the three robots. It is observed that during the first eight seconds the robots keep their common initial pose, then the robots pose change because a human operator injects forces to the robot Omni (Node 1) from the second 8 to second 112. In the last eight seconds no more forces are injected to the network. It can be appreciated that the pose errors are small and bounded when forces are injected and how the robots converge to a common pose when no more forces are injected to the network. The behavior of the linear and the angular velocities are shown in Figures 4.33.(a) and 4.33.(b), respectively.

$*T_{ji}$ [s]	Mean [s]	Variance [ $\mu s$ ]
$*T_{12}=0.21$	0.12	500
$*T_{21}=0.16$	0.10	200
$*T_{13}=0.20$	0.17	50
$*T_{31}=0.20$	0.12	450

Table 4.8: Upper-bounds of the variable time-delays and Gaussian distribution parameters.

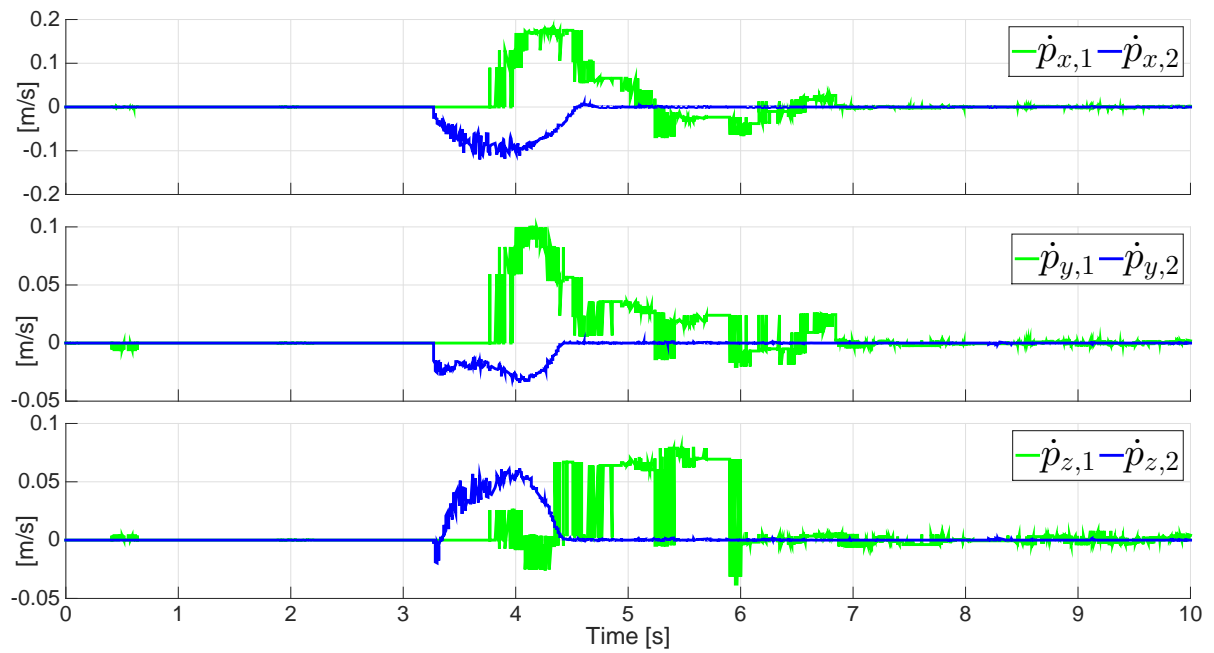


(a) Positions

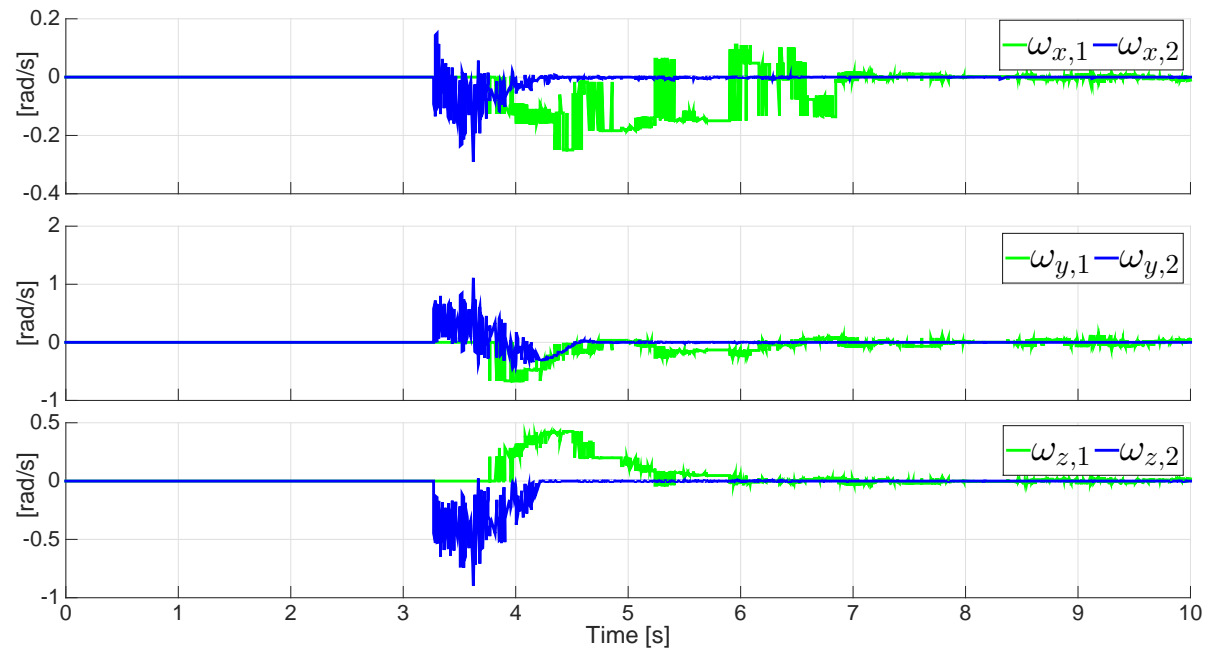


(b) Unit-quaternions (Orientations)

Figure 4.30: Pose of the robots for the leaderless case using the consensus control scheme with variable time-delays.

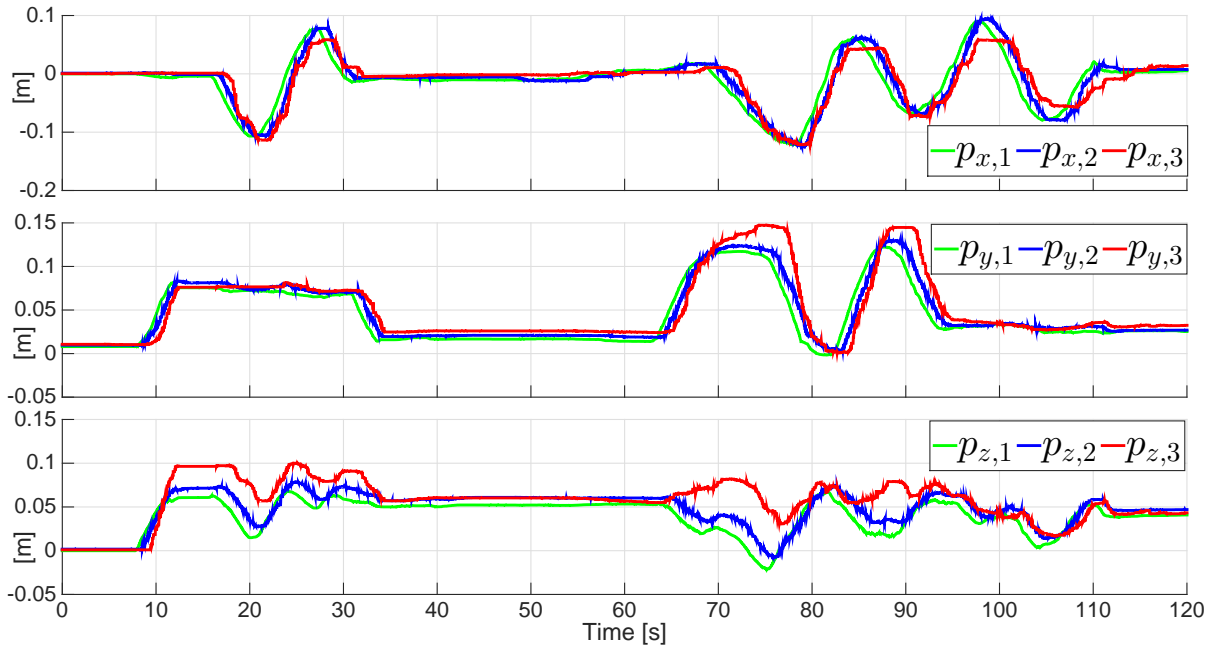


(a) Linear velocities

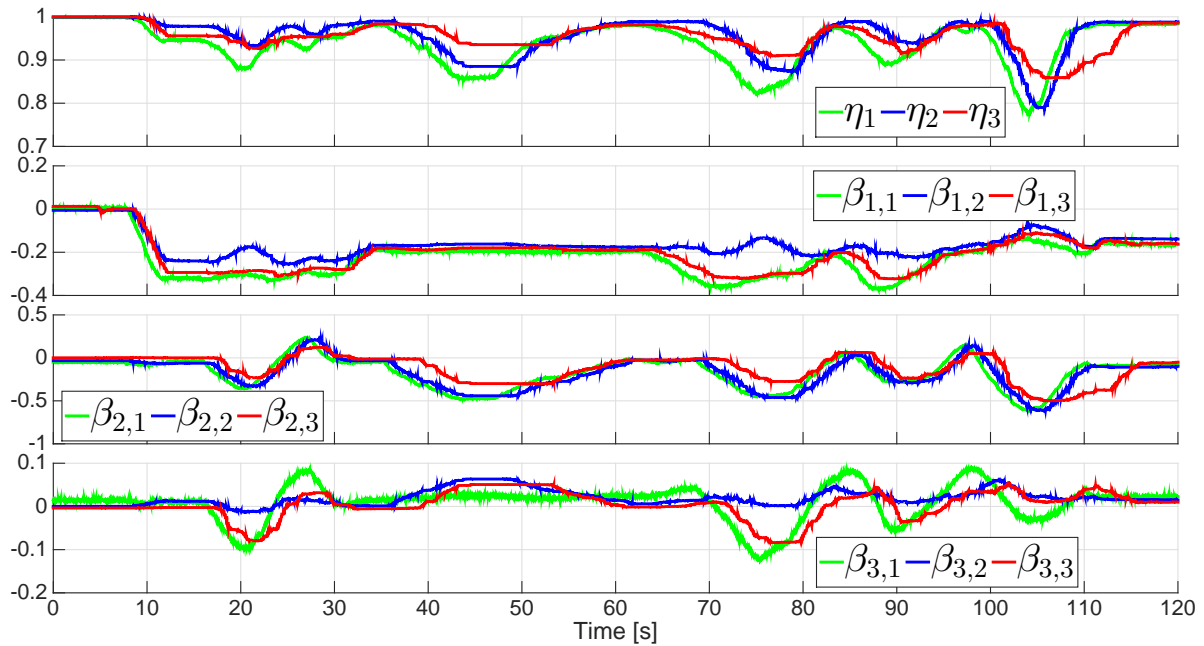


(b) Angular velocities

Figure 4.31: Velocities of the robots for the leaderless case using the consensus control scheme with variable time-delays.

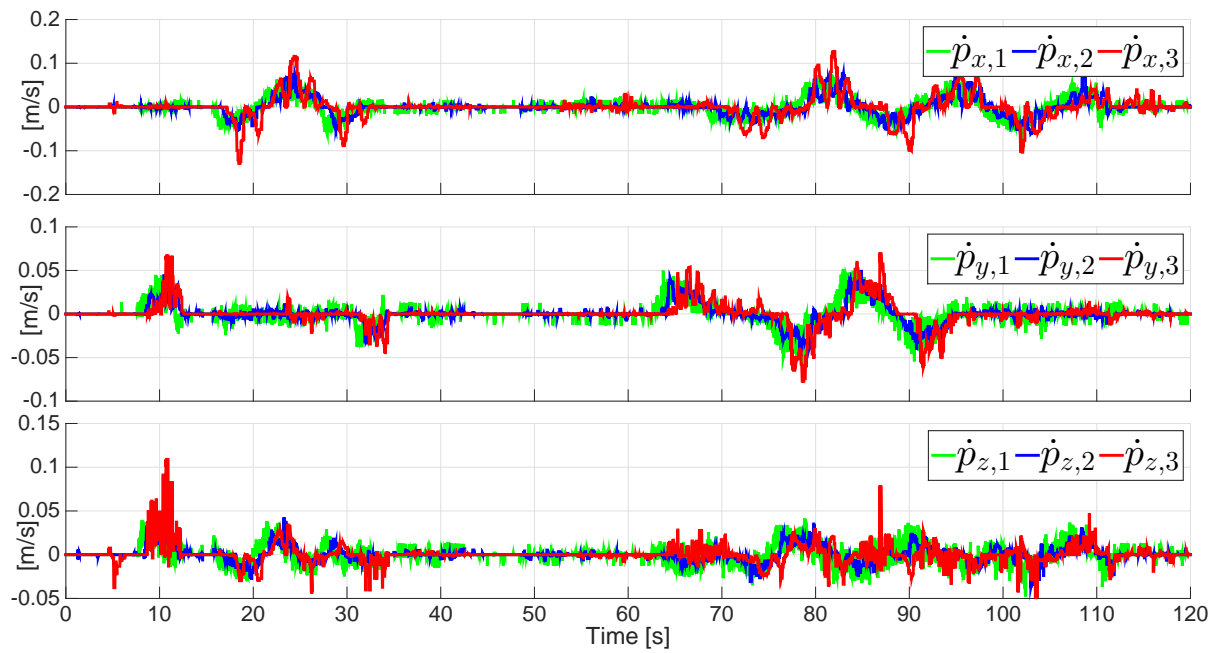


(a) Positions

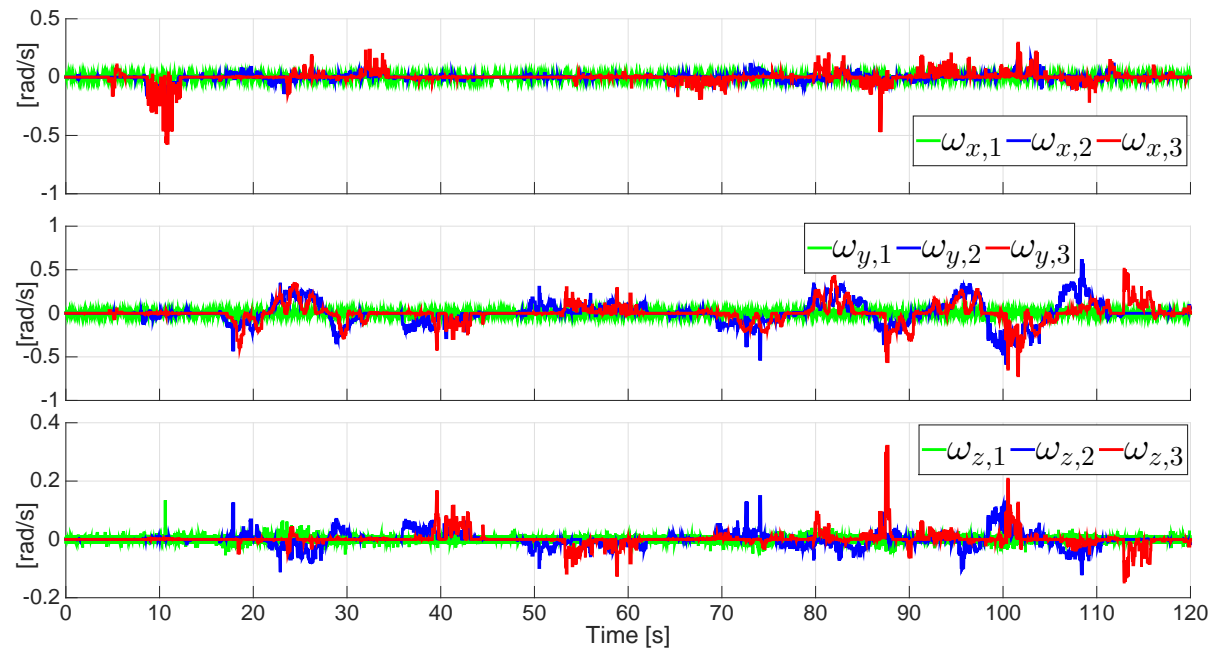


(b) Unit-quaternions (Orientations)

Figure 4.32: Pose of the robots for the leaderless with human interaction case using the consensus control scheme with variable time-delays.



(a) Linear velocities



(b) Angular velocities

Figure 4.33: Velocities of the robots for the leaderless with human interaction case using the consensus control scheme with variable time-delays.



**TELEOPERATION CONTROL**

*This chapter proposes control algorithms for Single Local and Single Remote (SL-SR) teleoperation systems and for Cooperative Teleoperation Systems (CTS) derived from the consensus control schemes presented in Chapter 4. Simulations and experimental validations that show the effectiveness of the proposed controllers are presented at the end of this chapter.*

## **5.1 Controllers for SL-SR teleoperation systems**

In this section three control algorithms for SL-SR teleoperation systems under the scenarios described in Section 4.1 are detailed.

In general, the single robot teleoperation control problem can be viewed as a special case of the Leaderless Consensus Problem with one robot interacting with a remote environment and another robot that is handled by a human operator. Hence, the proofs of the results in this section are referred to those of the corresponding leaderless consensus case.

### **5.1.1 Teleoperation control without velocity measurements**

For the case of SL-SR teleoperation systems, for which only pose measurements of the robots are available, the following controller for the local ( $\ell$ ) and remote ( $r$ ) manipulators is derived

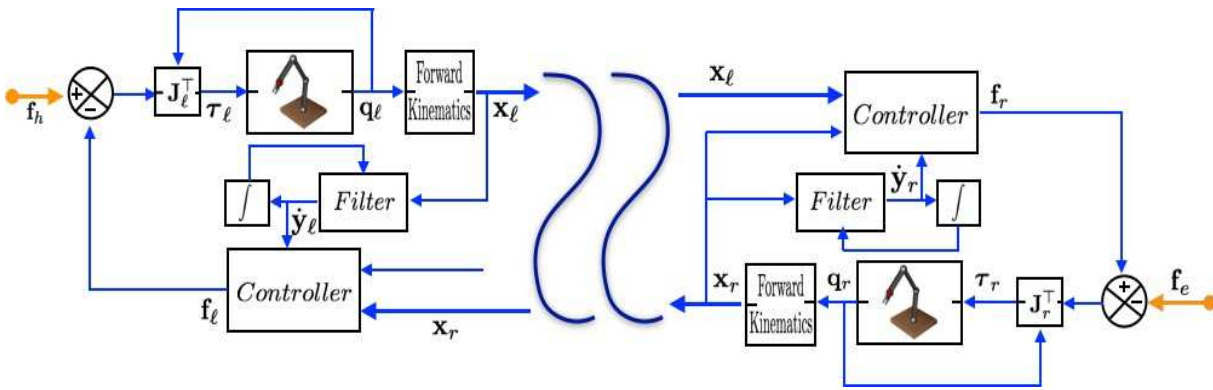


Figure 5.1: Control scheme for teleoperation systems without velocity measurements. The controller is defined in (5.1).

from the consensus control scheme proposed in Section 4.2:

$$\left. \begin{aligned} \dot{\mathbf{y}}_l &= \mathbf{x}_l - k_{yl}\mathbf{y}_l \\ \mathbf{f}_l &= k_l\Phi(\boldsymbol{\xi}_l)\mathbf{e}_{lr} - \mathbf{g}_l(\mathbf{q}_l) + d_l\Phi(\boldsymbol{\xi}_l)\dot{\mathbf{y}}_l \\ \dot{\mathbf{y}}_r &= \mathbf{x}_r - k_{yr}\mathbf{y}_r \\ \mathbf{f}_r &= -k_r\Phi(\boldsymbol{\xi}_r)\mathbf{e}_{rl} + \mathbf{g}_r(\mathbf{q}_r) - d_r\Phi(\boldsymbol{\xi}_r)\dot{\mathbf{y}}_r \end{aligned} \right\} \quad (5.1)$$

Figure 5.1 shows a block diagram of this control scheme.

The local and remote dynamics (3.58) in closed-loop with the controller (5.1) are

$$\left. \begin{aligned} \mathbf{M}_l(\mathbf{q}_l)\dot{\mathbf{v}}_l + \mathbf{C}_l(\mathbf{q}_l, \dot{\mathbf{q}}_l)\mathbf{v}_l + k_l\Phi(\boldsymbol{\xi}_l)\mathbf{e}_{lr} + d_l\Phi(\boldsymbol{\xi}_l)\dot{\mathbf{y}}_l &= \mathbf{f}_h \\ \mathbf{M}_r(\mathbf{q}_r)\dot{\mathbf{v}}_r + \mathbf{C}_r(\mathbf{q}_r, \dot{\mathbf{q}}_r)\mathbf{v}_r + k_r\Phi(\boldsymbol{\xi}_r)\mathbf{e}_{rl} + d_r\Phi(\boldsymbol{\xi}_r)\dot{\mathbf{y}}_r &= -\mathbf{f}_e \end{aligned} \right\} \quad (5.2)$$

**PROPOSITION 5.1:**

Consider the bilateral teleoperation system (3.58) and assume that the linear and the angular velocities are not available for measurements. Then, controller (5.1) ensures:

i) Convergence to zero of the velocities and pose errors, that is

$$\lim_{t \rightarrow \infty} \mathbf{v}_l(t) = \lim_{t \rightarrow \infty} \mathbf{e}_{lr}(t) = \mathbf{0}, \quad \lim_{t \rightarrow \infty} \mathbf{v}_r(t) = \lim_{t \rightarrow \infty} \mathbf{e}_{rl}(t) = \mathbf{0},$$

if the human operator does not inject forces on the local manipulator and the remote manipulator does not interact with the environment, i.e.,  $\mathbf{f}_h = \mathbf{f}_e = \mathbf{0}$ .  $\diamond$

ii) Boundedness of the velocities and pose errors, i.e.  $\mathbf{v}_l, \mathbf{v}_r, \mathbf{e}_{lr}, \mathbf{e}_{rl} \in \mathcal{L}_\infty$ , if the human operator



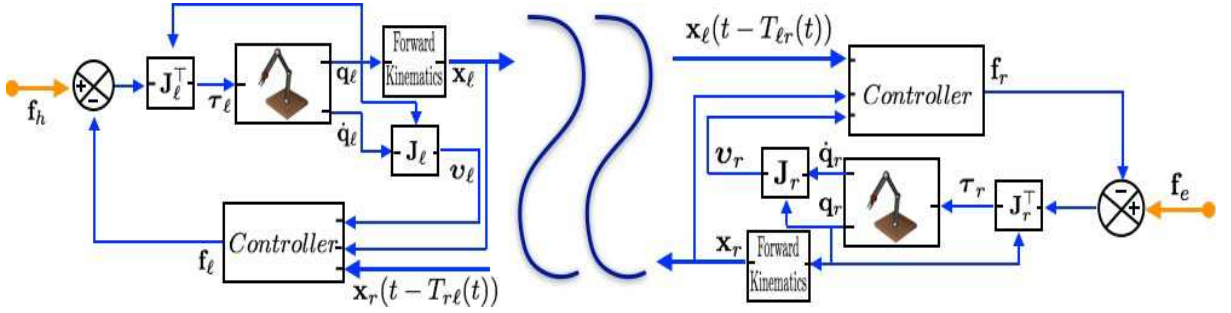


Figure 5.2: Control scheme for teleoperation systems with variable time-delays in the communication channel. The controller is defined in (5.5).

and the environment define passive velocity to force maps, that is,  $\forall t \geq 0$ ,  $\gamma \geq 0$  and  $\psi \geq 0$ ,

$$-\int_0^t \mathbf{v}_\ell^\top(\sigma) \mathbf{f}_h(\sigma) d\sigma + \gamma \geq 0, \quad \int_0^t \mathbf{v}_r^\top(\sigma) \mathbf{f}_e(\sigma) d\sigma - \psi \geq 0. \quad (5.3)$$

*Proof.* The proof of Claim i) is given by the proof of Proposition 4.2 for  $\bar{N} = \{\ell, r\}$  and interconnection weights set to:  $a_{\ell r} = a_{r\ell} = 1$ .

The proof of Claim ii) follows the same steps as in the proof of the Proposition 4.3, but in this case, the energy function is defined as  $\mathcal{D} := \mathcal{D}_\ell + \mathcal{D}_r$ , with:

$$\begin{aligned} \mathcal{D}_\ell &= \frac{1}{k_\ell} \mathcal{K}_\ell(\mathbf{v}_\ell) + \frac{1}{4} |\mathbf{x}_\ell - \mathbf{x}_r|^2 + \frac{1}{k_\ell} \left( \gamma - \int_0^t \mathbf{v}_\ell^\top(\sigma) \mathbf{f}_h(\sigma) d\sigma \right), \\ \mathcal{D}_r &= \frac{1}{k_r} \mathcal{K}_r(\mathbf{v}_r) + \frac{1}{4} |\mathbf{x}_r - \mathbf{x}_\ell|^2 - \frac{1}{k_r} \left( \psi - \int_0^t \mathbf{v}_r^\top(\sigma) \mathbf{f}_e(\sigma) d\sigma \right). \end{aligned} \quad (5.4)$$

◇◇◇

### 5.1.2 Teleoperation control with variable time-delays

The control law for SL-SR teleoperation systems with variable time-delay in the communication channel is derived from the consensus control scheme proposed in Section 4.3, and it is given by

$$\begin{aligned} \mathbf{f}_\ell &= k_\ell \Phi(\boldsymbol{\xi}_\ell) \mathbf{e}_{\ell r} + d_\ell \mathbf{v}_\ell - \mathbf{g}_\ell(\mathbf{q}_\ell), \\ \mathbf{f}_r &= -k_r \Phi(\boldsymbol{\xi}_r) \mathbf{e}_{r\ell} - d_r \mathbf{v}_r + \mathbf{g}_r(\mathbf{q}_r). \end{aligned} \quad (5.5)$$

Figure 5.2 shows a diagram of this control scheme.

The closed-loop system of control law (5.5) evaluated along (3.58) is given by

$$\left. \begin{aligned} \mathbf{M}_\ell(\mathbf{q}_\ell)\dot{\mathbf{v}}_\ell + \mathbf{C}_\ell(\mathbf{q}_\ell, \dot{\mathbf{q}}_\ell)\mathbf{v}_\ell + k_\ell\mathbf{e}_{\ell r} + d_\ell\mathbf{v}_\ell &= \mathbf{f}_h \\ \mathbf{M}_r(\mathbf{q}_r)\dot{\mathbf{v}}_r + \mathbf{C}_r(\mathbf{q}_r, \dot{\mathbf{q}}_r)\mathbf{v}_r + k_r\mathbf{e}_{r\ell} + d_r\mathbf{v}_r &= -\mathbf{f}_e \end{aligned} \right\} \quad (5.6)$$

**PROPOSITION 5.2:**

Consider the bilateral teleoperation system (3.58) and assume that **A3** holds. In this scenario the controller (5.5) ensures:

i) Convergence to zero of the velocities and pose errors, that is

$$\lim_{t \rightarrow \infty} \mathbf{v}_\ell(t) = \lim_{t \rightarrow \infty} \mathbf{e}_{\ell r}(t) = \mathbf{0}, \quad \lim_{t \rightarrow \infty} \mathbf{v}_r(t) = \lim_{t \rightarrow \infty} \mathbf{e}_{r\ell}(t) = \mathbf{0},$$

if the human operator does not inject forces on the local manipulator and the remote manipulator does not interact with the environment, i.e.,  $\mathbf{f}_h = \mathbf{f}_e = \mathbf{0}$ , and condition (4.40) is satisfied for any  $\alpha_\ell, \alpha_r > 0$ .

ii) Boundedness of the velocities and pose errors, i.e.  $\mathbf{v}_\ell, \mathbf{v}_r \in \mathcal{L}_\infty \cap \mathcal{L}_2$  and  $|\mathbf{x}_\ell - \mathbf{x}_r|, |\mathbf{x}_r - \mathbf{x}_\ell| \in \mathcal{L}_\infty$ , if:

- Condition (4.40) is satisfied for any  $\alpha_\ell, \alpha_r > 0$  and the inequalities (5.3) are fulfilled.
- The damping condition (4.49) holds, for any  $\delta_\ell, \delta_r, \alpha_\ell, \alpha_r > 0$  and  $c_\ell = c_r = 1$ .

◇

*Proof.* The proof of Claim i) is given by the proof of Proposition 4.6 for  $\bar{N} = \{\ell, r\}$  and interconnection weights set to:  $a_{\ell r} = a_{r\ell} = 1$ .

Claim ii) is proved following the same steps as in the proof of Proposition 4.7 but, in this case, the proof for the first damping condition uses the energy functions (5.4). ◇◇◇

### 5.1.3 Teleoperation control with uncertain parameters and variable time-delays

The controller for SL-SR teleoperation systems with uncertain kinematic and dynamic parameters and variable time-delay in the communication channel is derived from the consensus control

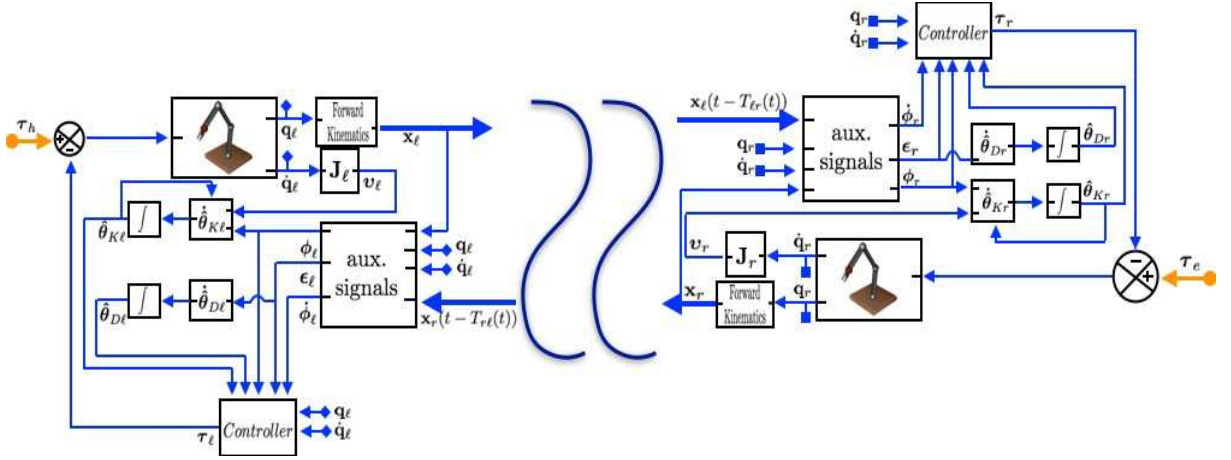


Figure 5.3: Control scheme for teleoperation systems with uncertain parameters and variable time-delays. The controller is defined in (5.7).

scheme proposed in Section 4.4, and it is given by

$$\begin{aligned}\tau_\ell &= \mathbf{Y}_{D\ell}(\mathbf{q}_\ell, \dot{\mathbf{q}}_\ell, \phi_\ell, \dot{\phi}_\ell) \hat{\boldsymbol{\theta}}_{D\ell} + \kappa_\ell \hat{\mathbf{J}}_\ell^\top(\mathbf{q}_\ell) \hat{\mathbf{J}}_\ell(\mathbf{q}_\ell) \epsilon_\ell, \\ \tau_r &= -\mathbf{Y}_{Dr}(\mathbf{q}_r, \dot{\mathbf{q}}_r, \phi_r, \dot{\phi}_r) \hat{\boldsymbol{\theta}}_{Dr} - \kappa_r \hat{\mathbf{J}}_r^\top(\mathbf{q}_r) \hat{\mathbf{J}}_r(\mathbf{q}_r) \epsilon_r.\end{aligned}\quad (5.7)$$

The Figure 5.2 shows a diagram of this control scheme. The joint space dynamic model of the SL-SR teleoperation system is defined as

$$\begin{aligned}\bar{\mathbf{M}}_\ell(\mathbf{q}_\ell) \ddot{\mathbf{q}}_\ell + \bar{\mathbf{C}}_\ell(\mathbf{q}_\ell, \dot{\mathbf{q}}_\ell) \dot{\mathbf{q}}_\ell + \bar{\mathbf{g}}_\ell(\mathbf{q}_\ell) &= \tau_h - \tau_\ell, \\ \bar{\mathbf{M}}_r(\mathbf{q}_r) \ddot{\mathbf{q}}_r + \bar{\mathbf{C}}_r(\mathbf{q}_r, \dot{\mathbf{q}}_r) \dot{\mathbf{q}}_r + \bar{\mathbf{g}}_r(\mathbf{q}_r) &= \tau_r - \tau_e,\end{aligned}\quad (5.8)$$

where  $\tau_h$  and  $\tau_e$  are the joints torques corresponding to the forces exerted by the human and the environment, respectively (Nuño et al. 2011). The closed-loop system of (5.8) together with the controller (5.7) is given by

$$\left. \begin{aligned}\bar{\mathbf{M}}_\ell(\mathbf{q}_\ell) \dot{\epsilon}_\ell + \bar{\mathbf{C}}_\ell(\mathbf{q}_\ell, \dot{\mathbf{q}}_\ell) \epsilon_\ell + \kappa_\ell \hat{\mathbf{J}}_\ell^\top(\mathbf{q}_\ell) \hat{\mathbf{J}}_\ell(\mathbf{q}_\ell) \epsilon_\ell &= \mathbf{Y}_{D\ell} \tilde{\boldsymbol{\theta}}_{D\ell} + \tau_h \\ \bar{\mathbf{M}}_r(\mathbf{q}_r) \dot{\epsilon}_r + \bar{\mathbf{C}}_r(\mathbf{q}_r, \dot{\mathbf{q}}_r) \epsilon_r + \kappa_r \hat{\mathbf{J}}_r^\top(\mathbf{q}_r) \hat{\mathbf{J}}_r(\mathbf{q}_r) \epsilon_r &= \mathbf{Y}_{Dr} \tilde{\boldsymbol{\theta}}_{Dr} - \tau_e\end{aligned}\right\} \quad (5.9)$$

### PROPOSITION 5.3:

Consider a SL-SR teleoperation system (5.8) in which the kinematic and the dynamic physical parameters of the robots are uncertain and the Assumption A3 holds. Then controller given by (5.7), (4.57), (4.58) and (4.59) together with the kinematic and dynamic parameter estimation

laws (4.55) and (4.56), ensures:

i) Convergence to zero of the velocities and pose errors, that is

$$\lim_{t \rightarrow \infty} \mathbf{v}_\ell(t) = \lim_{t \rightarrow \infty} \mathbf{e}_{\ell r}(t) = \mathbf{0}, \quad \lim_{t \rightarrow \infty} \mathbf{v}_r(t) = \lim_{t \rightarrow \infty} \mathbf{e}_{r\ell}(t) = \mathbf{0},$$

if the human operator does not inject torques on the local manipulator and the remote manipulator does not interact with the environment, i.e.,  $\boldsymbol{\tau}_h = \boldsymbol{\tau}_e = \mathbf{0}$ , and condition (4.64) is satisfied for any  $\alpha_\ell, \alpha_r > 0$ .

ii) Boundedness of  $\epsilon_i$ , that is  $\epsilon_\ell, \epsilon_r \in \mathcal{L}_\infty$ , if the joint torques injected by the human and the environment are bounded, i.e.  $\boldsymbol{\tau}_h, \boldsymbol{\tau}_e \in \mathcal{L}_\infty$ .  $\diamond$

*Proof.* The proof of Claim i) is given by the proof of Proposition 4.9 for  $\bar{N} = \{\ell, r\}$  and interconnection weights set to:  $a_{\ell r} = a_{r\ell} = 1$ .

Claim ii) is proved following the same steps as in the proof of Proposition 4.10.  $\diamond \diamond \diamond$

## 5.2 Control of cooperative teleoperation system with uncertain parameters and variable time-delays

The controller detailed in Remark 4.5 is used to derive the control law for the cooperative teleoperation system modeled by (3.67) with uncertain dynamic parameters and variable time-delays. The controller for the local manipulator ( $\mathbf{f}_\ell$ ) and the control law ( $\mathbf{f}_i$ ) of the robots that compose the cooperative system are given by

$$\begin{aligned} \mathbf{f}_\ell &= \hat{\mathbf{M}}_\ell(\mathbf{q}_\ell) \dot{\boldsymbol{\phi}}_\ell + \hat{\mathbf{C}}_\ell(\mathbf{q}_\ell, \dot{\mathbf{q}}_\ell) \boldsymbol{\phi}_\ell - \hat{\mathbf{g}}_\ell(\mathbf{q}_\ell) + \kappa_\ell \boldsymbol{\epsilon}_\ell, \\ \mathbf{f}_i &= -\hat{\mathbf{M}}_i \mathbf{W}_i^\top \dot{\boldsymbol{\phi}}_o - \left( \hat{\mathbf{M}}_i \dot{\mathbf{W}}_i^\top + \hat{\mathbf{C}}_i \mathbf{W}_i^\top \right) \boldsymbol{\phi}_o + \hat{\mathbf{g}}_i + \mathbf{f}_{i,\text{int}}^d \\ &\quad - (\mathbf{W}^\dagger)_i [\hat{\mathbf{M}}_o \dot{\boldsymbol{\phi}}_o + \hat{\mathbf{C}}_o \boldsymbol{\phi}_o - \hat{\mathbf{g}}_o + \kappa_o \boldsymbol{\epsilon}_o], \end{aligned} \tag{5.10}$$

where  $\mathbf{f}_{i,\text{int}}^d \in \mathbb{R}^6$  is the desired internal force, which is selected such that  $\sum_{i=1}^N \mathbf{W}_i \mathbf{f}_{i,\text{int}}^d = \mathbf{0}$ . It should be underscored that these control laws do not require force and moment measurements.

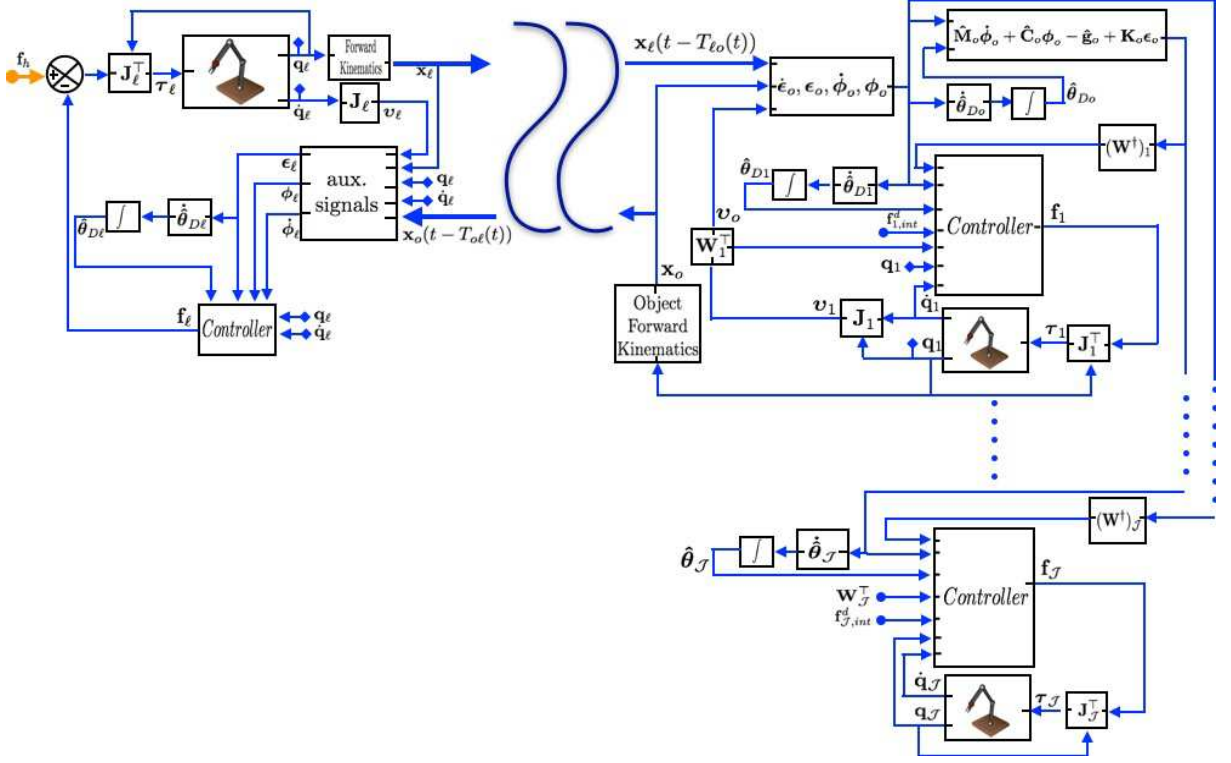


Figure 5.4: Control scheme for a cooperative teleoperation systems with uncertain parameters and variable time-delays. The controller is defined in (5.10).

A key observation on controller (5.10) is that

$$\sum_{i=1}^N \mathbf{W}_i \mathbf{f}_i = -\hat{\mathbf{M}}_{rcs} \dot{\phi}_o - \hat{\mathbf{C}}_{rcs} \phi_o + \hat{\mathbf{g}}_{rcs} - \kappa_o \epsilon_o, \quad (5.11)$$

that is due to the fact that  $\sum_{i=1}^N \mathbf{W}_i \mathbf{f}_{i,int}^d = \mathbf{0}$  and that  $\sum_{i=1}^N \mathbf{W}_i (\mathbf{W}^\dagger)_i = \mathbf{W} \mathbf{W}^\dagger = \mathbf{I}_6$ . This last derives from the full row rank property of  $\mathbf{W}$ . In the Figure 5.4 it can be seen a diagram of this control scheme.

The closed-loop system (3.67) and (5.10) is given by

$$\left. \begin{aligned} \mathbf{M}_l(\mathbf{q}_l) \dot{\epsilon}_l + \mathbf{C}_l(\mathbf{q}_l, \dot{\mathbf{q}}_l) \epsilon_l + \kappa_l \epsilon_l &= \mathbf{Y}_l \tilde{\theta}_l + \mathbf{f}_h \\ \mathbf{M}_{rcs} \dot{\epsilon}_o + \mathbf{C}_{rcs} \epsilon_o + \kappa_o \epsilon_o &= \mathbf{Y}_{rcs} \tilde{\theta}_{rcs} - \mathbf{f}_e \end{aligned} \right\} \quad (5.12)$$

**PROPOSITION 5.4:**

Consider a cooperative teleoperation system modeled as (3.67) in which the dynamic physical parameters of the robots and the grasped object are uncertain and the Assumption A3 holds. Then,

the controller given by (5.10), (4.57), (4.58) and (4.59) together with the dynamic parameter estimation law (4.56), ensures:

- i) Convergence to zero of the velocities and pose errors between the local robot and the object handled by the remote cooperative system, that is

$$\lim_{t \rightarrow \infty} \mathbf{v}_\ell(t) = \lim_{t \rightarrow \infty} \mathbf{e}_{\ell o}(t) = \mathbf{0}, \quad \lim_{t \rightarrow \infty} \mathbf{v}_o(t) = \lim_{t \rightarrow \infty} \mathbf{e}_{o\ell}(t) = \mathbf{0},$$

if the human operator does not inject forces on the local manipulator and the object does not interact with the environment, i.e.,  $\mathbf{f}_h = \mathbf{f}_e = \mathbf{0}$ , and condition (4.64) is satisfied for any  $\alpha_\ell, \alpha_o > 0$ .

- ii) Boundedness of the velocities and pose errors, i.e.  $\epsilon_\ell, \epsilon_o \in \mathcal{L}_\infty$ , if the forces injected by the human and the environment are bounded, i.e.  $\mathbf{f}_h, \mathbf{f}_e \in \mathcal{L}_\infty$ .  $\diamond$

*Proof.* The proof of Claim i) is established following verbatim the same steps of the proof of Proposition 4.9 for  $\bar{N} = \{\ell, r\}$  and interconnection weights set to:  $a_{\ell o} = a_{o\ell} = 1$ .

Claim ii) is proved following the same procedure as in the proof of Proposition 4.10.  $\diamond \diamond \diamond$

### 5.3 Simulation results

The simulation platform and robots described in Section 4.5 are used to test the control algorithms proposed in this chapter. The results are presented in two parts, the first one details the results of the control algorithms for SL-SR teleoperation systems and the second part shows the results of the CTS controller.

#### SL-SR teleoperation system simulations

Figure 5.5 shows the teleoperation system in which the control algorithms detailed in Sections 5.1.1 and 5.1.2 are simulated. It is composed of one OMNI robot at the local site and one LWR robot at the remote site. The controller proposed in Section 5.1.3 is simulated in the teleoperation system depicted in Figure 5.6, it is composed of one 2-DoF robot at the local site and one OMNI robot at the remote site.

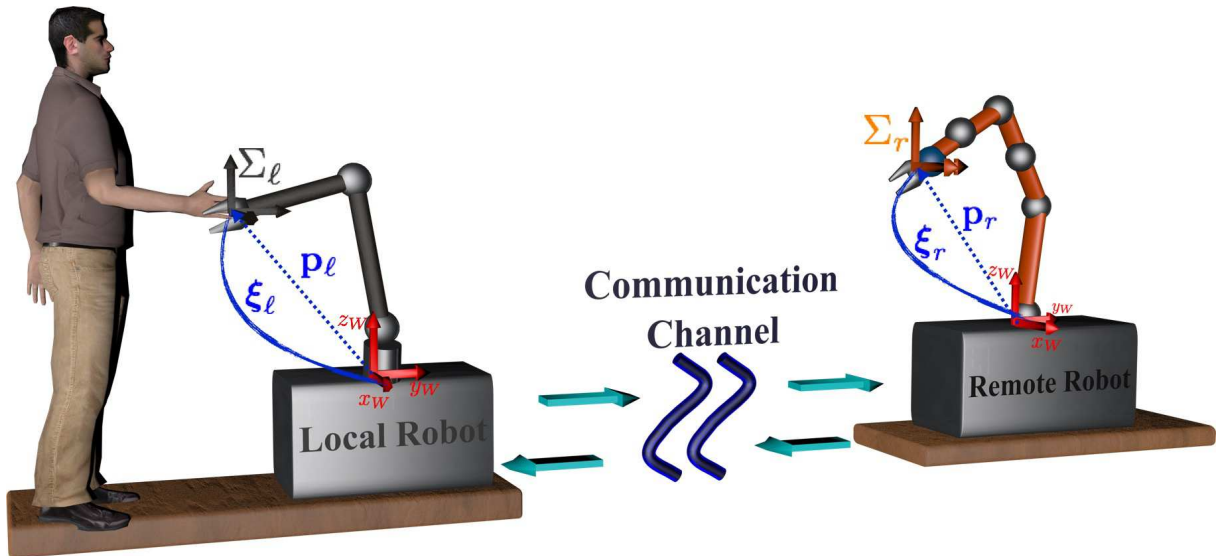


Figure 5.5: Teleoperation system used in the simulations of the control algorithms without velocity measurements and with variable time-delays.

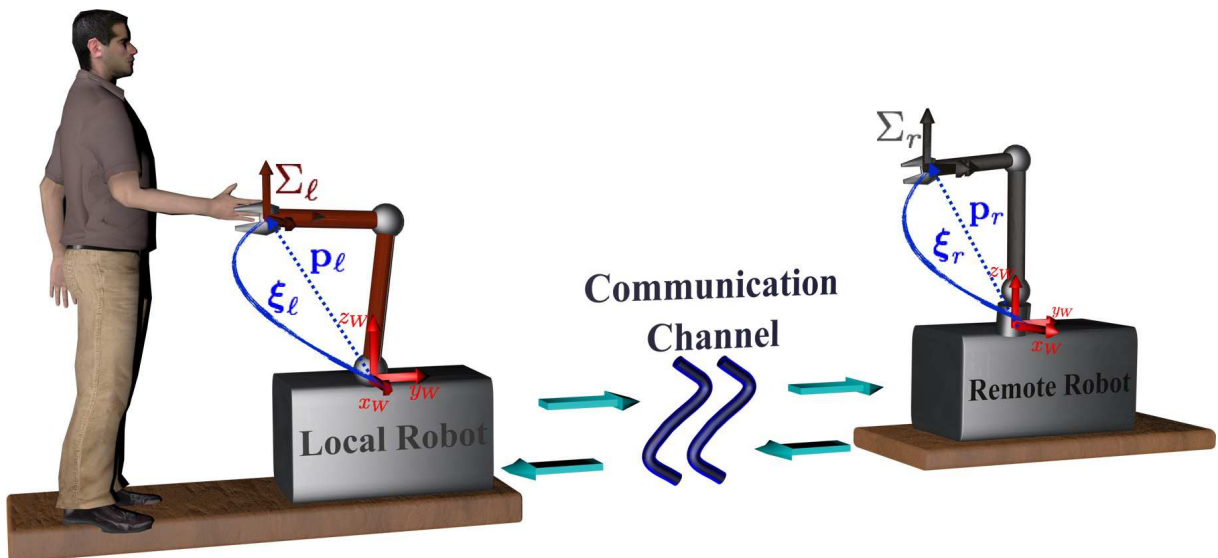


Figure 5.6: Teleoperation system used in the simulations of the control algorithm with uncertain parameters and variable time-delays.

The three control algorithms are evaluated under a similar simulation that is composed of the following steps:

- 1) The local and remote robots are set to have different initial poses and it is expected that, asymptotically, in free space (no external forces injected), both robots converge to a common pose.
- 2) When the robots have reached a common pose, human forces are injected to the local robot producing the movement of the local robot along a desired trajectory, and it is expected that the remote robot will follow closely the local robot trajectory.
- 3) At the remote site, and in order to test the robustness of the controller, a high stiff wall is simulated at the cartesian coordinate  $z$  in the trajectory of the remote robot for a short period.
- 4) The injection of human forces finishes and the robots have to converge again to a common pose.

The forces injected by the human ( $\mathbf{f}_h$ ) are applied through a spring–damper system, modeled as

$$\mathbf{f}_h = \mathbf{K}_h \Phi(\xi_\ell)(\mathbf{x}_\ell - \mathbf{x}_d) + \mathbf{B}_h \mathbf{v}_\ell,$$

where  $\mathbf{x}_d$  is a given desired pose, and  $\mathbf{K}_h$  and  $\mathbf{B}_h$  are the spring and damper gains, respectively.

The controllers gains and simulations parameters used in the experiments are the following:

**- Without velocity measurements**

$$k_\ell=15, k_r=550, d_\ell=150, d_r=850, k_{y\ell}=500, k_{yr}=50, \mathbf{K}_h = 25\mathbf{I}_6, \mathbf{B}_h = 2\mathbf{I}_6.$$

**- With variable time-delays**

$$k_\ell=15, k_r=500, d_\ell=5, d_r=150, {}^*T_{r\ell}=0.21, {}^*T_{\ell r}=0.16, \alpha_\ell=0.4, \alpha_r=0.3, \mathbf{K}_h = 300\mathbf{I}_6, \mathbf{B}_h = \mathbf{I}_6.$$

**- With uncertain parameters and variable time-delays**

$$\kappa_\ell=5, \kappa_r=10, \Gamma_{D\ell} = 5\mathbf{I}_5, \Gamma_{Dr} = 7\mathbf{I}_8, \Gamma_{K\ell} = 3\mathbf{I}_2, \Gamma_{Kr} = 5\mathbf{I}_2, {}^*T_{r\ell}=0.207, {}^*T_{\ell r}=0.152, \alpha_\ell=0.3, \alpha_r=0.3, \mathbf{K}_h = 2000\mathbf{I}_6, \mathbf{B}_h = \mathbf{I}_6.$$

Figures 5.7, 5.8, 5.9, 5.10, 5.11 and 5.12 show the simulation results for each one of the controllers evaluated under the previously detailed simulations. It can be observed that the three



Parameters	Robot P1	Robot P2	Robot P3	Object
Mass(kg) and Inertia(kgm <sup>2</sup> )	$m_1=4$ $m_2=4$ $m_3=3$ $I_1=1$ $I_2=1$ $I_3=0.50$	$m_1=2.50$ $m_2=2.50$ $m_3=2$ $I_1=0.60$ $I_2=0.60$ $I_3=0.30$	$m_1=1.8$ $m_2=1.7$ $m_3=1.1$ $I_1=0.465$ $I_2=0.45$ $I_3=0.22$	$m_o=3$ $I_o=1$
Length(m) and Center of mass (m)	$l_1=0.40$ $l_2=0.40$ $l_3=0.25$ $lc_1=0.20$ $lc_2=0.20$ $lc_3=0.125$	$l_1=0.90$ $l_2=0.60$ $l_3=0.40$ $lc_1=0.45$ $lc_2=0.30$ $lc_3=0.20$	$l_1=0.80$ $l_2=0.80$ $l_3=0.65$ $lc_1=0.40$ $lc_2=0.40$ $lc_3=0.325$	$l_o=0.45$ $lc_o=0.225$

Table 5.1: Robots' and object's dynamic parameters.

controllers perform accordingly to the stated in the Propositions 5.1, 5.2 and 5.3, respectively. That is, when no external forces are injected to the SL-SR teleoperation systems ( $\mathbf{f}_h = \mathbf{f}_e = 0$ ) the velocities and pose error converge to zero, and when forces are injected the errors remain bounded.

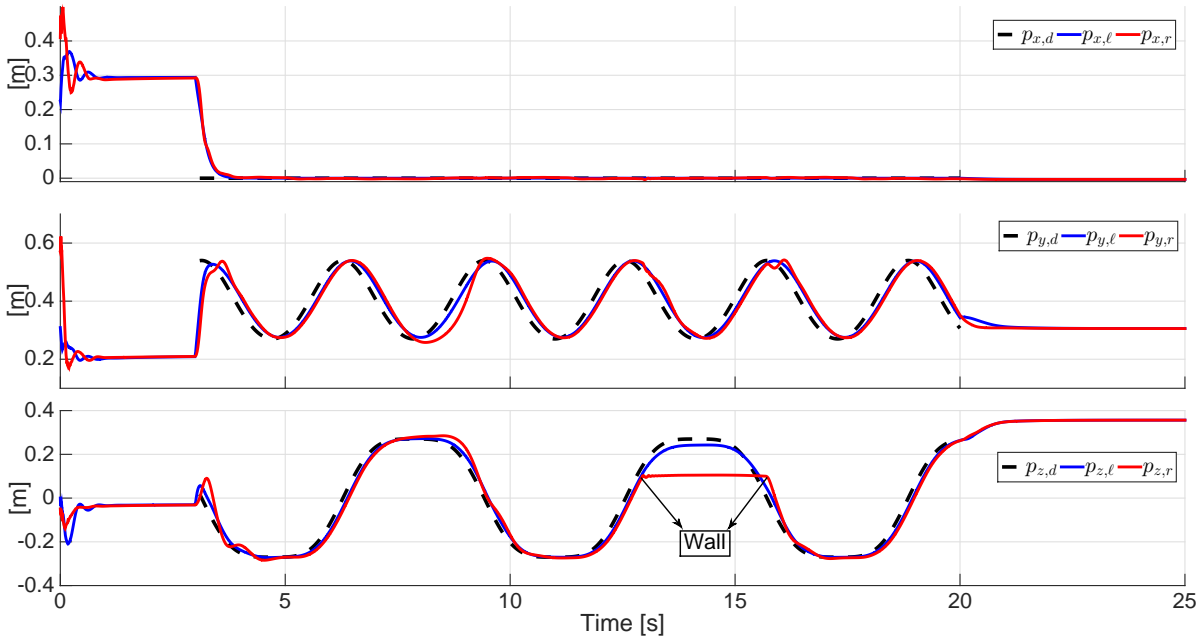
### Cooperative teleoperation system simulation

The teleoperator system shown in Figure 5.13 is composed of three different 3-DoF robot manipulators, one for the local site (Type P1 of Table 5.1), and two for the remote site (Type P2 and Type P3 of Table 5.1), that are rigidly grasping an object. This object is modeled as a pure mass system whose inertia matrix and gravity vector are  $\mathbf{M}_o = \text{diag}(m_o, m_o, I_{n_o})$  and  $\mathbf{g}_o = \text{col}(0, -m_o g, 0)$ . The grasp matrices are defined as:

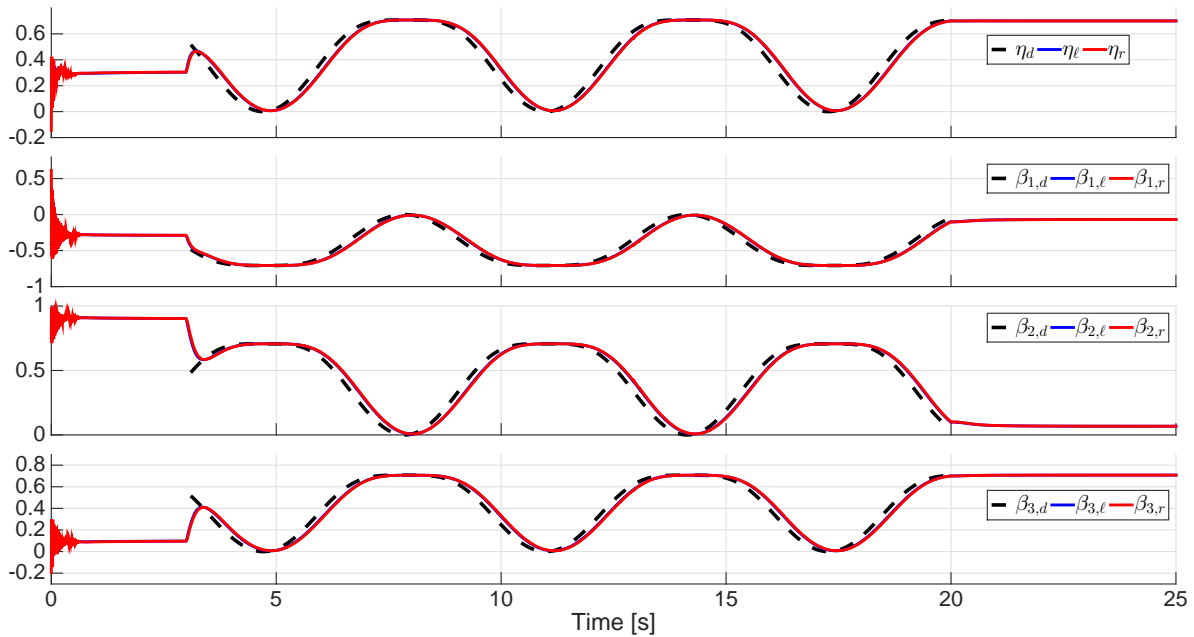
$$\mathbf{W}_1 = \begin{bmatrix} 1 & 0 & 0 \\ 0 & 1 & 0 \\ -|\mathbf{d}_1| \sin(\varphi_o) & |\mathbf{d}_1| \cos(\varphi_o) & 1 \end{bmatrix}$$

$$\mathbf{W}_2 = \begin{bmatrix} 1 & 0 & 0 \\ 0 & 1 & 0 \\ |\mathbf{d}_2| \sin(\varphi_o) & -|\mathbf{d}_2| \cos(\varphi_o) & 1 \end{bmatrix},$$

with  $\mathbf{d}_1 = [-.225, 0, 0]^\top$ ,  $\mathbf{d}_2 = [.225, 0, 0]^\top$ , and  $\varphi_o = q_{1,1} + q_{1,2} + q_{1,3}$ .

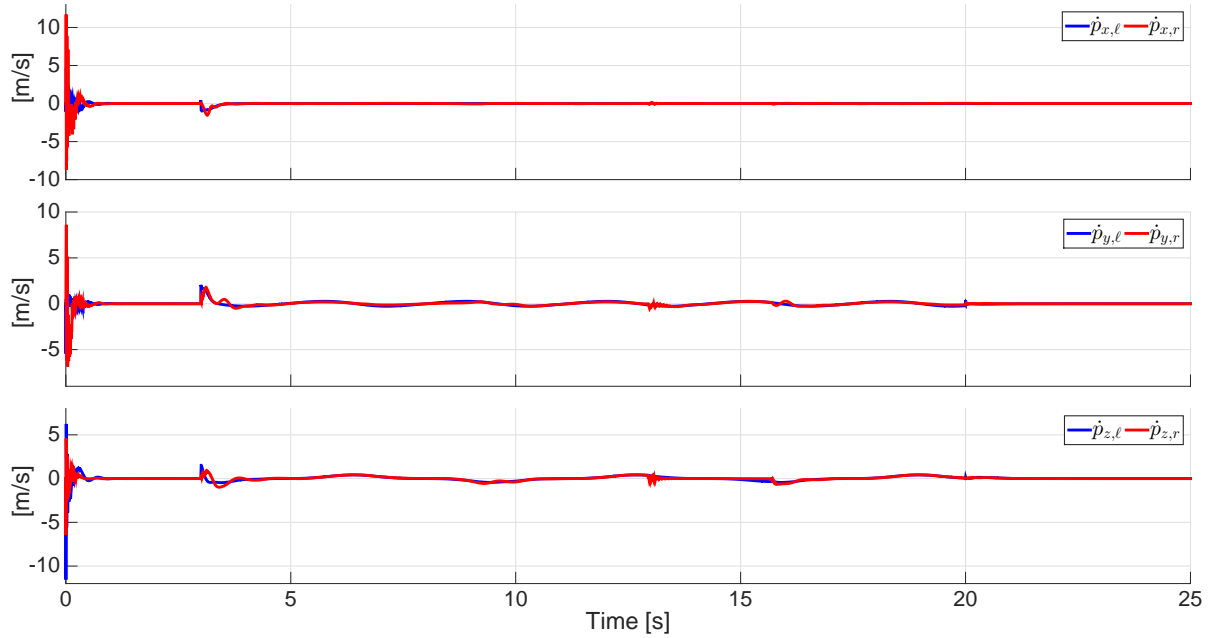


(a) Positions

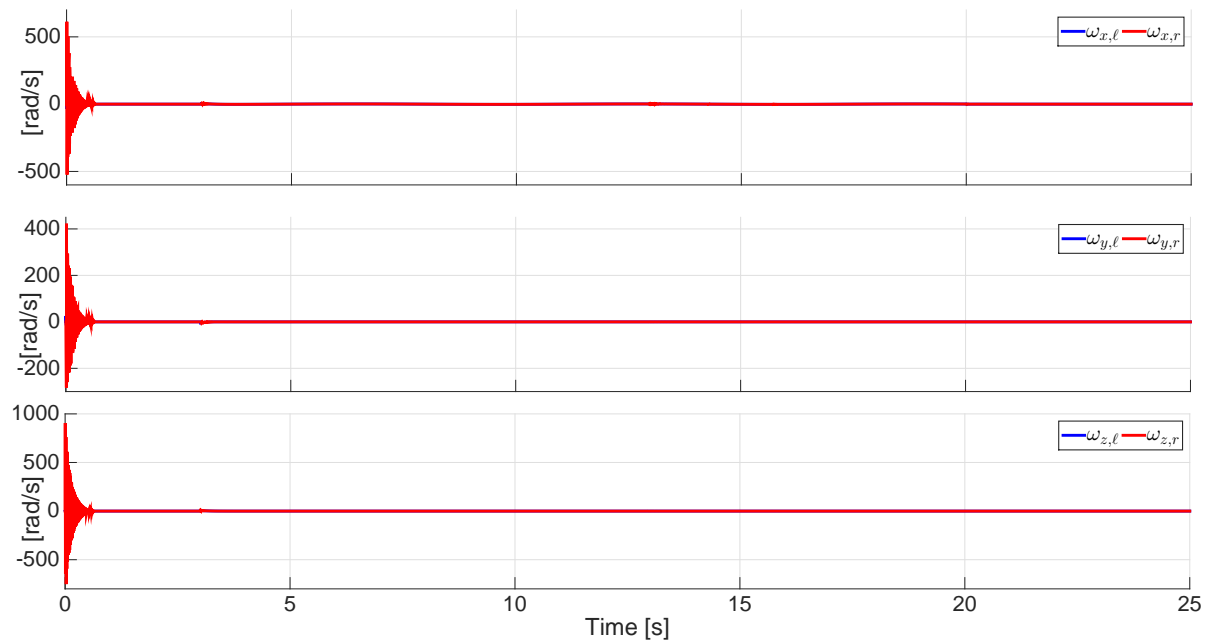


(b) Unit-quaternions (Orientations)

Figure 5.7: Pose of the robots that compose the teleoperation system shown in Figure 5.5 using the control algorithm without velocity measurements.

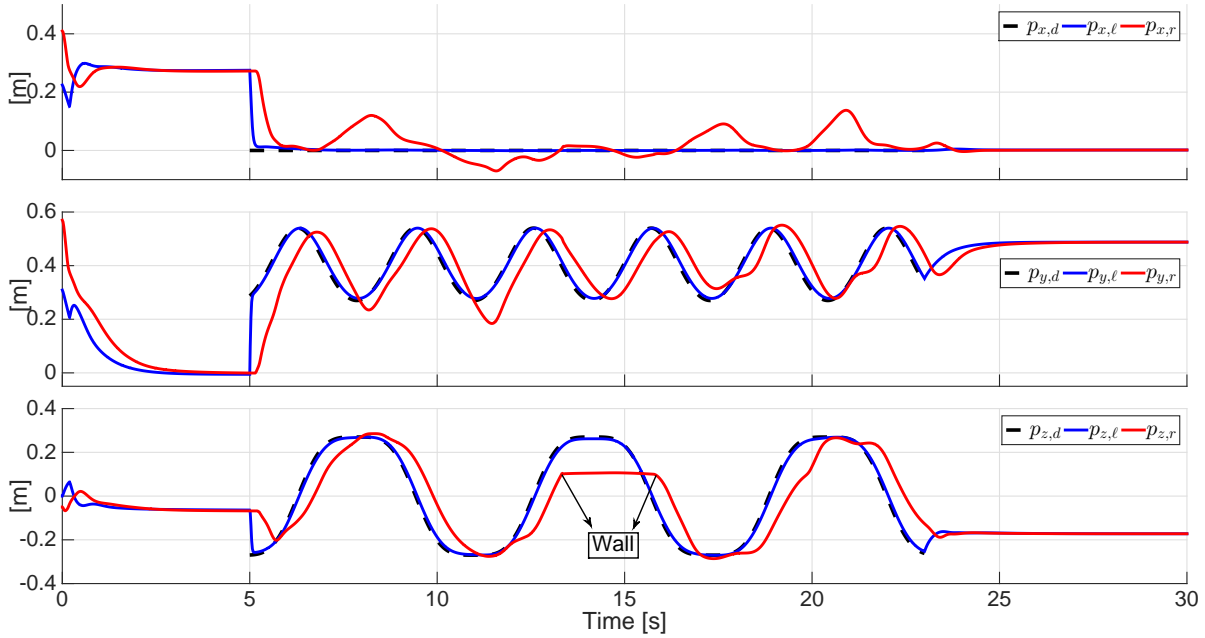


(a) Linear velocities

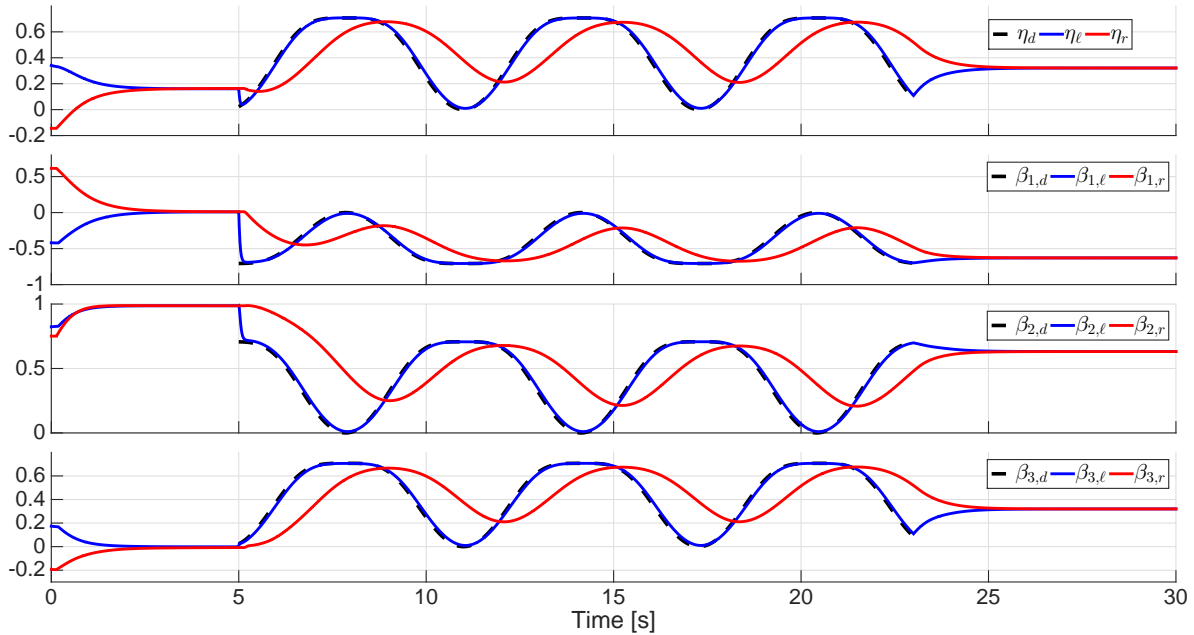


(b) Angular velocities

Figure 5.8: Velocities of the robots that compose the teleoperation system shown in Figure 5.5 using the control algorithm without velocity measurements.

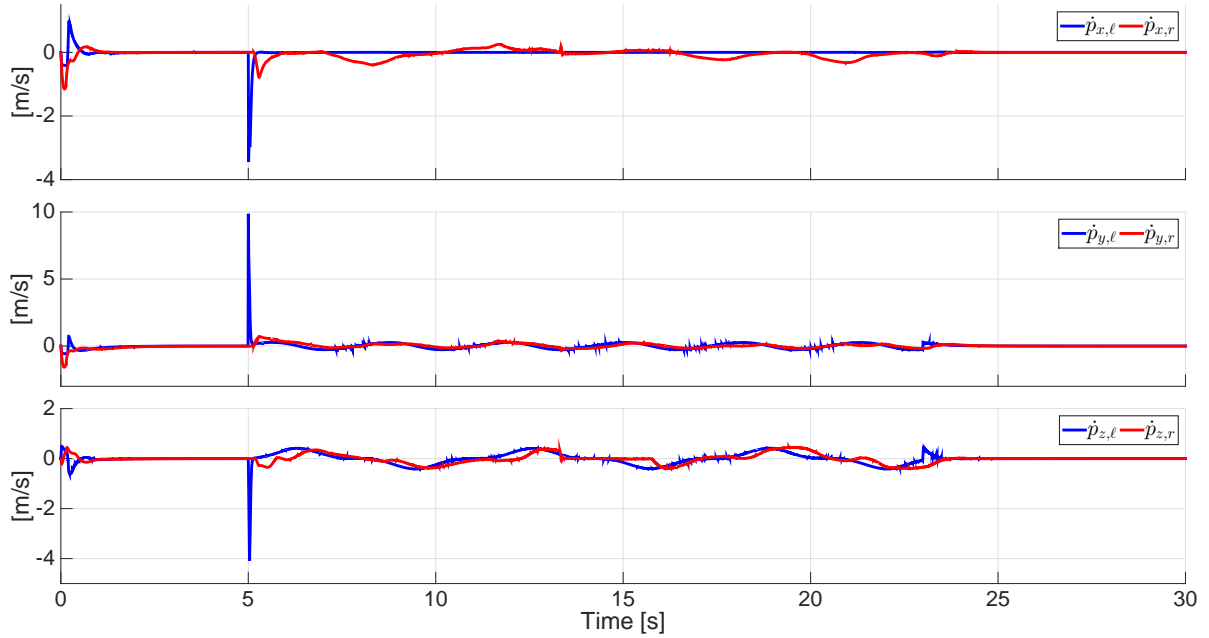


(a) Positions

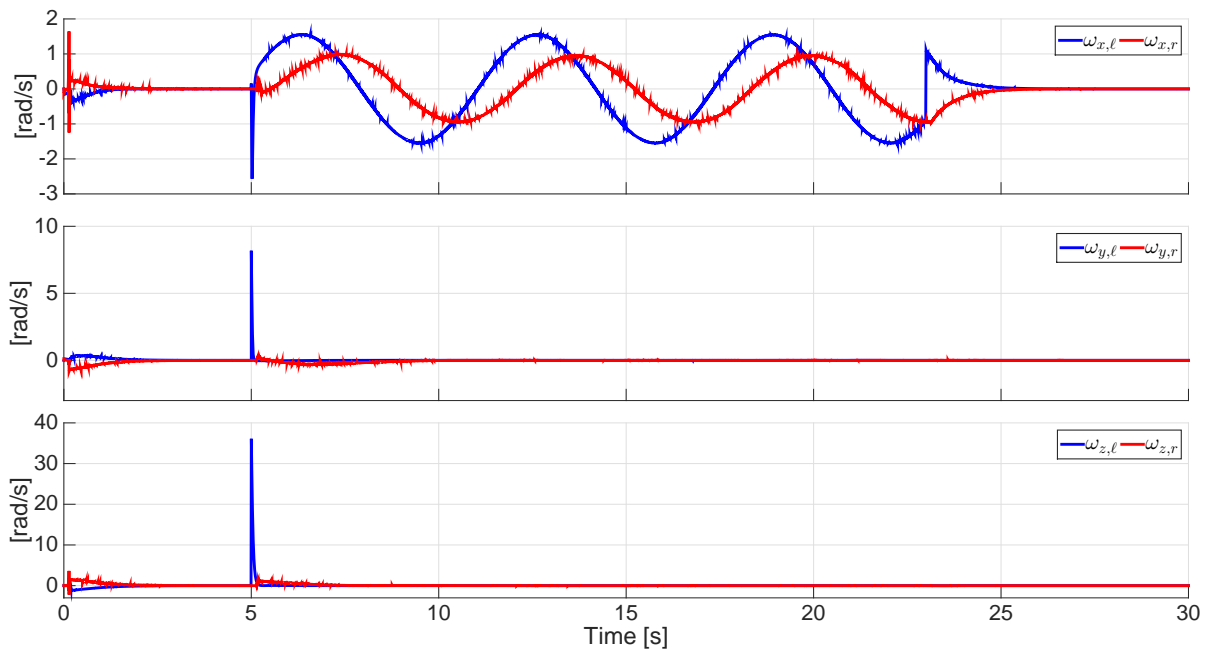


(b) Unit-quaternions (Orientations)

Figure 5.9: Pose of the robots that compose the teleoperation system shown in Figure 5.5 using the control algorithm with variable time-delays.

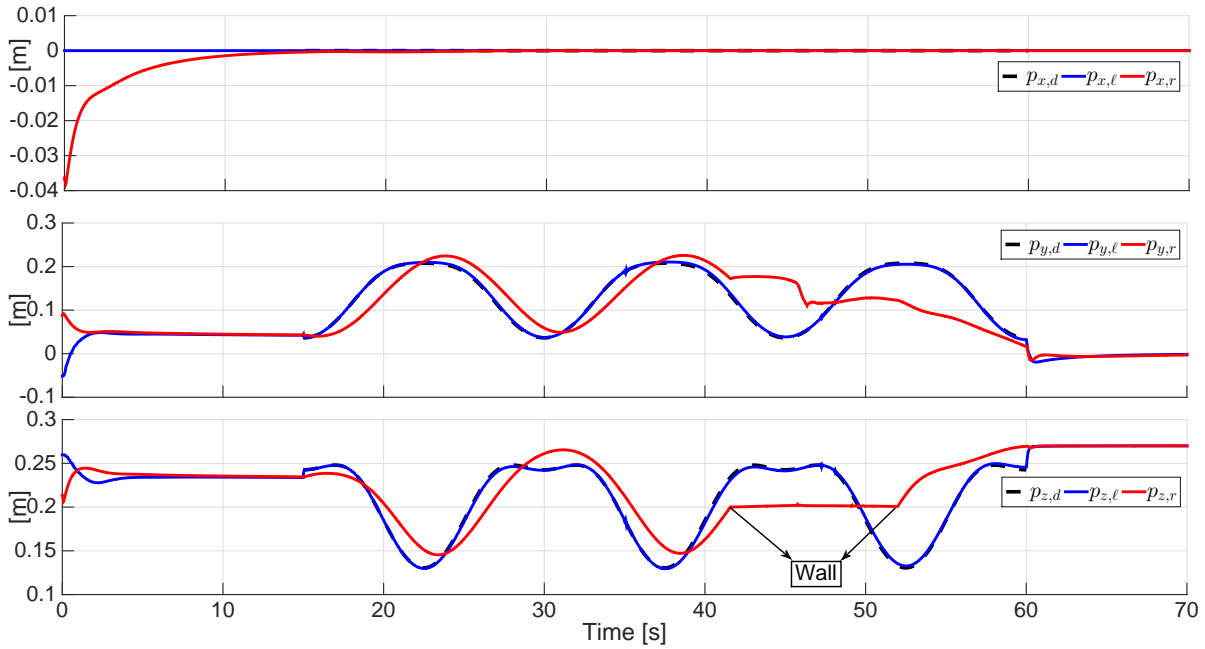


(a) Linear velocities

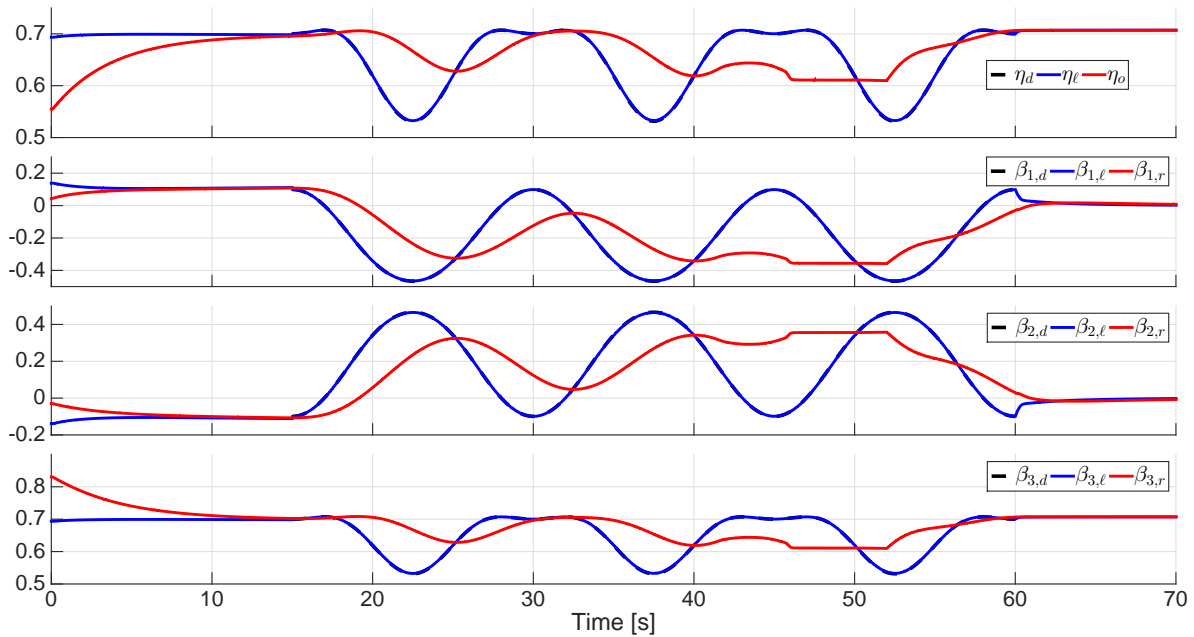


(b) Angular velocities

Figure 5.10: Velocities of the robots that compose the teleoperation system shown in Figure 5.5 using the control algorithm with variable time-delays.



(a) Positions



(b) Unit-quaternions (Orientations)

Figure 5.11: Pose of the robots that compose the teleoperation system shown in Figure 5.6 using the control algorithm with uncertain parameters and variable time-delays.

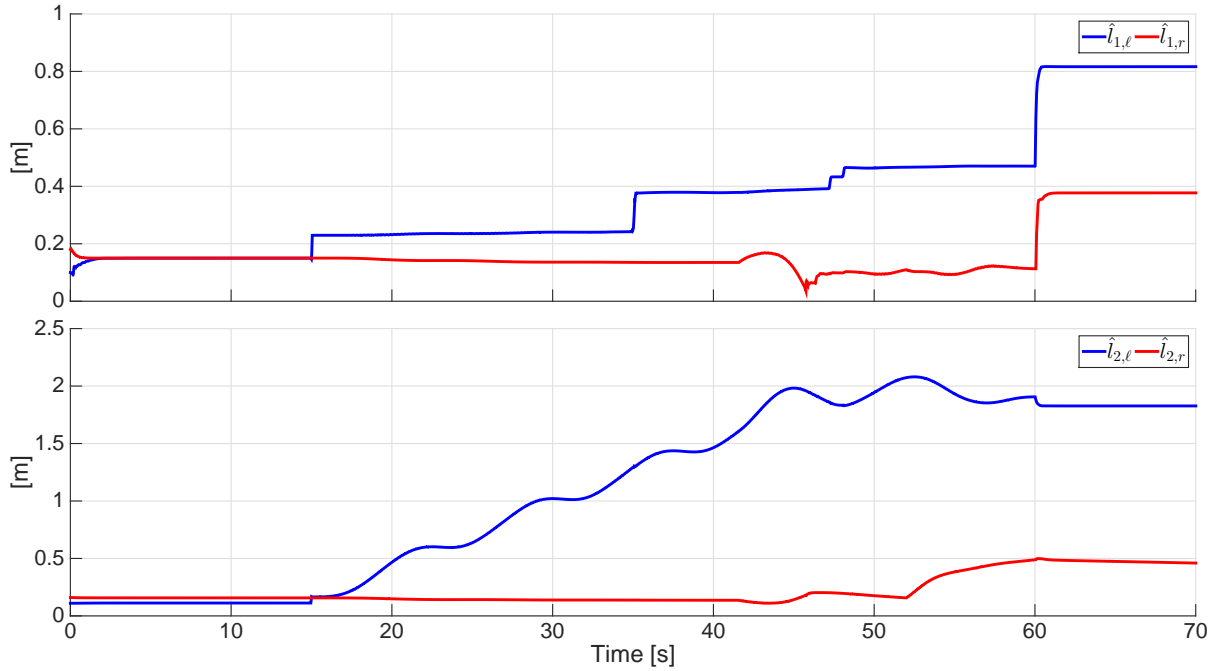


Figure 5.12: Kinematic parameters estimation of the robots that compose the teleoperation system shown in Figure 5.6 using the control algorithm with uncertain parameters and variable time-delays.

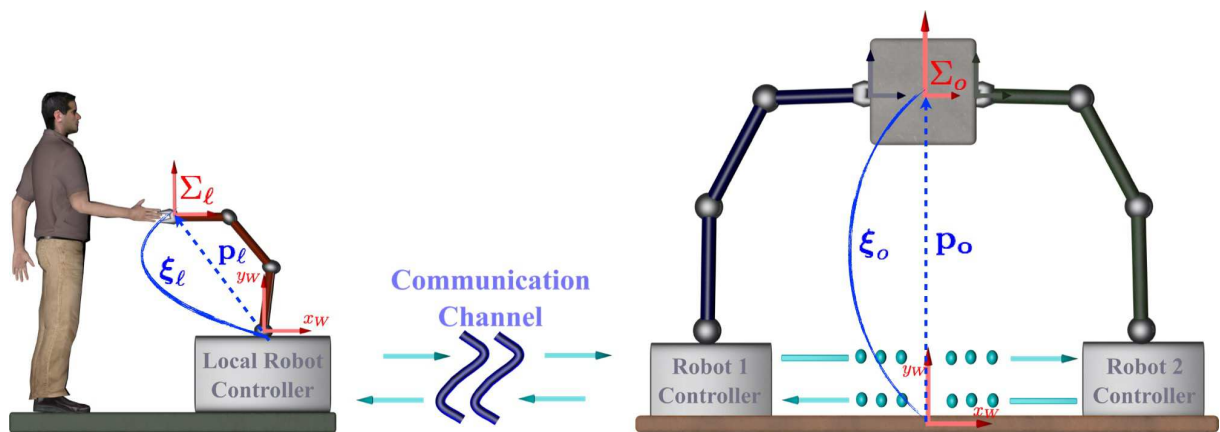
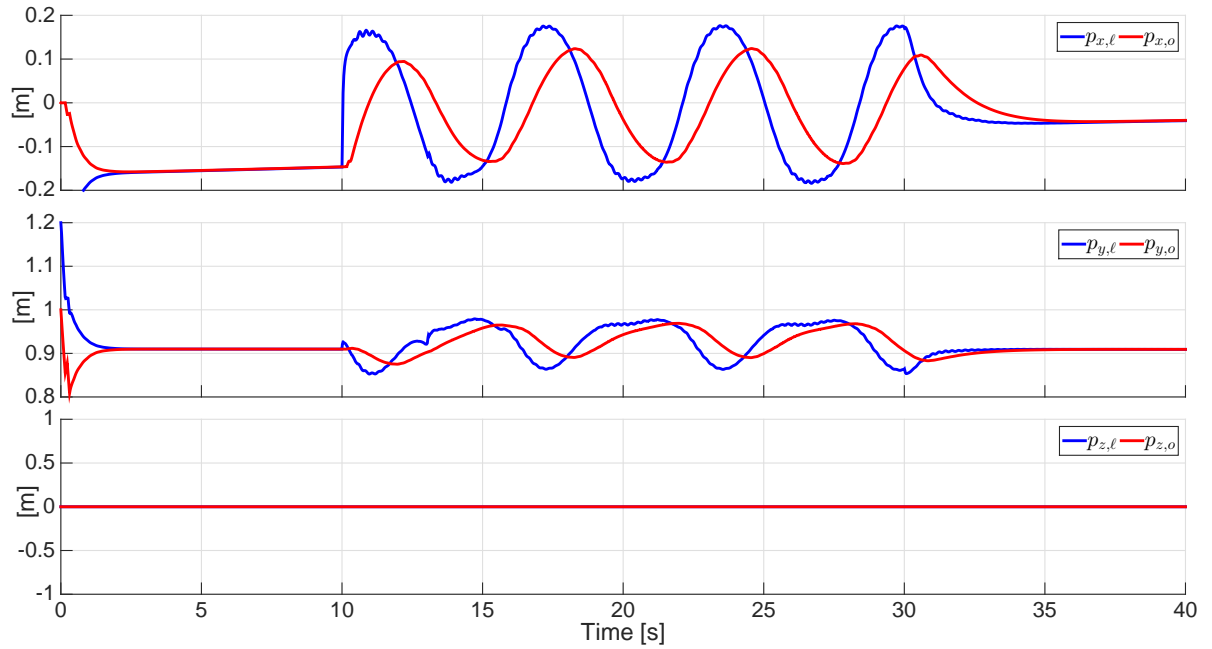


Figure 5.13: Teleoperator System with the reference frame and parameters description.

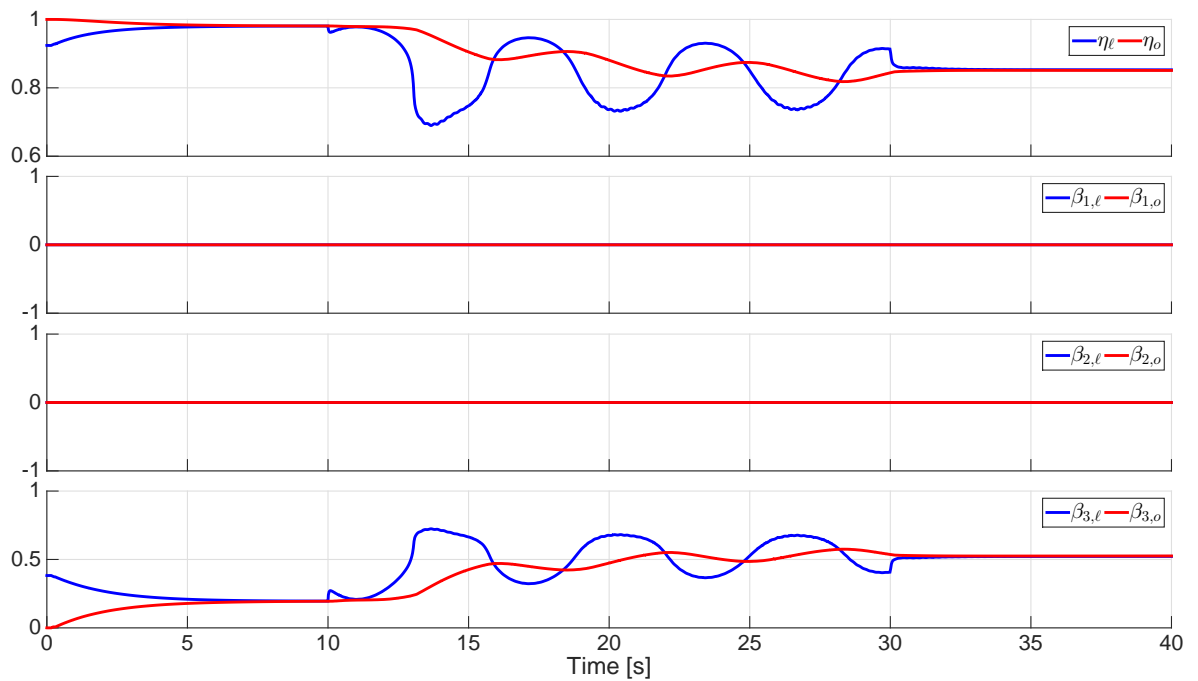
The controller gains and simulation parameters used in this experiments are:  $\kappa_\ell = 1500$  and  $\kappa_o = 20000$ ,  $\Gamma_i = 450\mathbf{I}_{25}$ ,  ${}^*T_{o\ell} = 0.28$ ,  ${}^*T_{\ell o} = 0.34$ ,  $\alpha_\ell = 0.33$ ,  $\alpha_o = 0.33$ .

In Figure 5.14.(a) and Figure 5.14.(b) it is observed the pose behavior of the cooperative teleoperator system. The object and the local manipulator begin with different initial pose and after 5 seconds they reach a common pose. From the second 10 to second 30, forces ( $f_h$ ) are injected to the local manipulator, and it can be appreciated the movement they produce on the local manipulator and how the object's pose follows closely the local pose. After second 30, when no more forces are injected, the object and the local manipulator reach again a common pose. The behavior of the linear and angular velocities is shown in Figures 5.15.(a) and 5.15.(b), respectively.



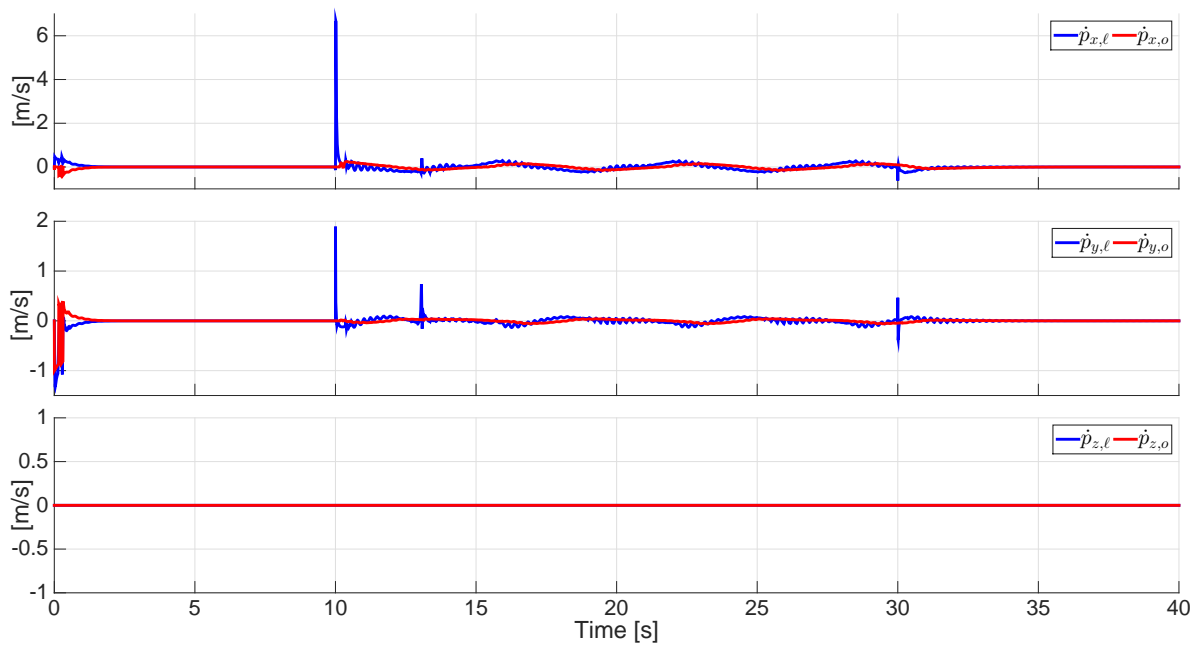


(a) Positions

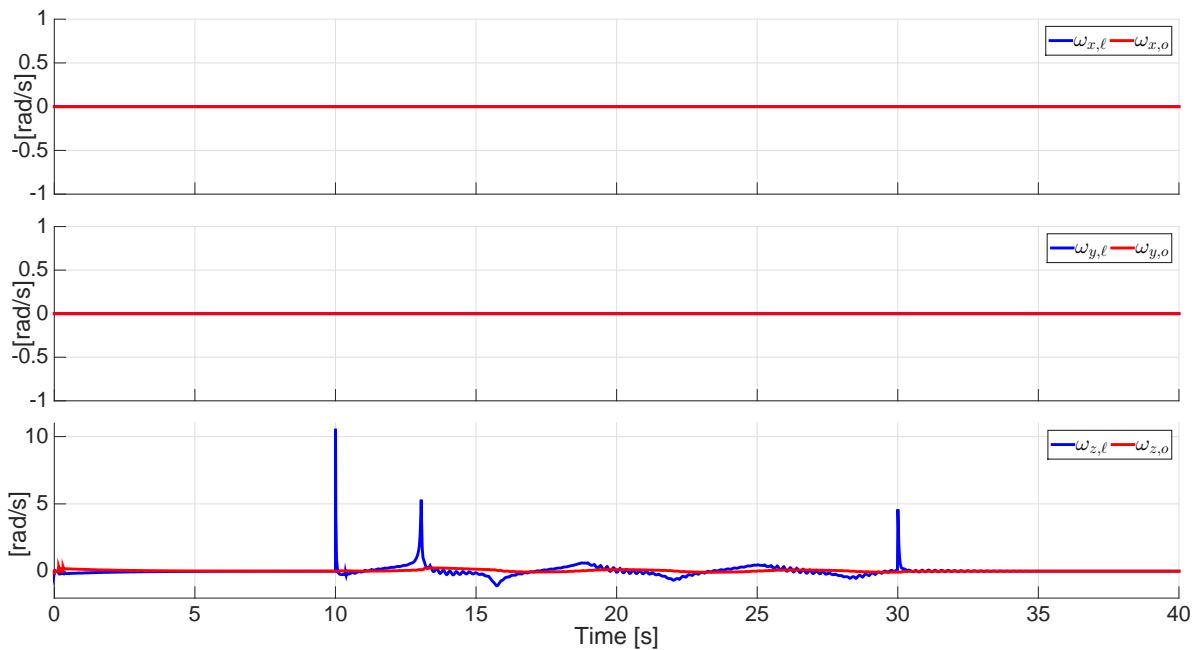


(b) Unit-quaternions (Orientations)

Figure 5.14: Pose of the robots that compose the cooperative teleoperation system.



(a) Linear velocities



(b) Angular velocities

Figure 5.15: Velocities of the robots that compose the cooperative teleoperation system.

## 5.4 Experimental results

In this section the teleoperation control algorithms detailed in Proposition 5.1 and Proposition 5.2 are validated in the test-bed shown in Figure 5.16. The software and hardware used in the validation are described in Section 4.6. The algorithms detailed in Proposition 5.3 and Proposition 5.4 could not be experimentally validated due to the lack of the robot dynamic regressors.

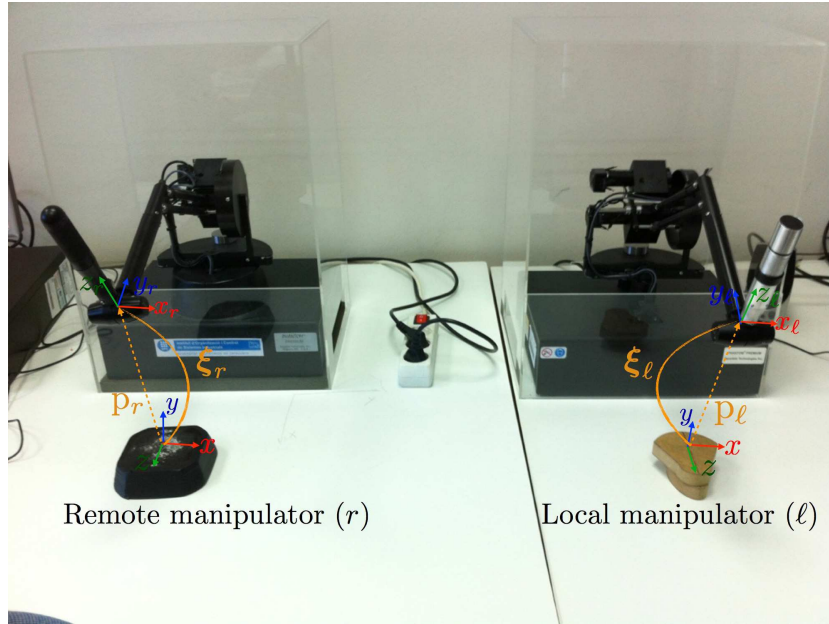


Figure 5.16: Test-bed used in the experimental validation of the teleoperation control algorithms.

The performed experiments pursue the same objectives as the simulations, which are described in Section 5.3.

The controllers gains used in the experiments are the following:

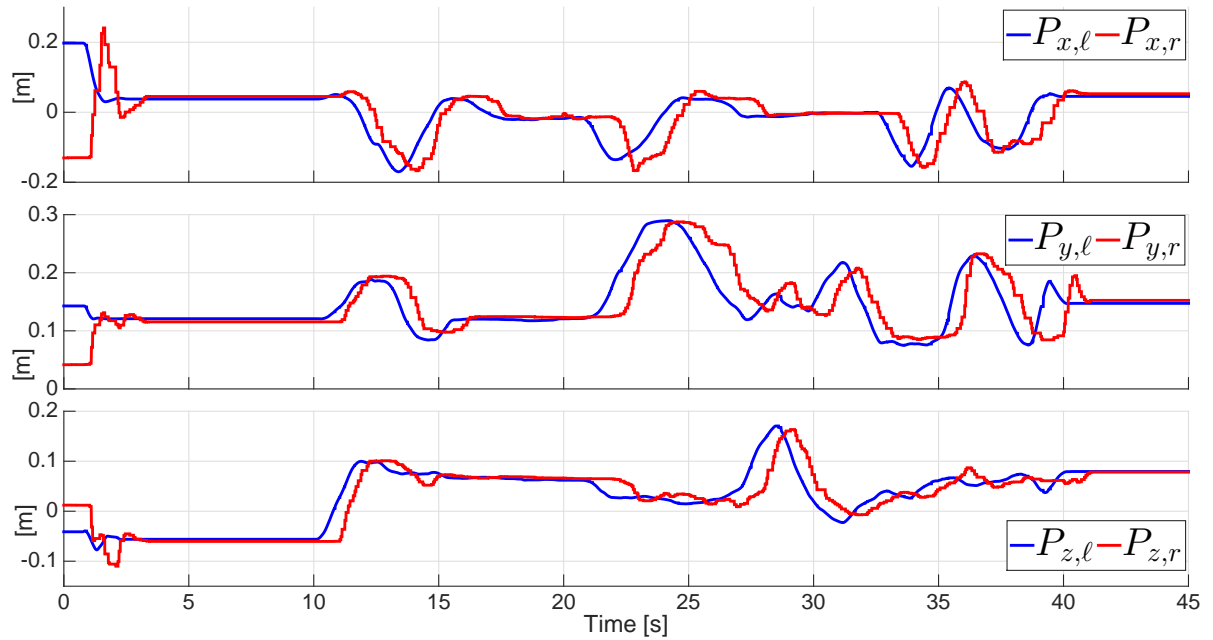
**- Teleoperation without velocity measurements**

$$k_\ell=5, k_r=11, d_\ell=2, d_r=3, k_{y\ell}=1000, k_{yr}=1000.$$

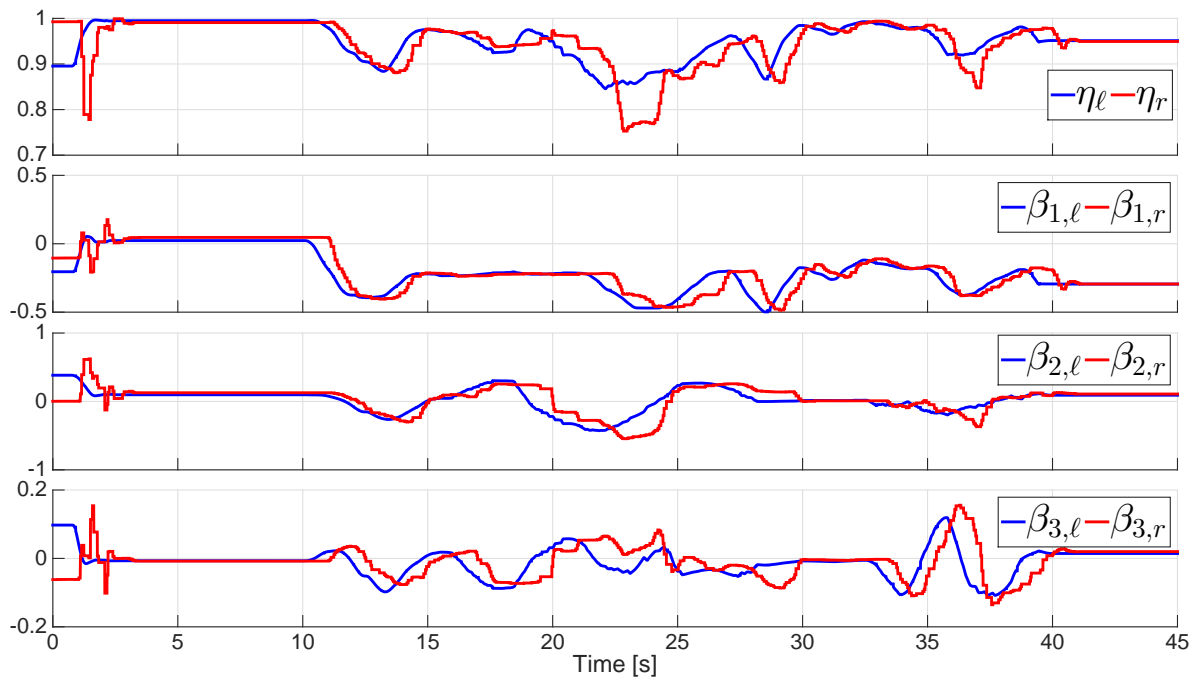
**- Teleoperation with variable time-delays**

$$k_\ell=5, k_r=10, d_\ell=1.1, d_r=1.9, {}^*T_{r\ell}=0.19, {}^*T_{\ell r}=0.21, \alpha_\ell=0.25, \alpha_r=0.2.$$

Figures 5.17, 5.18, 5.19 and 5.20 show the behaviors of the pose and velocities for each one of the controllers evaluated under the experiment detailed previously, and it can be observed that the two control algorithms performed accordingly to the stated in Propositions 5.1 and 5.2. That is, when external forces are injected to the teleoperation system the velocities and pose errors are bounded.

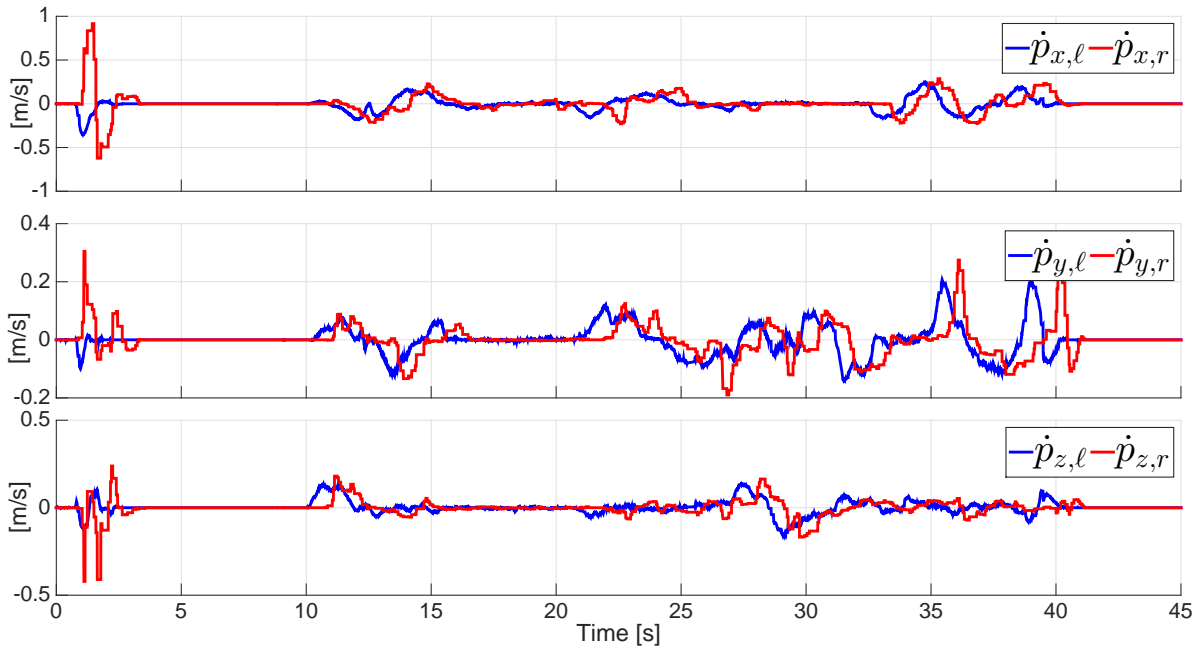


(a) Positions

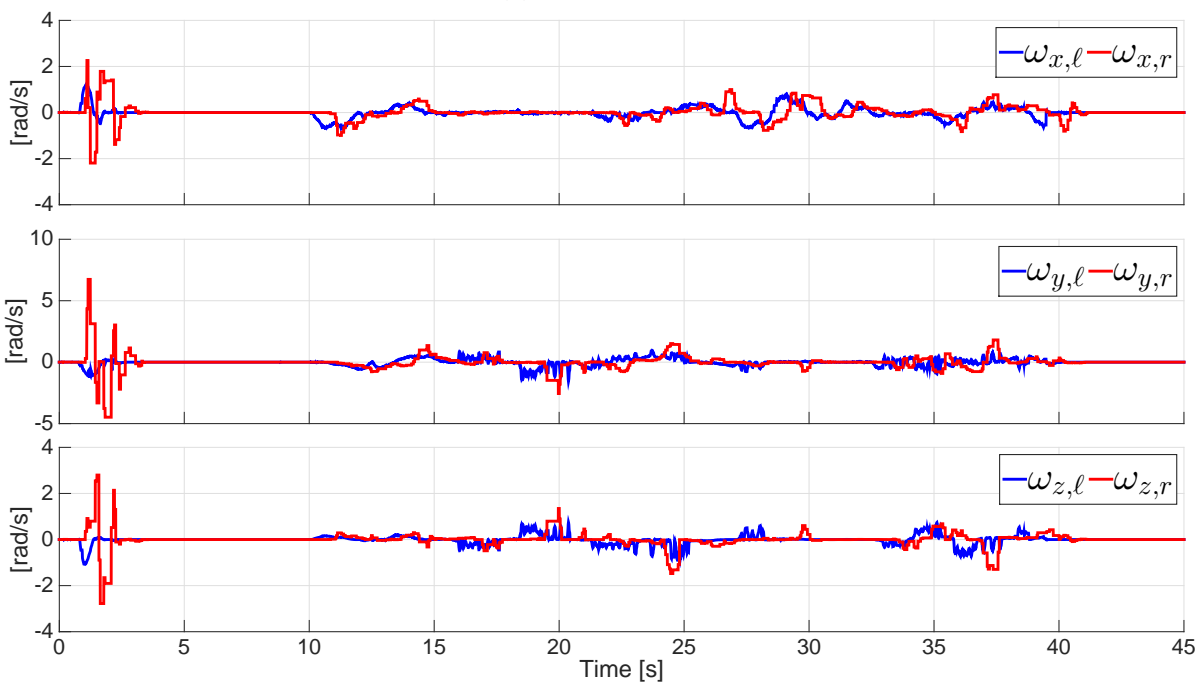


(b) Unit-quaternions (Orientations)

Figure 5.17: Pose of the robots using the teleoperation control algorithm without velocity measurements.

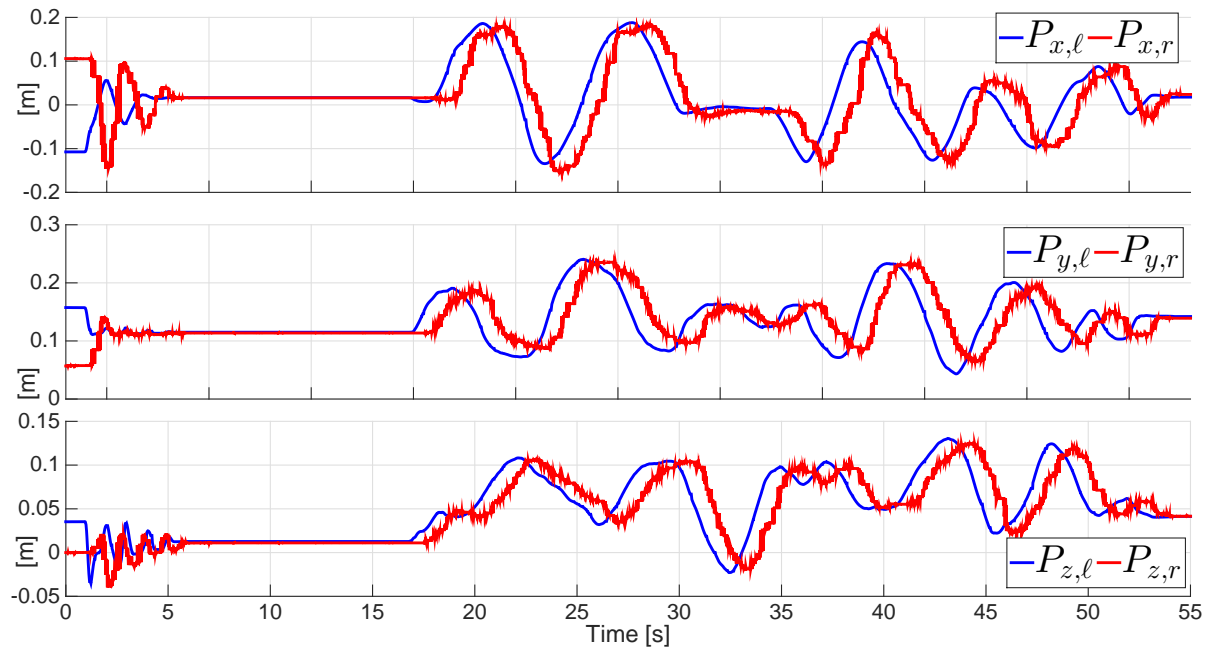


(a) Linear velocities

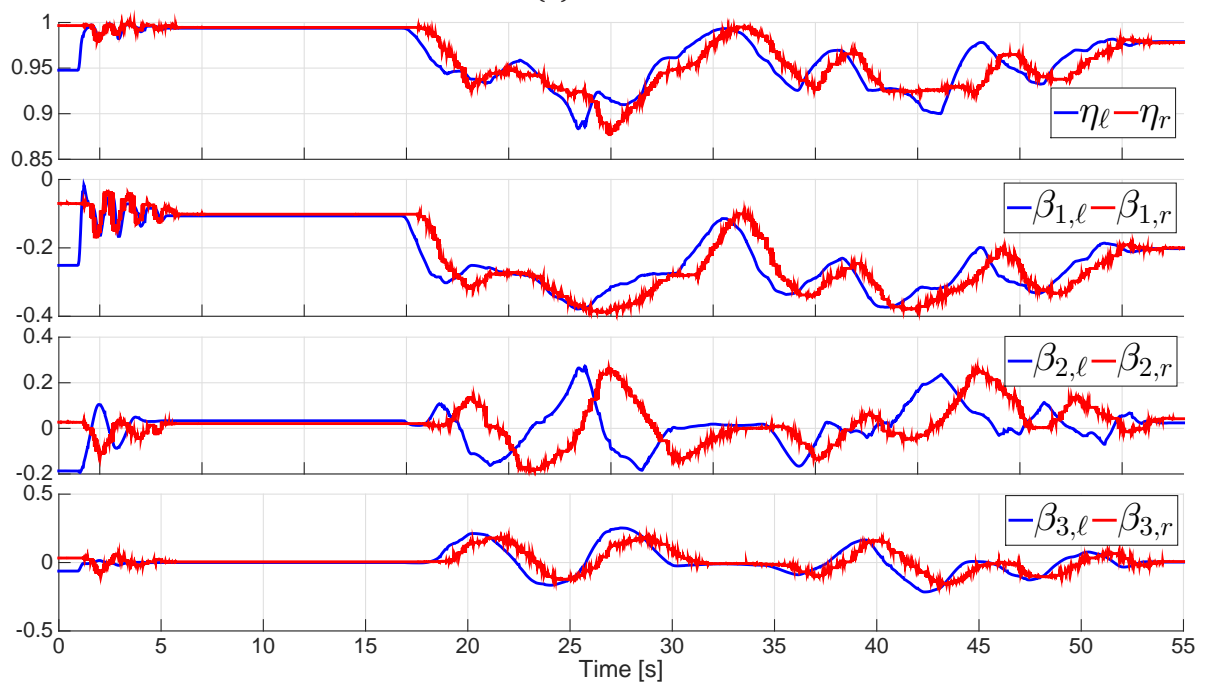


(b) Angular velocities

Figure 5.18: Velocities of the robots using the teleoperation control algorithm without velocity measurements.

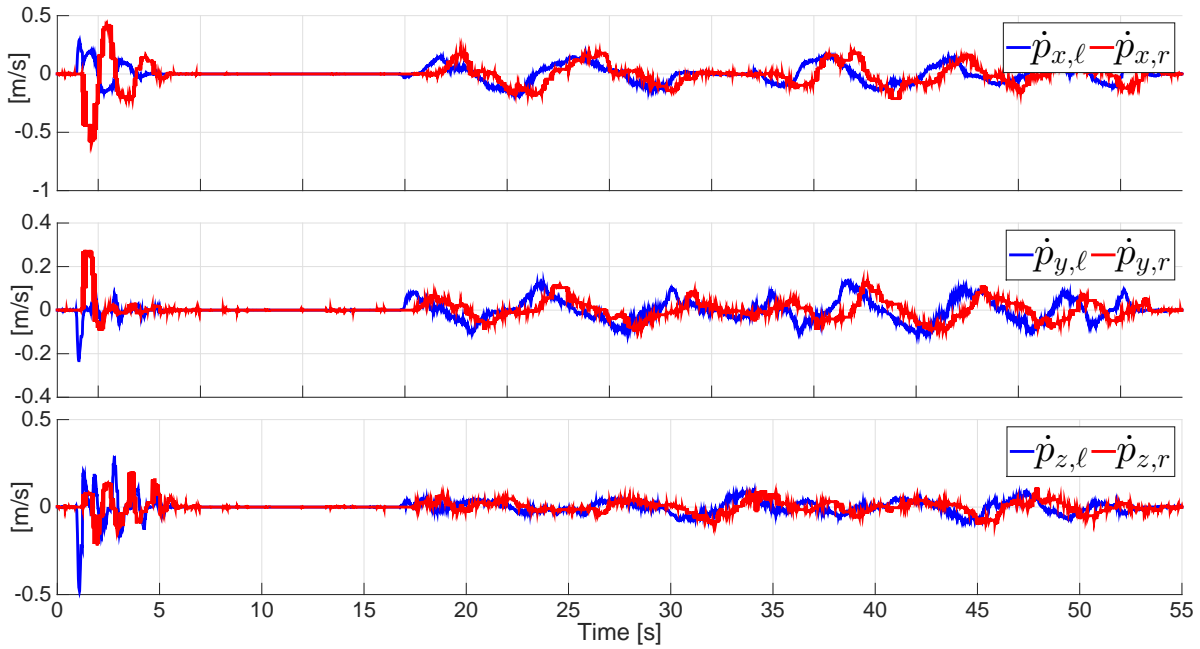


(a) Positions

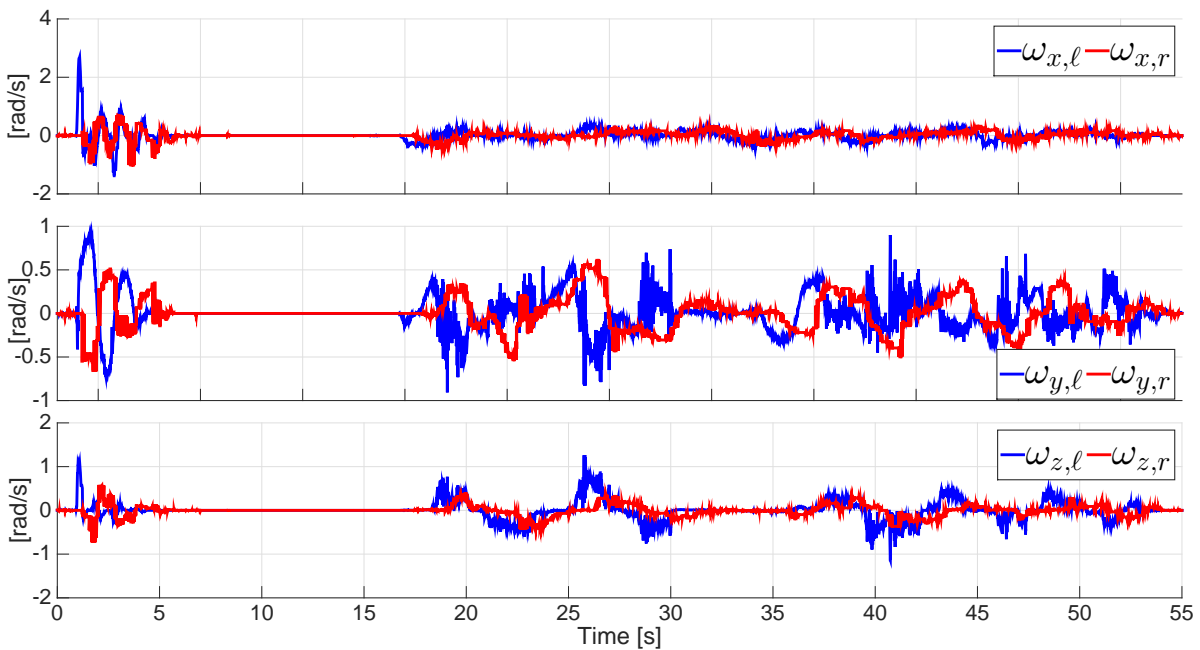


(b) Unit-quaternions (Orientations)

Figure 5.19: Pose of the robots using the teleoperation control algorithm with variable time-delays.



(a) Linear velocities



(b) Angular velocities

Figure 5.20: Velocities of the robots using the teleoperation control algorithm with variable time-delays.



*This chapter presents the conclusions, summarizes the contributions of the thesis and discusses the future work. Finally, the publications generated from this work are listed.*

## **6.1 Conclusions and contributions**

This thesis proposes new control schemes that provide solutions to the consensus problems of robot networks and to the position tracking problem in bilateral teleoperation systems. The main contributions of this work are:

- The proposed control schemes deal with the complete pose of the robots, and not only with the orientation part as do most of the controllers found in the literature. Moreover, the unit-quaternions are used to represent the orientation because they are a singularity-free representation.
- The proposed control schemes are applicable to robots with different dynamic parameters and dissimilar degrees of freedom (heterogeneous).
- In the leader-follower consensus problem, the proposed control schemes, require that at least one follower robot has access to the leader information. This requirement facilitates the implementation of the proposed schemes in comparison to similar control algorithms found in the literature that require that the leader information arrives to all the followers.

The different control schemes proposed in this work can be summarized in the following way:

- **Proportional plus filter.** This controller is composed of three terms: a proportional pose error term, a filter whose input is the robot pose and a gravity cancellation term. This scheme does not depend on velocity measurements. It has been proved that this scheme solves the leader-follower and the leaderless consensus problems for networks without interconnecting time-delays. Furthermore, for bilateral teleoperation systems and under the reasonable assumption that the human and the environment define passive maps from velocity to force, pose error and velocities are bounded. Similar to the leaderless consensus problem with two robots, if the human and the environment forces are zero, the pose error asymptotically converges to zero.
- **Proportional plus damping.** This controller is composed of three terms, as the previous controller, but instead of the filter it has a damping term whose input is the velocity, the other two terms are the proportional pose error and the gravity cancellation terms. It has been proved that this control scheme solves both the leader-follower and the leaderless pose consensus problems considering *variable time-delays in the interconnection of the network*. The teleoperation case has been derived and convergence to zero of the velocities and the pose errors between the local and remote robot manipulators has also been proved. Besides, using the human passivity assumption, it is shown that velocities and pose errors are bounded when a human interacts with the robot network.
- **Adaptive Controller. Uncertain Dynamic and Kinematic parameters.** This controller is composed of two terms and two estimation laws. The first term consists of the regressor matrix and the estimated dynamic parameter vector, and the second term is composed of the estimated Jacobian and an auxiliary signal whose inputs are velocity and pose errors. It has been proved that this controller solves the leader-follower and the leaderless pose consensus problems in networks of *robots with uncertain dynamic and kinematic parameters and variable time-delays in the robots' interconnection*. Similar to the previous control schemes, using the human passivity assumption, it is shown boundedness of velocities and pose errors when a human injects forces to the network. A control algorithm is derived for teleoperation systems composed of robots with uncertain parameters and variable time-delays in the communication channel.
- **Adaptive Controller. Uncertain Dynamic parameters.** This controller has been designed to solve the *control of cooperative teleoperation systems*. It is composed of two terms and one estimation law. The first term consists of the regressor matrix and the estimated dynamic parameters vector and the second term is composed of an auxiliary signal whose inputs are the velocity and pose errors. Besides, the controllers of the remote robots of the cooperative system have a third term to fix a desired internal force to be applied to the handled object. It has been proved that, in spite of variable time-delays in the com-

munication channel and uncertain dynamic parameters, the velocities and the pose errors between the local manipulator end-effector and the object handled by the cooperative system at the remote site converge to zero.

In addition to the above controllers, other elements are also original contributions of this work. These are:

- **Phantorque Libraries.** These are two communication libraries developed to facilitate the implementation of the different control algorithms from Simulink<sup>®</sup> to Geomagic<sup>®</sup> devices. The two libraries are: The PhantTorque\_6Dof library which is designed to be used with the PHANTOM Premium 1.5<sup>®</sup> and the PhanTorque\_3Dof library designed to work with the PHANTOM Omni<sup>®</sup> and PHANTOM Desktop<sup>®</sup>. It should be underscored that these libraries are publicly available at:

<https://sir.upc.edu/wikis/roblab/index.php/Projects/PhanTorqueLibraries>

- **Gravity vectors of the two Phantom Premium 1.5 Haptics.** The physical parameters and the vector functions of the gravity forces of the two Premium haptic devices have been experimentally calculated.

## 6.2 Future work

There are several interesting topics that can be treated in future work, like the relaxation of the interconnection assumptions. Instead of fixed (constant) and undirected interconnection topologies, it could be desirable to extend these topologies to be time-varying (switching) and simply connected.

In this work, due to the nonlinear network dynamics, the final agreement pose in the leaderless consensus problem cannot be a priori predicted. Hence, another future research avenue is the estimation of such agreement pose.

In order to analyze the behavior of the system when packet losses, multiple sample rates and signal quantization appear, the stability analysis should be made considering the system as discrete time. This is an interesting and difficult topic for future work.

In this work the interactions of the human and the environment are modeled as passive systems, but the extension of these models to a more general case would require further research.

A clear theoretical extension for the proportional plus filter scheme is the inclusion of time-delays in the interconnection.

The proportional plus damping and the adaptive controllers derived for teleoperation systems use a damping condition to ensure stability, but further research has to be done to also improve the transparency of the teleoperation system.

In the proposed CTS algorithm it is assumed that a rigid object is firmly grasped by the remote cooperative system. Future work will try to relax this assumption, allowing that flexible objects be handled by the cooperative system.

### 6.3 List of publications

The following list contains the published and submitted papers generated during the course of this thesis.

#### Journal publications:

- Aldana, C. I., Nuño, E., Basañez, L., Romero, E. (2014). Operational space consensus of multiple heterogeneous robots without velocity measurements. *Journal of the Franklin Institute*, 351(3), 1517–1539.
- Aldana, C. I., Romero, E., Nuño, E., Basañez, L. (2014). Pose consensus in networks of heterogeneous robots with variable time-delays. *Journal of Robust and Nonlinear Control*. In press. doi: 10.1002/rnc.3200.
- Nuño, E., Aldana, C. I., Basañez, L. (2014). Task space consensus in networks of heterogeneous and uncertain robotic systems with variable time-delays. Submitted to the *IET Control Theory & Applications*.

#### Book chapters:

- Aldana, C., Romero, E., Nuño, E., Basañez, L. (2014). Operational Space Consensus in Networks of Robots: The Leader-Follower Case. In M. A. Armada, A. Sanfeliu, M. Ferre (Eds.), *ROBOT2013: First Iberian Robotics Conference* (Vol. 253, 585–599). Springer International Publishing.

**Refereed conference publications:**

- Aldana, C.I., Nuño, E., Basañez, L. (2014). Leader-follower Pose Consensus for Heterogeneous Robot Networks with Variable Time-Delays. *19th IFAC World Congress*, Cape Town, South Africa, pp. 6674-6679, 24-29 August.
- Nuño, E., Aldana, C. I., Basañez, L. (2014). Leader-Follower Consensus in Networks of Uncertain Manipulators in the  $SE(3)$ . *XVI Congreso Latinoamericano de Control Automático (CLCA)*, 14-17 October.
- Aldana, C.I., Nuño, E., Basañez, L. (2013), Control of bilateral teleoperators in the operational space without velocity measurements, *IEEE/RSJ International Conference on Intelligent Robots and Systems (IROS)*, 5445-5450, 3-7 Nov.
- Aldana, C., Nuño, E., Basañez, L. (2012), Bilateral teleoperation of cooperative manipulators, *IEEE International Conference on Robotics and Automation (ICRA)*, 4274-4279, 14-18 May.



## MATH AND CONTROL BACKGROUND

*This appendix provides an overview of some of the mathematical notions and stability concepts that are employed throughout the dissertation. Norms,  $\mathcal{L}_q$  spaces, inequalities and quaternions are some of the mathematical tools that are reviewed in the first part. In the second part, Lyapunov theory and passivity concepts are described, since these are the basics tools used in the design of the proposed controllers. All these concepts are presented with the intention to be a quick reference and not an exhaustive one and, for that reason, all the theorems and lemmas are stated without proofs. References are provided for readers interested in such proofs.*

## A.1 Mathematical preliminaries

In this section some of the mathematical concepts used along this dissertation are defined. They have been gathered from several mathematical books and papers, like (Strang 1986; Hardy et al. 1988; Chou 1992; Kelly et al. 2005; van der Schaft Arjan 1999; Sontag 1998; Kuipers 2002).

### A.1.1 Matrix types and Kronecker product

**Definition A.1** (Matrix). A matrix is a system of  $m \times n$  elements, e.g., real or complex numbers, arranged in  $m$  rows and  $n$  columns, such as:

$$\mathbf{A} = \begin{bmatrix} a_{11} & a_{12} & \dots & a_{1n} \\ a_{21} & a_{22} & \dots & a_{2n} \\ \vdots & \vdots & \ddots & \vdots \\ a_{m1} & a_{m2} & \dots & a_{mn} \end{bmatrix}.$$

If  $m = n$ ,  $\mathbf{A}$  is called a *square matrix* of size  $n$ . The identity matrix or unit matrix is a square matrix with ones on the main diagonal and zeros elsewhere, denoted by  $\mathbf{I}_n$ . The set of all  $m \times n$  matrices with real entries is denoted by  $\mathbb{R}^{m \times n}$ .

**Definition A.2** (Matrix Transpose). If  $\mathbf{A}$  is a  $m \times n$  matrix, the transpose of  $\mathbf{A}$  is the  $n \times m$  matrix, denoted by  $\mathbf{A}^\top$ , whose columns are formed from the corresponding rows of  $\mathbf{A}$ . Some properties of the matrix transpose are:  $(\mathbf{A}^\top)^\top = \mathbf{A}$  and  $(\mathbf{AB})^\top = \mathbf{B}^\top \mathbf{A}^\top$ , where  $\mathbf{B}$  is a  $n \times p$  matrix.

**Definition A.3** (Eigenvalues and eigenvectors of a matrix). Consider a square matrix  $\mathbf{A}$  of size  $n$ . Then,  $\lambda$  is an eigenvalue of  $\mathbf{A}$  if there exists a nonzero vector  $\mathbf{v} \in \mathbb{R}^n$  such that

$$\mathbf{A}\mathbf{v} = \lambda\mathbf{v},$$

where  $\mathbf{v}$  is called eigenvector. In general,  $\mathbf{A}$  has  $n$  eigenvalues and they are the roots of the characteristic polynomial:

$$\det(\mathbf{A} - \lambda\mathbf{I}_n) = 0.$$

The set of eigenvalues of a matrix  $\mathbf{A}$  is called its spectrum and is denoted by  $\sigma(\mathbf{A})$ .

**THEOREM A.1 (Gershgorin circle theorem):**

Every eigenvalue of matrix  $\mathbf{A} \in \mathbb{R}^{n \times n}$ , with entries  $a_{ij}$ , lies in the union of the complex plane disks

$$D_i = \{z : |z - a_{ii}| \leq \sum_{j \neq i} |a_{ij}|\}, \quad 1 \leq i \leq n.$$

A Gershgorin disc is a closed disc centered at  $a_{ii}$  with radius  $r_i = \sum_{j \neq i} |a_{ij}|$ .

**Definition A.4** (Symmetric matrix). A matrix  $\mathbf{A}$  which is equal to its transpose, that is  $\mathbf{A} = \mathbf{A}^\top$ , is called symmetric. Clearly, every symmetric matrix is square.

**Definition A.5** (Positive definite matrix). A matrix  $\mathbf{A}$  is positive definite if and only if, for all  $\mathbf{x} \neq \mathbf{0}$ :

$$\mathbf{x}^\top \mathbf{A} \mathbf{x} > 0,$$

it is positive semi-definite if and only if, for all  $\mathbf{x}$ :

$$\mathbf{x}^\top \mathbf{A} \mathbf{x} \geq 0.$$

If  $\mathbf{A}$  is positive definite then its  $n$  eigenvalues  $\lambda_1, \dots, \lambda_n$  are strictly positive.

**Definition A.6** (Kronecker product). Let  $\mathbf{A}$  be a  $n \times p$  matrix and  $\mathbf{B}$  a  $m \times q$  matrix, then the



Kronecker product is the matrix  $nm \times pq$ , defined as

$$\mathbf{A} \otimes \mathbf{B} = \begin{pmatrix} a_{11}\mathbf{B} & a_{12}\mathbf{B} & \dots & a_{1p}\mathbf{B} \\ a_{21}\mathbf{B} & a_{22}\mathbf{B} & \dots & a_{2p}\mathbf{B} \\ \vdots & \vdots & \ddots & \vdots \\ a_{n1}\mathbf{B} & a_{n2}\mathbf{B} & \dots & a_{np}\mathbf{B} \end{pmatrix}. \quad (\text{a.1})$$

Some properties of the Kronecker product are:

1.  $\mathbf{A} \otimes (\mathbf{B} \otimes \mathbf{C}) = (\mathbf{A} \otimes \mathbf{B}) \otimes \mathbf{C}$
2.  $\mathbf{A} \otimes (\mathbf{B} + \mathbf{C}) = (\mathbf{A} \otimes \mathbf{B}) + (\mathbf{A} \otimes \mathbf{C})$
3.  $(\mathbf{A} \otimes \mathbf{B})(\mathbf{C} \otimes \mathbf{D}) = (\mathbf{AC} \otimes \mathbf{BD})$
4.  $a \otimes \mathbf{A} = \mathbf{A} \otimes a = a\mathbf{A}$
5.  $a\mathbf{A} \otimes b\mathbf{B} = ab\mathbf{A} \otimes \mathbf{B}$

where  $\mathbf{A}$ ,  $\mathbf{B}$ ,  $\mathbf{C}$  and  $\mathbf{D}$  are matrices of proper dimensions and  $a$  and  $b$  scalars.

### A.1.2 Vectors products and norms

**Definition A.7** (Vector). A vector is a column matrix. The set of all vectors (or column matrices) of dimension  $n$  is denoted by  $\mathbb{R}^n$ . For example:

$$\mathbf{x} = \begin{bmatrix} x_1 \\ x_2 \\ \vdots \\ x_n \end{bmatrix},$$

where  $x_1, x_2, \dots, x_n \in \mathbb{R}$ .

**Definition A.8** (Dot product). Let  $\mathbf{x}$  and  $\mathbf{y}$  be two vectors in  $\mathbb{R}^n$ , then the dot product (or inner product) of  $\mathbf{x}$  and  $\mathbf{y}$  is the scalar  $\mathbf{x} \cdot \mathbf{y}$  given by

$$\mathbf{x} \cdot \mathbf{y} = x_1y_1 + x_2y_2 + \dots + x_ny_n = \mathbf{x}^\top \mathbf{y} \quad (\text{a.2})$$

**Definition A.9** (Cross product). Let  $\mathbf{x} = [x_1 \ x_2 \ x_3]^\top$  and  $\mathbf{y} = [y_1 \ y_2 \ y_3]^\top$  be two vectors in  $\mathbb{R}^3$ , then the cross product of  $\mathbf{x}$  and  $\mathbf{y}$  is the vector

$$\mathbf{x} \times \mathbf{y} = \begin{bmatrix} x_2y_3 - x_3y_2 \\ x_3y_1 - x_1y_3 \\ x_1y_2 - x_2y_1 \end{bmatrix}. \quad (\text{a.3})$$

The cross product is only defined for vectors in  $\mathbb{R}^3$ . The vector cross product can also be expressed using the skew-symmetric matrix operator  $\mathbf{S}(\cdot)$ :

$$\mathbf{x} \times \mathbf{y} = \mathbf{S}(\mathbf{x})\mathbf{y},$$

where

$$\mathbf{S}(\mathbf{x}) := \begin{bmatrix} 0 & -x_3 & x_2 \\ x_3 & 0 & -x_1 \\ -x_2 & x_1 & 0 \end{bmatrix}. \quad (\text{a.4})$$

For all  $\mathbf{x}, \mathbf{y}, \mathbf{z} \in \mathbb{R}^3$  and  $a, b \in \mathbb{R}$  the skew-symmetric matrix operator satisfies:

$$\begin{aligned} \mathbf{S}(a\mathbf{x} + b\mathbf{y}) &= a\mathbf{S}(\mathbf{x}) + b\mathbf{S}(\mathbf{y}) \\ \mathbf{S}(\mathbf{x})^\top &= \mathbf{S}(-\mathbf{x}) = -\mathbf{S}(\mathbf{x}) \\ \mathbf{S}(\mathbf{x})(\mathbf{y} + \mathbf{z}) &= \mathbf{S}(\mathbf{x})\mathbf{y} + \mathbf{S}(\mathbf{x})\mathbf{z} \\ \mathbf{S}(\mathbf{x})\mathbf{y} &= -\mathbf{S}(\mathbf{y})\mathbf{x} \\ \mathbf{S}(\mathbf{x})\mathbf{x} &= 0 \\ \mathbf{y}^\top \mathbf{S}(\mathbf{x})\mathbf{y} &= 0 \\ \mathbf{x}^\top \mathbf{S}(\mathbf{y})\mathbf{z} &= \mathbf{z}^\top \mathbf{S}(\mathbf{x})\mathbf{y} \\ \mathbf{S}(\mathbf{x})\mathbf{S}(\mathbf{x}) &= \mathbf{x}\mathbf{x}^\top - \mathbf{x}^\top \mathbf{x} \mathbf{I}_3 \\ \mathbf{S}(\mathbf{x})\mathbf{S}(\mathbf{y}) &= \mathbf{y}\mathbf{x}^\top - \mathbf{x}^\top \mathbf{y} \mathbf{I}_3 \\ \mathbf{S}[\mathbf{S}(\mathbf{x})\mathbf{y}] &= \mathbf{y}\mathbf{x}^\top - \mathbf{x}\mathbf{y}^\top \end{aligned} \quad (\text{a.5})$$

**Definition A.10** (Norm of a vector). A positive number is called a norm for a vector  $\mathbf{x} \in \mathbb{R}^n$  and is denoted by  $|\mathbf{x}|$ , if it has the following four properties:

1.  $|\mathbf{x}| \geq 0$ ;
2.  $|\mathbf{x}| = 0$  if and only if  $\mathbf{x} \equiv 0$ ;
3.  $|a\mathbf{x}| = |a||\mathbf{x}| \quad \forall a \in \mathbb{R}$ ;
4.  $|\mathbf{x} + \mathbf{y}| \leq |\mathbf{x}| + |\mathbf{y}|$ .

The vector  $q$ -norm,  $|\mathbf{x}|_q$ , for  $q \geq 1$  is defined as

$$|\mathbf{x}|_q = \left( \sum_{i=1}^n |x_i|^q \right)^{\frac{1}{q}}.$$

All the norms are equivalent, in a sense that if  $|\mathbf{x}|_p$  and  $|\mathbf{x}|_q$  are two different norms, then there exist two constants  $a_1 > 0$  and  $a_2 > 0$  such that

$$a_1 |\mathbf{x}|_p \leq |\mathbf{x}|_q \leq a_2 |\mathbf{x}|_p.$$

**Definition A.11 ( $\infty$ -norm).** For a vector  $\mathbf{x} := [x_1, x_2, \dots, x_n]^\top \in \mathbb{R}^n$  the infinity norm is defined as

$$|\mathbf{x}|_\infty = \max_i |x_i|.$$

**Definition A.12 (Euclidean norm or 2-norm).** For a vector  $\mathbf{x} := [x_1, x_2, \dots, x_n]^\top \in \mathbb{R}^n$  is defined as

$$|\mathbf{x}|_2 = \sqrt{\mathbf{x}^\top \mathbf{x}}.$$

### A.1.3 Function properties

**Definition A.13 (Continuity).** A function  $f : [0, \infty) \rightarrow \mathbb{R}$  is continuous on  $[0, \infty)$  if for any given  $\epsilon_0 > 0$  there exists a  $\delta(\epsilon_0, t_0)$  such that  $\forall t_0, t \in [0, \infty)$  for which  $|t - t_0| < \delta(\epsilon_0, t_0)$  we have  $|f(t) - f(t_0)| < \epsilon_0$ .

**Definition A.14 (Uniform Continuity).** A function  $f : [0, \infty) \rightarrow \mathbb{R}$  is uniformly continuous on  $[0, \infty)$  if for any given  $\epsilon_0 > 0$  there exists a  $\delta(\epsilon_0)$  such that  $\forall t_0, t \in [0, \infty)$  for which  $|t - t_0| < \delta(\epsilon_0)$  we have  $|f(t) - f(t_0)| < \epsilon_0$ .

**Definition A.15 (Piecewise Continuity).** A function  $f : [0, \infty) \rightarrow \mathbb{R}$  is piecewise continuous on  $[0, \infty)$  if  $f$  is continuous on any finite interval  $[t_0, t_1] \subset [0, \infty)$  except for a finite number of points.

**Definition A.16 (Absolute Continuity).** A function  $f : [a, b] \rightarrow \mathbb{R}$  is absolute continuous on  $[a, b]$  iff, for any  $\epsilon > 0$ , there is a  $\delta > 0$  such that

$$\sum_{i=1}^n |f(\alpha_i) - f(\beta_i)| < \epsilon,$$

for any finite collection of subintervals  $(\alpha_i, \beta_i)$  of  $[a, b]$  with  $\sum_{i=1}^n |\alpha_i - \beta_i| < \delta$ .

**Definition A.17 (Lipschitz).** A function  $f : [a, b] \rightarrow \mathbb{R}$  is Lipschitz on  $[a, b]$  if

$$|f(x_1) - f(x_2)| \leq k|x_1 - x_2| \quad \forall x_1, x_2 \in [a, b],$$

where  $k \geq 0$  is a constant referred to as the Lipschitz constant.

**Definition A.18 (Locally and Globally Positive Definiteness).**  $V : \mathbb{R}^n \rightarrow \mathbb{R}_{\geq 0}$  is locally positive definite in  $B$  if  $V(\mathbf{0}) = 0$  and  $V(\mathbf{x}) > 0 \forall \mathbf{x} \in B, \mathbf{x} \neq \mathbf{0}$ . If in addition  $V(\mathbf{x}) > 0, \forall \mathbf{x} \neq \mathbf{0}$ , then  $V$  is said to be globally positive definite. For time dependent functions like  $W : \mathbb{R}^n \times \mathbb{R}_{\geq 0} \rightarrow \mathbb{R}_{\geq 0}$ .  $W(\mathbf{x}, t)$  is locally or globally positive definite if  $W(\mathbf{0}, t) = 0$  and  $W(\mathbf{x}, t) \geq V(\mathbf{x}), \forall t \geq 0$ , where  $V(\mathbf{x})$  is a locally or globally positive definite function.

**Definition A.19 (Negative Definiteness).** The function  $V(\mathbf{x})$  is negative definite if  $-V$  is posi-

tive definite.

**Definition A.20 (Positive and Negative Semi-Definiteness).** The function  $V(\mathbf{x})$  is positive semi-definite if  $V(\mathbf{0}) = 0$  and  $V(\mathbf{x}) \geq 0$  for  $\mathbf{x} \neq \mathbf{0}$ .  $V(\mathbf{x})$  is negative semi-definite if  $-V(\mathbf{x})$  is positive semi-definite.

**Definition A.21 (Radially Unboundedness).** A continuous function  $V(\mathbf{x})$  is radially unbounded if  $V(\mathbf{x}) \rightarrow \infty$  when  $|\mathbf{x}| \rightarrow \infty$ .  $W(\mathbf{x}, t)$  is radially unbounded if  $W(\mathbf{x}, t) \geq V(\mathbf{x})$ ,  $\forall t \geq 0$ , where  $V(\mathbf{x})$  is radially unbounded.

**Definition A.22 (Inner Product).** The inner product (denoted by  $\langle \cdot, \cdot \rangle$ ) is a generalization of the dot product. In a vector space, it is a way to multiply vectors together, with the result of this multiplication being a scalar. Examples of inner product spaces are:

- For two real numbers  $\{x, y\} \in \mathbb{R}$ ,  $\langle x, y \rangle = xy$ .
- For two vectors in the Euclidian space  $\{\mathbf{x}, \mathbf{y}\} \in \mathbb{R}^n$ ,  $\langle \mathbf{x}, \mathbf{y} \rangle = x_1y_1 + x_2y_2 + \dots + x_ny_n$ .
- For two real functions on in the interval  $[a, b]$ ,  $\{\mathbf{f}_1(x), \mathbf{f}_2(x)\} \in \mathbb{R}^n$ ,  $\langle \mathbf{f}_1, \mathbf{f}_2 \rangle = \int_a^b \mathbf{f}_1(x)\mathbf{f}_2(x)dx$ .

#### A.1.4 Norms for functions and $\mathcal{L}_q$ spaces

Using the vectors' norms definitions next are defined the norms of functions.

**Definition A.23 ( $\mathcal{L}_\infty$  Space and  $\mathcal{L}_\infty$ -norm).**  $\mathcal{L}_\infty$  space consists of all functions  $f : \mathbb{R}_{\geq 0} \rightarrow \mathbb{R}$  which are bounded, and the  $\mathcal{L}_\infty$ -norm of  $f$  is the least upper bound of its vector norm

$$\|f\|_\infty = \sup_{t \in [0, \infty)} |f(t)|.$$

**Definition A.24 ( $\mathcal{L}_2$  Space and  $\mathcal{L}_2$ -norm).** The  $\mathcal{L}_2$ -norm of  $f$  is given by

$$\|f\|_2 = \sqrt{\int_0^\infty f(t)^\top f(t) dt} = \sqrt{\int_0^\infty |f(t)|_2^2 dt}.$$

The  $\mathcal{L}_2$  space consists of all functions  $f : \mathbb{R}_{\geq 0} \rightarrow \mathbb{R}$  which have finite  $\mathcal{L}_2$ -norm i.e.  $\|f\|_2 < \infty$ .

**Definition A.25 ( $\mathcal{L}_q$  Space and  $\mathcal{L}_q$ -norm).** For  $1 \leq q < \infty$ , the set  $\mathcal{L}_q[0, \infty) = \mathcal{L}_q$  consists of all functions  $f : \mathbb{R}_{\geq 0} \rightarrow \mathbb{R}$ , which have bounded  $\mathcal{L}_q$ -norm defined as

$$\|f\|_q = \left( \int_0^\infty |f(t)|^q dt \right)^{\frac{1}{q}}.$$

**Definition A.26 ( $\mathcal{L}_{q_e}$  Space).** Let  $f : \mathbb{R}_{\geq 0} \rightarrow \mathbb{R}$ . Then, for each  $T \in \mathbb{R}_{>0}$ , the function

$f_T : \mathbb{R}_{>0} \rightarrow \mathbb{R}$  is defined by

$$f_T(t) = \begin{cases} f(t) & 0 \leq t \leq T \\ 0 & t > T \end{cases}$$

and is called the truncation of  $f$  to the interval  $[0, T]$ . For each  $q = 1, 2, \dots, \infty$ , the set  $\mathcal{L}_{q_e}$  consists of all measurable functions  $f : \mathbb{R}_{\geq 0} \rightarrow \mathbb{R}$  such that  $f_T \in \mathcal{L}_q$  for all  $T$  with  $0 \leq T < \infty$ .  $\mathcal{L}_{q_e}$  is called the extended  $\mathcal{L}_q$ -space.

**Remark A.1.** Note that  $\mathcal{L}_2$  is related to the inner product as  $\langle f, f \rangle = \int_0^\infty f^2(t)dt = \|f\|_2^2$ . Thus,  $\mathcal{L}_2$  is a Hilbert space, *i.e.*, complete linear space endowed with inner product.

**Remark A.2.** It is important to stress that in some applications, the inner product  $\langle y, u \rangle$  will usually denote the instantaneous power (electrical if  $u, y$  are voltage and current and mechanical if  $u, y$  are force and velocity). Thus  $\langle y, u \rangle_T$  denotes the supplied energy during the time interval  $[0, T]$  given by

$$\langle y, u \rangle_T := \int_0^T y(t)u(t)dt.$$

Note that (Schwarz inequality)

$$\langle y, u \rangle := \int_0^\infty y(t)u(t)dt \leq \|y\|_2^2 \|u\|_2^2.$$

Hence, if such a system is represented as an input-output map, from an input  $u$  to a controlled output  $y$ , and  $u \in \mathcal{L}_2$ , then the control system could be designed to make the input-output map  $\mathcal{L}_2$ -stable and to minimize its  $\mathcal{L}_2$ -gain<sup>3</sup>.  $\mathcal{L}_2$  signals are said to be finite-energy signals.

### A.1.5 Sets

**Definition A.27 (Invariant Set (Blanchini 1999)).** A set  $M$  is said to be an invariant set with respect to  $\dot{x} = f(x)$  if

$$x(0) \in M \Rightarrow x(t) \in M, \quad \forall t \in \mathbb{R}_{\geq 0}.$$

That is, if a solution belongs to  $M$  at some time instant, then it belongs to  $M$  for all future and past time. A set  $M$  is said to be a positively invariant set if

$$\forall x(0) \in M \Rightarrow x(t) \in M, \quad \forall t \geq \mathbb{R}_{\geq 0}.$$

**Definition A.28 (dist (Blanchini 1999)).** Consider any norm  $\|\cdot\| \in \mathbb{R}^n$ . Given a point  $\mathbf{x}(t) \in \mathbb{R}^n$  and a set  $M$ , the distance of  $\mathbf{x}$  from  $M$  is defined as

$$dist(\mathbf{x}, M) = \inf_{\mathbf{y} \in M} \|\mathbf{x} - \mathbf{y}\|.$$

<sup>3</sup>Refer to Section A.2.2 for the definition of  $\mathcal{L}_q$ -gain and  $\mathcal{L}_q$ -stability.

**LEMMA A.1 (Limit Sets):**

If a solution  $x(t)$  of  $\dot{x} = f(x)$  is bounded and belongs to  $D \subset \mathbb{R}^n$  for  $t \geq 0$ , then its positive limit set  $L^+$  is a nonempty, compact, invariant set. Moreover  $x(t)$  approaches  $L^+$  as  $t \rightarrow \infty$ .  $\diamond$

**Definition A.29 (Group (Murray, Li, and Sastry 1994)).** A set  $G$  together with a binary operator  $\circ$  defined on elements of  $G$  is called a group if it satisfies the following axioms:

1. *Closure:* If  $g_1, g_2 \in G$ , then  $g_1 \circ g_2 \in G$ .
2. *Identity:* There exists an identity element,  $e$ , such that  $g \circ e = e \circ g = g$  for every  $g \in G$ .
3. *Inverse:* For each  $g \in G$ , there exists a (unique) inverse,  $g^{-1} \in G$ , such that  $g \circ g^{-1} = g^{-1} \circ g = e$ .
4. *Associativity:* If  $g_1, g_2, g_3 \in G$ , then  $(g_1 \circ g_2) \circ g_3 = g_1 \circ (g_2 \circ g_3)$ .

**A.1.6 Inequalities**

**Inequality A.1 (Schwarz (Kreyszig 1978)).** Let  $\mathbf{f}_1(x), \mathbf{f}_2(x) \in \mathbb{R}^n$  be any two integrable functions in  $[a, b]$ , then Schwarz's inequality is given by

$$|\langle \mathbf{f}_1, \mathbf{f}_2 \rangle|^2 \leq \langle \mathbf{f}_1, \mathbf{f}_1 \rangle \langle \mathbf{f}_2, \mathbf{f}_2 \rangle$$

or, written out explicitly

$$\left[ \int_a^b \mathbf{f}_1(x) \mathbf{f}_2(x) dx \right]^2 \leq \int_a^b |\mathbf{f}_1(x)|^2 dx \int_a^b |\mathbf{f}_2(x)|^2 dx.$$

The equality holds if  $\mathbf{f}_1(x) = \alpha \mathbf{f}_2(x)$  with  $\alpha$  being a constant. Schwarz's inequality is sometimes also called Cauchy-Schwarz inequality or Buniakowsky inequality.

**Inequality A.2 (Hölder (Hardy et al. 1988)).** It states that if  $\mathbf{f}_1 : \mathbb{R}_{\geq 0} \rightarrow \mathcal{L}_{p_e}$  and  $\mathbf{f}_2 : \mathbb{R}_{\geq 0} \rightarrow \mathcal{L}_{q_e}$  where  $p, q \in (1, \infty)$  and  $\frac{1}{p} + \frac{1}{q} = 1$ , then

$$\int_0^\tau |\mathbf{f}_1(t) \mathbf{f}_2(t)| dt \leq \left( \int_0^\tau |\mathbf{f}_1(t)|^p dt \right)^{\frac{1}{p}} \left( \int_0^\tau |\mathbf{f}_2(t)|^q dt \right)^{\frac{1}{q}} \quad \forall \tau \in [0, \infty).$$

Which in the case of norms we have

$$|\mathbf{f}_1^\top(t) \mathbf{f}_2(t)| \leq \|\mathbf{f}_1(t)\|_p \|\mathbf{f}_2(t)\|_q.$$

**Inequality A.3 (Young (Hardy et al. 1988)).** Suppose  $\exists \{a, b, p, q\} \in \mathbb{R}_{>0}$  and  $\frac{1}{p} + \frac{1}{q} = 1$  then we have

$$ab \leq \frac{a^p}{p} + \frac{b^q}{q}.$$

Young's inequality is a special case of the inequality of weighted arithmetic and geometric means.

**Inequality A.4 (Minkowski (Hardy et al. 1988)).** Let  $\{\mathbf{x}, \mathbf{y}\} \in \mathbb{R}^n$ , and  $p \in [1, \infty)$ . Then the Minkowski inequality is given by

$$\|\mathbf{x}\|_p - \|\mathbf{y}\|_p \leq \|\mathbf{x} + \mathbf{y}\|_p \leq \|\mathbf{x}\|_p + \|\mathbf{y}\|_p.$$

**Inequality A.5 (Rayleigh (Strang 1986)).** For any  $\mathbf{x} \in \mathbb{R}^n$  and  $\mathbf{P} \in \mathbb{R}^{n \times n}$  if  $\mathbf{P} > 0$  and symmetric, then

$$\lambda_m\{\mathbf{P}\}|\mathbf{x}|^2 \leq \langle \mathbf{x}, \mathbf{P}\mathbf{x} \rangle \leq \lambda_M\{\mathbf{P}\}|\mathbf{x}|^2$$

where  $\lambda_m$  and  $\lambda_M$  are the minimum and the maximum eigenvalues of  $\mathbf{P}$ , respectively. Note that  $\langle \mathbf{x}, \mathbf{P}\mathbf{x} \rangle = \mathbf{x}^\top \mathbf{P}\mathbf{x}$ .

### A.1.7 Quaternions

**Definition A.30 (Quaternions).** The quaternions are a generalization of the complex numbers and are defined as

$$\boldsymbol{\alpha} = a_0 + a_1\mathbf{i} + a_2\mathbf{j} + a_3\mathbf{k}, \quad (\text{a.6})$$

where  $\mathbf{i}, \mathbf{j}$  and  $\mathbf{k}$  are three orthogonal unit spatial vectors and  $a_i \in \mathbb{R}$  for  $i = 0, 1, 2, 3$ . The quaternions set  $\mathbb{H}$  is  $\mathbb{R}^4$  together with the quaternion addition(+), subtraction(-) and multiplication( $\odot$ )

$$\mathbb{H} = \{\mathbb{R} \times \mathbb{R} \times \mathbb{R} \times \mathbb{R}, \pm, \odot\}$$

The column vector representation of an arbitrary quaternion  $\boldsymbol{\alpha}$  with respect to the basis  $(1, \mathbf{i}, \mathbf{j}, \mathbf{k})$  is the collection of its parameters

$$\boldsymbol{\alpha} = \begin{bmatrix} a_0 \\ a_1 \\ a_2 \\ a_3 \end{bmatrix} := \begin{bmatrix} a_0 \\ \mathbf{a} \end{bmatrix}, \quad (\text{a.7})$$

where  $\mathbf{a} = [a_1 \ a_2 \ a_3]^\top$ .

**Definition A.31 (Quaternion conjugate).** The conjugate of a quaternion  $\boldsymbol{\alpha}$ , denoted  $\boldsymbol{\alpha}^*$ , is given by

$$\boldsymbol{\alpha}^* = \begin{bmatrix} a_0 \\ -\mathbf{a} \end{bmatrix}. \quad (\text{a.8})$$

**Definition A.32 (Quaternions addition and subtraction).** The addition and subtraction of two quaternions  $\boldsymbol{\alpha}$  and  $\boldsymbol{\beta}$  are defined as

$$\boldsymbol{\alpha} + \boldsymbol{\beta} = (a_0 + b_0) + (a_1 + b_1)\mathbf{i} + (a_2 + b_2)\mathbf{j} + (a_3 + b_3)\mathbf{k}, \quad (\text{a.9})$$

$$\alpha - \beta = (a_0 - b_0) + (a_1 - b_1)\mathbf{i} + (a_2 - b_2)\mathbf{j} + (a_3 - b_3)\mathbf{k}. \quad (\text{a.10})$$

**Definition A.33 (Quaternions multiplication).** The quaternion multiplication, designated by  $\odot$ , is defined so that the following fundamental special products are satisfied:

$$\begin{aligned} \mathbf{i}^2 = \mathbf{j}^2 = \mathbf{k}^2 = \mathbf{ijk} = -1, \\ \mathbf{ij} = -\mathbf{ji} = \mathbf{k}, \quad \mathbf{jk} = -\mathbf{kj} = \mathbf{i}, \quad \mathbf{ki} = -\mathbf{ik} = \mathbf{j}. \end{aligned}$$

which yields

$$\alpha \odot \beta = \begin{bmatrix} a_0 \\ \mathbf{a} \end{bmatrix} \odot \begin{bmatrix} b_0 \\ \mathbf{b} \end{bmatrix} = \begin{bmatrix} a_0 b_0 - \mathbf{a}^\top \mathbf{b} \\ a_0 \mathbf{b} + b_0 \mathbf{a} + \mathbf{S}(\mathbf{a})\mathbf{b} \end{bmatrix} = \begin{bmatrix} b_0 a_0 - \mathbf{b}^\top \mathbf{a} \\ b_0 \mathbf{a} + a_0 \mathbf{b} - \mathbf{S}(\mathbf{b})\mathbf{a} \end{bmatrix}. \quad (\text{a.11})$$

It is straightforward to verify that  $\alpha = [1, \mathbf{0}]^\top$  is the identity element for quaternion multiplication. The quaternion multiplication is associative and distributive, *i.e.*, for the three quaternions,  $\alpha, \beta, \gamma$ :

$$\begin{aligned} (\alpha \odot \beta) \odot \gamma &= \alpha \odot (\beta \odot \gamma), \\ \alpha \odot (\beta \pm \gamma) &= \alpha \odot \beta \pm \alpha \odot \gamma, \end{aligned}$$

but it is not commutative:  $\alpha \odot \beta \neq \beta \odot \alpha$ .

**Definition A.34 (Quaternion norm).** The norm of a quaternion  $\alpha$ , denoted by  $\mathcal{N}(\alpha)$ , is defined as

$$\mathcal{N}(\alpha) := \alpha^* \odot \alpha = \alpha \odot \alpha^* = a_0^2 + a_1^2 + a_2^2 + a_3^2 = |\alpha|_2^2. \quad (\text{a.12})$$

**Definition A.35 (Quaternion inverse).** For each nonzero quaternion  $\alpha$  there is an inverse  $\alpha^{-1}$  such that  $\alpha \odot \alpha^{-1} = \alpha^{-1} \odot \alpha = 1$ , and the inverse is given by

$$\alpha^{-1} = \frac{\alpha^*}{\mathcal{N}(\alpha)}. \quad (\text{a.13})$$

For a detailed list of properties and operations involving quaternions, refer to (Chou 1992; Kuipers 2002).

## A.2 Stability concepts

### A.2.1 Lyapunov theory

**Definition A.36 (Equilibrium Point).** Consider the non-autonomous system

$$\dot{\mathbf{x}} = \mathbf{f}(\mathbf{x}, t), \quad (\text{a.14})$$



where  $f : \mathbb{R}^n \times \mathbb{R}_{\geq 0} \rightarrow \mathbb{R}^n$ . If  $\mathbf{f}$  does not depend explicitly on time, *i.e.*,

$$\dot{\mathbf{x}} = \mathbf{f}(\mathbf{x}), \quad (\text{a.15})$$

the system (a.15) is called autonomous. The equilibrium points  $\mathbf{x}^*$ , for a non-autonomous and for an autonomous system, are defined by  $\mathbf{f}(\mathbf{x}^*, t) \equiv \mathbf{0} \ \forall t \geq t_0$  and  $\mathbf{f}(\mathbf{x}^*) \equiv \mathbf{0}$ , respectively.

**Definition A.37 (Stability).** Let the origin  $\mathbf{x} = \mathbf{0}$  be an equilibrium point for (a.14). This equilibrium point is stable if  $\forall \epsilon > 0, t_0 \geq 0 \exists \delta = \delta(\epsilon, t_0) > 0$  s.t.

$$|\mathbf{x}(t_0)| < \delta \Rightarrow |\mathbf{x}(t)| < \epsilon \quad \forall t \geq t_0 \geq 0.$$

Correspondingly,  $\mathbf{x} = \mathbf{0}$  is a stable equilibrium point for (a.15) if  $\forall \epsilon > 0, \exists \delta = \delta(\epsilon) > 0$  s.t.

$$|\mathbf{x}(0)| < \delta \Rightarrow |\mathbf{x}(t)| < \epsilon \quad \forall t \geq 0.$$

**Definition A.38 (Uniform Stability (US)).** The origin of (a.14) is uniformly stable if  $\forall \epsilon \exists \delta = \delta(\epsilon) > 0$  s.t.

$$|\mathbf{x}(t_0)| < \delta \Rightarrow |\mathbf{x}(t)| < \epsilon \quad \forall t \geq t_0 \geq 0.$$

For the autonomous system (a.15) US and stability of the equilibrium are equivalent.

**Definition A.39 (Asymptotic Stability (AS)).** An equilibrium point of (a.14),  $\mathbf{x} = \mathbf{0}$ , is AS if it is stable, and if in addition  $\forall t_0 \geq 0, \exists \delta' = \delta'(t_0) > 0$  s.t.

$$|\mathbf{x}(t_0)| < \delta' \Rightarrow |\mathbf{x}(t)| \rightarrow 0 \quad t \rightarrow \infty.$$

The same equilibrium point for (a.15) is AS if it is stable, and if  $\exists \delta'$  s.t.  $|\mathbf{x}(0)| < \delta' \Rightarrow |\mathbf{x}(t)| \rightarrow 0$  as  $t \rightarrow \infty$ .

**Definition A.40 (Uniform Asymptotic Stability (UAS)).** The origin is a UAS equilibrium of (a.14) if the origin is uniformly stable and if  $\exists \delta' > 0$  s.t.  $|\mathbf{x}(t_0)| < \delta' \Rightarrow |\mathbf{x}(t)| \rightarrow 0 \quad t \rightarrow \infty \quad \forall t_0$ . For (a.15) UAS and AS of the equilibrium are equivalent.

**Definition A.41 (Global Asymptotic Stability (GAS)).** The origin is a GAS equilibrium of (a.14) and (a.15) if the origin is stable and if

$$|\mathbf{x}(t)| \rightarrow 0 \quad t \rightarrow \infty, \quad \forall \mathbf{x}(t_0) \in \mathbb{R}^n, t_0 \geq 0.$$

**Definition A.42 (Global Uniform Asymptotic Stability (GUAS)).** The origin is a GUAS equilibrium of (a.14) if it is US and GAS with a convergence rate independent of  $t_0$ . For (a.15) GUAS and GAS are equivalent.

**Definition A.43 (Lyapunov Function Candidate).** A continuous and differentiable function  $V : \mathbb{R}^n \times \mathbb{R}_{\geq 0} \rightarrow \mathbb{R}_{\geq 0}$  is said to be a Lyapunov function candidate for the equilibrium  $\mathbf{x} = \mathbf{0}$  of (a.14) if:

1.  $V(\mathbf{x}, t)$  is positive definite;
2.  $\frac{\partial V(\mathbf{x}, t)}{\partial t}$  and  $\frac{\partial V(\mathbf{x}, t)}{\partial \mathbf{x}}$  are continuous on  $t$  and  $\mathbf{x}$ .

Let  $\mathbf{x} = \mathbf{0}$  be an equilibrium of (a.15). Then  $V : \mathbb{R}^n \rightarrow \mathbb{R}_{\geq 0}$  is a Lyapunov function candidate if  $V(\mathbf{x})$  is positive definite and  $\frac{dV(\mathbf{x})}{dx}$  is continuous.

**Definition A.44 (Lyapunov Function).** The Lyapunov function candidate  $V(\mathbf{x}, t)$  is a Lyapunov function for the system (a.14) if its total time derivative<sup>4</sup> along any state trajectory of (a.14) is negative semi-definite, *i.e.*,

$$\dot{V}(\mathbf{x}, t) \leq 0 \quad \forall t \geq 0.$$

The Lyapunov function candidate  $V(\mathbf{x})$  is a Lyapunov function for (a.15) if

$$\dot{V}(\mathbf{x}) = \left[ \frac{\partial V(\mathbf{x})}{\partial \mathbf{x}} \right]^T \frac{d\mathbf{x}}{dt} \leq 0 \quad \forall t \geq 0.$$

**THEOREM A.2 (Lyapunov Local Stability):**

*The origin is a stable equilibrium of (a.14) if there exists a Lyapunov function candidate  $V(\mathbf{x}, t)$  s.t.  $\dot{V}(\mathbf{x}, t)$  is locally negative semi-definite, and is locally AS if  $\dot{V}(\mathbf{x}, t)$  is locally negative definite. For autonomous systems, (a.15), the origin is a stable equilibrium if there exists a Lyapunov function candidate  $V(\mathbf{x})$  s.t.  $\dot{V}(\mathbf{x})$  is locally negative semi-definite, and is locally AS if  $\dot{V}(\mathbf{x})$  is locally negative definite.*  $\diamond$

**THEOREM A.3 (Lyapunov Global Asymptotic Stability):**

*The origin of (a.14) is GAS if there exists a radially unbounded Lyapunov function candidate  $V(\mathbf{x}, t)$  s.t.  $\dot{V}(\mathbf{x}, t)$  is negative definite. For the system (a.15) the origin is GAS if there exists a radially unbounded Lyapunov function candidate  $V(\mathbf{x})$  s.t.  $\dot{V}(\mathbf{x})$  is negative definite.*  $\diamond$

**THEOREM A.4 (Lyapunov First Instability Theorem):**

*The origin is an unstable equilibrium of (a.14) if there exists a continuously differentiable, decrescent scalar function  $V(\mathbf{x}, t)$  s.t. i)  $\dot{V}(\mathbf{0}, t) = 0 \quad \forall t \geq t_0$ ; ii)  $V(\mathbf{x}, t_0) > 0 \quad \forall \mathbf{x} \neq \mathbf{0}$  and; iii)  $\dot{V}(\mathbf{x}, t) > 0$ . For the system (a.15) the origin is an unstable equilibrium if: i)  $V(\mathbf{0}) = 0$ ; ii)  $V(\mathbf{x}_0) > 0$  for  $\mathbf{x}_0 \neq \mathbf{0}$  arbitrarily small and; iii)  $\dot{V}(\mathbf{x}) > 0$ .*  $\diamond$

**THEOREM A.5 (Lyapunov Second Instability Theorem):**

*The origin is an unstable equilibrium of (a.14) if there exists a continuously differentiable, decrescent scalar function  $V(\mathbf{x}, t)$ , s.t. i)  $\dot{V}(\mathbf{0}, t) = 0 \quad \forall t \geq t_0$ ; ii)  $V(\mathbf{x}, t_0) > 0 \quad \forall \mathbf{x} \neq \mathbf{0}$  and; iii)  $\dot{V}(\mathbf{x}, t) - \lambda V(\mathbf{x}, t) \geq 0 \quad \forall t \geq t_0, \lambda > 0, \mathbf{x} \neq \mathbf{0}$ . For the system (a.15) the origin is*

---

<sup>4</sup> $\dot{V}(\mathbf{x}, t) = \frac{\partial}{\partial t} V(\mathbf{x}, t) + \left[ \frac{\partial}{\partial \mathbf{x}} V(\mathbf{x}, t) \right]^T \frac{d\mathbf{x}}{dt}$

an unstable equilibrium if: i)  $V(\mathbf{0}) = 0$ ; ii)  $V(\mathbf{x}_0) > 0$  for  $\mathbf{x}_0 \neq \mathbf{0}$  arbitrarily small and; iii)  $\dot{V}(\mathbf{x}) - \lambda V(\mathbf{x}) > 0 \quad \forall \lambda > 0$ .  $\diamond$

**THEOREM A.6 (La Salle (LaSalle and Lefschetz 1961)):**

Consider the continuous autonomous system (a.15). Assume that there exists a radially unbounded Lyapunov function candidate  $V(\mathbf{x})$ , s.t.  $\dot{V}(\mathbf{x}) \leq 0 \quad \forall \mathbf{x} \in \mathbb{R}^n$ . Define the set  $\Omega = \{\mathbf{x} \in \mathbb{R}^n : V(\mathbf{x}) < l, l \in \mathbb{R}_{>0} < \infty\}$ . Let  $\mathbf{R} \subset \Omega$  s.t.  $\mathbf{R} = \{\mathbf{x} \in \mathbb{R}^n : \dot{V}(\mathbf{x}) = 0\}$ , and let  $\mathbf{M}$  be the largest invariant set in  $\mathbf{R}$ . Then, every solution  $\mathbf{x}(t)$  originating in  $\Omega$  tends to  $\mathbf{M}$  as  $t \rightarrow \infty$ .  $\diamond$

**LEMMA A.2 (Barbălat's Lemma (Khalil 1996)):**

If  $\lim_{t \rightarrow \infty} \int_0^t \mathbf{f}(\tau) d\tau$  exists and is finite, and  $\mathbf{f}(t)$  is a uniformly continuous function, then

$$\lim_{t \rightarrow \infty} \mathbf{f}(t) = \mathbf{0}.$$

$\diamond$

**LEMMA A.3 (Barbălat's Lemma (Teel 1999)):**

If  $\mathbf{f}, \dot{\mathbf{f}} \in \mathcal{L}_\infty$  and  $\mathbf{f} \in \mathcal{L}_p$  for some  $p \in [1, \infty)$ , then  $\mathbf{f}(t) \rightarrow \mathbf{0}$  as  $t \rightarrow \infty$ .  $\diamond$

**LEMMA A.4 (Barbălat's Lemma (Tao 1997)):**

If  $\mathbf{f} \in \mathcal{L}_2$  and  $\dot{\mathbf{f}} \in \mathcal{L}_\infty$ , then  $\mathbf{f}(t) \rightarrow \mathbf{0}$  as  $t \rightarrow \infty$ .  $\diamond$

## A.2.2 Input–output stability

**Definition A.45 ( $\mathcal{L}_q$ -Stability).** A mapping  $\mathbf{f} : \mathcal{L}_{q_e} \rightarrow \mathcal{L}_{q_e}$  with input  $\mathbf{u}$ , is  $\mathcal{L}_q$ -stable<sup>5</sup> if

$$\mathbf{u} \in \mathcal{L}_q \Rightarrow \mathbf{f}(\mathbf{u}) \in \mathcal{L}_q.$$

$\mathbf{f}$  is said to have finite  $\mathcal{L}_q$ -gain if  $\exists \gamma_q, \beta_q < \infty$  s.t.

$$\|\mathbf{f}(\mathbf{u})_T\|_{q_e} \leq \gamma_q \|\mathbf{u}_T\|_{q_e} + \beta_q \quad \forall \mathbf{u} \in \mathcal{L}_{q_e}, T \in [0, \infty). \quad (\text{a.16})$$

$\mathbf{f}$  is said to have finite  $\mathcal{L}_q$ -gain with zero bias if  $\beta_q = 0$ .

**Remark A.3.** Existence of finite  $\mathcal{L}_q$ -gain of  $\mathbf{f}$  implies that  $\mathbf{f}$  is  $\mathcal{L}_q$ -stable.

**Definition A.46.** Let  $\mathbf{f} : \mathcal{L}_{q_e} \rightarrow \mathcal{L}_{q_e}$  have finite  $\mathcal{L}_q$ -gain. Then the  $\mathcal{L}_q$ -gain of  $\mathbf{f}$  is defined as  $\gamma_q(\mathbf{f}) = \inf\{\gamma_q | \exists \beta_q\}$  such that (a.16) holds.

---

<sup>5</sup>Note that  $\mathcal{L}_q \subset \mathcal{L}_{q_e}$ .

**THEOREM A.7 ( $\mathcal{L}_2$ -stable System):**

Consider the time-invariant nonlinear system

$$\begin{aligned}\dot{\mathbf{x}} &= \mathbf{f}(\mathbf{x}) + \mathbf{g}(\mathbf{x})\mathbf{u}, & \mathbf{x}(0) &= \mathbf{x}_0 \\ \mathbf{y} &= \mathbf{h}(\mathbf{x})\end{aligned}\tag{a.17}$$

where  $\mathbf{f}(\mathbf{x})$  is locally Lipschitz, and  $\mathbf{g}(\mathbf{x}), \mathbf{h}(\mathbf{x})$  are continuous over  $\mathbb{R}^n$ . The matrix  $\mathbf{g}$  is  $n \times m$  and  $\mathbf{h} : \mathbb{R}^n \rightarrow \mathbb{R}^q$ .  $\mathbf{f}(\mathbf{0}) = \mathbf{0}$  and  $\mathbf{h}(\mathbf{0}) = \mathbf{0}$ . Let  $\gamma$  be a positive number and suppose there is a continuously differentiable positive semidefinite function  $V(\mathbf{x})$  that satisfies the inequality

$$\frac{\partial V}{\partial \mathbf{x}} \mathbf{f}(\mathbf{x}) + \frac{1}{2\gamma^2} \frac{\partial V}{\partial \mathbf{x}} \mathbf{g}(\mathbf{x}) \mathbf{g}^\top(\mathbf{x}) \left( \frac{\partial V}{\partial \mathbf{x}} \right)^\top + \frac{1}{2} \mathbf{h}^\top(\mathbf{x}) \mathbf{h}(\mathbf{x}) \leq 0 \quad \forall \mathbf{x} \in \mathbb{R}^n,$$

Then, for each  $\mathbf{x}_0 \in \mathbb{R}^n$ , the system (a.17) is  $\mathcal{L}_2$ -stable and has finite  $\mathcal{L}_2$ -gain less than or equal to  $\gamma$ .

◇

**A.2.3 Passivity**

**Definition A.47 (Passive System).** The system  $\mathbf{y} = \mathbf{f}(\mathbf{u}, t)$  is

- passive, if  $\int_0^t \mathbf{u}^\top(\tau) \mathbf{y}(\tau) d\tau \geq -\beta \quad \forall \beta \in \mathbb{R}_{>0}$ ;
- lossless, if  $\int_0^t \mathbf{u}^\top(\tau) \mathbf{y}(\tau) d\tau = 0$ ;
- input strictly passive, if  $\exists \beta, \gamma > 0$  s.t.  $\int_0^t \mathbf{u}^\top(\tau) \mathbf{y}(\tau) d\tau \geq \gamma \|\mathbf{u}\|_2^2 - \beta \quad \forall \mathbf{u} \in \mathcal{L}_2$ ;
- output strictly passive if  $\exists \beta, \epsilon > 0$  s.t.  $\int_0^t \mathbf{u}^\top(\tau) \mathbf{y}(\tau) d\tau \geq \epsilon \|\mathbf{y}\|_2^2 - \beta \quad \forall \mathbf{u} \in \mathcal{L}_2$ .

**Definition A.48 (State Space Passivity).** Consider the system given by

$$\begin{aligned}\dot{\mathbf{x}} &= \mathbf{f}(\mathbf{x}, \mathbf{u}) \\ \mathbf{y} &= \mathbf{h}(\mathbf{x}, \mathbf{u})\end{aligned}\tag{a.18}$$

where  $\mathbf{f} : \mathbb{R}^n \times \mathbb{R}^p \rightarrow \mathbb{R}^n$  is locally Lipschitz,  $\mathbf{h} : \mathbb{R}^n \times \mathbb{R}^p \rightarrow \mathbb{R}^p$  is continuous,  $\mathbf{f}(\mathbf{0}, \mathbf{0}) = \mathbf{0}$  and  $\mathbf{h}(\mathbf{0}, \mathbf{0}) = \mathbf{0}$ . This system is said to be passive if there exists a continuously differentiable positive semidefinite function  $V(\mathbf{x})$  (called the storage function) s.t.

$$\mathbf{u}^T \mathbf{y} \geq \dot{V} = \frac{\partial V}{\partial \mathbf{x}} \mathbf{f}(\mathbf{x}, \mathbf{u}) \quad \forall (\mathbf{x}, \mathbf{u}) \in \mathbb{R}^n \times \mathbb{R}^p.$$

Moreover, it is said to be

- lossless, if  $\mathbf{u}^T \mathbf{y} = \dot{V}$ ;

- input-feedforward passive, if  $\mathbf{u}^\top \mathbf{y} \geq \dot{V} + \mathbf{u}^\top \boldsymbol{\varphi}(\mathbf{u})$  for  $\boldsymbol{\varphi} : \mathbb{R}^p \rightarrow \mathbb{R}$ ;
- input strictly passive, if  $\mathbf{u}^\top \mathbf{y} \geq \dot{V} + \epsilon |\mathbf{u}|^2, \forall \epsilon > 0$ ;
- output-feedback passive, if  $\mathbf{u}^\top \mathbf{y} \geq \dot{V} + \mathbf{y}^\top \boldsymbol{\rho}(\mathbf{u})$  for  $\boldsymbol{\rho} : \mathbb{R}^p \rightarrow \mathbb{R}$ ;
- output strictly passive, if  $\mathbf{u}^\top \mathbf{y} \geq \dot{V} + \delta |\mathbf{y}|^2, \forall \delta > 0$ ;
- strictly passive, if  $\mathbf{u}^\top \mathbf{y} \geq \dot{V} + \boldsymbol{\psi}(\mathbf{x})$  for  $\boldsymbol{\psi} : \mathbb{R}^n \rightarrow \mathbb{R}_{>0}$ .

In all cases, the inequality must hold for all input-output pair  $\{\mathbf{u}, \mathbf{y}\}$ .



VALIDATION TOOLS

*The kinematic and the dynamic models of the robot manipulators used in the validation experiments are presented in the first section of this appendix. In the second one, the PhanTorque libraries developed for the communication between Simulink<sup>®</sup> and the Geomagic<sup>®</sup> devices are detailed.*

### B.1 Robot kinematics and dynamics

In this section the kinematic and the dynamic models of the robot manipulators shown in Table 4.1 are detailed.

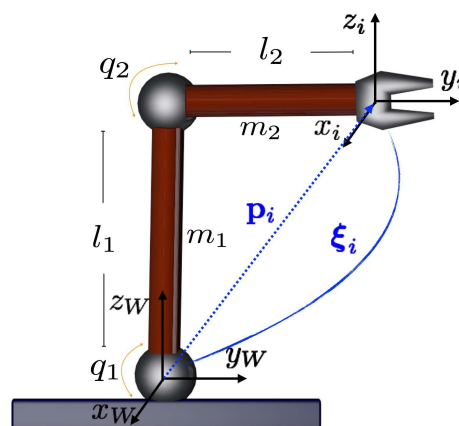


Figure B.1: 2-DoF planar manipulator.

### B.1.1 2-DoF robot

The direct kinematics of the 2-DoF planar robot shown in Figure B.1 is given by

$$\mathbf{T}(\mathbf{q}) = \begin{bmatrix} 0 & -1 & 0 & 0 \\ \sin(q_1 + q_2) & 0 & \cos(q_1 + q_2) & l_1 \cos(q_1) + l_2 \cos(q_1 + q_2) \\ -\cos(q_1 + q_2) & 0 & \sin(q_1 + q_2) & l_1 \sin(q_1) + l_2 \sin(q_1 + q_2) \\ 0 & 0 & 0 & 1 \end{bmatrix}.$$

The Jacobian is  $\mathbf{J}(\mathbf{q}) = [J_{ij}] \in \mathbb{R}^{2 \times 2}$ , where

$$J_{11} = -l_2 \sin(q_1 + q_2) - l_1 \sin(q_1);$$

$$J_{12} = -l_2 \sin(q_1 + q_2);$$

$$J_{21} = l_2 \cos(q_1 + q_2) + l_1 \cos(q_1);$$

$$J_{22} = l_2 \cos(q_1 + q_2).$$

The joint space dynamic model follows (3.45) with  $n = 2$ , The inertia matrix is  $\bar{\mathbf{M}}(\mathbf{q}) = [\bar{M}_{ij}]$ , where

$$\bar{M}_{11} = p_1 + 2p_2 \cos(q_2);$$

$$\bar{M}_{12} = p_3 + p_2 \cos(q_2);$$

$$\bar{M}_{21} = \bar{M}_{12};$$

$$\bar{M}_{22} = p_3.$$

Similarly, the Coriolis and centrifugal matrix is  $\bar{\mathbf{C}}(\mathbf{q}, \dot{\mathbf{q}}) = [\bar{C}_{ij}]$ , where

$$\bar{C}_{11} = -p_2 \sin(q_2) \dot{q}_2;$$

$$\bar{C}_{12} = -p_2 \sin(q_2) (\dot{q}_1 + \dot{q}_2);$$

$$\bar{C}_{21} = p_2 \sin(q_2) \dot{q}_1;$$

$$\bar{C}_{22} = 0.$$

The gravity vector is  $\bar{\mathbf{g}}(\mathbf{q}) = [\bar{g}_i]$ , where

$$\bar{g}_1 = g \frac{1}{l_2} p_3 \cos(q_1 + q_2) + g \frac{1}{l_1} (p_1 - p_3) \cos(q_1)$$

$$\bar{g}_2 = g \frac{1}{l_2} p_3 \cos(q_1 + q_2);$$

The parameters ( $p_j, j = 1 \dots 3$ ), that are used in the previous definitions are given by

$$p_1 = m_2 l_2^2 + (m_1 + m_2) l_1^2$$

$$p_2 = m_2 l_1 l_2;$$

$$p_3 = m_2 l_2^2.$$

The meaning of each physical parameter is depicted in Table B.1.



Parameters	Meaning
$m_i$	link mass
$I_{n_i}$	link inertia
$l_i$	link length
$l_{c,i}$	center of mass
$g$	gravity constant

Table B.1: Robots' parameters description.

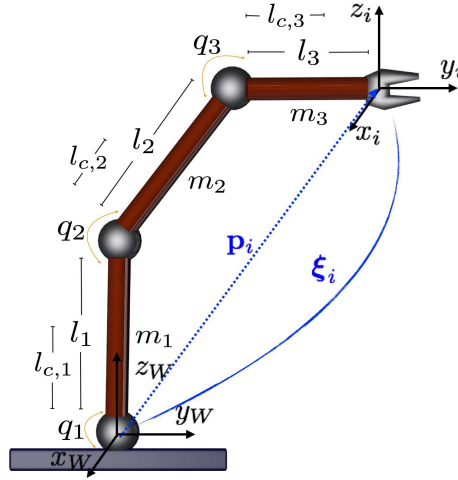


Figure B.2: 3-DoF planar manipulator.

### B.1.2 3-DoF robot

The direct kinematics of the 3-DoF planar robot shown in Figure B.1 is given by

$$\mathbf{T}(\mathbf{q}) = \begin{bmatrix} 0 & -1 & 0 & 0 \\ \sin(q_1+q_2+q_3) & 0 & \cos(q_1+q_2+q_3) & l_1 \cos(q_1)+l_2 \cos(q_1+q_2)+l_3 \cos(q_1+q_2+q_3) \\ -\cos(q_1+q_2+q_3) & 0 & \sin(q_1+q_2+q_3) & l_1 \sin(q_1)+l_2 \sin(q_1+q_2)+l_3 \sin(q_1+q_2+q_3) \\ 0 & 0 & 0 & 1 \end{bmatrix}.$$

The Jacobian is  $\mathbf{J}(\mathbf{q}) = [J_{ij}] \in \mathbb{R}^{3 \times 3}$ , where

$$\begin{aligned} J_{11} &= -l_1 \sin(q_1) - l_2 \sin(q_1 + q_2) - l_3 \sin(q_1 + q_2 + q_3); \\ J_{12} &= -l_2 \sin(q_1 + q_2) - l_3 \sin(q_1 + q_2 + q_3); \\ J_{13} &= -l_3 \sin(q_1 + q_2 + q_3); \\ J_{21} &= l_1 \cos(q_1) + l_2 \cos(q_1 + q_2) + l_3 \cos(q_1 + q_2 + q_3); \\ J_{22} &= l_2 \cos(q_1 + q_2) + l_3 \cos(q_1 + q_2 + q_3); \\ J_{23} &= l_3 \cos(q_1 + q_2 + q_3); \\ J_{31} &= 1; \\ J_{32} &= 1; \\ J_{33} &= 1. \end{aligned}$$

The joint space dynamic model follows (3.45) with  $n = 3$ . The inertia matrix is  $\bar{M}(\mathbf{q}) = [\bar{M}_{ij}]$ , where

$$\begin{aligned}
\bar{M}_{11} &= p_1 + 2p_2 \cos(q_2) + 2p_3 \cos(q_3) + 2p_4 \cos(q_2 + q_3); \\
\bar{M}_{12} &= p_5 + p_2 \cos(q_2) + 2p_3 \cos(q_3) + p_4 \cos(q_2 + q_3); \\
\bar{M}_{13} &= p_6 + p_3 \cos(q_3) + p_4 \cos(q_2 + q_3); \\
\bar{M}_{21} &= \bar{M}_{12}; \\
\bar{M}_{22} &= p_5 + 2p_3 \cos(q_3); \\
\bar{M}_{23} &= p_6 + p_3 \cos(q_3); \\
\bar{M}_{31} &= \bar{M}_{13}; \\
\bar{M}_{32} &= \bar{M}_{23}; \\
\bar{M}_{33} &= p_6.
\end{aligned}$$

Similarly, the Coriolis and centrifugal matrix is  $\bar{C}(\mathbf{q}, \dot{\mathbf{q}}) = [\bar{C}_{ij}]$ , where

$$\begin{aligned}
\bar{C}_{11} &= -p_2 \sin(q_2) \dot{q}_2 - p_3 \sin(q_3) \dot{q}_3 - p_4 \sin(q_2 + q_3) (\dot{q}_2 + \dot{q}_3); \\
\bar{C}_{12} &= -p_2 \sin(q_2) (\dot{q}_1 + \dot{q}_2) - p_3 \sin(q_3) \dot{q}_3 - p_4 \sin(q_2 + q_3) (\dot{q}_1 + \dot{q}_2 + \dot{q}_3); \\
\bar{C}_{13} &= -p_3 \sin(q_3) (\dot{q}_1 + \dot{q}_2 + \dot{q}_3) - p_4 \sin(q_2 + q_3) (\dot{q}_1 + \dot{q}_2 + \dot{q}_3); \\
\bar{C}_{21} &= p_2 \sin(q_2) \dot{q}_1 - p_3 \sin(q_3) \dot{q}_3 + p_4 \sin(q_2 + q_3) (\dot{q}_1); \\
\bar{C}_{22} &= -p_3 \sin(q_3) \dot{q}_3; \\
\bar{C}_{23} &= -p_3 \sin(q_3) (\dot{q}_1 + \dot{q}_2 + \dot{q}_3); \\
\bar{C}_{31} &= p_3 \sin(q_3) (\dot{q}_1 + \dot{q}_2) + p_4 \sin(q_2 + q_3) \dot{q}_1; \\
\bar{C}_{32} &= p_3 \sin(q_3) (\dot{q}_1 + \dot{q}_2); \\
\bar{C}_{33} &= 0.
\end{aligned}$$

The gravity vector is  $\bar{g}(\mathbf{q}) = [\bar{g}_i]$ , where

$$\begin{aligned}
\bar{g}_1 &= p_7 \cos(q_1) + p_8 \cos(q_1 + q_2) + p_9 \cos(q_1 + q_2 + q_3); \\
\bar{g}_2 &= p_8 \cos(q_1 + q_2) + p_9 \cos(q_1 + q_2 + q_3); \\
\bar{g}_3 &= p_9 \cos(q_1 + q_2 + q_3).
\end{aligned}$$

The parameters ( $p_j, j = 1 \dots 9$ ) (Ahmad and Zribi 1993), that are used in the previous definitions are given by

$$\begin{aligned}
p_1 &= m_1 l_{c,1}^2 + I n_1 + m_2 l_1^2 + m_2 l_{c,2}^2 + I n_2 + m_3 l_1^2 + m_3 l_2^2 + m_3 l_{c,3}^2 + I n_3; \\
p_2 &= m_2 l_1 l_{c,2} + m_3 l_1 l_2 \\
p_3 &= m_3 l_2 l_{c,3}; \\
p_4 &= m_3 l_1 l_{c,3};
\end{aligned}$$

$$\begin{aligned}
p_5 &= m_2 l_{c,2}^2 + I n_2 + m_3 l_2^2 + m_3 l_{c,3}^2 + I n_3; \\
p_6 &= m_3 l_{c,3}^2 + I n_3; \\
p_7 &= m_2 g l_{c,2} + m_3 g l_2; \\
p_8 &= m_2 g l_{c,2} + m_3 g l_2; \\
p_9 &= m_3 g l_{c,3}.
\end{aligned}$$

The meaning of each physical parameter is depicted in Table B.1.

### Operational space dynamics and regressor matrix

As detailed in Chapter 3, the nonlinear operational space dynamics of the 3-DoF robot can be derived from the joint space dynamic model described previously and from relation (3.47). Using Property P13, the operational space model can be expressed as

$$\mathbf{M}(\mathbf{q})\dot{\mathbf{v}} + \mathbf{C}(\mathbf{q}, \dot{\mathbf{q}})\mathbf{v} + \mathbf{g}(\mathbf{q}) = \mathbf{Y}(\dot{\mathbf{q}}, \mathbf{q}, \dot{\mathbf{v}}, \mathbf{v})\Theta.$$

In this case, there exist 25 different parameters and hence  $\mathbf{Y}(\dot{\mathbf{q}}, \mathbf{q}, \dot{\mathbf{v}}, \mathbf{v}) \in \mathbb{R}^{3 \times 25}$  and  $\Theta \in \mathbb{R}^{25}$ . These parameters are shown in Table B.2.

$\Theta_1 = p_7/l_1$	$\Theta_{10} = p_5/l_1^2$	$\Theta_{19} = p_9$
$\Theta_2 = p_8/l_2$	$\Theta_{11} = (l_3 p_1)/l_1^2$	$\Theta_{20} = (l_3^2 p_5)/l_1^2$
$\Theta_3 = p_2/(l_1 l_2)$	$\Theta_{12} = (l_3 p_5)/l_2^2$	$\Theta_{21} = (l_3^2 p_2)/(l_1 l_2)$
$\Theta_4 = p_3/l_2$	$\Theta_{13} = (l_3 p_6)/l_2^2$	$\Theta_{22} = (l_3 p_3)/l_2$
$\Theta_5 = p_4/l_1$	$\Theta_{14} = (l_3 p_5)/l_1^2$	$\Theta_{23} = (l_3 p_4)/l_1$
$\Theta_6 = (l_3 p_2)/(l_1 l_2)$	$\Theta_{15} = (l_3^2 p_6)/l_2^2$	$\Theta_{24} = (l_3 p_8)/l_2$
$\Theta_7 = p_6/l_2^2$	$\Theta_{16} = (l_3^2 p_1)/l_1^2$	$\Theta_{25} = l_3 p_7/l_1$
$\Theta_8 = p_5/l_2^2$	$\Theta_{17} = p_6$	
$\Theta_9 = p_1/l_1^2$	$\Theta_{18} = (l_3^2 p_5)/l_2^2$	

Table B.2: Elements of the parameters vector  $\Theta$ .

The components of the regressor matrix,  $\mathbf{Y}(\dot{\mathbf{q}}, \mathbf{q}, \dot{\mathbf{v}}, \mathbf{v}) \in \mathbb{R}^{3 \times 25}$ , are

$$\begin{aligned}
Y_{1,1} &= (g(\cos(2q_1 + q_2) + \cos(q_2)))/(2 \sin(q_2)); \\
Y_{1,2} &= -(g(\cos(2q_1 + q_2) + \cos(q_2)))/(2 \sin(q_2)); \\
Y_{1,3} &= (\dot{v}_1 \cos(q_2)^2 + v_2 \dot{q}_1 + (v_2 \dot{q}_2)/2)/(\cos(q_2)^2 - 1) - ((\dot{v}_2 \cos(2q_1 + 3q_2))/4 \\
&\quad - (\dot{v}_2 \cos(2q_1 - q_2))/4 + (\dot{v}_1 \sin(2q_1 - q_2))/4 - (\dot{v}_1 \sin(2q_1 + 3q_2))/4 \\
&\quad + (3v_1 \dot{q}_2 \cos(2q_1 + q_2))/4 + (3v_2 \dot{q}_2 \sin(2q_1 + q_2))/4 \\
&\quad + (v_1 \dot{q}_1 \cos(2q_1 - q_2))/4 - (v_1 \dot{q}_1 \cos(2q_1 + 3q_2))/4 \\
&\quad + (v_1 \dot{q}_2 \cos(2q_1 - q_2))/4 + (v_2 \dot{q}_1 \sin(2q_1 - q_2))/4 \\
&\quad - (v_2 \dot{q}_1 \sin(2q_1 + 3q_2))/4 + (v_2 \dot{q}_2 \sin(2q_1 - q_2))/4 \\
&\quad + v_1 \dot{q}_2 \cos(q_2))/(\sin(q_2)(\cos(q_2)^2 - 1));
\end{aligned}$$

$$\begin{aligned}
Y_{1,4} &= (\cos(q_1)(v_3\dot{q}_1 \sin(q_3) - \dot{v}_3 \cos(q_3) + v_3\dot{q}_2 \sin(q_3) + v_3\dot{q}_3 \sin(q_3)))/\sin(q_2); \\
Y_{1,5} &= -(\cos(q_1 + q_2)(v_3\dot{q}_1 \sin(q_2 + q_3) - \dot{v}_3 \cos(q_2 + q_3) + v_3\dot{q}_2 \sin(q_2 + q_3) \\
&\quad + v_3\dot{q}_3 \sin(q_2 + q_3)))/\sin(q_2); \\
Y_{1,6} &= (\dot{v}_3 \cos(q_1) \cos(q_2) \sin(q_3) + \dot{v}_3 \cos(q_1 + q_2) \sin(q_2 + q_3) \cos(q_2) \\
&\quad + v_3\dot{q}_2 \cos(q_1 + q_2) \cos(q_2 + q_3) \cos(q_2) + v_3\dot{q}_3 \cos(q_1 + q_2) \cos(q_2 + q_3) \cos(q_2) \\
&\quad + v_3\dot{q}_3 \cos(q_1) \cos(q_2) \cos(q_3))/(\cos(q_2)^2 - 1) \\
&\quad - ((v_3\dot{q}_2 \sin(2q_2 + q_3) \cos(q_1))/4 - (v_3\dot{q}_2 \sin(2q_2 - q_3) \cos(q_1))/4 \\
&\quad + v_3\dot{q}_1 \cos(q_1 + q_2) \sin(q_2 + q_3) + (3v_3\dot{q}_2 \cos(q_1 + q_2) \sin(q_2 + q_3))/2 \\
&\quad - v_3\dot{q}_1 \cos(q_1) \sin(q_3) + (v_3\dot{q}_2 \cos(q_1) \sin(q_3))/2 \\
&\quad - (v_3\dot{q}_2 \sin(q_2 - q_3) \cos(q_1 + q_2))/4 + (v_3\dot{q}_2 \sin(3q_2 + q_3) \cos(q_1 + q_2))/4 \\
&\quad + v_3\dot{q}_1 \cos(q_1) \cos(q_2)^2 \sin(q_3) - v_3\dot{q}_1 \cos(q_1 + q_2) \sin(q_2 + q_3) \cos(q_2)^2 \\
&\quad - v_3\dot{q}_2 \cos(q_1 + q_2) \sin(q_2 + q_3) \cos(q_2)^2)/(\sin(q_2)(\cos(q_2)^2 - 1)); \\
Y_{1,7} &= (\cos(q_1)(v_1\dot{q}_2 \cos(q_1) \cos(q_2) + v_2\dot{q}_2 \cos(q_2) \sin(q_1)))/\sin(q_2)^3 \\
&\quad - (\cos(q_1)(\dot{v}_1 \cos(q_1) + \dot{v}_2 \sin(q_1) - v_1\dot{q}_1 \sin(q_1) + v_2\dot{q}_1 \cos(q_1)))/\sin(q_2)^2; \\
Y_{1,8} &= (\cos(q_1)(\dot{v}_1 \cos(q_1) + \dot{v}_2 \sin(q_1) - v_1\dot{q}_1 \sin(q_1) + v_2\dot{q}_1 \cos(q_1)))/\sin(q_2)^2 \\
&\quad - (\cos(q_1)(v_1\dot{q}_2 \cos(q_1) \cos(q_2) + v_2\dot{q}_2 \cos(q_2) \sin(q_1)))/\sin(q_2)^3; \\
Y_{1,9} &= (2\dot{v}_1 + 2\dot{v}_1 \cos(2q_1 + 2q_2) + 2v_2\dot{q}_1 + 2v_2\dot{q}_2 \\
&\quad + 2\dot{v}_2 \sin(2q_1 + 2q_2))/(4\sin(q_2)^2) + (v_1\dot{q}_1 \cos(2q_1 + q_2) \\
&\quad + 2v_1\dot{q}_2 \cos(2q_1 + q_2) + v_2\dot{q}_1 \sin(2q_1 + q_2) + 2v_2\dot{q}_2 \sin(2q_1 + q_2) \\
&\quad - v_1\dot{q}_1 \cos(2q_1 + 3q_2) - v_2\dot{q}_1 \sin(2q_1 + 3q_2) \\
&\quad + 2v_1\dot{q}_2 \cos(q_2))/(\sin(3q_2) - 3\sin(q_2)); \\
Y_{1,10} &= -(2\dot{v}_1 + 2\dot{v}_1 \cos(2q_1 + 2q_2) + 2v_2\dot{q}_1 + 2v_2\dot{q}_2 \\
&\quad + 2\dot{v}_2 \sin(2q_1 + 2q_2))/(4\sin(q_2)^2) - (v_1\dot{q}_1 \cos(2q_1 + q_2) \\
&\quad + 2v_1\dot{q}_2 \cos(2q_1 + q_2) + v_2\dot{q}_1 \sin(2q_1 + q_2) \\
&\quad + 2v_2\dot{q}_2 \sin(2q_1 + q_2) - v_1\dot{q}_1 \cos(2q_1 + 3q_2) \\
&\quad - v_2\dot{q}_1 \sin(2q_1 + 3q_2) + 2v_1\dot{q}_2 \cos(q_2))/(\sin(3q_2) - 3\sin(q_2)); \\
Y_{1,11} &= (\cos(q_1 + q_2) \sin(q_2)(\dot{v}_3 \sin(q_3) + v_3\dot{q}_3 \cos(q_3)) \\
&\quad - v_3\dot{q}_2 \cos(q_1 + q_2) \cos(q_2) \sin(q_3))/\sin(q_2)^3; \\
Y_{1,12} &= (\cos(q_1)(\dot{v}_3 \sin(q_2 + q_3) + v_3\dot{q}_2 \cos(q_2 + q_3) + v_3\dot{q}_3 \cos(q_2 + q_3)))/\sin(q_2)^2 \\
&\quad - (v_3\dot{q}_2 \sin(q_2 + q_3) \cos(q_1) \cos(q_2))/\sin(q_2)^3; \\
Y_{1,13} &= (v_3\dot{q}_2 \sin(q_2 + q_3) \cos(q_1) \cos(q_2))/\sin(q_2)^3 - (\cos(q_1)(\dot{v}_3 \sin(q_2 + q_3) \\
&\quad + v_3\dot{q}_2 \cos(q_2 + q_3) + v_3\dot{q}_3 \cos(q_2 + q_3)))/\sin(q_2)^2; \\
Y_{1,14} &= -(\cos(q_1 + q_2) \sin(q_2)(\dot{v}_3 \sin(q_3) + v_3\dot{q}_3 \cos(q_3)) \\
&\quad - v_3\dot{q}_2 \cos(q_1 + q_2) \cos(q_2) \sin(q_3))/\sin(q_2)^3; \\
Y_{1,15} &= Y_{1,16} = Y_{1,17} = Y_{1,18} = Y_{1,19} = 0; \\
Y_{1,20} &= Y_{1,21} = Y_{1,22} = Y_{1,23} = Y_{1,24} = 0; \\
Y_{1,25} &= 0; \\
Y_{2,1} &= g/2 + (g \sin(2q_1 + q_2))/(2 \sin(q_2)); \\
Y_{2,2} &= g/2 - (g \sin(2q_1 + q_2))/(2 \sin(q_2));
\end{aligned}$$

$$\begin{aligned}
Y_{2,3} &= -(-\dot{v}_2 \cos(q_2)^2 + v_1 \dot{q}_1 + (v_1 \dot{q}_2)/2)/(\cos(q_2)^2 - 1) - ((\dot{v}_1 \cos(2q_1 + 3q_2))/4 \\
&\quad - (\dot{v}_1 \cos(2q_1 - q_2))/4 - (\dot{v}_2 \sin(2q_1 - q_2))/4 + (\dot{v}_2 \sin(2q_1 + 3q_2))/4 \\
&\quad - (3v_2 \dot{q}_2 \cos(2q_1 + q_2))/4 + (3v_1 \dot{q}_2 \sin(2q_1 + q_2))/4 \\
&\quad - (v_2 \dot{q}_1 \cos(2q_1 - q_2))/4 + (v_2 \dot{q}_1 \cos(2q_1 + 3q_2))/4 \\
&\quad - (v_2 \dot{q}_2 \cos(2q_1 - q_2))/4 + (v_1 \dot{q}_1 \sin(2q_1 - q_2))/4 \\
&\quad - (v_1 \dot{q}_1 \sin(2q_1 + 3q_2))/4 + (v_1 \dot{q}_2 \sin(2q_1 - q_2))/4 \\
&\quad + v_2 \dot{q}_2 \cos(q_2))/(\sin(q_2)(\cos(q_2)^2 - 1)); \\
Y_{2,4} &= (\sin(q_1)(v_3 \dot{q}_1 \sin(q_3) - \dot{v}_3 \cos(q_3) + v_3 \dot{q}_2 \sin(q_3) + v_3 \dot{q}_3 \sin(q_3)))/\sin(q_2); \\
Y_{2,5} &= -(\sin(q_1 + q_2)(v_3 \dot{q}_1 \sin(q_2 + q_3) - \dot{v}_3 \cos(q_2 + q_3) + v_3 \dot{q}_2 \sin(q_2 + q_3) \\
&\quad + v_3 \dot{q}_3 \sin(q_2 + q_3)))/\sin(q_2); \\
Y_{2,6} &= -(v_3 \dot{q}_1 \sin(q_1) \sin(q_3) - v_3 \dot{q}_1 \sin(q_1 + q_2) \sin(q_2 + q_3) \\
&\quad + v_3 \dot{q}_2 \sin(q_1) \sin(q_3))/\sin(q_2) - (v_3 \dot{q}_2 \sin(q_1 + q_2) \sin(q_2 + q_3) \\
&\quad - \cos(q_2)(\dot{v}_3 \sin(q_1 + q_2) \sin(q_2 + q_3) \sin(q_2) + \dot{v}_3 \sin(q_1) \sin(q_2) \sin(q_3) \\
&\quad + v_3 \dot{q}_2 \cos(q_2 + q_3) \sin(q_1 + q_2) \sin(q_2) \\
&\quad + v_3 \dot{q}_3 \cos(q_2 + q_3) \sin(q_1 + q_2) \sin(q_2) + v_3 \dot{q}_3 \cos(q_3) \sin(q_1) \sin(q_2)) \\
&\quad + v_3 \dot{q}_2 \sin(q_1) \sin(q_3))/(\sin(q_2)(\cos(q_2)^2 - 1)); \\
Y_{2,7} &= (-v_2 \dot{q}_2 \cos(q_2) \cos(q_1)^2 + v_1 \dot{q}_2 \cos(q_2) \sin(q_1) \cos(q_1) \\
&\quad + v_2 \dot{q}_2 \cos(q_2))/(\sin(q_2) - \cos(q_2)^2 \sin(q_2)) \\
&\quad + (\dot{v}_2 - v_1 \dot{q}_1 - \dot{v}_2 \cos(q_1)^2 + v_1 \dot{q}_1 \cos(q_1)^2 + \dot{v}_1 \cos(q_1) \sin(q_1) \\
&\quad + v_2 \dot{q}_1 \cos(q_1) \sin(q_1))/(\cos(q_2)^2 - 1); \\
Y_{2,8} &= -(-v_2 \dot{q}_2 \cos(q_2) \cos(q_1)^2 + v_1 \dot{q}_2 \cos(q_2) \sin(q_1) \cos(q_1) \\
&\quad + v_2 \dot{q}_2 \cos(q_2))/(\sin(q_2) - \cos(q_2)^2 \sin(q_2)) - (\dot{v}_2 - v_1 \dot{q}_1 - \dot{v}_2 \cos(q_1)^2 \\
&\quad + v_1 \dot{q}_1 \cos(q_1)^2 + \dot{v}_1 \cos(q_1) \sin(q_1) + v_2 \dot{q}_1 \cos(q_1) \sin(q_1))/(\cos(q_2)^2 - 1); \\
Y_{2,9} &= (v_1 \dot{q}_1 \sin(2q_1 + q_2) - 2v_2 \dot{q}_2 \cos(2q_1 + q_2) - v_2 \dot{q}_1 \cos(2q_1 + q_2) \\
&\quad + 2v_1 \dot{q}_2 \sin(2q_1 + q_2) + v_2 \dot{q}_1 \cos(2q_1 + 3q_2) - v_1 \dot{q}_1 \sin(2q_1 + 3q_2) \\
&\quad + 2v_2 \dot{q}_2 \cos(q_2))/(\sin(3q_2) - 3 \sin(q_2)) - (2\dot{v}_2 \cos(2q_1 + 2q_2) \\
&\quad - 2\dot{v}_2 + 2v_1 \dot{q}_1 + 2v_1 \dot{q}_2 - 2\dot{v}_1 \sin(2q_1 + 2q_2))/(4 \sin(q_2)^2); \\
Y_{2,10} &= (2\dot{v}_2 \cos(2q_1 + 2q_2) - 2\dot{v}_2 + 2v_1 \dot{q}_1 + 2v_1 \dot{q}_2 \\
&\quad - 2\dot{v}_1 \sin(2q_1 + 2q_2))/(4 \sin(q_2)^2) - (v_1 \dot{q}_1 \sin(2q_1 + q_2) \\
&\quad - 2v_2 \dot{q}_2 \cos(2q_1 + q_2) - v_2 \dot{q}_1 \cos(2q_1 + q_2) \\
&\quad + 2v_1 \dot{q}_2 \sin(2q_1 + q_2) + v_2 \dot{q}_1 \cos(2q_1 + 3q_2) \\
&\quad - v_1 \dot{q}_1 \sin(2q_1 + 3q_2) + 2v_2 \dot{q}_2 \cos(q_2))/(\sin(3q_2) - 3 \sin(q_2)); \\
Y_{2,11} &= (\sin(q_1 + q_2) \sin(q_2)(\dot{v}_3 \sin(q_3) - v_3 \dot{q}_3(2 \sin(q_3/2)^2 - 1)) \\
&\quad + v_3 \dot{q}_2 \sin(q_1 + q_2) \sin(q_3)(2 \sin(q_2/2)^2 - 1))/\sin(q_2)^3; \\
Y_{2,12} &= -(\sin(q_1)((\dot{v}_3 \cos(2q_2 + q_3))/2 - (\dot{v}_3 \cos(q_3))/2 + v_3 \dot{q}_2 \sin(q_3) \\
&\quad + (v_3 \dot{q}_3 \sin(q_3))/2 - (v_3 \dot{q}_3 \sin(2q_2 + q_3))/2))/\sin(q_2)^3; \\
Y_{2,13} &= (\sin(q_1)((\dot{v}_3 \cos(2q_2 + q_3))/2 - (\dot{v}_3 \cos(q_3))/2 + v_3 \dot{q}_2 \sin(q_3) \\
&\quad + (v_3 \dot{q}_3 \sin(q_3))/2 - (v_3 \dot{q}_3 \sin(2q_2 + q_3))/2))/\sin(q_2)^3;
\end{aligned}$$

$$\begin{aligned}
Y_{2,14} &= -(\sin(q_1 + q_2) \sin(q_2) (\dot{v}_3 \sin(q_3) - v_3 \dot{q}_3 (2 \sin(q_3/2)^2 - 1)) \\
&\quad + v_3 \dot{q}_2 \sin(q_1 + q_2) \sin(q_3) (2 \sin(q_2/2)^2 - 1)) / \sin(q_2)^3; \\
Y_{2,15} &= Y_{2,16} = Y_{2,17} = Y_{2,18} = Y_{2,19} = 0; \\
Y_{2,20} &= Y_{2,21} = Y_{2,22} = Y_{2,23} = Y_{2,24} = 0; \\
Y_{2,25} &= 0; \\
Y_{3,1} &= Y_{3,2} = Y_{3,3} = 0; \\
Y_{3,4} &= (\cos(q_2) (v_1 \dot{q}_2 \cos(q_1) \cos(q_3) \sin(q_2) \\
&\quad + v_2 \dot{q}_2 \cos(q_3) \sin(q_1) \sin(q_2))) / (\sin(q_2) - \cos(q_2)^2 \sin(q_2)) - (\dot{v}_1 \cos(q_1) \cos(q_3) \\
&\quad + \dot{v}_2 \cos(q_3) \sin(q_1) + v_2 \dot{q}_1 \cos(q_1) \cos(q_3) + v_1 \dot{q}_1 \cos(q_1) \sin(q_3) \\
&\quad - v_1 \dot{q}_1 \cos(q_3) \sin(q_1) + v_1 \dot{q}_2 \cos(q_1) \sin(q_3) + v_2 \dot{q}_1 \sin(q_1) \sin(q_3) \\
&\quad + v_2 \dot{q}_2 \sin(q_1) \sin(q_3)) / \sin(q_2); \\
Y_{3,5} &= (\dot{v}_1 \cos(q_1 + q_2) \cos(q_2 + q_3) + \dot{v}_2 \cos(q_2 + q_3) \sin(q_1 + q_2) \\
&\quad + v_2 \dot{q}_1 \cos(q_1 + q_2) \cos(q_2 + q_3) + v_2 \dot{q}_2 \cos(q_1 + q_2) \cos(q_2 + q_3) \\
&\quad + v_1 \dot{q}_1 \cos(q_1 + q_2) \sin(q_2 + q_3) - v_1 \dot{q}_1 \cos(q_2 + q_3) \sin(q_1 + q_2) \\
&\quad - v_1 \dot{q}_2 \cos(q_2 + q_3) \sin(q_1 + q_2) + v_2 \dot{q}_1 \sin(q_1 + q_2) \sin(q_2 + q_3)) / \sin(q_2) \\
&\quad - (\cos(q_2) (v_1 \dot{q}_2 \cos(q_1 + q_2) \cos(q_2 + q_3) \sin(q_2) \\
&\quad + v_2 \dot{q}_2 \cos(q_2 + q_3) \sin(q_1 + q_2) \sin(q_2))) / (\sin(q_2) - \cos(q_2)^2 \sin(q_2)); \\
Y_{3,6} &= (\dot{v}_1 \cos(q_1) \cos(q_2) \sin(q_3) + \dot{v}_2 \cos(q_2) \sin(q_1) \sin(q_3) \\
&\quad + \dot{v}_1 \cos(q_1 + q_2) \sin(q_2 + q_3) \cos(q_2) + \dot{v}_2 \sin(q_1 + q_2) \sin(q_2 + q_3) \cos(q_2) \\
&\quad + v_2 \dot{q}_1 \cos(q_1 + q_2) \sin(q_2 + q_3) \cos(q_2) + v_2 \dot{q}_2 \cos(q_1 + q_2) \sin(q_2 + q_3) \cos(q_2) \\
&\quad - v_1 \dot{q}_1 \sin(q_1 + q_2) \sin(q_2 + q_3) \cos(q_2) - v_1 \dot{q}_2 \sin(q_1 + q_2) \sin(q_2 + q_3) \cos(q_2) \\
&\quad + v_2 \dot{q}_1 \cos(q_1) \cos(q_2) \sin(q_3) - v_1 \dot{q}_1 \cos(q_2) \sin(q_1) \sin(q_3)) / (\cos(q_2)^2 - 1) \\
&\quad - (v_1 \dot{q}_1 \cos(q_1) \sin(q_3) - v_2 \dot{q}_1 \sin(q_1 + q_2) \sin(q_2 + q_3) \\
&\quad - v_1 \dot{q}_1 \cos(q_1 + q_2) \sin(q_2 + q_3) + v_1 \dot{q}_2 \cos(q_1) \sin(q_3) \\
&\quad + v_2 \dot{q}_1 \sin(q_1) \sin(q_3) + v_2 \dot{q}_2 \sin(q_1) \sin(q_3) \\
&\quad - v_1 \dot{q}_1 \cos(q_1) \cos(q_2)^2 \sin(q_3) - v_2 \dot{q}_1 \cos(q_2)^2 \sin(q_1) \sin(q_3) \\
&\quad + v_1 \dot{q}_1 \cos(q_1 + q_2) \sin(q_2 + q_3) \cos(q_2)^2 + v_1 \dot{q}_2 \cos(q_1 + q_2) \sin(q_2 + q_3) \cos(q_2)^2 \\
&\quad + v_2 \dot{q}_1 \sin(q_1 + q_2) \sin(q_2 + q_3) \cos(q_2)^2 \\
&\quad + v_2 \dot{q}_2 \sin(q_1 + q_2) \sin(q_2 + q_3) \cos(q_2)^2) / (\sin(q_2) (\cos(q_2)^2 - 1)); \\
Y_{3,7} &= Y_{3,8} = Y_{3,9} = Y_{3,10} = 0; \\
Y_{3,11} &= -(\sin(q_3) ((\dot{v}_1 \sin(q_1)) / 2 - (\dot{v}_2 \cos(q_1)) / 2 + (\dot{v}_2 \cos(q_1 + 2q_2)) / 2 \\
&\quad - (\dot{v}_1 \sin(q_1 + 2q_2)) / 2 + (v_2 \dot{q}_1 \sin(q_1)) / 2 + v_2 \dot{q}_2 \sin(q_1) \\
&\quad - (v_1 \dot{q}_1 \cos(q_1 + 2q_2)) / 2 - (v_2 \dot{q}_1 \sin(q_1 + 2q_2)) / 2 \\
&\quad + (v_1 \dot{q}_1 \cos(q_1)) / 2 + v_1 \dot{q}_2 \cos(q_1))) / \sin(q_2)^3; \\
Y_{3,12} &= (\sin(q_2 + q_3) (\dot{v}_1 \cos(q_1) + \dot{v}_2 \sin(q_1) - v_1 \dot{q}_1 \sin(q_1) \\
&\quad + v_2 \dot{q}_1 \cos(q_1))) / \sin(q_2)^2 - (\sin(q_2 + q_3) (v_1 \dot{q}_2 \cos(q_1) \cos(q_2) \\
&\quad + v_2 \dot{q}_2 \cos(q_2) \sin(q_1))) / \sin(q_2)^3;
\end{aligned}$$

$$\begin{aligned}
Y_{3,13} &= (\sin(q_2 + q_3)(v_1 \dot{q}_2 \cos(q_1) \cos(q_2) + v_2 \dot{q}_2 \cos(q_2) \sin(q_1)))/\sin(q_2)^3 \\
&\quad - (\sin(q_2 + q_3)(\dot{v}_1 \cos(q_1) + \dot{v}_2 \sin(q_1) - v_1 \dot{q}_1 \sin(q_1) \\
&\quad + v_2 \dot{q}_1 \cos(q_1)))/\sin(q_2)^2; \\
Y_{3,14} &= (\sin(q_3)((\dot{v}_1 \sin(q_1))/2 - (\dot{v}_2 \cos(q_1))/2 + (\dot{v}_2 \cos(q_1 + 2q_2))/2 \\
&\quad - (\dot{v}_1 \sin(q_1 + 2q_2))/2 + (v_2 \dot{q}_1 \sin(q_1))/2 + v_2 \dot{q}_2 \sin(q_1) \\
&\quad - (v_1 \dot{q}_1 \cos(q_1 + 2q_2))/2 - (v_2 \dot{q}_1 \sin(q_1 + 2q_2))/2 \\
&\quad + (v_1 \dot{q}_1 \cos(q_1))/2 + v_1 \dot{q}_2 \cos(q_1)))/\sin(q_2)^3; \\
Y_{3,15} &= -(\dot{v}_3 - \dot{v}_3(\cos(2q_2 + 2q_3)/2 + 1/2))/\sin(q_2)^2 - ((v_3 \dot{q}_2 \cos(q_2 + 2q_3))/2 \\
&\quad + (v_3 \dot{q}_3 \cos(q_2 + 2q_3))/4 - (v_3 \dot{q}_3 \cos(3q_2 + 2q_3))/4 \\
&\quad - (v_3 \dot{q}_2 \cos(q_2))/2)/\sin(q_2)^3; \\
Y_{3,16} &= (\dot{v}_3 - \dot{v}_3(\cos(2q_3)/2 + 1/2) + (v_3 \dot{q}_3 \sin(2q_3))/2)/\sin(q_2)^2 \\
&\quad - (v_3 \dot{q}_2 \cos(q_2) - v_3 \dot{q}_2 \cos(q_2)(\cos(2q_3)/2 + 1/2))/\sin(q_2)^3; \\
Y_{3,17} &= \dot{v}_3; \\
\\
Y_{3,18} &= (\dot{v}_3 - \dot{v}_3(\cos(2q_2 + 2q_3)/2 + 1/2))/\sin(q_2)^2 + ((v_3 \dot{q}_2 \cos(q_2 + 2q_3))/2 \\
&\quad + (v_3 \dot{q}_3 \cos(q_2 + 2q_3))/4 - (v_3 \dot{q}_3 \cos(3q_2 + 2q_3))/4 \\
&\quad - (v_3 \dot{q}_2 \cos(q_2))/2)/\sin(q_2)^3; \\
Y_{3,19} &= g \cos(q_1 + q_2 + q_3); \\
Y_{3,20} &= (v_3 \dot{q}_2 \cos(q_2) - v_3 \dot{q}_2 \cos(q_2)(\cos(2q_3)/2 + 1/2))/\sin(q_2)^3 - (\dot{v}_3 \\
&\quad - \dot{v}_3(\cos(2q_3)/2 + 1/2) + (v_3 \dot{q}_3 \sin(2q_3))/2)/\sin(q_2)^2; \\
Y_{3,21} &= -(-4\dot{v}_3 \sin(q_2) \cos(q_2)^2 + 4v_3 \dot{q}_2 \cos(q_2) + \dot{v}_3 \sin(3q_2 + 2q_3) \\
&\quad + \dot{v}_3 \sin(q_2 - 2q_3) - v_3 \dot{q}_2 \cos(q_2 - 2q_3) - 3v_3 \dot{q}_2 \cos(q_2 + 2q_3) \\
&\quad - v_3 \dot{q}_3 \cos(q_2 - 2q_3) + v_3 \dot{q}_3 \cos(3q_2 + 2q_3))/(4 \sin(q_2)(\cos(q_2)^2 - 1)); \\
Y_{3,22} &= -(v_3 \dot{q}_2 \cos(q_2 - 2q_3) - v_3 \dot{q}_2 \cos(q_2 + 2q_3) + v_3 \dot{q}_3 \cos(q_2 - 2q_3) \\
&\quad - 2v_3 \dot{q}_3 \cos(q_2 + 2q_3) + v_3 \dot{q}_3 \cos(3q_2 + 2q_3))/(\sin(3q_2) - 3 \sin(q_2)) \\
&\quad - (2\dot{v}_3 - 2\dot{v}_3 \cos(2q_2 + 2q_3) - 2\dot{v}_3 \cos(2q_2) \\
&\quad + 2\dot{v}_3 \cos(2q_3))/(4 \sin(q_2)^2); \\
Y_{3,23} &= (v_3 \dot{q}_2 \cos(q_2 - 2q_3) - v_3 \dot{q}_2 \cos(q_2 + 2q_3) + v_3 \dot{q}_3 \cos(q_2 - 2q_3) \\
&\quad - 2v_3 \dot{q}_3 \cos(q_2 + 2q_3) + v_3 \dot{q}_3 \cos(3q_2 + 2q_3))/(\sin(3q_2) - 3 \sin(q_2)) \\
&\quad - (2\dot{v}_3 + 2\dot{v}_3 \cos(2q_2 + 2q_3) - 2\dot{v}_3 \cos(2q_2) \\
&\quad - 2\dot{v}_3 \cos(2q_3))/(4 \sin(q_2)^2); \\
Y_{3,24} &= (g(\sin(q_1 - q_3) - \sin(q_1 + 2q_2 + q_3)))/(2 \sin(q_2)); \\
Y_{3,25} &= (g \cos(q_1) \sin(q_3))/\sin(q_2).
\end{aligned}$$

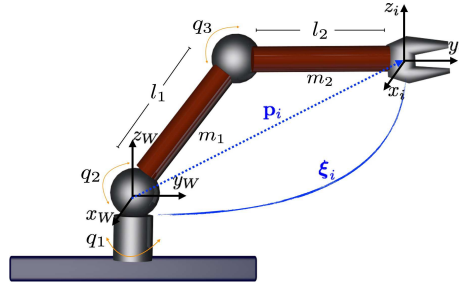


Figure B.3: 3-DoF robot Omni.

### B.1.3 3-DoF robot Omni

The direct kinematics of the 3-DoF robot Omni shown in Figure B.4 is given by

$$\mathbf{T}(\mathbf{q}) = \begin{bmatrix} -\sin(q_1) \sin(q_2+q_3) & -\cos(q_1) & -\sin(q_1) \cos(q_2+q_3) & -\sin(q_1)(l_1 \cos(q_2)+l_2 \cos(q_2+q_3)) \\ \cos(q_1) \sin(q_2+q_3) & -\sin(q_1) & \cos(q_1) \cos(q_2+q_3) & \cos(q_1)(l_1 \cos(q_2)+l_2 \cos(q_2+q_3)) \\ -\cos(q_2+q_3) & 0 & \sin(q_2+q_3) & l_1 \sin(q_2)+l_2 \sin(q_2+q_3) \\ 0 & 0 & 0 & 1 \end{bmatrix}.$$

The Jacobian is  $\mathbf{J}(\mathbf{q}) = [J_{ij}] \in \mathbb{R}^{3 \times 3}$ , where

$$\begin{aligned} J_{11} &= -\sin(q_1)(l_1 \cos(q_2) + l_2 \cos(q_2 + q_3)); \\ J_{12} &= -\cos(q_1)(l_1 \sin(q_2) + l_2 \sin(q_2 + q_3)); \\ J_{13} &= -l_2 \cos(q_1) \sin(q_2 + q_3); \\ J_{21} &= \cos(q_1)(l_1 \cos(q_2) + l_2 \cos(q_2 + q_3)); \\ J_{22} &= -\sin(q_1)(l_1 \sin(q_2) + l_2 \sin(q_2 + q_3)); \\ J_{23} &= l_2 \sin(q_1) \sin(q_2 + q_3); \\ J_{31} &= 0; \\ J_{32} &= l_1 \cos(q_2) + l_2 \cos(q_2 + q_3); \\ J_{33} &= l_2 \cos(q_2 + q_3). \end{aligned}$$

The joint space dynamic model follows (3.45) with  $n = 3$ . The inertia matrix is  $\bar{\mathbf{M}}(\mathbf{q}) = [\bar{M}_{ij}]$ , where

$$\begin{aligned} \bar{M}_{11} &= \frac{1}{2}In_{2z} - \frac{1}{2}In_{2y} \cos(2q_2) + \frac{1}{2}In_{3y} + \frac{1}{2}In_{2y} - \frac{1}{2}In_{3y} \cos(2q_2 + 2q_3) + \frac{1}{2}In_{2z} \cos(2q_2) \\ &\quad \frac{1}{2}In_{3z} \cos(2q_2 + 2q_3) + \frac{1}{2}In_{3z} + In_{1z} + \frac{1}{8}m_2l_1^2 + \frac{1}{2}m_3l_1^2 \cos(2q_2) + \frac{1}{2}m_3l_1l_2 \sin(2q_2 + q_3) \\ &\quad \frac{1}{2}m_3l_1^2 + \frac{1}{8}m_2l_1^2 \cos(2q_2) + \frac{1}{8}m_3l_2^2 - \frac{1}{8}m_3l_2^2 \cos(2q_2 + 2q_3) + \frac{1}{2}m_3l_1l_2 \sin(q_3); \\ \bar{M}_{12} &= 0; \\ \bar{M}_{13} &= 0; \end{aligned}$$



$$\begin{aligned}
\bar{M}_{21} &= 0; \\
\bar{M}_{22} &= In_{2_x} + In_{3_x} + m_3 l_1^2 + m_3 l_1 l_2 \sin(q_3) + \frac{1}{4} m_3 l_2^2 + \frac{1}{4} m_2 l_1^2; \\
\bar{M}_{23} &= In_{3_x} + \frac{1}{4} m_3 l_2^2 + \frac{1}{2} m_3 l_1 l_2 \sin(q_3); \\
\bar{M}_{31} &= 0; \\
\bar{M}_{32} &= \bar{M}_{23}; \\
\bar{M}_{33} &= In_{3_x} + \frac{1}{4} m_3 l_2^2.
\end{aligned}$$

Similarly, the Coriolis and centrifugal matrix is  $\bar{C}(\mathbf{q}, \dot{\mathbf{q}}) = [\bar{C}_{ij}]$ , where

$$\begin{aligned}
\bar{C}_{11} &= \left( \frac{1}{8} m_3 l_2^2 \sin(2q_2 + 2q_3) - \frac{1}{2} m_3 l_1^2 \sin(2q_2) + \frac{3}{8} m_2 l_1^2 \sin(2q_2) - \frac{1}{2} m_2 l_1^2 \sin(2q_2) + \frac{1}{2} m_3 l_1 l_2 \cos(2q_2 + q_3) \right. \\
&\quad \left. - \frac{1}{2} In_{2_z} \sin(2q_2) + \frac{1}{2} In_{2_y} \sin(2q_2) - \frac{1}{2} In_{3_z} \sin(2q_2 + 2q_3) + \frac{1}{2} In_{3_y} \sin(2q_2 + 2q_3) \right) \dot{\theta}_2 \\
&\quad + \left( \frac{1}{8} m_3 l_2^2 \sin(2q_2 + 2q_3) + \frac{1}{4} m_2 l_1 l_2 \cos(2q_2 + q_3) + \frac{1}{4} m_3 l_1 l_2 \cos(q_3) + \frac{1}{2} In_{3_y} \sin(2q_2 + 2q_3) \right. \\
&\quad \left. - \frac{1}{2} In_{3_x} \sin(2q_2 + 2q_3) \right) \dot{\theta}_3; \\
\bar{C}_{12} &= \left( \frac{1}{8} m_3 l_2^2 \sin(2q_2 + 2q_3) - \frac{1}{2} m_3 l_1^2 \sin(2q_2) + \frac{3}{8} m_2 l_1^2 \sin(2q_2) + \frac{1}{2} m_3 l_1 l_2 \cos(2q_2 + q_3) - \frac{1}{2} m_2 l_1^2 \sin(2q_2) \right. \\
&\quad \left. + \frac{1}{2} In_{2_y} \sin(2q_2) - \frac{1}{2} In_{3_z} \sin(2q_2 + 2q_3) - \frac{1}{2} In_{2_z} \sin(2q_2) \right) \dot{\theta}_1; \\
\bar{C}_{13} &= \left( \frac{1}{8} m_3 l_2^2 \sin(2q_2 + 2q_3) + \frac{1}{4} m_3 l_1 l_2 \cos(2q_2 + q_3) + \frac{1}{4} m_3 l_1 l_2 \cos(q_3) - \frac{1}{2} In_{3_z} \sin(2q_2 + 2q_3) \right. \\
&\quad \left. + \frac{1}{2} In_{3_y} \sin(2q_2 + 2q_3) \right) \dot{\theta}_1; \\
\bar{C}_{21} &= -\bar{C}_{12}; \\
\bar{C}_{22} &= \frac{1}{2} m_3 l_1 l_2 \cos(q_3) \dot{\theta}_3; \\
\bar{C}_{23} &= \frac{1}{2} m_3 l_1 l_2 \cos(q_3) \dot{\theta}_2 + \frac{1}{2} m_3 l_1 l_2 \cos(q_3) \dot{\theta}_3; \\
\bar{C}_{31} &= -\bar{C}_{13}; \\
\bar{C}_{32} &= -\frac{1}{2} m_3 l_1 l_2 \cos(q_3) \dot{\theta}_2; \\
\bar{C}_{33} &= 0.
\end{aligned}$$

The gravity vector is  $\bar{\mathbf{g}}(\mathbf{q}) = [\bar{g}_i]$ , where

$$\begin{aligned}
\bar{g}_1 &= 0; \\
\bar{g}_2 &= \frac{1}{2} g m_3 l_2 \sin(q_2 + q_3) + \frac{1}{2} g m_3 l_1 \cos(q_2) + \frac{1}{2} g m_2 l_1 \cos(q_2); \\
\bar{g}_3 &= \frac{1}{2} g m_3 l_2 \sin(q_2 + q_3).
\end{aligned}$$

The meaning of the physical parameters is depicted in Table B.1.

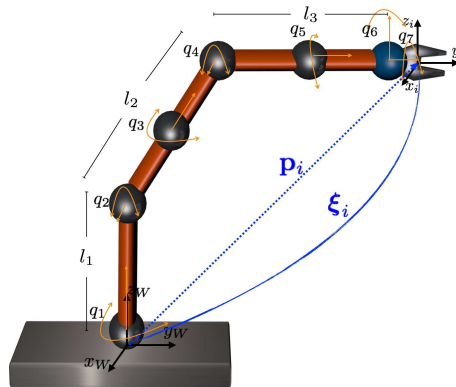


Figure B.4: 7-DoF robot LWR.

### B.1.4 7-DoF robot LWR

The kinematics and dynamics of this robot can be found in (Bargsten, Zometa, and Findeisen 2013) and in (Ejarque and Basañez 2014).

## B.2 PhanTorque libraries

The PhanTorque libraries<sup>6</sup> are devised to facilitate the implementation of control algorithms from Simulink<sup>®</sup> to Geomagic<sup>®</sup> devices. In particular the *PhanTorque\_6Dof*, shown in Figure B.5, is designed to be used with the PHANTOM Premiums 1.5<sup>®</sup> and the *PhanTorque\_3Dof*, shown in Figure B.8, with the PHANTOM Omni<sup>®</sup> and PHANTOM Desktop<sup>®</sup> devices. These libraries follow the same idea of the Phansim library detailed in (Mohammadi, Tavakoli, and Jazayeri 2011). The PhanTorque libraries use C/C++ S-functions and the OpenHaptics libraries<sup>7</sup> to make the communication between the haptics and Simulink. The main characteristics of the PhanTorque libraries are that they allow to set the torques of the Geomagic devices and read the transformation matrix of the robot's end-effector with respect to the base and their linear and angular velocities.

### PhanTorque\_6Dof library

Figure B.5 shows the blocks that compose the PhanTorque\_6Dof library. The masks of the two principal blocks, *PhanTorque\_6Dof* and *PhanTorque\_6Dof\_vels*, are detailed in Figure B.6 and Figure B.7, respectively. The Jacobian derived in (Rodriguez and Basañez 2005) is used to program the blocks *Phantom 1.5/6DOF Jacobian* and *Phantom 1.5/6DOF Jacobian Transpose*, it is given by  $\mathbf{J}(\mathbf{q}) = [J_{ij}] \in \mathbb{R}^{6 \times 6}$ , where

<sup>6</sup>The libraries are publicly available at <https://sir.upc.edu/wikis/roblab/index.php/Projects/PhanTorqueLibraries>

<sup>7</sup><http://geomagic.com/en/products/open-haptics/overview/>

$$\begin{aligned}
J_{11} &= \cos(q_1) (l_1 \cos(q_2) + l_2 \sin(q_3)); \\
J_{12} &= \sin(q_1) (-l_1 \sin(q_2) + l_2 \sin(q_3)); \\
J_{13} &= l_2 \sin(q_1) \cos(q_3); \\
J_{14} &= J_{15} = J_{16} = 0; \\
J_{21} &= 0; \\
J_{22} &= l_1 \cos(q_2) + l_2 \sin(q_3); \\
J_{23} &= l_2 \sin(q_3); \\
J_{24} &= J_{25} = J_{26} = 0; \\
J_{31} &= -\sin(q_1) (l_1 \cos(q_2) + l_2 \sin(q_3)); \\
J_{32} &= \cos(q_1) (-l_1 \sin(q_2) + l_2 \cos(q_3)); \\
J_{33} &= l_2 \cos(q_1) \cos(q_3); \\
J_{34} &= J_{35} = J_{36} = 0; \\
J_{41} &= 0; \\
J_{42} &= -\cos(q_1); \\
J_{43} &= -\cos(q_1); \\
J_{44} &= \sin(q_1) \sin(q_3); \\
J_{45} &= -\sin(q_1) \cos(q_3) \sin(q_4) - \cos(q_1) \cos(q_4); \\
J_{46} &= \sin(q_1) \cos(q_3) \cos(q_4) \cos(q_5) - \cos(q_1) \sin(q_4) \cos(q_5) - \sin(q_1) \sin(q_3) \sin(q_5); \\
J_{51} &= 1; \\
J_{52} &= 0; \\
J_{53} &= 0; \\
J_{54} &= -\cos(q_3); \\
J_{55} &= -\sin(q_3) \sin(q_4); \\
J_{56} &= \sin(q_3) \cos(q_4) \cos(q_5) + \cos(q_3) \sin(q_5); \\
J_{61} &= 0; \\
J_{62} &= \sin(q_1); \\
J_{63} &= \sin(q_1); \\
J_{64} &= \cos(q_1) \sin(q_3); \\
J_{65} &= -\cos(q_1) \cos(q_3) \sin(q_4) + \sin(q_1) \cos(q_4); \\
J_{66} &= \cos(q_1) \cos(q_3) \cos(q_4) \cos(q_5) + \sin(q_1) \sin(q_4) \cos(q_5) - \cos(q_1) \sin(q_3) \sin(q_5).
\end{aligned}$$

The *Clock Generator* block is the same of the Phansim library. The *Homogeneous Matrix* block changes the vector  $\mathbf{h} \in \mathbb{R}^{16}$  to a matrix  $\mathbf{H} \in \mathbb{R}^{4 \times 4}$  and the *Rotation Matrix* block extracts the rotation matrix data from  $\mathbf{h}$ .

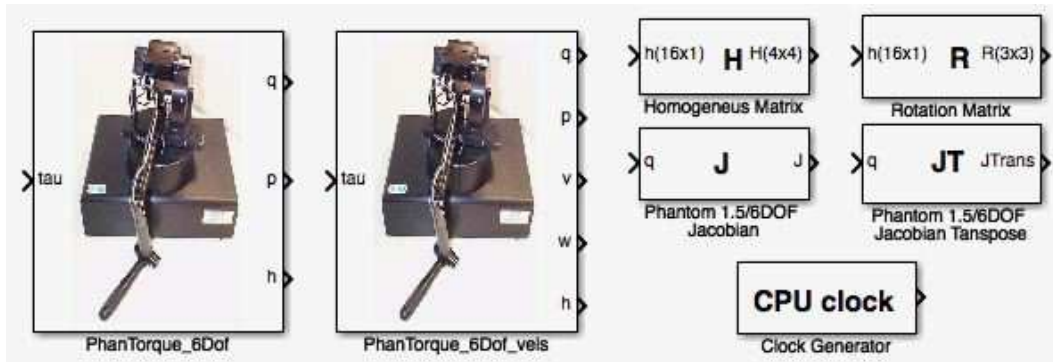


Figure B.5: PhanTorque\_6Dof library.

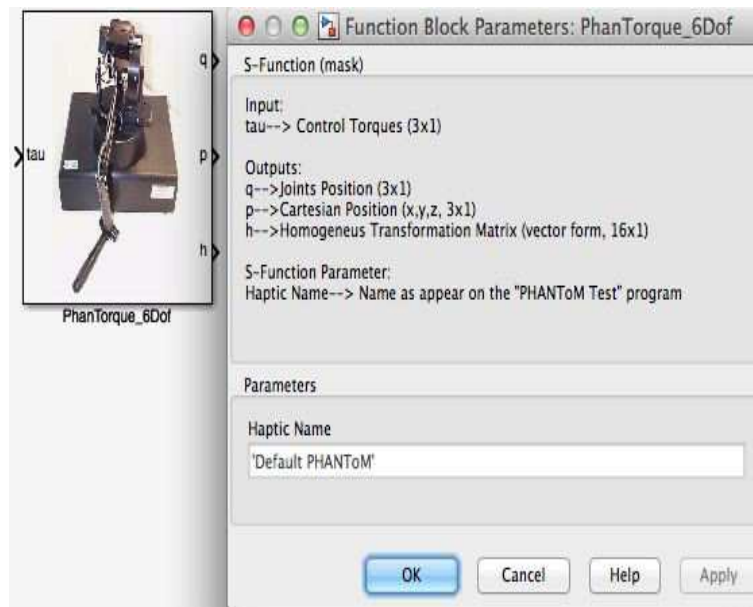


Figure B.6: PhanTorque\_6Dof block.

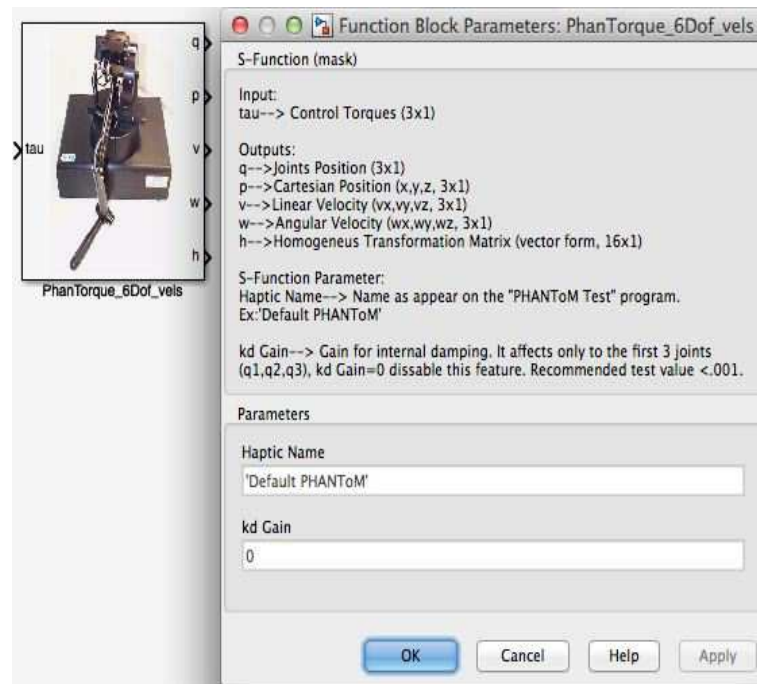


Figure B.7: PhanTorque\_6Dof\_vels block.

### PhanTorque\_3Dof library

The blocks that compose the PhanTorque\_3Dof library are shown in Figure B.8 . In Figure B.9 and Figure B.11 the masks of the two principal blocks of the library are detailed. The Jacobian derived in (Nuño, Sarras, Panteley, and Basañez 2012) is used to program the blocks *Omni Jacobian* and *Omni Jacobian Transpose*. The rest of the blocks are the same as those of the PhanTorque\_6Dof. All the blocks, except *Omni Jacobian* and *Omni Jacobian Transpose*, work also with the Phantom Desktop<sup>®</sup> device.



Figure B.8: PhanTorque\_3Dof library.

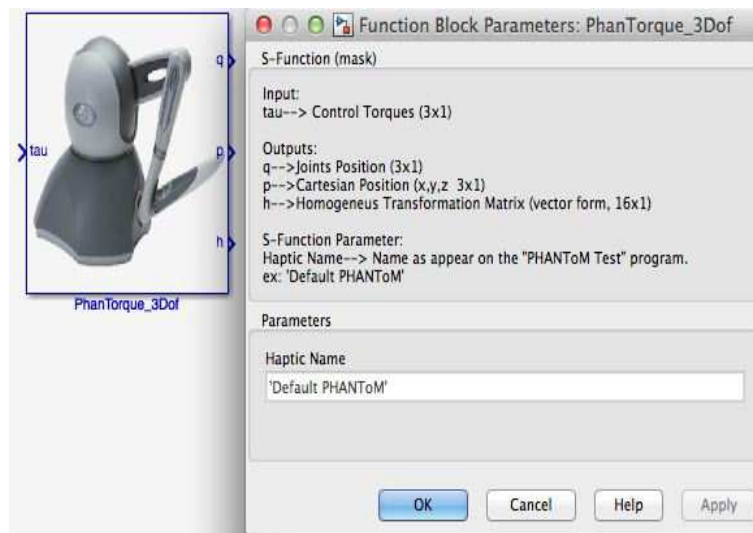


Figure B.9: PhanTorque\_3Dof block.

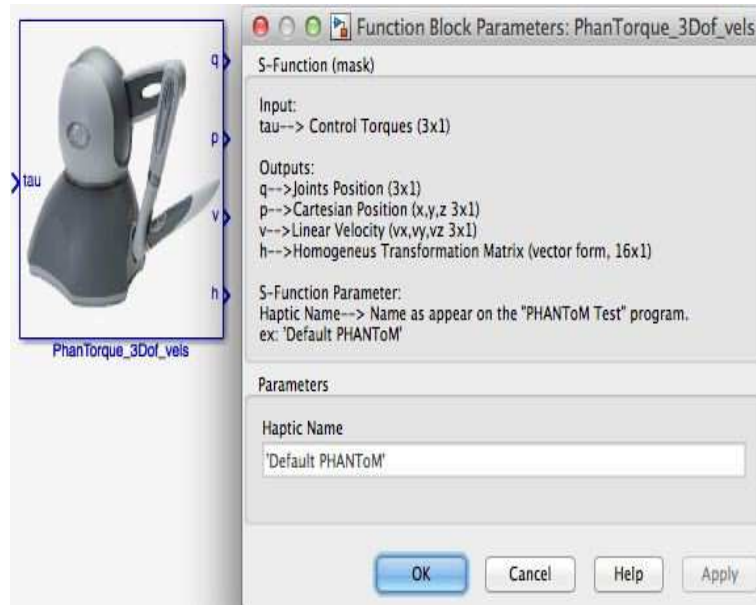


Figure B.10: PhanTorque\_3Dof\_vels block.

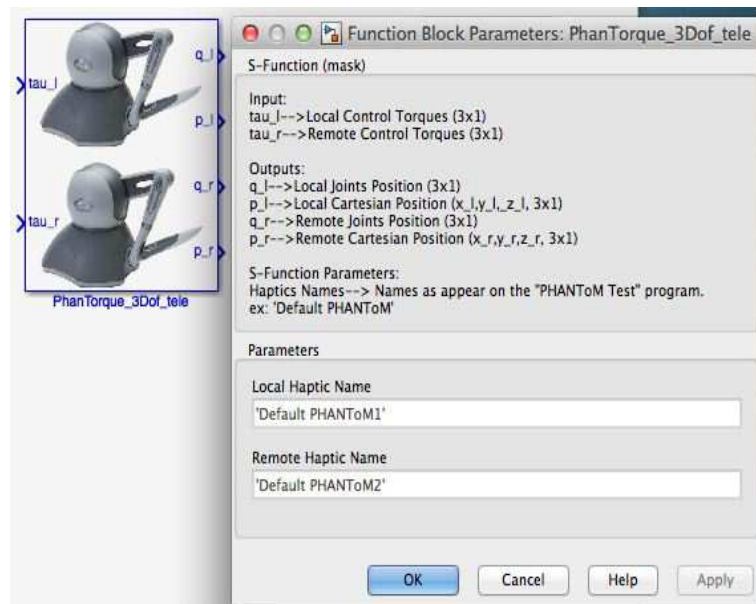


Figure B.11: PhanTorque\_3Dof\_tele block.





## REFERENCES

---

- Abdessameud, A. and A. Tayebi (2009). Attitude synchronization of a group of spacecraft without velocity measurements. *IEEE Transactions on Automatic Control* 54(11), 2642–2648.
- Abdessameud, A. and A. Tayebi (2011a). A unified approach to the velocity-free consensus algorithms design for double integrator dynamics with input saturations. *IEEE Conference on Decision and Control and European Control Conference*, 4903–4908.
- Abdessameud, A. and A. Tayebi (2011b). Formation control of VTOL unmanned aerial vehicles with communication delays. *Automatica* 47(11), 2383–2394.
- Abdessameud, A., A. Tayebi, and I.-G. Polushin (2012). Attitude synchronization of multiple rigid bodies with communication delays. *IEEE Transactions on Automatic Control* 57(9), 2405–2411.
- Ahmad, S. and M. Zribi (1993). Lyapunov-based control design for multiple robots handling a common object. *Dynamics and Control* 3(2), 127–157.
- Ahn, H.-S. and J. Ryu (2008). Passivity and transparency of teleoperation systems with lossy delay: Transmission line-based analysis. *IEEE International Conference on Systems, Man and Cybernetics*, 2730–2735.
- Anderson, R. and M. Spong (1989). Bilateral control of teleoperators with time delay. *IEEE Transactions on Automatic Control* 34(5), 494–501.
- Aracil, R., J. M. Azorin, M. Ferre, and C. Peña (2013). Bilateral control by state convergence based on transparency for systems with time delay. *Robotics and Autonomous Systems* 61(2), 86–94.
- Arcak, M. (2007). Passivity as a design tool for group coordination. *IEEE Transactions on Automatic Control* 52(8), 1380–1390.
- Artigas, J., J. Ryu, and C. Preusche (2010). Time domain passivity control for position-position teleoperation architectures. *Presence* 19(5), 482–497.
- Astolfi, A., R. Ortega, and A. Venkatraman (2010). A globally exponentially convergent immersion and invariance speed observer for mechanical systems with non-holonomic constraints. *Automatica* 46(1), 182–189.
- Azorin, J., R. Aracil, C. Perez, N. Garcia, and J. Sabater (2008). Transparent bilateral control

- for time-delayed teleoperation by state convergence. In *IEEE International Conference on Robotics and Automation (ICRA)*, pp. 643–648.
- Bargsten, V., P. Zometa, and R. Findeisen (2013). Modeling, parameter identification and model-based control of a lightweight robotic manipulator. *IEEE International Conference on Control Applications (CCA)*, 134–139.
- Blanchini, F. (1999). Set invariance in control. *Automatica* 35(11), 1747–1767.
- Bonitz, R. G. and T. C. Hsia (1996). Internal force-based impedance control for cooperating manipulators. *IEEE Transactions on Robotics and Automation* 12(1), 78–89.
- Caccavale, F., P. Chiacchio, and S. Chiaverini (1999). Stability analysis of a joint space control law for a two-manipulator system. *IEEE Transactions on Automatic Control* 44(1), 85–88.
- Caccavale, F., P. Chiacchio, and S. Chiaverini (2000). Task-space regulation of cooperative manipulators. *Automatica* 36(6), 879–887.
- Caccavale, F., P. Chiacchio, A. Marino, and L. Villani (2008). Six-dof impedance control of dual-arm cooperative manipulators. *IEEE/ASME Transactions On Mechatronics* 13(5), 576–586.
- Caccavale, F., B. Siciliano, and L. Villani (1999). The role of Euler parameters in robot control. *Asian Journal of Control* 1(1), 25–34.
- Camazine, S. (2003). *Self-Organization in Biological Systems*. Princeton University Press.
- Campa, R. (2005). *Control de robots manipuladores en espacio de tarea*. Ph. D. thesis, CICESE.
- Campa, R. and K. Camarillo (2008). *Robot manipulators*, Chapter Unit quaternions: A mathematical tool for modeling, path planning and control of robot manipulators, pp. 21–48. InTech.
- Campa, R. and H. de la Torre (2009). Pose control of robot manipulators using different orientation representations: A comparative review. *American Control Conference (ACC)*, 2855–2860.
- Cao, Y. and W. Ren (2011). *Distributed Coordination of Multi-agent Networks: Emergent Problems, Models, and Issues*. Springer-Verlag.
- Cheah, C. C., C. Liu, and J. E. Slotine (2006). Adaptive jacobian tracking control of robots with uncertainties in kinematic, dynamic and actuator models. *IEEE Transactions on Automatic Control* 51(6), 1024–1029.
- Chopra, N. and M. Spong (2005). On synchronization of networked passive systems with time delays and application to bilateral teleoperation. In *Proceedings of the SICE Annual Conference*, pp. 3424–3429.
- Chopra, N., M. Spong, R. Ortega, and N. Barbanov (2006). On tracking performance in bilateral teleoperation. *IEEE Transactions on Robotics* 22(4), 844–847.

- Chou, J. C. K. (1992). Quaternion kinematic and dynamic differential equations. *IEEE Transactions on Robotics and Automation* 8(1), 53–64.
- Chung, S.-J., U. Ahsun, and J.-J. Slotine (2009). Application of synchronization to formation flying spacecraft: Lagrangian approach. *Journal of Guidance, Control and Dynamics* 32(2), 512–526.
- Chung, S.-J. and J.-J. Slotine (2009). Cooperative robot control and concurrent synchronization of lagrangian systems. *IEEE Transactions on Robotics*. 25(3), 686–700.
- Craig, J. J. (2005). *Introduction to Robotics: Mechanics and Control* (3rd ed.). Addison-Wesley Longman Publishing Co., Inc.
- Dauchez, P., X. Delebarre, Y. Bouffar-Vercelli, and E. Degoulange (1992). Force control experiments with a two-arm robot. *Journal of Intelligent and Robotic Systems* 5(3), 253–269.
- De Persis, C. and B. Jayawardhana (2012). Coordination of passive systems under quantized measurements. *SIAM Journal on Control and Optimization* 50(6), 3155–3177.
- Ejarque, R. and L. Basañez (2014). Control adaptatiu per al robot manipulador KUKA Light Weight Robot 4+ (<http://hdl.handle.net/2099.1/24233>). Technical report, Institute of Industrial and Control Engineering, Technical University of Catalonia.
- Fax, J. and R. Murray (2004). Information flow and cooperative control of vehicle formations. *IEEE Transactions on Automatic Control* 49(9), 1465–1476.
- Feng, Y., S. Xu, F. Lewis, and B. Zhang (2013). Consensus of heterogeneous first- and second-order multi-agent systems with directed communication topologies. *International Journal of Robust and Nonlinear Control*, 362–375.
- Fjellstad, O. E. (1994). *Control of unmanned underwater vehicles in six degrees of freedom: a quaternion feedback approach*. Ph. D. thesis, Norwegian Institute of Technology, University of Trondheim.
- Franchi, A., C. Secchi, H. I. Son, H. Bulthoff, and P. Giordano (2012). Bilateral teleoperation of groups of mobile robots with time-varying topology. *IEEE Transactions on Robotics* 28(5), 1019–1033.
- Garcia-Valdovinos, L., V. Parra-Vega, and M. Arteaga (2007). Observer-based sliding mode impedance control of bilateral teleoperation under constant unknown time delay. *Robotics and Autonomous Systems* 55(8), 609–617.
- Ge, C., W. Zhang, H. Wang, and X. Li (2014). An adaptive regulator for space teleoperation system in task space. *Abstract and Applied Analysis* 2014, 7.
- Gu, D.-B. and Z. Wang (2009). Leader-follower flocking: Algorithms and experiments. *IEEE Transactions on Control Systems Technology* 17(5), 1211–1219.
- Hainsworth, D. W. (2001). Teleoperation user interfaces for mining robotics. *Autonomous*

- Robots* 11(1), 19–28.
- Hardy, G., J. Littlewood, and G. Polya (1988). *Inequalities (2nd ed.)*. Cambridge Mathematical Library. Cambridge University Press.
- Hatanaka, T., Y. Igarashi, M. Fujita, and M. Spong (2012). Passivity-based pose synchronization in three dimensions. *IEEE Transactions on Automatic Control* 57(2), 360–375.
- Hokayem, P. and M. Spong (2006). Bilateral teleoperation: An historical survey. *Automatica* 42(12), 2035–2057.
- Hsu, P. (1993). Coordinated control of multiple manipulator systems. *IEEE Transactions on Robotics and Automation* 9(4), 400–410.
- Hu, H.-X., L. Yu, W.-A. Zhang, and H. Song (2013). Group consensus in multi-agent systems with hybrid protocol. *Journal of The Franklin Institute* 350(3), 575–597.
- Hu, J. and Y. Lin (2010). Consensus control for multi-agent systems with double-integrator dynamics and time delays. *IET Control Theory and Applications* 4(1), 109.
- Hu, Y., H. Su, and J. Lam (2013). Adaptive consensus with a virtual leader of multiple agents governed by locally Lipschitz nonlinearity. *International Journal of Robust and Nonlinear Control* 23(9), 978–990.
- Hua, C. and X. Liu (2011). Teleoperation over the internet with/without velocity signal. *IEEE Transactions on Instrumentation and Measurement* 60(1), 4–13.
- Igarashi, Y., T. Hatanaka, M. Fujita, and M. Spong (2009). Passivity-based attitude synchronization in SE(3). *IEEE Transactions on Control Systems Technology* 17(5), 1119–1134.
- Jadbabaie, A., J. Lin, and A. S. Morse (2003). Coordination of groups of mobile autonomous agents using nearest neighbor rules. *IEEE Transactions on Automatic Control* 48(6), 988–1001.
- Kelly, R., V. Santibáñez, and A. Loria (2005). *Control of Robot Manipulators in Joint Space*. Advanced textbooks in control and signal processing. Springer-Verlag.
- Khalil, H. (1996). *Nonlinear Systems (2nd ed.)*. Englewood Cliffs, NJ: Prentice-Hall.
- Khatib, O. (1995). Inertial properties in robotic manipulation: an object-level framework. *The International Journal of Robotics Research* 13(1), 19–36.
- Klumpp, A. R. (1976). Singularity-free extraction of a quaternion from a direction-cosine matrix. *Journal of Spacecraft and Rockets* 13(12), 754–755.
- Kreyszig, E. (1978). *Introductory Functional Analysis with Applications*. London UK: John Wiley and Sons.
- Kuipers, J. B. (2002). *Quaternions and rotation sequences: A primer with applications to orbits, aerospace and virtual reality*. Princeton University Press.

- LaSalle, J. and S. Lefschetz (1961). *Stability by Lyapunov's Direct Method with Applications, volume 4 of Mathematics in Science and Engineering*. Academic Press.
- Lau, H. Y. K. and L. C. C. Wai (2005). Implementation of position–force and position–position teleoperator controllers with cable-driven mechanisms. *Robotics and Computer-Integrated Manufacturing* 21(2), 145–152.
- Launay, J.-P. (1998). Teleoperation and nuclear services advantages of computerized operator-assistance tools. *Nuclear Engineering and Design* 180(1), 47–52.
- Lawrence, D. A. (1993). Stability and transparency in bilateral teleoperation. *IEEE Transactions on Robotics and Automation* 9(5), 624–637.
- Le, M. Q., M. T. Pham, M. Tavakoli, and R. Moreau (2011a). An enhanced sliding-mode control for a pneumatic-actuated teleoperation system. *IEEE/RSJ International Conference on Intelligent Robots and Systems (IROS)*, 659–664.
- Le, M. Q., M. T. Pham, M. Tavakoli, and R. Moreau (2011b). Sliding mode control of a pneumatic haptic teleoperation system with on/off solenoid valves. *IEEE International Conference on Robotics and Automation (ICRA)*, 874–879.
- Lee, D. and M. Spong (2005). Bilateral teleoperation of multiple cooperative robots over delayed communication networks: Theory. *IEEE International Conference on Robotics and Automation (ICRA)*, 360–365.
- Lee, D. and M. W. Spong (2007). Stable flocking of multiple inertial agents on balanced graphs. *IEEE Transactions on Automatic Control* 52(8), 1469–1475.
- Li, Z., Z. Duan, and F. L. Lewis (2014). Distributed robust consensus control of multi-agent systems with heterogeneous matching uncertainties. *Automatica* 50(3), 883–889.
- Liu, X., R. Tao, and M. Tavakoli (2014). Adaptive control of uncertain nonlinear teleoperation systems. *Mechatronics* 24(1), 66–78.
- Liu, Y. and N. Chopra (2012). Controlled synchronization of heterogeneous robotic manipulators in the task space. *IEEE Transactions on Robotics* 28(1), 268–275.
- Liu, Y.-C. and N. Chopra (2013). Control of semi-autonomous teleoperation system with time delays. *Automatica* 49(6), 1553–1565.
- Luecke, G. R. and K. W. Lai (1997). A joint error-feedback approach to internal force regulation in cooperating manipulator systems. *Journal of Robotic Systems* 14(9), 631–648.
- Malysz, P. and S. Sirouspour (2011). A Kinematic Control Framework for Single-Slave Asymmetric Teleoperation Systems. *IEEE Transactions on Robotics* 27(5), 901–917.
- Markley, F. L. (2008). Unit quaternion from rotation matrix. *Journal of Guidance, Control and Dynamics* 31(2), 440–442.
- Mei, J., W. Ren, and G. Ma (2011). Distributed coordinated tracking with a dynamic leader

- for multiple Euler-Lagrange systems. *IEEE Transactions on Automatic Control* 56(6), 1415–1421.
- Meng, Z., W. Ren, Y. Cao, and Z. You (2011). Leaderless and leader-following consensus with communication and input delays under a directed network topology. *IEEE Transactions on Systems, Man and Cybernetics, Part B: Cybernetics* 41(1), 75–88.
- Mohammadi, A., M. Tavakoli, and A. Jazayeri (2011). Phansim : A simulink toolkit for the phantom haptic devices. *Proceedings of 23rd Canadian Congress of Applied Mechanics*, 787–790.
- Moosavian, S. A. A. and M. Mostafavi (2006). Multiple impedance control of redundant manipulators. *Proceeding of IEEE Conference on Robotics, Automation and Mechatronics*, 1–6.
- Moreau, L. (2005). Stability of multiagent systems with time-dependent communication links. *IEEE Transactions on Automatic Control* 50(2), 169–182.
- Murata, S. and H. Kurokawa (2012). *Self-Organizing Robots*, Volume 77 of *Springer Tracts in Advanced Robotics*. Springer Tokyo.
- Murray, R., Z. Li, and S. Sastry (1994). *A Mathematical Introduction to Robot Modelling and Control*. CRC Press.
- Murray, R. M. (2007). Recent research in cooperative control of multivehicle systems. *Journal of Dynamic Systems, Measurement, and Control* 129(5), 571–583.
- Nakamura, Y., K. Nagai, and T. Yoshikawa (1987). Mechanics of coordinative manipulation by multiple robotic mechanisms. *IEEE International Conference on Robotics and Automation (ICRA)*, 991–998.
- Natale, C. (2003). *Interaction Control of Robot Manipulators: Six-Degrees-of-Freedom Tasks*, Volume 3. Springer.
- Ni, W. and D. Cheng (2010). Leader-following consensus of multi-agent systems under fixed and switching topologies. *Systems and Control Letters* 59(3–4), 209–217.
- Niemeyer, G. and J. Slotine (1991). Stable adaptive teleoperation. *IEEE Journal of Oceanic Engineering* 16(1), 152–162.
- Nuño, E., L. Basañez, G. Obregon-Pulido, and G. Solis-Perales (2011). Bilateral teleoperation control without velocity measurements. In *18th IFAC World Congress*.
- Nuño, E., L. Basañez, and R. Ortega (2011). Passivity-based control for bilateral teleoperation: A tutorial. *Automatica* 47(3), 485–495.
- Nuño, E., L. Basañez, R. Ortega, and M. Spong (2009). Position tracking for nonlinear teleoperators with variable time-delay. *International Journal of Robotics Research* 28(7), 895–910.

- Nuño, E., R. Ortega, and L. Basañez (2010). An adaptive controller for nonlinear teleoperators. *Automatica* 46(1), 155–159.
- Nuño, E., R. Ortega, L. Basañez, and D. Hill (2011). Synchronization of networks of nonidentical Euler-Lagrange systems with uncertain parameters and communication delays. *IEEE Transactions on Automatic Control* 56(4), 935–941.
- Nuño, E., I. Sarras, and L. Basañez (2013). Consensus in networks of nonidentical Euler-Lagrange systems using P+d controllers. *IEEE Transactions on Robotics* 29(6), 1503–1508.
- Nuño, E., I. Sarras, E. Panteley, and L. Basañez (2012). Consensus in networks of nonidentical Euler-Lagrange systems with variable time-delays. In *IEEE Conference on Decision and Control (CDC)*, Maui, Hawaii, USA, pp. 4721–4726.
- Okura, F., Y. Ueda, T. Sato, and N. Yokoya (2013). Teleoperation of mobile robots by generating augmented free-viewpoint images. *IEEE/RSJ International Conference on Intelligent Robots and Systems (IROS)*, 665–671.
- Olfati-Saber, R., J. A. Fax, and R. M. Murray (2007). Consensus and cooperation in networked multi-agent systems. *Proceedings of the IEEE* 95(1), 215–233.
- Olfati-Saber, R. and R. Murray (2004). Consensus problems in networks of agents with switching topology and time-delays. *IEEE Transactions on Automatic Control* 49(9), 1520–1533.
- Polushin, I., P. X. Liu, and C.-H. Lung (2007). A force-reflection algorithm for improved transparency in bilateral teleoperation with communication delay. *IEEE/ASME Transactions on Mechatronics* 12(3), 361–374.
- Polushin, I. G., S. N. Dashkovskiy, A. Takhmar, and R. V. Patel (2013). A small gain framework for networked cooperative force-reflecting teleoperation. *Automatica* 49(2), 338–348.
- Preusche, C., T. Ortmaier, and G. Hirzinger (2002). Teleoperation concepts in minimal invasive surgery. *Control Engineering Practice* 10(11), 1245–1250.
- Qian, K., A. Song, J. Bao, and H. Zhang (2012). Small teleoperated robot for nuclear radiation and chemical leak detection. *International Journal of Advanced Robotic Systems* 9(70), 1–9.
- Qin, J., W. Zheng, and H. Gao (2012). Coordination of multiple agents with double-integrator dynamics under generalized interaction topologies. *IEEE Transactions on Systems, Man and Cybernetics, Part B: Cybernetics* 42(1), 44–57.
- Qin, J., W. X. Zheng, and H. Gao (2011). Consensus of multiple second-order vehicles with a time-varying reference signal under directed topology. *Automatica* 47(9), 1983–1991.
- Ren, W. (2007). Distributed attitude alignment in spacecraft formation flying. *International Journal of Adaptive Control and Signal Processing* 21(2-3), 95–113.

- Ren, W. (2008). On consensus algorithms for double-integrator dynamics. *IEEE Transactions on Automatic Control* 53(6), 1503–1509.
- Ren, W. (2009). Distributed leaderless consensus algorithms for networked Euler-Lagrange systems. *International Journal of Control* 82(11), 2137–2149.
- Ren, W. (2010a). Consensus tracking under directed interaction topologies: Algorithms and experiments. *IEEE Transactions on Control Systems Technology* 18(1), 230–237.
- Ren, W. (2010b). Distributed cooperative attitude synchronization and tracking for multiple rigid bodies. *IEEE Transactions on Control Systems Technology* 18(2), 383–392.
- Ren, W. and E. Atkins (2007). Distributed multi-vehicle coordinated control via local information exchange. *International Journal of Robust and Nonlinear Control* 17(10-11), 1002–1033.
- Ren, W. and R. W. Beard (2005). Consensus seeking in multiagent systems under dynamically changing interaction topologies. *IEEE Transactions on Automatic Control* 50(5), 655–661.
- Ren, W., R. W. Beard, and E. Atkins (2007). Information consensus in multivehicle cooperative control. *IEEE Control Systems* 27(2), 71–82.
- Rodriguez, A. and L. Basañez (2005). Modelo cinemático de la interfase háptica PHAN-ToM 1.5/6DOF (<http://upcommons.upc.edu/pfc/handle/2099.1/14587>). Technical report, Institute of Industrial and Control Engineering, Technical University of Catalonia.
- Rodriguez-Angeles, A. and H. Nijmeijer (2004). Mutual synchronization of robots via estimated state feedback: a cooperative approach. *IEEE Transactions on Control Systems Technology* 12(4), 542–554.
- Rodriguez-Seda, E. J., J. J. Troy, C. A. Erignac, P. Murray, D. M. Stipanovic, and M. W. Spong (2010). Bilateral teleoperation of multiple mobile agents: coordinated motion and collision avoidance. *IEEE Transactions on Control Systems Technology* 18(4), 984–992.
- Rubio, A., A. Avello, and J. Florez (2000). On the use of virtual springs to avoid singularities and workspace boundaries in force-feedback teleoperation. *IEEE International Conference on Robotics and Automation (ICRA)* 3, 2690–2695.
- Salvo-Rossi, P., G. Romano, F. Palmieri, and G. Iannello (2006). Joint end-to-end loss-delay hidden markov model for periodic UDP traffic over the internet. *IEEE Transactions on Signal Processing* 54(2), 530–541.
- Sarlette, A., R. Sepulchre, and N. E. Leonard (2009). Autonomous rigid body attitude synchronization. *Automatica* 45(2), 572–577.
- Sarras, I., E. Nuño, L. Basañez, and M. Kinnaert. Output feedback control of bilateral teleoperators without velocity measurements. *International Journal of Robust and Nonlinear Control*.



- Scardovi, L. and R. Sepulchre (2009). Synchronization in networks of identical linear systems. *Automatica* 45(11), 2557–2562.
- Secchi, C., L. Sabattini, and C. Fantuzzi (2013). Decentralized global connectivity maintenance for interconnected lagrangian systems in the presence of data corruption. *European Journal of Control* 19(6), 461 – 468. Lagrangian and Hamiltonian Methods for Modelling and Control.
- Seung, S., B. Kang, H. Je, J. Park, K. Kim, and S. Park (2009). Tele-operation master-slave system for minimal invasive brain surgery. *IEEE International Conference on Robotics and Biomimetics (ROBIO)*, 177–182.
- Shuster, M. D. (1993). A survey of attitude representations. *The Journal of the Astronautical Sciences* 41(4), 439–517.
- Siciliano, B., L. Sciavicco, L. Villani, and G. Oriolo (2009). *Robotics: Modelling, Planning and Control*. Advanced Textbooks in Control and Signal Processing. Springer.
- Sirospour, S. (2005). Modeling and control of cooperative teleoperation systems. *IEEE Transactions on Robotics* 21(6), 1220–1225.
- Sirospour, S. and A. Shahdi (2006). Model predictive control for transparent teleoperation under communication time delay. *IEEE Transactions on Robotics* 22(6), 1131–1145.
- Sontag, E. (1998). *Mathematical Control Theory. Deterministic Finite-Dimensional Systems (Second ed.)*, Volume 6 of *Applied mathematics*. New York: Springer-Verlag.
- Spong, M., S. Hutchinson, and M. Vidyasagar (2005). *Robot Modeling and Control*. Wiley.
- Spurrier, R. A. (1978). Comment on singularity-free extraction of a quaternion from a direction-cosine matrix. *Journal of Spacecraft and Rockets* 15(4), 255.
- Stramigioli, S., A. van der Schaft, B. Maschke, and C. Melchiorri (2002). Geometric scattering in robotic telemanipulation. *IEEE Transactions on Robotics and Automation* 18(4), 588–596.
- Strang, G. (1986). *Introduction to applied mathematics*. Cambridge UK: Wellesley-Cambridge Press.
- Su, Y. and J. Huang (2012a). Cooperative output regulation with application to multi-agent consensus under switching network. *IEEE transactions on systems, man, and cybernetics. Part B, Cybernetics : a publication of the IEEE Systems, Man, and Cybernetics Society* 42(3), 864–875.
- Su, Y. and J. Huang (2012b). Stability of a class of linear switching systems with applications to two consensus problems. *IEEE Transactions on Automatic Control* 57(6), 1420–1430.
- Su, Y. and J.-P. Huang (2012c). Cooperative output regulation of linear multi-agent systems. *IEEE Transactions on Automatic Control* 57(4), 1062–1066.

- Sun, D. and J. K. Mills (2002). Adaptive synchronized control for coordination of multirobot assembly tasks. *IEEE Transactions on Automatic Control* 18(4), 498–510.
- Sun, Y. (2012). Average consensus in networks of dynamic agents with uncertain topologies and time-varying delays. *Journal of The Franklin Institute* 349(3), 1061–1073.
- Tao, G. (1997). A simple alternative to the barbălat lemma. *IEEE Transactions on Automatic Control* 42(5), 698.
- Teel, A. R. (1999). Asymptotic convergence from  $\mathcal{L}_p$  stability. *IEEE Transactions on Automatic Control* 44(11), 2169–2170.
- Terelius, H., G. Shi, and K. Johansson (2013). Consensus control for multi-agent systems with a faulty node. In *4th IFAC Workshop on Distributed Estimation and Control in Networked Systems*, pp. 425–432.
- Torres, F., S. Puente, and C. Díaz (2009). Automatic cooperative disassembly robotic system: Task planner to distribute tasks among robots. *Control Engineering Practice* 17(1), 112 – 121.
- Uchiyama, M. (1998). *Control problems in robotics and automation*, Volume 230 of *Lecture Notes in Control and Information Sciences*, Chapter 2. Multirobots and Cooperative Systems, pp. 18–34. Springer Berlin / Heidelberg.
- Uchiyama, M. and P. Dauchez (1993). Symmetric kinematic formulation and non-master/slave coordinated control of two-arm robots. *Advanced Robotics* 7(4), 361–383.
- Uchiyama, M., N. Iwasawa, and K. Hakomori (1987). Hybrid position/force control for coordination of a two-arm robot. *IEEE International Conference on Robotics and Automation (ICRA)*, 1242–1247.
- Uzmay, I., R. Burkan, and H. Sarikaya (2004). Application of robust and adaptive control techniques to cooperative manipulation. *Control Engineering Practice* 12(2), 139–148.
- van der Schaft Arjan (1999).  *$\mathcal{L}_2$ -Gain and Passivity in Nonlinear Control*. Springer-Verlag New York, Inc.
- Vertut, J. and P. Coiffet (1985). *Robot Technology*, Volume 3B, pp. 205–212. Springer Netherlands.
- Vicsek, T., A. Czirók, E. Ben-Jacob, I. Cohen, and O. Shochet (1995). Novel type of phase transitions in a system of self-driven. *Physical review letters* 75(6), 1226–1229.
- Walker, I. D., R. a. Freeman, and S. I. Marcus (1991). Analysis of Motion and Internal Loading of Objects Grasped by Multiple Cooperating Manipulators. *The International Journal of Robotics Research* 10(4), 396–409.
- Wang, H. (2013a). Passivity based synchronization for networked robotic systems with uncertain kinematics and dynamics. *Automatica* 49(3), 755–761.

- Wang, H. (2013b). Task-space synchronization of networked robotic systems with uncertain kinematics and dynamics. *IEEE Transactions on Automatic Control* 58(12), 3169–3174.
- Wang, H. and Y. Xie (2012). Task-space framework for bilateral teleoperation with time delays. *Journal of Dynamic Systems, Measurement, and Control* 134(5).
- Wang, X., C. Yu, and Z. Lin (2012). A dual quaternion solution to attitude and position control for rigid-body coordination. *IEEE Transactions on Robotics* 28(5), 1162–1170.
- Wen, G., Z. Duan, W. Yu, and G. Chen (2012). Consensus in multi-agent systems with communication constraints. *International Journal of Robust and Nonlinear Control* 22(2), 170–182.
- Wen, G., Z. Li, Z. Duan, and G. Chen (2013). Distributed consensus control for linear multi-agent systems with discontinuous observations. *International Journal of Control* 86(1), 95–106.
- Wen, J. T. and K. K. Delgado (1992). Motion and force control of multiple robotic manipulators. *Automatica* 28(4), 729–743.
- Wen, J.-Y. and K. Kreutz-Delgado (1991). The attitude control problem. *IEEE Transactions on Automatic Control* 36(10), 1148–1162.
- Willaert, B., B. Corteville, D. Reynaerts, H. Van Brussel, and E. B. Vander Poorten (2009). Bounded environment passivity of the classical position-force teleoperation controller. *IEEE/RSJ International Conference on Intelligent Robots and Systems (IROS)*, 4622–4628.
- Williams, D. and O. Khatib (1993). Experiments in multi-grasp manipulation. *Experimental Robotics III, The 3rd Int. Symposium, Kyoto, Japan, October 28-30*, 14–28.
- Xi, N., T.-J. Tarn, and A. K. Bejczy (1996). Intelligent planning and control for multi-robot coordination: an event-based approach. *IEEE Transactions on Robotics and Automation* 12(3), 439–452.
- Yu, W., G. Chen, M. Cao, and J. Kurths (2010). Second-order consensus for multiagent systems with directed topologies and nonlinear dynamics. *IEEE transactions on systems, man, and cybernetics. Part B, Cybernetics : a publication of the IEEE Systems, Man, and Cybernetics Society* 40(3), 881–891.
- Yu, W., W. Ren, W. X. Zheng, G. Chen, and J. Lü (2013). Distributed control gains design for consensus in multi-agent systems with second-order nonlinear dynamics. *Automatica* 49(7), 2107–2115.
- Yuan, J. (1988). Closed-loop manipulator control using quaternion feedback. *IEEE Journal of Robotics and Automation* 4(4), 434–440.
- Zergeroglu, E., D. D. Dawson, I. W. Walker, and P. Setlur (2004). Nonlinear tracking control of kinematically redundant robot manipulators. *IEEE/ASME Transactions on Mechatronics* 9(1), 129–132.



## Keyword Index

- $\mathcal{L}_2$ -Gain, 158
- $\mathcal{L}_2$ -Stability, 158
- $\mathcal{L}_q$ -Stability, 157
- Autonomous System, 155
- Axis-angle representation
  - definition, 24
  - from rotation matrix, 24
- Barbālat's Lemma, 157
- Dynamic model
  - joint space, 35
  - operational space, 36
  - properties, 36
- Euler angles
  - definition, 21
  - ZYX convention, 22
  - ZYZ convention, 21
- Function properties
  - absolute Continuity, 149
  - continuity, 149
  - uniform Continuity, 149
  - Lipschitz, 149
  - piecewise Continuity, 149
- Functions
  - negative semi-definite, 150
  - positive definite, 149
  - radially unbounded, 150
  - negative Definite, 149
  - positive Semi-Definite, 150
- Gershgorin theorem, 146
- Hilbert space, 151
- Inequality
  - Hölder, 152
  - Minkowski, 153
  - Rayleigh, 153
  - Schwarz, 152
  - Young, 152
- Inner product, 150
- Joint space, 18
- Kronecker product, 146
- La Salle's Theorem, 157
- Laplacian, 39
- LCP definition, 47
- Lemma
  - equilibrium points leader-follower, 48
  - equilibrium points leaderless, 50
- LFCP definition, 47
- Lyapunov Theory
  - equilibrium point, 154
  - local stability, 156
  - stability, 155
  - AS, 155
  - GAS, 155, 156
  - GUAS, 155
  - instability, 156
  - Lyapunov function, 156
  - Lyapunov function candidate, 155
  - UAS, 155
  - US, 155
- Matrix
  - definition, 145, 146
  - eigenvalues, 146
  - Identity, 146
  - square, 146
  - symmetric, 146
  - transpose, 146
- Non-Autonomous System, 154
- Norm
  - $\mathcal{L}_2$ , 150
  - $\mathcal{L}_\infty$ , 150
- Operational space, 18
- Passivity, 158
- Pose
  - definition, 28
  - error, 31
- Proposition
  - cooperative teleoperation with uncertain parameters and time-delays, 120
  - equilibrium points for a network with delays, 58
  - LCP solution with uncertain parameters and time-delays, 70
  - LCP solution with uncertain parameters, time-delays and human interaction, 71

- LCP solution with variable time-delays, 61
- LCP solution with variable time-delays and human interaction, 63
- LCP solution without velocity measurement and human interaction, 56
- LCP solution without velocity measurements, 54
- LFCP solution with uncertain parameters and time-delays, 67
- LFCP solution with variable time-delays, 59
- LFCP solution without velocity measurements, 52
- teleoperation with uncertain parameters and time-delays, 118
- teleoperation with variable time-delays, 116
- teleoperation without velocity measurements, 115
  
- Quaternions
  - addition, 153
  - conjugate, 153
  - definition, 153
  - inverse, 154
  - multiplication, 154
  - norm, 154
  - unit-quaternions, 25
  
- Rotation matrix
  - composition, 20
  - definition, 19
  
- Sets
  - dist, 151
  - group, 152
  - invariance, 151
  - limit set, 151
  - positively invariant, 151
  
- Topological Spaces
  - $\mathcal{L}_q$ , 150
  - $\mathcal{L}_{q_e}$ , 150
  
- Unit-quaternions
  - definition, 25
  - from axis-angle representation, 26
  - from rotation matrix, 26
  
- Vector
  - $\infty$ -norm, 149
  - cross product, 147
  - definition, 147
  - dot product, 147
  
- Euclidean-norm, 149
- norm definition, 148
- q-norm, 148

## First Authors Index

- Abdessameud A., 7, 9, 11  
Ahmad S., 14  
Ahn HS., 13  
Anderson R., 13  
Aracil R., 13  
Arcak M., 10  
Artigas J., 12  
Azorin J.M., 13
- Blanchini F., 151  
Bonitz R., 14
- Caccavale F., 11, 14, 28  
Camazine S., 7  
Campa R., 19, 30, 32  
Cheah C., 12  
Chopra N., 10  
Chou J.C.K., 145  
Chung S., 11  
Craig J., 21, 34
- Dauchez P., 14  
DePersis C., 10
- Fax J., 8  
Feng Y., 9  
Fjellstad O., 11, 30, 32  
Franchi A., 15
- Garcia-Valdovinos L., 13  
Ge C., 12, 13  
Gu D., 7, 12
- Hainsworth D., 12  
Hardy G., 145, 152, 153  
Hatanaka T., 7, 12  
Hsu P., 14  
Hu H., 9, 10  
Hu J., 9  
Hua C., 13
- Igarashi Y., 11
- Jadbabaie, A., 8
- Kelly R., 35, 145  
Khalil H.K., 157  
Khatib O., 14  
Kreyszig E., 152
- Kuipers J.B., 145
- Lau H., 12  
Launay JP., 12  
Lawrence D., 12  
Le M., 12  
Lee D., 7  
Li Z., 9  
Liu X., 14  
Liu Y., 12, 14, 73  
Luecke G., 14
- Malysz P., 15  
Mei J., 10  
Meng Z., 9, 10  
Moosavian S., 14  
Moreau L., 8  
Murata S., 7  
Murray R., 8, 152
- Nakamura Y., 14  
Natale C., 27, 28  
Ni W., 9  
Niemeyer G., 13  
Nuño E., 10, 13, 42, 73
- Okura F., 12  
Olfati-Saber R., 8, 40
- Polushin I.G., 13, 15  
Preusche C., 12
- Qian K., 12  
Qin J., 9
- Ren W., 8–11, 42  
Rodriguez A., 7, 10  
Rodriguez-Angeles A., 14  
Rodriguez-Seda E., 15  
Rubio A., 12
- Sarlette A., 11  
Scardovi L., 7  
Schaft A. van der, 145  
Secchi C., 10  
Seung S., 12  
Shuster M., 28  
Siciliano B., 26  
Sirouspour S., 13, 15

Slotine J., 10  
Sontag E.D., 145  
Spong M., 15, 34  
Spurrier R., 74  
Strang G., 145, 153  
Su Y., 9  
Sun D., 14  
Sun Y., 9  
  
Tao G., 157  
Teel A.R., 157  
Terelius H., 9  
Torres F., 14  
  
Uchiyama M., 14  
Uzmay I., 14  
  
Vertut J, 12  
Vicsek, T, 8  
  
Wang H., 12, 13, 73  
Wang X, 12  
Wen G., 9  
Wen J., 11, 14, 32  
Willaert B., 12  
Williams D., 14  
  
Xi N., 14  
  
Yu W., 10  
Yuan J., 11, 33  
  
Zergeroglu E., 73